Effects of clay-organic association on hydrocarbon generation in shale

Submitted to Macquarie University in fulfillment of the requirements for the degree of

Doctor of Philosophy

February 2018

Md Habibur Rahman

Macquarie University

Faculty of Sciences

Department of Earth and Planetary Sciences

New South Wales, Australia

Statement of Authenticity

I hereby declare that this thesis entitled "Effects of clay-organic association on hydrocarbon generation in shale" has not been submitted for the award of a degree at any other university or institution other than Macquarie University. I also certify that this thesis is an original piece of research that has been written by me and that the help in preparing this study and all sources used have been appropriately acknowledged.

Md Habibur Rahman

'I know nothing except the fact of my ignorance'

(Socrates, 470 BC - 399 BC)

Dedicated to

My sister, ***Meherun-nesa Rozina*** *(1982-2014)*

The kindest person I have ever seen who fought an incredibly valiant battle against cancer

Acknowledgments

I owe a great deal of gratitude to my principal supervisor Martin Kennedy for the encouragement and support he has provided throughout my PhD studies. Martin has been extraordinary in mentoring me to develop my ideas and assisting me in problem solving. The lessons he taught have helped me to become a better researcher and made it possible to finish this PhD.

I would also like to thank the co-supervisors of my PhD study. From the beginning of the study, my co-supervisor Stefan Loëhr has been encouraging and supportive. He helped me a lot to find my way through this long journey. I am also grateful to my external supervisor David Dewhurst from CSIRO Energy, Western Australia. He has been very keen on providing support throughout my PhD. He has remained continuously enthusiastic to my research.

My sincere thanks to Tony Hall from the University of Adelaide for helping and supporting me on planning the PhD project during early days. Tony has been amazingly helpful to guide me with the initial experimental set-up. I would also like to thank Neil Sherwood from CSIRO Earth Science and Resource Engineering, New South Wales. He has been incredibly welcoming of me in his lab and has remained extremely helpful to my countless queries. My sincere thanks goes to Brian Horsfield from GFZ German Research Centre for Geosciences for helping me with the kinetic experiments. I would like to thank Simon George from Macquarie University for helping me with experiments and allowing me to use his lab.

I would like to thank my colleagues Soumaya Abbasi, Catherine Straford, Elizabeth Baruch, Paolo Abballe, Natalie Debenham, Karita Negandhi and Alexander Tunnadine from our research group for the invaluable supports they have provided during this long journey.

This PhD study would not have been possible without the Macquarie University Research Excellence Scholarship (iMQRES) awarded by Macquarie University. This thesis work is also partly supported by the Australian Research Council project (ARC Linkage Project LP120200086 to M. Kennedy).

I would like to thank my wife Mili for her continuous encouragement during this whole journey. She has been extraordinarily supportive and has selflessly given more to me than I could have ever asked for. Words cannot describe how lucky I am to have her in my life. Special thanks to my daughter little Viyana, her divine smiles have been taking away the tiredness of the journey during the final days.

I would have never asked for a better parents and siblings. My parents, Md Mostofa and Jahanara Begum, and brother Sumon have always been unbelievably supportive. From commencement to completion, this PhD would have never been completed without the constant support and encouragement from them.

Abstract

Widely variable and inconsistent results are reported in many previous studies while investigating the influence of mineral matrix on hydrocarbon generation using laboratory pyrolysis experiments. Some studies show greater hydrocarbon generation in mixtures of clay minerals and organic matter while others report an inhibiting effect of clay minerals. The effect of physical association of organic matter and mineral matrices on hydrocarbon generation has not been tested yet. This thesis investigates the forms of organic carbon in shale and their physical relationship to the mineral matrix as a control on hydrocarbon yield and generation kinetics. Two distinct shale textures are compared with varying degree of surface contact between minerals and organic matter. Samples of the Micoene Monterey Formation in California, USA demonstrate a complex intimate association of amorphous organic matter with clay minerals at sub-micron scale in a nanocomposite shale fabric. Organic matter in the Permian Stuart Range Formation of South Australia is present as discrete organic particles of > 5 μm size that are largely unrelated to the mineral matrix. The relationship between organic matter and mineral surfaces is also evident in the scaling between total organic carbon (TOC) and mineral surface area (MSA). Samples with intercalated clay mineral and organic matter (nanocomposite) typical of the Monterey Formation show a strong first-order relationship between TOC and MSA (R^2 = 0.91) identifying a genetic relationship between these structures leading to a molecular scale coating of organic matter on mineral surfaces. Samples from the Stuart Range Formation have a poor relationship between

TOC and MSA (R^2 = 0.54) indicating independence of organic matter accumulation without mineral matrix influence. Pyrolysis experiments of whole rock samples compared to the extracted kerogen isolates show greater hydrocarbon generation of the kerogen isolates than the whole rocks (containing minerals and organic matter) in both sample suites. Between the two sample sets, however, there is a significant difference of hydrocarbon generation potential (HI) between extracted kerogen and whole rock with the Stuart Range Formation showing a much greater range (56 to 210 mgHC/g TOC) than in the Monterey Formation (85 to 142 mgHC/gTOC). This is interpreted to result from greater hydrocarbon retention by the mineral surfaces unoccupied by organic matter in the Stuart Range Formation. Kinetic experiments are performed on paired samples of whole rock and the extracted kerogen component from both Monterey and Stuart Range formations using open system, non-isothermal pyrolysis at three different heating rates (0.7, 2 and 5 K/min). The majority of the samples of the Stuart Range Formation show nearly identical generation pattern for whole rock and kerogen isolate pairs in kinetic models, which is consistent with the independent distribution of organic matter and minerals. The Monterey Formation, however, show a significant clay catalytic effect by reducing the onset temperature of hydrocarbon generation by 20°C when compared to kerogen isolates. This finding is consistent with the nanocomposite fabric of samples of the Monterey Formation where reactive clay minerals are intimately associated with organic matter. The results show that shale fabric, and in particular, the physical relationship between clay mineral surfaces and organic matter at sub-micron scales can influence timing and yield of

hydrocarbon generation. In turn, this association is determined by conditions in the depositional environment leading to a predictable effect between different types of shale.

Table of contents

List of Figures

List of Table

Chapter 1. Introduction

Fine-grained sedimentary rocks are the most abundant lithology that constitutes approximately two-thirds of the stratigraphic record, among them shale is most common. Oil and gas extracted from conventional petroleum systems are generated in organically rich shale before migrating to reservoirs. Generation of hydrocarbon includes physical and chemical transformations of organic matter, processes that begin soon after the deposition of sediments. Transformation of organic matter involves complex organic reactions in different phases of sediment lithification and diagenesis as they occur with increasing burial and temperature, though only a tiny fraction of the organic matter produced in marine and continental settings gets preserved in sediment (Hedges and Keil, 1995). Following preservation in sediments, with geologic time, organic matter transforms to oil and gas by slow chemical and physical alteration with a key intermediate called kerogen (Vandenbroucke and Largeau, 2007).

Kerogen is the most abundant form of organic carbon in the sedimentary record and accounting for ~ 90% of the organic carbon in the global carbon cycle (Durand, 1980; Hedges and Keil, 1995; Vandenbroucke and Largeau, 2007). The transformation of organic matter with increasing burial and temperature is classically subdivided into three stages, diagenesis, catagenesis, and metagenesis (Tissot and Welte, 1984). Diagenesis starts in recently deposited sediments and includes low temperature transformations of sedimentary organic matter by microbial actions and chemical reactions. Through diagenesis, a new structure of organic matter is formed which is

called kerogen. Kerogens are complex mixtures of organic components that often lack any distinctive chemical composition and are defined as the fraction of organic matter dispersed in sediments that are insoluble in organic solvents (Durand, 1980). Diagenesis also produces a heavier component of organic matter called bitumen. Bitumen differs from kerogen being the fraction of organic matter soluble in organic solvents (Durand, 1980). Diagenesis is restricted to within a few hundred meters of burial depth. An increase in temperature during burial of sediments leads to catagenesis that induces the formation of oil and gas through thermal breakdown. Thermal maturation of kerogen during sediment burial results in a net loss of carbon, hydrogen and oxygen as shown by a continuous decrease in total organic carbon (TOC) content with increasing maturity in homogenous sedimentary series (Vandenbroucke and Largeau, 2007). The subsequent last stage of the evolution of sedimentary organic matter at high temperature (commonly > 150°C) is called metagenesis. The van Krevelen (van Krevelen, 1961) diagram illustrates the maturity stages of organic matter that are separated according to carbon losses over oxygen and hydrogen. During these complex burial transformations of organic matter in sediments, the minerals in rock matrices also undergo simultaneous diagenetic transformations in response to increasing burial and temperature and exposure to geofluids.

Shale is a fine-grained sedimentary rock with fissility that may contain a range of silicate and carbonate minerals. Clay minerals are major constituent of shale with clastic mineralogy (Shaw and Weaver, 1965). Among all clay minerals in sedimentary rocks, smectite, illite and their mixed-layer illite-

smectite (I-S) intermediates are more common and comprise 30% of all minerals (Garrels and Mackenzie, 1971). Illitization of smectites is a common clay minerals diagenetic process that occurs in shale. The diagenetic transformation of smectite to illite through a mixed layer I-S occurs over the temperature-depth interval associated with peak oil generation (Perry and Hower, 1970; Hower et al., 1976; Pevear, 1999; Kim et al., 2004; Abid and Hesse, 2007; Li et al., 2015). Illitization causes loss of Si, Na and H_2O and gain of K, Al and quartz cements (Hower et al., 1976) processes capable of significantly altering the detrital mineralogy of shale. The process of illitization is poorly understood, both solid state transformation (Pollard, 1971; Hower et al., 1976; Eslinger et al., 1979; Ehrlich, 1996; Drits et al., 1997) and partial dissolution and re-precipitation (Nadeau et al., 1985; Ahn and Peacor, 1986; Lynch et al., 1997) have been proposed as potential mechanisms. Smectite diagenesis provides a potential scope of physico-chemical interaction between physically associated organic compounds and charged (reactive) smectite surfaces during burial of shale.

The structure of smectite allows it to coordinate organic reactions, a property widely used in chemical and metallurgical industries for many decades (McCabe and Adams, 2013; Ray, 2013). Smectites are expandable 2:1 type clay minerals with a structure consisting of an octahedral layer sandwiched between two tetrahedral layers (Varma, 2002). The interlayer spaces of smectites can accommodate various cations (e.g. Na^+, K^+, Ca^{2+}, Mg^{2+}) and water molecules (Varma, 2002; Ray, 2013). A net negative layer charge of smectites makes them highly reactive in sediments (Brown and Rhodes, 1997;

McCabe and Adams, 2013). Most of the reactions catalyzed by smectites are due to their acidic character; both Lewis and BrØnsted activity are common (Kellendonk et al., 1987; Varma, 2002; McCabe and Adams, 2013). Hydrated and dehydrated cations in the interlayer space are the sources of Brønsted and Lewis acidity respectively (Wu et al., 2012). The acidic properties of clay minerals are strongly dependent on the presence of water. BrØnsted acidity (proton/H+ donation) is mainly due to the dissociation of adsorbed water that is induced by the polarizing power of the cations (e.g. K^{+}, Ca^{2+}, Al^{3+}) varying with the size and charge of the ions. Water molecules in the interlayer space of smectites can also be displaced by polar organic molecules (Varma, 2002). The Brønsted and Lewis acidity indicate the potential of smectite surfaces to associate with organic matter during diagenesis.

Organic matter in sedimentary rocks is commonly preserved as discrete, primary particles that have escaped mineralization (Tyson, 1994). However, a growing body of literature documents a class of mineral-bound organic matter that is frequently dominant both in modern organic-rich sediments (Bishop et al., 1992; Keil et al., 1994; Mayer, 1994; Blair and Aller, 2012) and in ancient mudstones (Salmon et al., 2000; Kennedy et al., 2014; Löhr and Kennedy, 2014). The intimate association of organic matter with clay minerals can have several potential effects. Firstly, sorption to mineral surfaces can stabilize organic molecules by slowing the degradation rates up to five orders of magnitude in marine sediments (Keil et al., 1994; Ray, 2013) aiding preservation of organic matter in sediments (Kennedy and Wagner, 2011). Kennedy and Wagner (2011) suggested that smectite acts to preserve

significant concentrations of organic matter in sediments with high TOC (TOC > 10%) resulting when water column anoxia facilitates a higher organic carbon loading on mineral surfaces. Secondly, the cation exchange capacity of smectites make them a potential catalyst of associated organic reactions (Lagaly et al., 2013).

The majority of organic matter in continental margin settings is oxidised/mineralized within the water column or in sediments and only a small fraction, as low as < 0.5% of the primary organic matter ultimately is preserved in the geologic record (Hedges and Keil, 1995). Several models of organic carbon enrichment in sediments have been proposed including the control of oxygen depleted conditions (Arthur and Sageman, 1994; Hartnett et al., 1998), high primary productivity (Calvert et al., 1992; Tyson, 2005), flux of organic carbon through water column (Jahnke, 1990) and sedimentation rate (Müller and Suess, 1979; Arthur and Sageman, 1994; Tyson, 2001). In addition to the earlier mentioned models, organic carbon in sedimentary rocks may also be preserved through association with high surface area (i.e. smectite) clay minerals (Kennedy et al., 2002). The clay mineral associated organic matter preservation model is potentially significant because of the abundance of clay minerals in stratigraphic record, shale comprising > 60% clay minerals as constituent (Shaw and Weaver, 1965). Moreover, many studies have also shown that in modern continental margin sediments TOC is quantitatively associated with mineral surface area (MSA) that is mainly contributed by the clay minerals (Keil et al., 1994; Mayer, 1994; Hedges and Keil, 1995; Keil and Mayer, 2014).

The TOC and MSA relationship shown previously in different studies are almost entirely based on bulk geochemical analyses and there are few petrographic images at sufficient scale to show the physical relationship of organic matter and mineral surfaces in shale. It is not established how the mineral surface area facilitates organic matter preservation. It is not established how the mineral surface area facilitates organic matter preservation. Compared to the quantitative and qualitative analyses of organic content, the diversity of distribution of organic matter in shale is not well studied and speculation exists in many studies on the uniformity of its arrangement in sediments (Kuila et al., 2014). The organic matter that is visible in optical or scanning electron imaging in sediments often does not add up to the total organic carbon measured in the bulk rocks identifying the presence of a significant fraction of organic matter in shale in different forms (Bishop et al., 1992) that might not visible by standard methods.

One significant impact that mineral surfaces may have on organic matter is to influence hydrocarbon generation. The form of organic matter in shale depends on several factors including initial composition, depositional environment, and diagenetic alteration. Depending on these variables, organic matter may range from particulate to structure-less textures (Belin, 1992). These organic matter fabrics, such as particulate or clay mineral associated organic matter, could potentially have a significant control on the contact and exposure of organic matter to highly reactive mineral surfaces in shale (Fig. 1.1).

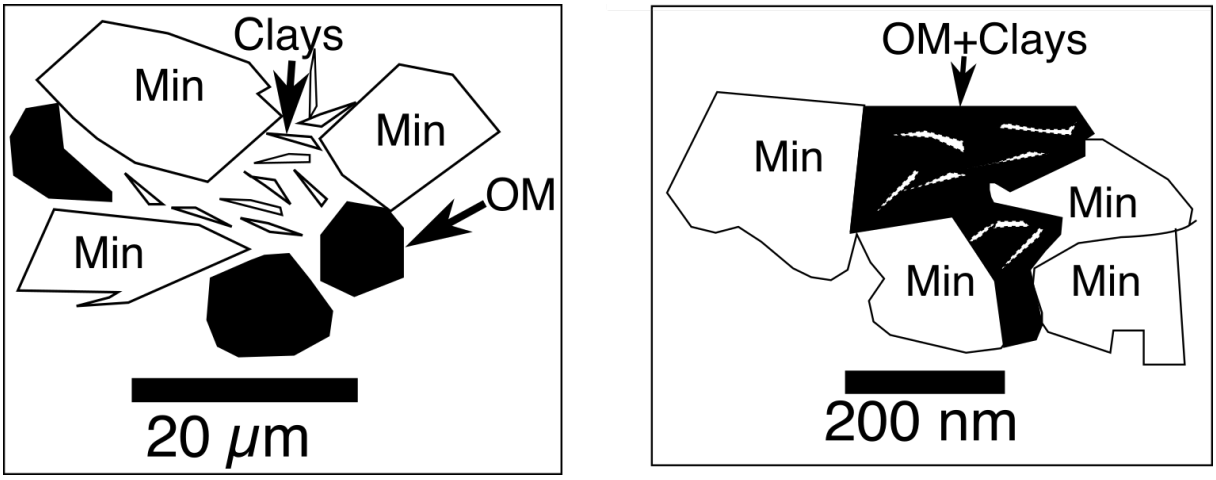

Fig. 1.1. Schematic diagrams showing two potential organic matter textures in shale. a) Organic matter is present as discrete particles without an intimate association with clay minerals. b) Organic matter is present in an intimate association with clay minerals.

The study of shale fabric is a challenge because of the fine (few microns) grain size of clay minerals and relatively homogenous appearance in hand specimen and at optical microscopy scale (Macquaker and Adams, 2003; Macquaker et al., 2010). However, with the advancement of high resolution scanning and transmission electron imaging, grain to grain contacts are more frequently imaged and show complex sedimentary depositional and diagenetic processes active on these apparently homogenous sediments (Macquaker and Adams, 2003; Macquaker et al., 2010; Aplin and Macquaker, 2011; Kennedy et al., 2014; Macquaker et al., 2014; Milliken et al., 2014; Shaldybin et al., 2017). Shale contains a varying proportion of detrital, alteration/replacement and authigenic minerals (Macquaker and Adams, 2003). The authigenic components of shale mainly depend on fluid chemistry, burial temperature and initial (detrital) mineralogy (Setti et al., 2004). The detrital components depend on the original mineralogy of the continental provenance and intensity of continental weathering (Boggs, 2009). The amount and type of organic matter and mineralogy can vary significantly in shale based on the

physical and chemical processes acting on sediments during and after deposition (Lazar et al., 2015). Therefore, a variation in organic-inorganic fabric would be expected in shale formations where organic productivity, mineralogy, depositional and diagenetic settings are widely variable.

Experimental studies have investigated the impact of smectite clays on hydrocarbon generation (Shimoyama and Johns, 1971; Galwey, 1972; Johns and Shimoyama, 1972; Johns, 1979; Espitalie et al., 1980; Heller-Kallai et al., 1984; Tannenbaum and Kaplan, 1985; Pan et al., 2010; Yuan et al., 2013; Yang and Horsfield, 2016). These studies show variable results regarding the impact of clay minerals on hydrocarbon yield, composition and temperature. Espitalie et al. (1980) showed a decrease in total hydrocarbon yield from pyrolysis of kerogen-clay mixtures relative to kerogen isolates which they attributed to the retention of heavier hydrocarbon by clay mineral surfaces. They showed that the light hydrocarbons do not show considerable reduction in quantity due to mineral matrix effects. Strong catalytic effects of clay minerals are also observed while pyrolysis experiments were done on organic materials (either kerogen isolates or synthetic organic compounds) with the presence of smectite minerals. A five fold higher yield of lighter hydrocarbon (C_1-C_6) was reported for pyrolysis of kerogen with smectite clays (i.e. montmorillonite) compared to kerogen alone (Tannenbaum and Kaplan, 1985). Similarly, a significant 43 fold higher lighter hydrocarbon (C_1-C_5) yield was also observed from pyrolysis of a synthetic organic compound (aminolauric acid) interlayered to smectites compared to the hydrocarbon yield from the organic compound alone (Yuan et al., 2013). However, a recent

pyrolysis heating rate-related study suggested that mineral-organic interactions at high temperature and short time scale relative to geologic time scales are extremely unlikely to be a representation of processes occurring in nature and speculated that the mineral matrix does not have any effect at all on hydrocarbon generation on longer time scales. Their results on natural rock samples show that the mineral matrix effect is weakened with decreasing heating rate in laboratory experiments (Yang and Horsfield, 2016). None of these previous studies have considered the effects of the natural variation in physical contact between organic matter and mineral surfaces on hydrocarbon generation that occur in shale textures, rather they have assumed a uniform distribution of organic particles in mineral matrix. The potential that the physical relationship between organic matter and mineral surfaces may have a significant impact on hydrocarbon generation is indicated by more than 8 times higher lighter hydrocarbon (C_1-C_5) generation from smectite (montmorillonite) interlayered organic compound (aminolauric acid) compared to hydrocarbon generation from a general mixture of the same organic compound and smectite (Yuan et al., 2013). Mineral influenced catalytic processes on hydrocarbon generation have not been tested in natural samples even though clay minerals and organics may occur in substantially different degree of associations in shale. An integrated approach to study the physical association of organic matter to mineral matrices petrographically combined with geochemical experiments is required to understand the clay mineral catalytic effects on hydrocarbon generation in the range of textures that occur in natural samples.

The rate of hydrocarbon generation from a given organic carbon rich sediment depends on ambient temperature, exposure time and the activation energies of a series of transformation reactions (Burnham et al., 1988; Behar et al., 1997; Schenk et al., 1997). Hydrocarbon generation from different shale fabrics can be tested using laboratory pyrolysis techniques with a modelled heating rate using kinetic pyrolysis techniques. By varying heating rates, kinetic experiments provide a simulated model of kerogen transformation with temperature that attempts to simulate geological conditions. Kinetic experiments are widely used tools for predicting the timing and rate of hydrocarbon generation of a given source rock (Braun and Burnham, 1987; Tissot et al., 1987; Espitalie et al., 1988; Ungerer et al., 1988; Pepper and Corvi, 1995; Peters et al., 2015; Abbassi et al., 2016; Romero-Sarmiento et al., 2016). Kinetic models provide the activation energy distribution and transformation patterns in response to increasing temperature. Kinetic experiments performed on the Kimmeridge shale to understand the mineral matrix effects show that based on organic matter content, smectite clays have a catalytic effect that shifted kinetic parameters (e.g. activation energy) (Dembicki, 1992).

1.1. Thesis Objectives

This thesis demonstrates two major shale fabrics controlling the nature of association between organic matter and mineral phases and mineral matrix effect on hydrocarbon generation in whole rock paired with their kerogen isolates in shale with different fabrics. The specific consideration of how the range of mineral matrices present in shale could influence hydrocarbon

generation has not previously been focused on. This approach requires integration of bulk geochemical and mineralogical analyses with detailed optical and electron microscopic characterization of organic matter morphology and distribution relative to mineral surfaces in shale (Appendices 1-5). Two shale rich formations were studied, the Stuart Range Formation of South Australia and the Monterey Formation of California, USA. They were selected because they are comprised of two very different shale fabrics; a) a particulate fabric in which organic matter is present as discrete organic particles at > 5 μm in scale and b) a nanocomposite fabric, in which organic carbon and clay mineral surfaces are intimately associated at the sub- μm scale to form organoclay aggregates and nanocomposites. The main objectives of this thesis are as follows:

a. Characterize the organic and inorganic phases in two end-member shale fabrics, particulate and nanocomposite.

b. Evaluate and compare mineral matrix effects on hydrocarbon yield using pyrolysis technique in shale with these different fabrics.

c. Determine the mineral matrix effects on hydrocarbon generation kinetics in these two shale fabrics with a modelled geological heating rate.

1.2. Thesis Structure:

This thesis contains five chapters. This first, chapter 1 is an introductory chapter.

Chapters 2, 3, and 4 are presented as a series of self-contained chapters and they correspond to papers that are either published, or are ready to be submitted. These chapters are organised as follows:

Chapter 2 addresses the characterization of organic and inorganic phases in two endmember shale fabrics.

Chapter 3 compares the hydrocarbon generation potential of two shale formations with the particulate and nanocomposite fabrics (Rahman et al., 2017).

Chapter 4 tests the effects of particulate and nanocomposite shale fabrics on hydrocarbon generation kinetics using a generation model with typical geological heating rate (Rahman et al., 2018).

Chapter 5 lists a summary and the main conclusions drawn from this study. This chapter also includes recommendations and scope for further research.

References

Abbassi, S., Edwards, D.S., George, S.C., Volk, H., Mahlstedt, N., di Primio, R., Horsfield, B., 2016. Petroleum potential and kinetic models for hydrocarbon generation from the Upper Cretaceous to Paleogene Latrobe Group coals and shales in the Gippsland Basin, Australia. Organic Geochemistry 91, 54-67.

Abid, I., Hesse, R., 2007. Illitizing fluids as precursors of hydrocarbon migration along transfer and boundary faults of the Jeanne d'Arc Basin

offshore Newfoundland, Canada. Marine and Petroleum Geology 24, 237-245.

Ahn, J., Peacor, D., 1986. Transmission and analytical electron microscopy of the smectite-to-illite transition. Clays and Clay Minerals 34, 165-179.

Aplin, A.C., Macquaker, J.H., 2011. Mudstone diversity: Origin and implications for source, seal, and reservoir properties in petroleum systems. AAPG Bulletin 95, 2031-2059.

Arthur, M.A., Sageman, B.B., 1994. Marine shales: depositional mechanisms and environments of ancient deposits. Annual review of Earth and planetary sciences 22, 499-551.

Behar, F., Vandenbroucke, M., Tang, Y., Marquis, F., Espitalie, J., 1997. Thermal cracking of kerogen in open and closed systems: determination of kinetic parameters and stoichiometric coefficients for oil and gas generation. Organic Geochemistry 26, 321-339.

Belin, S., 1992. Application of backscattered electron imaging to the study of source rocks microtextures. Organic Geochemistry 18, 333-346.

Bishop, A., Kearsley, A., Patience, R., 1992. Analysis of sedimentary organic materials by scanning electron microscopy: the application of backscattered electron imagery and light element X-ray microanalysis. Organic Geochemistry 18, 431-446.

Blair, N.E., Aller, R.C., 2012. The fate of terrestrial organic carbon in the marine environment. Annual Review of Marine Science 4, 401-423.

Boggs, S., 2009. Petrology of sedimentary rocks. Cambridge University Press.

Braun, R.L., Burnham, A.K., 1987. Analysis of chemical reaction kinetics using a distribution of activation energies and simpler models. Energy & fuels 1, 153-161.

Brown, D., Rhodes, C., 1997. Brønsted and Lewis acid catalysis with ion-exchanged clays. Catalysis Letters 45, 35-40.

Burnham, A.K., Braun, R.L., Samoun, A.M., 1988. Further comparison of methods for measuring kerogen pyrolysis rates and fitting kinetic parameters. Organic Geochemistry 13, 839-845.

Calvert, S., Nielsen, B., Fontugne, M., 1992. Evidence from nitrogen isotope ratios for enhanced productivity during formation of eastern Mediterranean sapropels.

Dembicki, H., 1992. The effects of the mineral matrix on the determination of kinetic parameters using modified Rock Eval pyrolysis. Organic Geochemistry 18, 531-539.

Drits, V., Sakharov, B., Lindgreen, H., Salyn, A., 1997. Sequential structure transformation of illite-smectite-vermiculite during diagenesis of Upper Jurassic shales from the North Sea and Denmark. Clay Minerals 32, 351-371.

Durand, B., 1980. Kerogen: Insoluble organic matter from sedimentary rocks. Editions technip.

Ehrlich, H.L., 1996. How microbes influence mineral growth and dissolution. Chemical Geology 132, 5-9.

Eslinger, E., Highsmith, P., Albers, D., DeMayo, B., 1979. Role of iron reduction in the conversion of smectite to illite in bentonites in the Disturbed Belt, Montana. Clays and Clay Minerals 27, 327-338.

Espitalie, J., Madec, M., Tissot, B., 1980. Role of mineral matrix in kerogen pyrolysis: influence on petroleum generation and migration. AAPG Bulletin 64, 59-66.

Espitalie, J., Ungerer, P., Irwin, I., Marquis, F., 1988. Primary cracking of kerogens. Experimenting and modelling C 1, C 2–C 5, C 6–C 15 and C 15+ classes of hydrocarbons formed. Organic Geochemistry 13, 893-899.

Galwey, A.K., 1972. The rate of hydrocarbon desorption from mineral surfaces and the contribution of heterogeneous catalytic-type processes to petroleum genesis. Geochimica et Cosmochimica Acta 36, 1115-1130.

Garrels, R.M., Mackenzie, F.T., 1971. Evolution of sedimentary rocks.

Hartnett, H.E., Keil, R.G., Hedges, J.I., Devol, A.H., 1998. Influence of oxygen exposure time on organic carbon preservation in continental margin sediments. Nature 391, 572-575.

Hedges, J.I., Keil, R.G., 1995. Sedimentary organic matter preservation: an assessment and speculative synthesis. Marine chemistry 49, 81-115.

Heller-Kallai, L., Aizenshtat, Z., Miloslavski, I., 1984. The effect of various clay minerals on the thermal decomposition of stearic acid under 'bulk flow'conditions. Clay Miner 19, 779-788.

Hower, J., Eslinger, E.V., Hower, M.E., Perry, E.A., 1976. Mechanism of burial metamorphism of argillaceous sediment: 1. Mineralogical and chemical evidence. Geological Society of America Bulletin 87, 725-737.

Jahnke, R.A., 1990. Early diagenesis and recycling of biogenic debris at the seafloor, Santa Monica Basin, California. Journal of marine research 48, 413-436.

Johns, W.D., 1979. Clay mineral catalysis and petroleum generation. Annual review of Earth and planetary sciences 7, 183.

Johns, W.D., Shimoyama, A., 1972. Clay minerals and petroleum-forming reactions during burial and diagenesis. AAPG Bulletin 56, 2160-2167.

Keil, R., Mayer, L., 2014. Mineral matrices and organic matter. Treatise on geochemistry 12, 337-359.

Keil, R.G., Montlucon, D.B., Prahl, F.G., Hedges, J.I., 1994. Sorptive preservation of labile organic matter in marine sediments. Nature 370, 549-552.

Kellendonk, F., Heinerman, J., van Santen, R., 1987. Clay-activated isomerization reactions. Preparative Chemistry using supported reagents, 455.

Kennedy, M.J., Löhr, S.C., Fraser, S.A., Baruch, E.T., 2014. Direct evidence for organic carbon preservation as clay-organic nanocomposites in a Devonian black shale; from deposition to diagenesis. Earth and Planetary Science Letters 388, 59-70.

Kennedy, M.J., Pevear, D.R., Hill, R.J., 2002. Mineral surface control of organic carbon in black shale. Science 295, 657-660.

Kennedy, M.J., Wagner, T., 2011. Clay mineral continental amplifier for marine carbon sequestration in a greenhouse ocean. Proceedings of the National Academy of Sciences 108, 9776-9781.

Kim, J., Dong, H., Seabaugh, J., Newell, S.W., Eberl, D.D., 2004. Role of Microbes in the Smectite-to-Illite Reaction. Science 303, 830-832.

Kuila, U., McCarty, D.K., Derkowski, A., Fischer, T.B., Topór, T., Prasad, M., 2014. Nano-scale texture and porosity of organic matter and clay minerals in organic-rich mudrocks. Fuel 135, 359-373.

Lagaly, G., Ogawa, M., Dékány, I., 2013. Clay mineral organic interactions. Handbook of clay science.

Lazar, O.R., Bohacs, K.M., Macquaker, J.H., Schieber, J., Demko, T.M., 2015. Capturing key attributes of fine-grained sedimentary rocks in outcrops, cores, and thin sections: nomenclature and description guidelines. Journal of Sedimentary Research 85, 230-246.

Li, Y., Cai, J., Song, G., Ji, J., 2015. DRIFT spectroscopic study of diagenetic organic–clay interactions in argillaceous source rocks. Spectrochimica Acta Part A: Molecular and Biomolecular Spectroscopy 148, 138-145.

Löhr, S.C., Kennedy, M.J., 2014. Organomineral nanocomposite carbon burial during Oceanic Anoxic Event 2. Biogeosciences 11, 4971-4983.

Lynch, F.L., Mack, L.E., Land, L.S., 1997. Burial diagenesis of illite/smectite in shales and the origins of authigenic quartz and secondary porosity in sandstones. Geochimica et Cosmochimica Acta 61, 1995-2006.

Macquaker, J.H., Adams, A., 2003. Maximizing information from fine-grained sedimentary rocks: An inclusive nomenclature for mudstones. Journal of Sedimentary Research 73, 735-744.

Macquaker, J.H., Keller, M.A., Davies, S.J., 2010. Algal blooms and "marine snow": Mechanisms that enhance preservation of organic carbon in ancient fine-grained sediments. Journal of Sedimentary Research 80, 934-942.

Macquaker, J.H., Taylor, K.G., Keller, M., Polya, D., 2014. Compositional controls on early diagenetic pathways in fine-grained sedimentary rocks: Implications for predicting unconventional reservoir attributes of mudstones. AAPG Bulletin 98, 587-603.

Mayer, L.M., 1994. Surface area control of organic carbon accumulation in continental shelf sediments. Geochimica et Cosmochimica Acta 58, 1271-1284.

McCabe, R.W., Adams, J.M., 2013. Clay Minerals as Catalysts, in: Bergaya, F., Gerhard, L. (Eds.), Developments in Clay Science. Elsevier, UK, pp. 491-538.

Milliken, K.L., Ko, L.T., Pommer, M., Marsaglia, K.M., 2014. SEM petrography of Eastern Mediterranean sapropels: Analogue data for assessing organic matter in oil and gas shales. Journal of Sedimentary Research 84, 961-974.

Müller, P.J., Suess, E., 1979. Productivity, sedimentation rate, and sedimentary organic matter in the oceans—I. Organic carbon preservation. Deep Sea Research Part A. Oceanographic Research Papers 26, 1347-1362.

Nadeau, P., Wilson, M., McHardy, W., Tait, J., 1985. The conversion of smectite to illite during diagenesis: evidence from some illitic clays from bentonites and sandstones. Mineralogical Magazine 49, 393-400.

Pan, C., Jiang, L., Liu, J., Zhang, S., Zhu, G., 2010. The effects of calcite and montmorillonite on oil cracking in confined pyrolysis experiments. Organic Geochemistry 41, 611-626.

Pepper, A.S., Corvi, P.J., 1995. Simple kinetic models of petroleum formation. Part I: oil and gas generation from kerogen. Marine and Petroleum Geology 12, 291-319.

Perry, E., Hower, J., 1970. Burial diagenesis in Gulf Coast pelitic sediments. Clays and Clay Minerals 18, 165-177.

Peters, K.E., Burnham, A.K., Walters, C.C., 2015. Petroleum generation kinetics: Single versus multiple heating-ramp open-system pyrolysis. AAPG Bulletin 99, 591-616.

Pevear, D.R., 1999. Illite and hydrocarbon exploration. Proceedings of the National Academy of Sciences 96, 3440-3446.

Pollard, C.O., 1971. Semidisplacive mechanism for diagenetic alteration of montmorillonite layers to illite layers. Geological Society of America Special Papers 134, 79-94.

Rahman, H.M., Kennedy, M., Löhr, S., Dewhurst, D.N., 2017. Clay-organic association as a control on hydrocarbon generation in shale. Organic Geochemistry 105, 42-55.

Rahman, H.M., Kennedy, M., Löhr, S., Dewhurst, D.N., Sherwood, N., Yang, S., Horsfield, B., 2018. The influence of shale depositional fabric on the kinetics of hydrocarbon generation through control of mineral surface contact area on clay catalysis. Geochimica et Cosmochimica Acta 220, 429-448.

Ray, S.S., 2013. Clay-containing polymer nanocomposites: from fundamentals to real applications. Newnes.

Romero-Sarmiento, M.-F., Euzen, T., Rohais, S., Jiang, C., Littke, R., 2016. Artificial thermal maturation of source rocks at different thermal

maturity levels: Application to the Triassic Montney and Doig formations in the Western Canada Sedimentary Basin. Organic Geochemistry 97, 148-162.

Salmon, V., Derenne, S., Lallier-Vergès, E., Largeau, C., Beaudoin, B., 2000. Protection of organic matter by mineral matrix in a Cenomanian black shale. Organic Geochemistry 31, 463-474.

Schenk, H.J., Di Primio, R., Horsfield, B., 1997. The conversion of oil into gas in petroleum reservoirs. Part 1: Comparative kinetic investigation of gas generation from crude oils of lacustrine, marine and fluviodeltaic origin by programmed-temperature closed-system pyrolysis. Organic Geochemistry 26, 467-481.

Setti, M., Marinoni, L., López-Galindo, A., 2004. Mineralogical and geochemical characteristics (major, minor, trace elements and REE) of detrital and authigenic clay minerals in a Cenozoic sequence from Ross Sea, Antarctica. Clay Minerals 39, 405-421.

Shaldybin, M., Lopushnyak, Y., Goncharov, I., Wilson, M., Wilson, L., Mendis, B., 2017. The mineralogy of the clayey-silty siliceous rocks in the Bazhenov Shale Formation (Upper Jurassic) in the west Siberian Basin, Russia: The role of diagenesis and possible implications for their exploitation as an unconventional hydrocarbon reservoir. Applied Clay Science 136, 75-89.

Shaw, D.B., Weaver, C.E., 1965. The mineralogical composition of shales. Journal of Sedimentary Research 35.

Shimoyama, A., Johns, W.D., 1971. Catalytic conversion of fatty acids to petroleum-like paraffins and their maturation. Nature 232, 140-144.

Tannenbaum, E., Kaplan, I.R., 1985. Role of minerals in the thermal alteration of organic matter—I: Generation of gases and condensates under dry condition. Geochimica et Cosmochimica Acta 49, 2589-2604.

Tissot, B., Pelet, R., Ungerer, P., 1987. Thermal history of sedimentary basins, maturation indices, and kinetics of oil and gas generation. AAPG Bulletin 71, 1445-1466.

Tissot, B.P., Welte, D.H., 1984. Petroleum formation and occurrence. Springer-Verlag.

Tyson, R., 2001. Sedimentation rate, dilution, preservation and total organic carbon: some results of a modelling study. Organic Geochemistry 32, 333-339.

Tyson, R., 2005. The "productivity versus preservation" controversy: cause, flaws, and resolution. SPECIAL PUBLICATION-SEPM 82, 17.

Tyson, R.V., 1994. Sedimentary organic matter : organic facies and palynofacies / R. V. Tyson. London : Chapman & Hall, London.

Ungerer, P., Behar, F., Villalba, M., Heum, O.R., Audibert, A., 1988. Kinetic modelling of oil cracking. Organic Geochemistry 13, 857-868.

van Krevelen, D.W., 1961. Coal. Elsevier.

Vandenbroucke, M., Largeau, C., 2007. Kerogen origin, evolution and structure. Organic Geochemistry 38, 719-833.

Varma, R.S., 2002. Clay and clay-supported reagents in organic synthesis. Tetrahedron 58, 1235-1255.

Wu, L.M., Zhou, C.H., Keeling, J., Tong, D.S., Yu, W.H., 2012. Towards an understanding of the role of clay minerals in crude oil formation, migration and accumulation. Earth-Science Reviews 115, 373-386.

Yang, S., Horsfield, B., 2016. Some Predicted Effects of Minerals on the Generation of Petroleum in Nature. Energy & fuels 30, 6677-6687.

Yuan, P., Liu, H., Liu, D., Tan, D., Yan, W., He, H., 2013. Role of the interlayer space of montmorillonite in hydrocarbon generation: An experimental study based on high temperature-pressure pyrolysis. Applied Clay Science 75-76, 82-91.

Chapter 2. Two examples of distinct shale fabrics: what they are composed of and how they are formed

Habibur M Rahman[a*], Martin Kennedy[a], Stefan Löhr[a], David N Dewhurst[b], Neil Sherwood[c]

[a] *Department of Earth and Planetary Sciences, Macquarie University, Sydney, New South Wales, Australia*

[b] *CSIRO Energy, Perth, Western Australia, Australia*

[c]*CSIRO Earth Science and Resource Engineering, North Ryde, New South Wales, Australia*

* *Corresponding author at: Department of Earth and Planetary Sciences, Macquarie University, Sydney, NSW 2109, Australia. Tel: +61-2-9850-8426.*

E-mail address: mdhabibur.rahman@mq.edu.au, hrahman039@gmail.com

Statement of authors' contribution

This Chapter is a final version of a manuscript that is ready to be submitted to *AAPG Bulletin*. This paper has been formatted to conform to the font and referencing style adopted in the thesis. Figures and tables included within the text are prefixed with the chapter number. This chapter characterizes organic and inorganic phases of two formations from distinct depositional environments to understand their rock fabrics, which is the first objective of the thesis. High-resolution petrography and organic petrology were used to study the association of organic matter and minerals. I am the primary author. I examined data including sample selection, sampling and sample preparation for this study. I performed all the experiments and analyses used in this manuscript. I processed and interpreted all data derived from the

conducted analyses and experiments. I wrote and designed the paper's structure. Martin Kennedy, Stefan Löhr, David Dewhurst and Neil Sherwood reviewed and provided feedback on the manuscript. This manuscript has not been published and is not being considered for publication elsewhere, except as described above.

Abstract

This study uses direct imaging of organic matter distribution and mineral mapping of organic rich shale samples to characterize fabric of two shale formations with distinctly different depositional environment. Shale samples from the Monterey Formation, USA containing abundant high surface area detrital clay minerals are compared with samples from the Stuart Range Formation, South Australia deposited in a cold climate setting without the influence of detrital clays. Samples of the Monterey Formation demonstrate a complex intimate association of amorphous organic matter with clay minerals at nanometre scale in a nanocomposite fabric. On the other hand, in samples of the Stuart Range Formation, organic matter is present as discrete particles of > 5 μm, that float within and are separate from the fine-grained mineral matrix resulting in a particulate fabric. These different shale fabrics influence the total organic carbon and mineral surface area (TOC-MSA) relationship of the samples studied. Samples with nanocomposite fabric show a strong first-order relationship between TOC and MSA (R^2 = 0.91), whereas samples with particulate fabric show no apparent relationship between TOC and MSA (R^2 = 0.54). The significant differences in clay mineral and organic

matter association in these two shale fabrics can potentially affect a range of geochemical properties including hydrocarbon generation.

Keywords

Shale fabric, organoclay nanocomposite, Monterey Formation, Stuart Range Formation, shale diagensis.

2.1. Introduction

Shale contains a varying proportion of authigenic, autochthonous, and detrital minerals (Macquaker and Adams, 2003). The relative contribution of each of these components in given sediment varies as a function of the depositional setting. The authigenic components of shale mainly depend on pore-water chemistry, temperature and detrital mineralogy (Setti et al., 2004). The detrital components are function of parent lithology and the extent of continental weathering. Including these inorganic mineral phases, a major constituent of shale is its organic content that may vary from less than 1% to more than 30% of the rock depending on various geological and geochemical factors (e.g. Isaacs, 2001). The nature and degree of association of its organic and inorganic phases define the fabric of shale. Direct imaging is a very common and effective approach to study the fabric of sedimentary rock. Imaging shale fabric has long been a challenge due to fine grain size of the sediment (Macquaker and Adams, 2003; Macquaker et al., 2010). However, the development of high resolution scanning and transmission electron imaging, together with improved sample preparation techniques such as ion milling, have revealed evidence of complex depositional and diagenetic

processes active on these apparently homogenous sediments (Macquaker and Adams, 2003; Macquaker et al., 2010; Aplin and Macquaker, 2011; Kennedy et al., 2014; Macquaker et al., 2014; Milliken et al., 2014; Shaldybin et al., 2017).

The significant variations of organic matter content in shale are function of physical and chemical processes acting on sediments during and after deposition (Lazar et al., 2015). Some important factors that control the distribution of organic matter in shale are chemical stability and primary depositional morphology of organic matter, depositional environment, and diagenesis. The majority of these factors also directly influence the mineralogy of the sediment (Potter et al., 2005). Distinct organic-inorganic fabrics are therefore predicted for shales where organic productivity, mineralogy, depositional and diagenetic settings, and organic matter type are widely variable.

The type of organic matter in shale can be determined based on the physico-optical properties of its microscopic organic component (i.e. macerals). Three major maceral groups are recognised in sedimentary rock and coal (Stach, 1982; Taylor, 1998). These macerals and maceral groups have distinctive morphologies with a wide range of size and shape (e.g. Stach, 1982; Suárez-Ruiz et al., 2012) that can limit or extend their level of exposures to mineral matrices and influence the distribution of organic carbon within given sediment.

Sedimentary rocks host the major reservoir of organic carbon in the global shallow carbon cycle (Zonneveld et al., 2010), among them nearly 95% of the organic carbon is preserved in continental margin sediment (Hedges and Keil, 1995). Burial of organic carbon is a critical component of biogeochemical processes that control the flux of oxygen to the atmosphere, temperature and therefore life on earth (Hedges, 1992; Hartnett et al., 1998). An intimate association of organic matter with some mineral phases increases their chemical and thermal stability compared to non-mineral associated organic particles (Ray, 2013). In fact, this process could potentially act as an organic matter preservation mechanism in nature (Keil and Mayer, 2014). Including other factors such as organic matter type, the transformation of organic matter in sedimentary rock depends to a great extent on their thermal and chemical stability in response to burial depth and increasing temperature after deposition (Tissot and Welte, 1984). An intimate association of labile organic matter with mineral matrices could potentially affect the maturation and transformation of organic matter substantially during burial. Therefore, the relationship between organic matter and associated (or not) mineral phases could be critical.

A first order relationship between TOC and mineral surface area (MSA) is reported in modern sediments (Keil et al., 1994; Mayer, 1994; Ransom et al., 1997) and in ancient rocks across a range of redox conditions and organic content (Kennedy et al., 2002; Kennedy et al., 2014; Löhr and Kennedy, 2014). The TOC and MSA relationships previously shown in different studies are based on bulk geochemical analyses. It is not generally established whether

there is a single/uniform or multiple varieties of organic matter association with mineral surfaces in shale. In addition, it is also not established whether the apparent mineral surface area control on organic matter preservation is connected to the composition, origin and reactivity of the organic matter. The organic matter that is visible in optical imaging in sediments often does not add up to the total organic carbon measured in the bulk rock, indicating the presence of organic matter bound to clays, that is not visible under optical microscopes. Compared to the quantitative and qualitative analyses on organic content, the diversity of organic matter morphology and distribution in shale is not well studied and speculations exist in many studies on the uniformity of their arrangement in sediment (e.g. Kuila et al., 2014).

This study aims to investigate the physical relationship between minerals and organic matter leading to distinct fabric types in shale. Two different types of organic-rich sediment are selected from very different depositional environments. Samples are selected from the peri-glacial, restricted marine Stuart Range Formation in the Arckaringa Basin, South Australia and the midbathyal slope, open marine Monterey Formation from California, USA. This study is based on optical petrography, electron microscopy and a new high-resolution mineral mapping technique to characterize the inorganic and organic phases and access shale fabrics at the micron to sub-micron scale.

2.2. Geological Settings

The Early Permian (299-290 Ma) Arckaringa Basin is a large sedimentary basin covering approximately 100,000 square kms of central to northern

South Australia (Wohling et al., 2013). The basin unconformably overlies the Neoproterozoic to Devonian Officer Basin and the Archean to Mesoproterozoic Gawler Craton (Fig. 2.1a). Seismic lines have identified a series of depocentres in the Arckaringa Basin (Carr et al., 2012). Glacial scours formed the troughs followed by a deglaciation and then a marine transgression. The Stuart Range Formation was deposited in a generally quiet, restricted marine environment during the deglaciation phase in the Arckaringa basin (Menpes et al., 2010). The Stuart Range Formation underlies the Mount Toondina Formation (Fig. 2.1b) consisting of marine shale with siltstone. Samples were collected from the recovered cores of Stuart Range Formation encountered in Arck 1 well drilled in the Arckaringa basin.

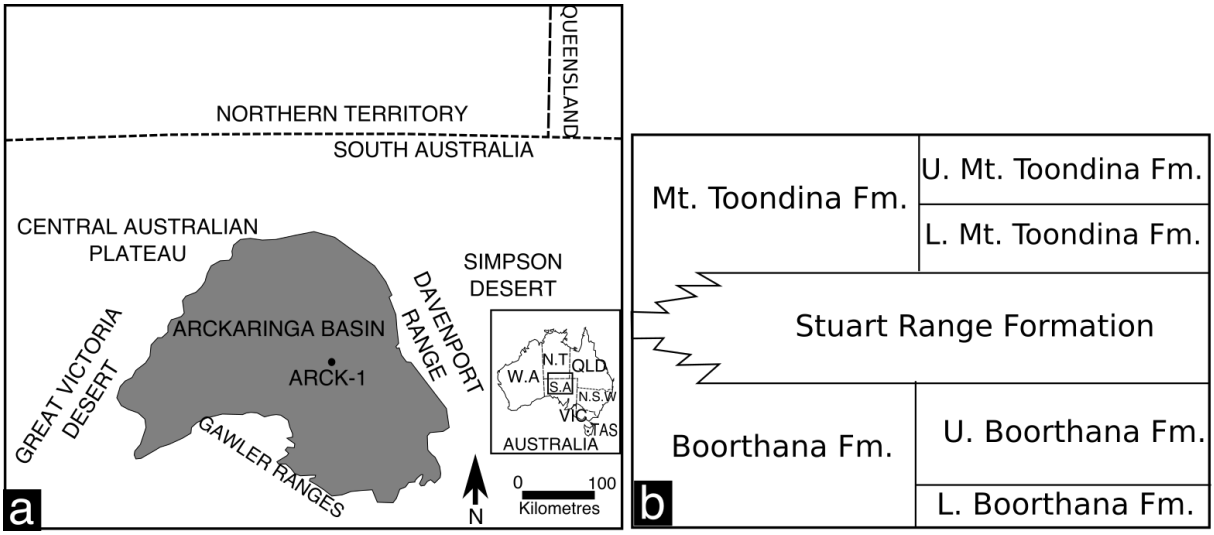

Fig. 2.1. a. Regional map showing the location of the Arckaringa basin. b. Stratigraphic position of Stuart Range Formation in Arckaringa basin. Modified after Wohling et al. (2013).

The Miocene Monterey Formation (19 to 5 Ma; Barron and Isaacs (2001) is studied at Naples Beach section of the Santa Barbara-Ventura Basin (Fig. 2.2a). Outcrop samples were collected from the carbonaceous marl member

(Fig. 2.2b). The carbonaceous marl member of the Monterey Formation represents a pelagic sequence predominantly composed of organic rich shale interstratified with phosphatic laminae. The organic content of the member varies from 1 to 25% by wt. (Isaacs, 2001; Föllmi et al., 2005).

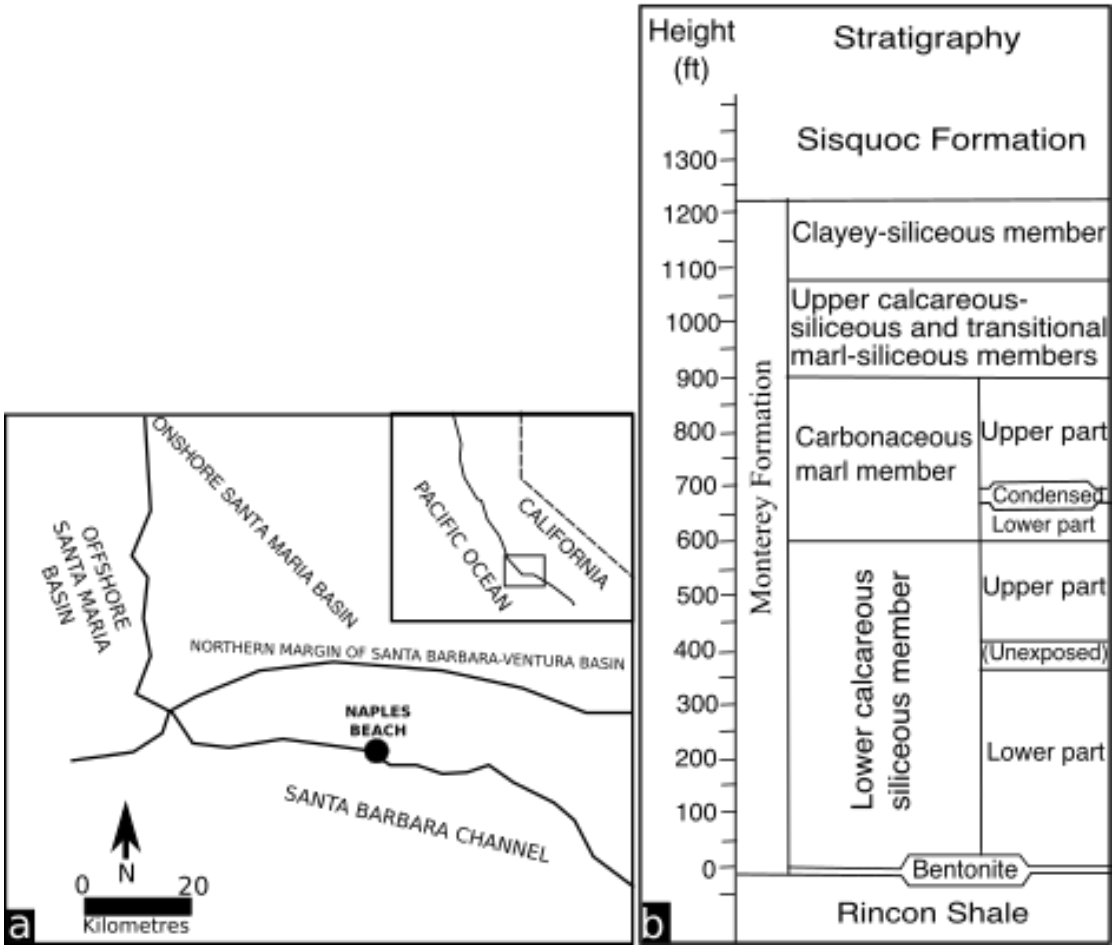

Fig. 2.2. a. Regional map of Southern Califonria showing the location of Naples Beach section. Modified after Brincat and Abbott (2001). b. Stratigraphic position of Monterey Formation, from Isaacs (2001).

2.3. Materials and methods

2.3.1. Samples

Seventeen subsamples were collected from the Stuart Range and Monterey formations (Table 2.1). Monterey samples (TOC: 5 to 21 wt.%) were collected

from the Naples Beach section. The samples are from the carbonaceous marl member (Isaacs, 2001) deposited as a pelagic to hemipelagic sequence mineralogically dominated by clay minerals with minor detrital quartz, feldspar, diagenetic dolomite and siderite concretions. Biogenic silica and their diagenetic derivatives are rare or absent in this interval (Barron, 1986; Garrison et al., 1994; Isaacs, 2001; Föllmi et al., 2005; Berndmeyer et al., 2012; Laurent et al., 2015).

Table 2.1. Lithofacies and TOC (wt.%) of samples studied from Monterey and Stuart Range formations.

Formation	Sample no.	Lithofacies	Depth (m)	TOC (wt.%)
Monterey	M59	Phosphatic mudstone	Outcrop	11.8
	M62	Black shale	Outcrop	21.4
	M22	Calcareous black mudstone	Outcrop	13.0
	M28	Phosphatic shale	Outcrop	16.9
	M33	Black shale	Outcrop	22.7
	M29	Phosphatic shale	Outcrop	5.4
	M21	Calcareous phosphatic shale	Outcrop	9.8
Stuart Range	S43	Fissile black shale	918.06	6.2
	S81	Silty mudstone	897.26	5.9
	S08	Silty Mudstone	951.3	4.7
	S77	Black shale	900.73	7.3
	S99	Argillaceous siltstone	888.5	1.3
	S51	Silty mudstone	990.17	0.06
	S64	Black shale	907.53	6.8
	S12	Silty mudstone	949.65	1.7
	S26	Fissile black shale	934.76	3.2

A subset of Stuart Range Formation samples (TOC: 2–7 wt.%) were collected from the Arck-1 well stored at the South Australian state core repository representing depth ranging from 888 to 990 m (Table 2.1). The samples are typical of the Stuart Range Formation being feldspar-rich siliceous shale with significant fraction of clay minerals. Presence of lonestones (Fig. 2.3) observed

in core indicates massflow deposits.

Fig. 2.3. Lonestones (arrow) in laminated pelagic marine deposits of the Stuart Range Formation, observed in drilled core.

2.3.2. Methods

2.3.2.1. X-ray diffraction

Sample mineralogy was determined by bulk powder X-ray Diffraction (XRD), on a Bruker D8 advance diffractometer with a Cu-radiation source. Samples were milled and passed through a 200 μm sieve before analysis. Mineral phases were identified using Bruker Diffrac.Eva software with Crystallography Open Database reference patterns.

2.3.2.2. Scanning electron microscopy

Polished blocks of samples were prepared using a Hitachi IM4000 Argon Ion Mill system. The samples were carbon-coated before SEM analysis. Zeiss EVO MA15 SEM, JEOL JSM 7100F field emission SEM and FEI Teneo field emission SEM, all equipped with energy dispersive X-ray spectroscopy (EDS)

systems for elemental analyses were used to analyse the samples. SEM analyses were performed at 13 mm working distance and 15 kV accelerating voltage. Backscatter scanning electron (BSE) images provide visual information of the distribution and morphology of organic matter, since organic matter appears dark relative to mineral phases.

2. 3.2.3. Nanomin mineral mapping

The Nanomin automated mineralogy and petrography technique was used for mineral mapping of the samples on an FEI Taneo field emission SEM equipped with dual Bruker Series 6 EDS detectors. Nanomin is a recently introduced technology to determine and map the mineralogy of fine-grained, heterogenous rock samples such as shale. Nanomin compares EDS spectra collected in the mapped area against reference spectra collected on known mineral standards. An X-ray spacing of 200 nm and 8 ms acquisition time were used for EDS mapping of the samples for Nanomin analyses. The Nanomin mineral classification system can de-convolve mixed X-ray spectra and assign up to three minerals per analysed spot, a significant development compared to earlier SEM-based mineral mapping techniques (e.g. QEMSCAN). This allows improved interpretation of the mixed phase X-ray spectra, characteristic of fine-grained sediments. Nanomin mineral maps provide visual information on the distribution of different mineral phases at micron resolution.

2.3.2.4. Mineral surface area

The mineral surface area (MSA) of samples were determined by Ethylene Glycol Monoethyl Ether (EGME) method (Tiller and Smith, 1990). MSA (in

m^2) was determined from conversion of the mass of sorbed EGME (in mg) using a factor of 3.2 based on an assumption of monolayer coverage (Kennedy and Wagner, 2011). Clay mineral standards obtained from the Clay Mineral Society were analysed with six replicates of a suite of clay in the same batch as the samples. MSA was corrected for $CaCO_3$ and organic carbon content, and is reported here as "silicate MSA". MSA measured on the clay mineral standards showed good reproducibility (SWy-2: 741 m^2/g ±1.93%; STx-1b: 771 m^2/g ±1.33%; IScZ-1: 296 m^2/g ±2.57%; IMt-2: 141 m^2/g ±1.04%; n = 6 for each clay standard).

2.3.2.5. Organic petrology

Macerals in each sample were characterized and quantified using point counting in accordance with the procedures of the Standards Association of Australia (1998) (AS 2856.2). On average, 500 points were counted for each of the white and fluorescent light observations on every sample. The point count data for the maceral analyses are reported as volume precents.

2.4. Results

Samples from the Monterey Formation represent laminated, intermittently burrowed shale. Quartz, feldspars, pyrite and clay minerals are the major minerals present (Tables 2.2 and 2.3). Biogenic silica and chert are absent/minor in the samples studied. Discrete, 5 to 20 μm size feldspar grains are observed frequently in all samples. Pyrite framboids of 2 to 10 μm are also abundant. The samples contain abundant clay minerals observed under SEM (Fig. 2.4 and 2.5), which is consistent with their high MSAs (215 to 676

m^2/g; Table 2.2). Smectite and mixed layer illite-smectites are the most abundant clays (Fig. 2.6). Smectite clays show parallel orientation to the lamination of the rock and in many cases differential compaction around rigid detrital grains (Fig. 2.4 and 2.5). The smectite and mixed layer illite-smectites are intimately associated with organic matter at the sub-micron scale (Fig. 2.6).

Table 2.2. Mineral surface area (MSA) and mineralogy of samples from Monterey and Stuart Range formations. Qz = Quartz, Ab = Albite/Plagioclase feldspars, Mc = Microcline, Ca = Calcite, Py = Pyrite, Ch = Chlorite, S = Smectite, I = Illite, Mu = Muscovite, Bt = Biotite, K = Kaolinite, Gp = Gypsum, Fp = Fluorapatite. Mineralogy is determined by bulk powder XRD and MSA is measured using the EGME method of Tiller and Smith (1990).

Sample No.	Silicate MSA (m2g-1)	Qz	Ab	Mc	Ca	Py	Ch	S	I	Mu	Bt	K	Gp	Fp
M59	318	*	*	*	*	*		*	*		*		*	
M62	676	*	*			*		*	*					
M28	477	*	*	*	*	*		*	*		*			
M33	635	*	*	*	*	*		*	*	*	*			
M21	215	*	*	*	*	*		*	*		*			*
S81	222	*	*			*			*	*		*		
S08	259	*	*			*	*	*	*	*		*	*	
S77	264	*	*			*		*	*			*		
S64	269	*	*			*		*	*			*	*	
S12	179	*	*	*		*		*	*	*		*		
S26	251	*	*			*		*	*			*	*	

Table 2.3: Quantitative mineralogy of Monterey (M28) and Stuart Range samples (S64) using Nanomin mineral mapping.

Mineral	Measurement area (%)	
	Monterey Formation (M28)	Stuart Range Formation (S64)
Quartz (Silica)	6	26
Alkali Feldspar	34	11
Plagioclase	2	< 1
Illite	4	< 1
Smectites	25	18
I/S Interstratified	3	26
Pyrite	6	5
Kaolinite	< 1	4
Glauconite	4	2
Unclassified	5	1

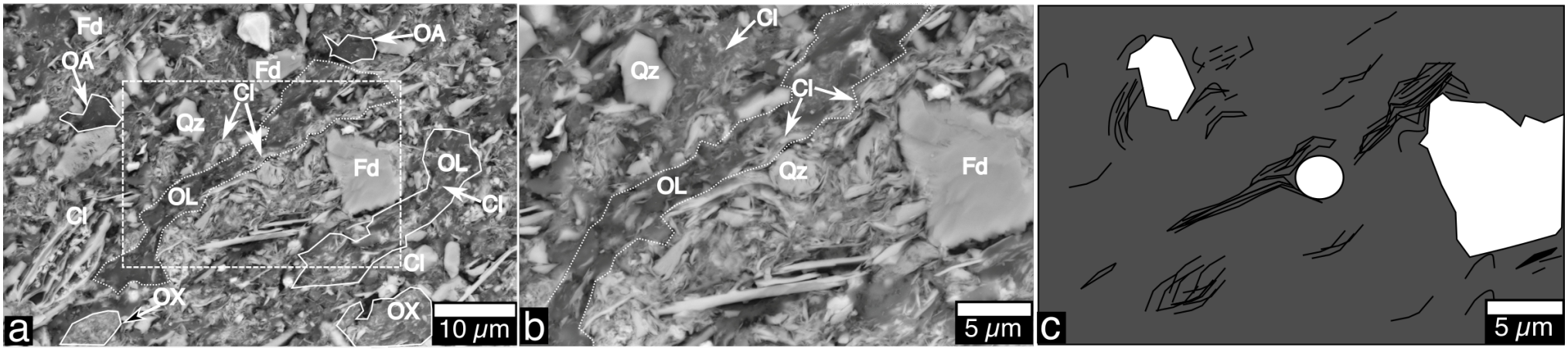

Fig. 2.4. Monterey Formation sample (M28). a, b: Backscatter SEM photomicrographs at a sequential higher resolution show a complex association of amorphous organic matter with clay minerals. Three types of organic matter are classified based on their morphology, OL= organoclay laminae, OA= organoclay aggregates and OX= infilling organoclay matrix. Dotted outline indicates a diffusive boundary of OL. Majority of the organic matter is present as OL fabric. c: Schematic illustration of Fig. b. The clay mineral flakes (black lines) shows differential compaction around rigid mineral grains (white) indicative of the possible detrital origin of the clay minerals.

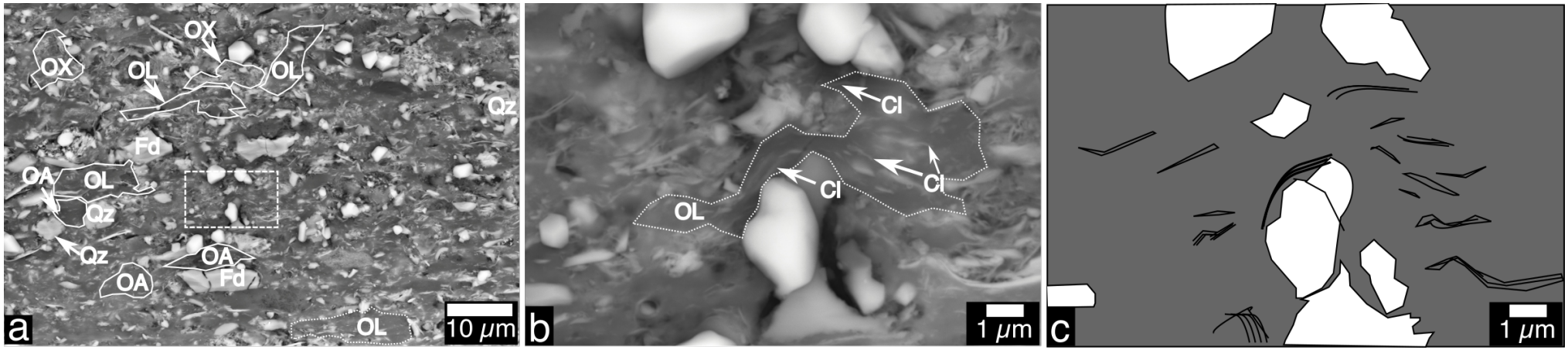

Fig. 2.5. Monterey Formation sample (M33). a, b: Backscatter SEM photomicrographs at a sequential higher resolution show three types of organic matter and mineral association, OL= organoclay laminae, OA= organoclay aggregates and OX= infilling organoclay matrix. Dotted outline indicates a diffusive boundary of OL. Majority of the organic matter is present as OL fabric. c: Schematic illustration of Fig. b. The clay mineral flakes (black lines) shows differential compaction around rigid mineral grains (white) indicative of the possible detrital origin of the clay minerals as also observed in Fig. 2.4.

Fig. 2.6. SEM photomicrograph and Nanomin mineral maps of a Monterey Formation sample (M28). a: Backscatter SEM photomicrograph showing the majority of organic matter is present in an intimate association with clay minerals. In rare occasions, discrete, particulate organic matter is observed (top middle side of the image). Majority of these discrete organic particles in Monterey samples are possibly migrated, early-generated bitumen as indicated by their rounded shape, homogenous appearance and pore-filling nature. b: Bulk mineralogy of the same view as Fig. a. Feldspars (blue), Clay (smectites and illite) (green) and quartz (grey) are the dominating minerals. c: Nanomin mineral map for smectite and mixed layer illite-smectite of the same view as Fig. a and b. Amorphous organic matter (black patches) is intimately mixed with smectite and mixed layer illite-smectite. Submicron size smectite and illite-smectite flakes are spotted within organic matter.

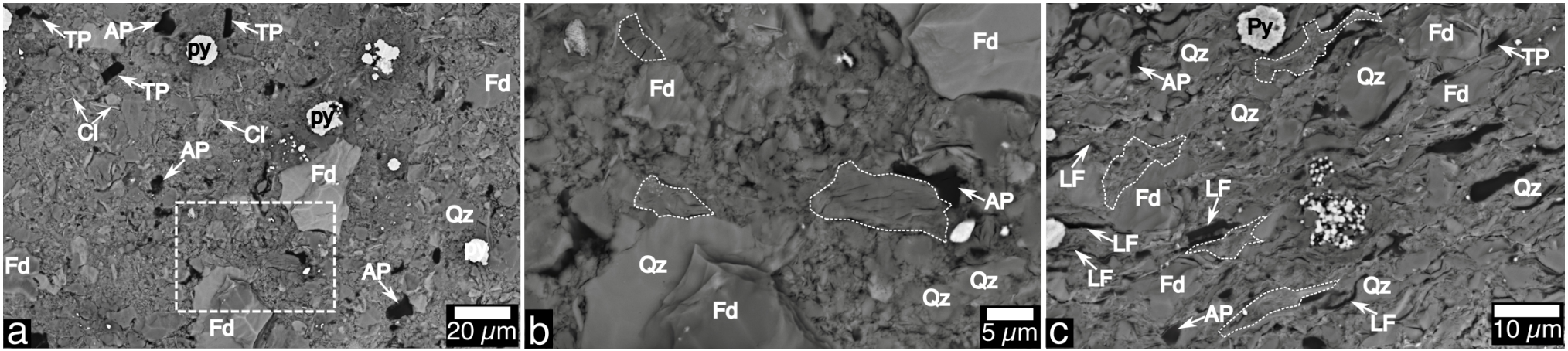

Fig. 2.7. SEM photomicrographs of Stuart Range samples (a,b: S26, c: S43). a,b: Backscatter SEM photomicrographs at a sequential higher resolution. Discrete organic particles are present as angular to sub-angular organic particles (AP), lamellar organic flakes (LF) and tabular organic particles (TP). Pyrite framboids (py) are abundant. c: Distribution of AP, LF and TP and pyrite framboids in a sample. Pore-filling nature of the clay minerals are pointed by arrows on Fig. a and c and dashed outline on Fig. b and c.

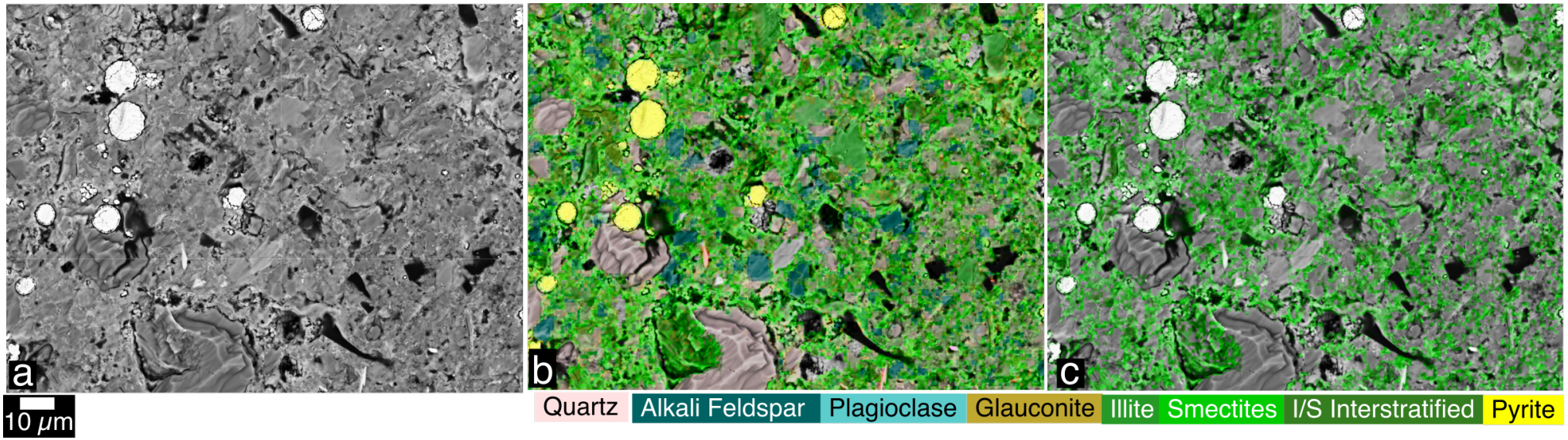

Fig. 2.8. SEM photomicrograph and Nanomin mineral map of a Stuart Range sample (S08). a: Backscatter SEM photomicrographs showing particulate organic matter (black patches) present in mineral matrix. b: Nanomin mineral map shows abundance of quartz (grey), feldspars (blue), smectites (green) and pyrite (yellow). c: Distribution of smectite and mixed layer illite-smectite in the same area as a and b. Smectite clays show pore filling nature and a random orientation in rock matrices.

Samples of the Stuart Range Formation contain 5 to 50 μm diameter, subangular to angular, poorly sorted quartz grains with abundant feldspars (Tables 2.2 and 2.3). The majority of the feldspar grains are 5 to 30 μm in size. Pyrite framboids of 2 to 20 μm consisting of sub-micron size pyrite crystals are readily observed (Fig. 2.7). They are randomly distributed in the rock matrix and in some cases occur nearby organic matter. Some samples also show polyframboid aggregates of pyrite containing multiple single framboid which can be > 50 μm in size. Smectite and illite are the abundant clays in the Stuart Range samples. The smectite clays are pore-filling and randomly oriented, they are not aligned parallel to the depositional laminae (Fig. 2.8).

Organic matter is present in an intimate association with clay minerals in Monterey samples across a range of TOC. The morphology of organic matter can be classified as a) organoclay laminae (OL), b) organoclay aggregates (OA) and c) infilling organoclay matrix (OX) (Fig. 2.4 and 2.5). Organoclay laminae are the most common organic matter morphology observed in the Monterey samples and vary widely in thickness from < 5 μm to ~50 μm. Two types of laminae are observed: discrete organoclay laminae have a sharp boundary whereas diffusive laminae show no sharp boundary and blend into the surrounding matrix (Fig. 2.4a and 2.4b). Organoclay aggregates are subrounded grains ranging from 5 to 20 μm in size (Fig. 2.5a). Infilling organoclay matrix contains the least organic carbon in the clay-organic association compared to the other two organic matter morphologies (Fig. 2.4a). In all three of the above mentioned organic matter morphologies,

organic matter is intimately mixed with clay minerals at the sub-micron scale. This observation is consistent with the organic petrography analyses showing > 70% of the organic matter across all samples is composed of bituminite mixed with clay minerals (Fig. 2.9 and Table 2.4) analogous to the 'mineral bituminous groundmass' class set by the ICCP (International Committee for Coal and Organic Petrology). Discrete organic particles of > 5 μm are rarely observed in samples of Monterey Formation. When present, they exhibit a rounded shape, pore-filling nature and homogenous textural appearance (Fig. 2.5).

Table 2.4. Quantitative maceral analyses demonstrate the dominance of clay-mixed bituminite over the other macerals in samples of Monterey Formation. Data are reported here as volume percent on a mineral-free basis. sp= Sporinite, tl= Telalginite, lm= Lamalginite, ld= Liptodetrinite, mc=Micrinite, bt= Bituminite, vt= Vitrinite, it= Inertinite/reworked vitrinite, bt-c= Bituminite-clay mixture.

Sample no	sp (%)	tl (%)	lm(%)	ld (%)	mc (%)	bt (%)	vt (%)	it (%)	bt-c (%)
M33	<1	4	<1	2	<1	18	<1	<1	74
M59	<1	4	<1	2	2	11	<1	<1	79
M21	<1	4	<1	2	<1	16	<1	<1	77
M44	<1	4	<1	2	<1	21	2	<1	70
M28	<1	9	1	4	<1	2	<1	2	80
M62	<1	5	<1	3	<1	5	1	<1	83

Table 2.5: Quantitative maceral analyses illustrate that telalginite and lamalginite are the dominating macerals in Stuart Range Formation. Data are reported here as volume percent on a mineral-free basis. tl= Telalginite, lm= Lamalginite, sp= Sporinite, ld= Liprodetrinite, mc= Micrinite, bt= Bituminite, vt= Vitrinite, it= Inertinite/reworked vitrinite.

Sample no	tl (%)	lm (%)	sp (%)	ld (%)	mc (%)	bt (%)	vt (%)	it (%)
S81	24	27	8	9	1	1	15	14
S12	21	40	4	6	< 1	5	11	12
S26	27	31	4	6	1	8	9	13
S64	30	24	6	6	< 1	11	11	12
S77	25	37	3	4	2	3	6	20
S08	63	20	1	5	< 1	< 1	2	8

Organic matter in samples of the Stuart Range Formation is mostly present as discrete particles of > 5 μm. According to their texture, they can be classified as a) angular to sub-angular organic particles (AP), b) lamellar organic flakes (LF), and c) tabular organic particles (TP). Angular to sub-angular organic particles are subrounded to angular shape, range in size from 5 to 50 μm in diameter (Fig. 2.7). Organic petrography shows that majority of these angular organic particles are vitrinite and inertinite derived from the higher plants (Fig. 2.10a and 2.10c). The occurrence of vitrinite and inertinite indicates moderate terrestrial organic matter input. Lamellar organic flakes are mostly < 5 μm in thickness and represent mostly lamalginite macerals. Tabular organic particles in the Stuart Range samples range from 5 to 10 μm thickness and represent bituminite and telalginite macerals (Fig. 2.10b and 2.10d). LF and TP together represent alginate macerals in Stuart Range samples that comprise on average, more than 60% of the total organic matter content (Table 2.5).

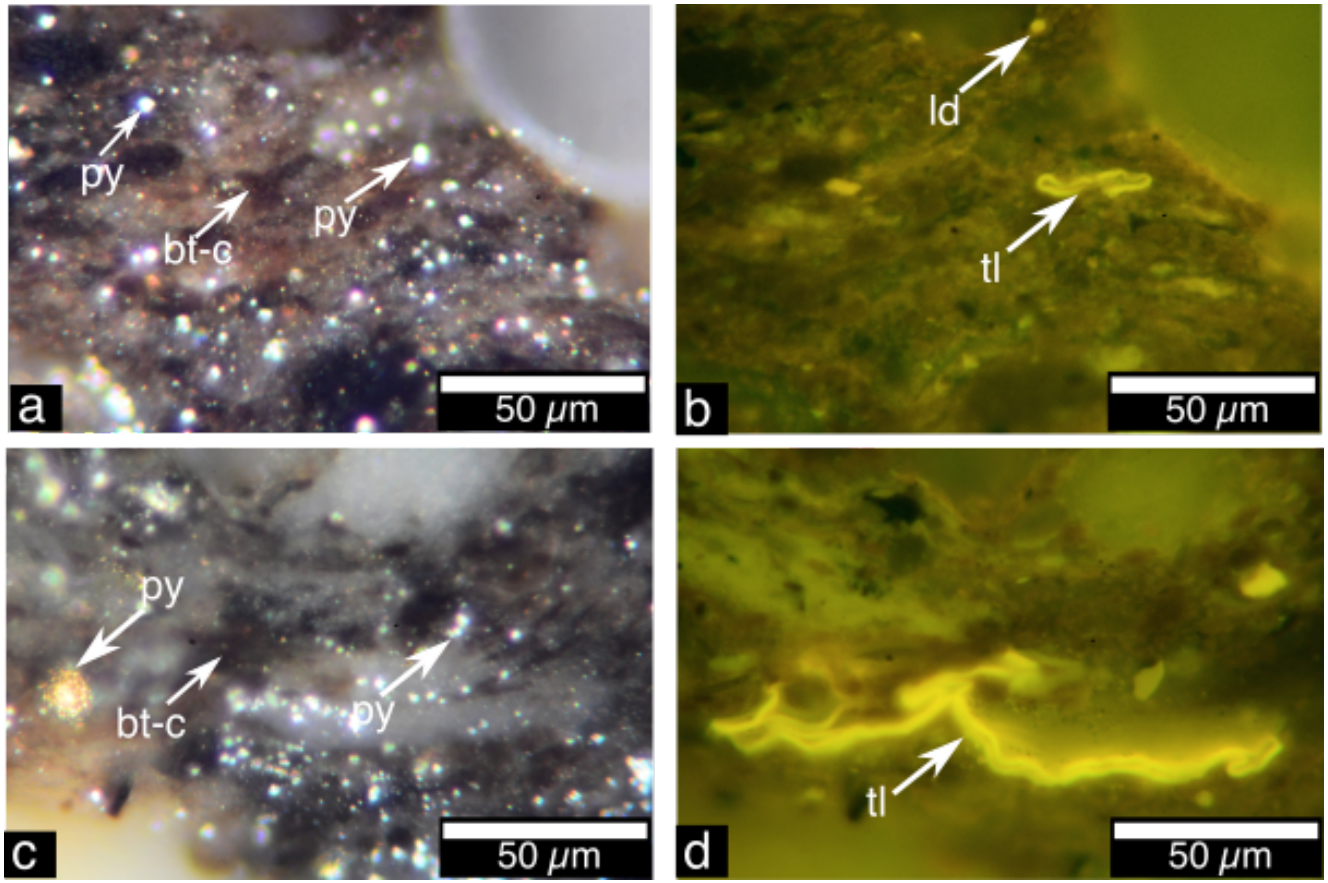

Fig. 2.9. Maceral distribution in a sample (M21) of Monterey Formation. a, c: Clay mineral mixed bituminite (bt-c) is the most abundant maceral. Vitrinite and interitine are rarely observed. Pyrite framboids (py) are abundant. b, d: Telalginite (tl) is occasionally present and liptodetrinite (ld) is more common. Here, a, and c represent observations under reflected white light and b and d represent the same views under fluorescent light.

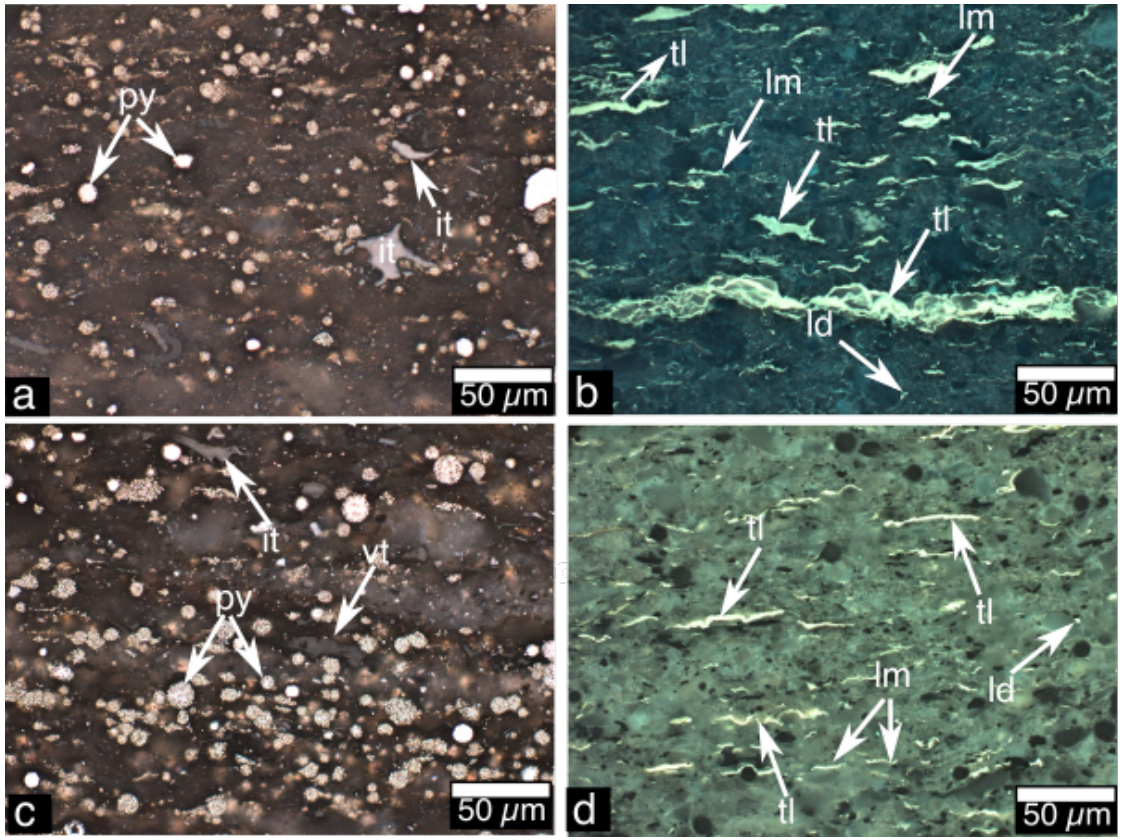

Fig. 2.10. Maceral distribution in samples of Stuart Range Formation (a,b: S64, c: S81, d: S12). Here a and b represent the same view. a: Pyrite framboids (py) are abundant. b: Telalginite (tl) and lamalginite (lm) are the abundant liptinite macerals in Stuart Range samples, liptodetrinite (ld) is also common. c: Vitrnite (vt) and inertinite (it) represent the terrestrial fraction of organic matter. d: lamalginite and telalginite are abundant in Stuart Range samples. Here a and c represent observations under reflected white light and b and d under fluorescent light.

Samples of Monterey Formation show a strong first order relationship between TOC and MSA (R^2 = 0.91) whereas samples of the Stuart Range Formation show no relationship between TOC and MSA (R^2 = 0.54; Fig. 2.11).

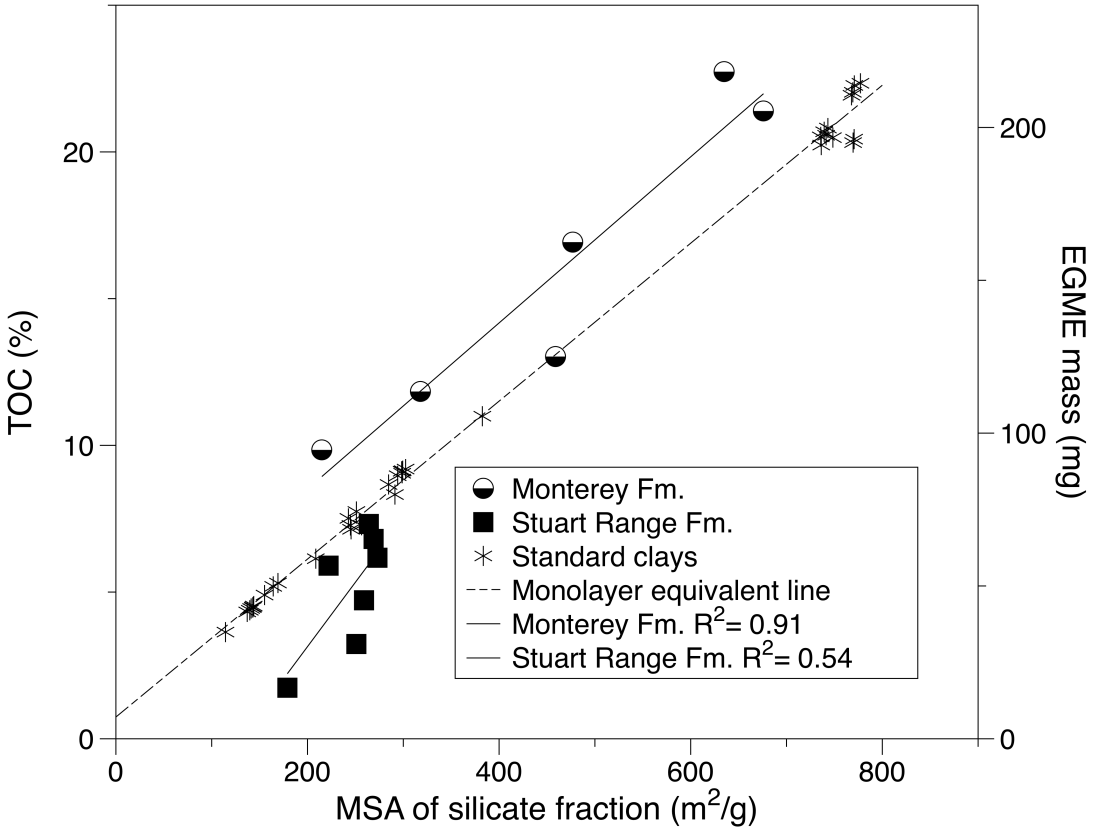

Fig. 2.11. Samples of Monterey Formation have a positive relationship between silicate MSA and TOC over a broad range of values. Stuart Range Formation samples show no relationship between silicate MSA and TOC.

2. 5. Discussion:

Optical and scanning electron microscopy including high-resolution mineral-mapping technique was used to characterize organic and inorganic phases and their physical associations in Monterey and Stuart Range samples. The fabric of shale samples of Monterey and Stuart Range formations are distinctly different. Monterey samples show a nanocomposite fabric where nanometre scale physical association of organic matter and clay minerals are

observed. Stuart Range samples have a particulate fabric comprising > 5 μm sized discrete organic particles.

The Monterey Formation samples represent a marine pelagic sequence deposited in a continental slope setting (Isaacs, 2001). The significant fraction of clay minerals observed in Monterey samples (Fig. 2.6c) is consistent with the high MSA (215 to 676 m^2/g; Table 2.2) measured. Clay minerals are orientated parallel to the lamination of sediments and in many cases, are deformed due to compaction around rigid detrital mineral grains (Fig. 2.4 and 2.5). These features indicate that the majority of the smectite and mixed layer illite-smectite clays that are associated with organic matter are of detrital origin. Moreover, nearly half of the mixed layer illite-smectite clays in Monterey samples from Naples beach section were reported with excess aluminium hydroxy interlayers (Isaacs et al., 2001), characteristic of formation from the chemical weathering of volcanic glass in the provenance area (Schultz et al., 1980; Chamley, 1989). The association of smectite clays with amorphous organic matter is visible at micro- to nano-metre scale under SEM in samples with a range of TOC (Fig. 2.4b and 2.5b). The results of the organic petrography analyses are consistent with the SEM observations indicating > 70% of the organic matter in the Monterey samples is bituminite maceral intimately mixed with clay minerals. The input of terrestrial higher plants in Monterey samples is minimal, with limited presence of vitrinite and inertinite (< 1 to 2 % of the organic matter; Table 2.4), which is consistent with their marine, pelagic depositional setting. Due to the fine grain size of clay crystals (< 4 μm), it is not possible to identify individual clay minerals in

mineral mixed bituminite macerals using optical microscopy technique. However, the SEM observations and high-resolution Nanomin mineral mapping revealed that these clay laths are smectites, present within amorphous organic matter (Fig. 2.4b, 2.5b and 2.6). Clay mineral mixed bituminite maceral class is recognized by the ICCP as materials containing bituminite maceral intimately mixed with fine-grained minerals as groundmass. This maceral class has also been observed in different sample sets in some previous studies (Ming et al., 1994; Pakdel et al., 1999). However, their origin and the process of formation are not completely understood yet. The exact fraction of bituminite in this mineral mixed maceral class is not resolved yet because of the very fine grain size of clay component in them. Based on SEM observations, morphological subclasses of organic matter in Monterey samples proposed in this study as OL, OA and OX indicates that there is probably a considerable variation in clay mineral fractions in bituminite mixed maceral subclass across the sediment.

The Stuart Range Formation was deposited during the waning stage of end-Permian glaciation (Menpes et al., 2010). Samples are collected from sediments of pelagic facies. Organic matter enrichment in cold climate deposit such as the Stuart Range Formation is rare; vast majority of organic-rich sediments in the geologic record are associated with greenhouse conditions (Klemme and Ulmishek, 1991). Sub-angular to angular, poorly sorted quartz and feldspar grains in Stuart Range samples (Fig. 2.7 and 2.8) indicate limited physical weathering. Abundance of feldspar (Fig. 2.8b) indicates the mineralogical immaturity of sediments and a dominance of physical over

chemical weathering, common for glacial deposits (Chamley, 1989). Unlike Monterey samples, the majority of smectite and illite clays in Stuart Range samples are authigenic as indicated by their pore-filling nature and randomly oriented texture (Fig. 2.8c). Clay minerals in Stuart Range samples are devoid of any intimate associations with organic matter unlike the Monterey samples. This indicates organic carbon preservation without the influence of detrital clay minerals. High surface area clay minerals typically formed in soils are not present in the cold climate physical weathering dominated condition and, thus, cannot account for organic carbon preservation.

Organic matter in Stuart Range samples is present as discrete particles of > 5 μm in size. Results of quantitative maceral analyses are consistent with depositional setting of these glacio-marine sediments. Alginite (telalginite and lamalginite) is the major maceral group present in Stuart Range samples as 51 to 83% of the organic matter (Table 2.5). This is indicative of a dominantly marine origin of Stuart Range sediments. Alginites are derived from algal materials with telalginite and lamalginite coming from different algae (Stach, 1982; Taylor, 1998; Suárez-Ruiz and Al-Juboury, 2012). Telalginite is derived from large colonial or thick walled unicellular algae with recognizable biologic structure, e.g. botryococcus and tasmanites. Lamalginites are derived from thin-wallled colonial or unicellular algae that occur as laminae with little or no recognizable biologic structure. Vitrinite and inertinite are derived from the humic component of land plants (Stach, 1982; Jinsheng, 2009). The terrestrial input in organic matter of Stuart Range samples is higher than that of Monterey samples, as indicated by the

content of vitrinite and inertinite (on average < 2% for Monterey and ~16% for Stuart Range samples; Tables 2.4 and 2.5). Results of organic petrography analyses are consistent with mineral mapping and SEM analyses. AP, LF, and TP subclasses of organic matter morphology (Fig. 2.7) indicate a link with organic matter type. With some expected overlap, AP, LF and TP mostly represent vitrinite/inertimie, lamalginite and telalgninite macerals respectively. None of the samples of Stuart Range Formation show any intimate association of mineral matrix with organic matter.

In spite of high TOC (~ 20% in some samples), the occurrence of particulate organic matter is insignificant (Fig. 2.4 and 2.5) and is rarely observed in Monterey Formation (Fig. 2.6). Their homogenous texture, rounded shape and pore-filling nature indicates they are possibly bitumen (Milliken et al., 2014) migrated from the early generation of detrital organic matter (kerogen) followed by infilling of some interparticle/mouldic pores in the rock matrix. The organic matter in Monterey Formation predominantly occurs in a nanocomposite fabric. The abundance of detrital clays during deposition may potentially have a strong control on the association of amorphous organic matter with mineral matrices.

The exact process of the formation of nanocomposite fabric in organic rich shale/mudstone is not completely understood yet. Some studies reported similar organic matter and mineral association before. Such mineral-organic associations were previously reported in upwelling sediment of the Peru continental margin, suggesting depositional environment could possibly have a strong control on the formation of these associations. The study also

speculated that adsorption of organic matter to clay minerals is likely to take place in the water column (Bishop et al., 1992). Organominerallic aggregates were also observed in the Middle Jurassic Whitby Mudstone Formation with shape and composition similar to nanocomposites observed in our study (Macquaker et al., 2010). They have similar compacted, wispy shape comprising organic matter mixed with clay and silt-sized debris as nanocomposite fabric observed in this study (Fig. 2.5a, b). Due to the analogous texture and composition to modern marine snow (e.g. Alldredge and Silver, 1988; Shanks, 2002), organominerallic aggregates were interpreted as 'ancient marine snow' formed in water column and reached to the sediment-water interface as aggregates instead of organic particles (Macquaker et al., 2010). The formation of ancient marine snow in water column increases their settling rate compared to pure organic particles that reduces their exposure time to oxygen (Shanks, 2002) and allows rapid burial of labile organic compound in sediment (Macquaker et al., 2010). The water column formation of nanocomposites is supported by the evidence of high concentration of organic carbon (TOC~ 20% in some samples) in shale with nanocomposite fabric. Another possible mechanism of nanocomposite formation in marine shale could be the microbial activity on sediments below the sediment-water interface. This is supported by the evidence of significant bacterial populations in recent (e.g. Lochte and Turley, 1988; Parkes et al., 1993b) and deeper sediments (Parkes et al., 1994). Nanocomposites could also form during diagenesis by a certain type of macerals (e.g. bituminite) interacting with reactive detrital clay surfaces. High TOC samples of the Monterey Formation analysed in this study have the greatest abundance of

high surface area clays (i.e. smectites) (Fig. 2.11). The slow accumulation rate of the Monterey Formation (0.6 to 9 mg/cm^2/yr) (Isaacs, 2001) might provide enough residence time for primary organic matter to interact and associate with reactive detrital clay surfaces.

Distinct association of organic matter and mineral matrix, in Monterey and Stuart Range formations, as nanocomposite and particulate fabric respectively is consistent with the relationship between TOC and MSA of studied sample sets. MSA and TOC of Stuart Range samples do not show any relationship (R^2 = 0.54) as the petrographic observations show that organic matter is present as discrete particles unrelated to clay mineral surfaces. On the contrary, samples from Monterey Formation show a strong correlation between MSA of the silicate fraction and TOC (R^2 = 0.91; Fig. 2.11) since the amorphous organic matter is intimately associated with clay minerals (Fig. 2.4-2.6). This indicates that the association of organic matter and clay minerals in Monterey samples, which is visible at sub-micron scale, could have a significant effect on thermal stability of labile organic matter compared to discrete organic particles without mineral association.

2.6. Conclusions

Physical association of organic matter and mineral phases of samples from two organic rich shale formations were studied by SEM analyses, Nanomin mineral mapping and organic petrography. The comparison of rock fabric in samples of the Monterey Formation of California, USA and the Stuart Range Formation of South Australia reveals major differences in organic matter and

clay mineral association. Both Monterey and Stuart Range formations comprise clay minerals with abundant smectite. However, the smectites in Monterey samples are detrital, subsequently, organic matter in the Monterey samples is preserved in a nanocomposite fabric showing an intimate association with clay minerals at sub-micron scale. This intimate physical association is also consistent with a strong positive relationship between TOC and MSA in Monterey samples (R^2 = 0.91). On the contrary, smectites in Stuart Range samples are pore-filling, authigenic and thus do not have a link with organic matter deposition, since authigenic clays are formed later during diagenesis. As a result, organic matter preserved in the Stuart Range Formation does not show any association with clay minerals, and occur as discrete organic particles. This is consistent with the absence of a relationship between TOC and MSA in Stuart Range samples (R^2 = 0.54).

The morphology of organic matter in nanocomposite fabric across a wide range of TOC samples can be classified as a) organoclay laminae b) organoclay aggregates and c) infilling organoclay matrix. Organoclay laminae are the most common organic matter morphology in Monterey samples. Organic petrology of Monterey and Stuart Range samples is consistent with SEM observations. Results show that > 70% of the organic matter across all Monterey samples is composed of bituminite mixed with clay minerals. Organic matter in samples of Stuart Range Formation are mostly present as discrete particles of > 5μm size. According to their texture, they can be classified as a) angular to sub-angular organic particles (AP), b) lamellar organic flakes (LF), and c) tabular organic particles (TP). With some expected

overlap, AP, LF and TP mostly represent the vitrinite/inertimie, lamalginite and telalgninite macerals respectively. None of the samples of Stuart Range Formation shows an intimate association of mineral matrix with organic matter. Depending on the depositional setting, organic matter may occur in shale in a nanocomposite fabric where detrital clay minerals are related to organic matter preservation, or in a particulate fabric, where the occurrence and preservation of discrete organic particles are not related to authigenic clay minerals. Intimate physical association of organic matter with clay minerals may have distinct influence on diagenesis and hydrocarbon generation properties compared to particulate organic matter without mineral association.

Acknowledgements

The Australian Research Council (ARC) is acknowledged for providing financial support (ARC Linkage Project LP120200086 to M. J. Kennedy) to conduct the research project. We thank Catherine Stafford and Soumaya Abbassi for providing critical comments on the manuscript. We thank Natalie Debenham for her help during sample collection. SEM analyses were conducted using microscope facilities at the Department of Earth and Planetary Sciences and the Biology Microscopy Unit at Macquarie University.

References

Alldredge, A.L., Silver, M.W., 1988. Characteristics, dynamics and significance of marine snow. Progress in oceanography 20, 41-82.

Aplin, A.C., Macquaker, J.H., 2011. Mudstone diversity: Origin and implications for source, seal, and reservoir properties in petroleum systems. AAPG Bulletin 95, 2031-2059.

Australian Standards, 1998. AS 2856.2: Coal Petrography. Part 2: Maceral Analysis.

Barron, J.A., 1986. Paleoceanographic and tectonic controls on deposition of the Monterey formation and related siliceous rocks in California. Palaeogeography, Palaeoclimatology, Palaeoecology 53, 27-45.

Barron, J.A., Isaacs, C.M., 2001. Updated chronostratigraphic framework for the California Miocene. The Monterey Formation: From Rocks to Molecules. Columbia University Press, New York, 393-395.

Berndmeyer, C., Birgel, D., Brunner, B., Wehrmann, L.M., Jöns, N., Bach, W., Arning, E.T., Föllmi, K.B., Peckmann, J., 2012. The influence of bacterial activity on phosphorite formation in the Miocene Monterey Formation, California. Palaeogeography, Palaeoclimatology, Palaeoecology 317–318, 171-181.

Bishop, A., Kearsley, A., Patience, R., 1992. Analysis of sedimentary organic materials by scanning electron microscopy: the application of backscattered electron imagery and light element X-ray microanalysis. Organic Geochemistry 18, 431-446.

Brincat, D., Abbott, G.D., 2001. Some aspects of the molecular biogeochemistry of laminated and massive rocks from the Naples Beach Section (Santa Barbara-Ventura Basin). The Monterey Formation: From Rocks to Molecules. Columbia University Press, New York, 140-149.

Carr, L., Korsch, R., Preiss, W., Menpes, S., Holzschuh, J., 2012. Key features of new deep seismic reflection lines across frontier sedimentary basins in central Australia: the Arckaringa, Officer, Amadeus and Georgina Basins. ASEG Extended Abstracts 2012, 1-4.

Chamley, H., 1989. Clay sedimentology / Hervé Chamley. Springer-Verlag, London New York.

Föllmi, K.B., Badertscher, C., de Kaenel, E., Stille, P., John, C.M., Adatte, T., Steinmann, P., 2005. Phosphogenesis and organic-carbon preservation in the Miocene Monterey Formation at Naples Beach, California—The Monterey hypothesis revisited. Geological Society of America Bulletin 117, 589-619.

Garrison, R.E., Hoppie, B.W., Grimm, K.A., 1994. Phosphates and dolomites in coastal upwelling sediments of the Peru margin and the Monterey Formation (Naples Beach section), California.

Hartnett, H.E., Keil, R.G., Hedges, J.I., Devol, A.H., 1998. Influence of oxygen exposure time on organic carbon preservation in continental margin sediments. Nature 391, 572-575.

Hedges, J.I., 1992. Global biogeochemical cycles: progress and problems. Marine chemistry 39, 67-93.

Hedges, J.I., Keil, R.G., 1995. Sedimentary organic matter preservation: an assessment and speculative synthesis. Marine chemistry 49, 81-115.

Isaacs, C.M., 2001. Depositional framework of the Monterey formation, California. The Monterey Formation: From Rocks to Molecules, 1-30.

Isaacs, C.M., Pollastro, R.M., Barron, J.A., Ingle Jr, J.C., Bukry, D., Dunbar, R.B., Keller, M.A., Tomson, J.H., Lewan, M.D., 2001. Geologic and

Paleontologic Features of Rock Samples in the Cooperative Monterey Organic Geochemistry Study, Naples Beach and Lions Head Sections, California. The Monterey Formation: From Rocks to Molecules, 373.

Jinsheng, G., 2009. Coal, Oil Shale, Natural Bitumen, Heavy Oil and Peat - Volume II.

Keil, R., Mayer, L., 2014. Mineral matrices and organic matter. Treatise on geochemistry 12, 337-359.

Keil, R.G., Montlucon, D.B., Prahl, F.G., Hedges, J.I., 1994. Sorptive preservation of labile organic matter in marine sediments. Nature 370, 549-552.

Kennedy, M.J., Löhr, S.C., Fraser, S.A., Baruch, E.T., 2014. Direct evidence for organic carbon preservation as clay-organic nanocomposites in a Devonian black shale; from deposition to diagenesis. Earth and Planetary Science Letters 388, 59-70.

Kennedy, M.J., Pevear, D.R., Hill, R.J., 2002. Mineral surface control of organic carbon in black shale. Science 295, 657-660.

Klemme, H., Ulmishek, G.F., 1991. Effective petroleum source rocks of the world: stratigraphic distribution and controlling depositional factors (1). AAPG Bulletin 75, 1809-1851.

Kuila, U., McCarty, D.K., Derkowski, A., Fischer, T.B., Topór, T., Prasad, M., 2014. Nano-scale texture and porosity of organic matter and clay minerals in organic-rich mudrocks. Fuel 135, 359-373.

Laurent, D., de Kaenel, E., Spangenberg, J.E., Föllmi, K.B., 2015. A sedimentological model of organic-matter preservation and

phosphogenesis in the Miocene Monterey Formation at Haskells Beach, Goleta (central California). Sedimentary Geology 326, 16-32.

Lazar, O.R., Bohacs, K.M., Macquaker, J.H., Schieber, J., Demko, T.M., 2015. Capturing key attributes of fine-grained sedimentary rocks in outcrops, cores, and thin sections: nomenclature and description guidelines. Journal of Sedimentary Research 85, 230-246.

Lochte, K., Turley, C., 1988. Bacteria and cyanobacteria associated with phytodetritus in the deep sea. Nature 333, 67.

Löhr, S.C., Kennedy, M.J., 2014. Organomineral nanocomposite carbon burial during Oceanic Anoxic Event 2. Biogeosciences 11, 4971-4983.

Macquaker, J.H., Adams, A., 2003. Maximizing information from fine-grained sedimentary rocks: An inclusive nomenclature for mudstones. Journal of Sedimentary Research 73, 735-744.

Macquaker, J.H., Keller, M.A., Davies, S.J., 2010. Algal blooms and "marine snow": Mechanisms that enhance preservation of organic carbon in ancient fine-grained sediments. Journal of Sedimentary Research 80, 934-942.

Macquaker, J.H., Taylor, K.G., Keller, M., Polya, D., 2014. Compositional controls on early diagenetic pathways in fine-grained sedimentary rocks: Implications for predicting unconventional reservoir attributes of mudstones. AAPG Bulletin 98, 587-603.

Mayer, L.M., 1994. Surface area control of organic carbon accumulation in continental shelf sediments. Geochimica et Cosmochimica Acta 58, 1271-1284.

Menpes, S., Korsch, R., Carr, L., 2010. 2008 Gawler Craton-Officer Basin-Musgrave Province-Amadeus Basin (GOMA) seismic survey, 08GA-OM1: Geological interpretation of the Arckaringa Basin, GOMA (Gawler Craton–Officer Basin–Musgrave Province–Amadeus Basin) Seismic and MT Workshop 2010, p. 16.

Milliken, K.L., Ko, L.T., Pommer, M., Marsaglia, K.M., 2014. SEM petrography of Eastern Mediterranean sapropels: Analogue data for assessing organic matter in oil and gas shales. Journal of Sedimentary Research 84, 961-974.

Ming, Q., Xilin, R., Dazhong, T., Jian, X., Wolf, M., 1994. Petrographic and geochemical characterization of pale and dark brown coal from Yunnan Province, China. International Journal of Coal Geology 25, 65-92.

Pakdel, H., Roy, C., Kalkreuth, W., 1999. Oil production by vacuum pyrolysis of Canadian oil shales and fate of the biological markers. Fuel 78, 365-375.

Parkes, R.J., Cragg, B.A., Bale, S., Getlifff, J., Goodman, K., Rochelle, P.A., Fry, J.C., Weightman, A.J., Harvey, S., 1994. Deep bacterial biosphere in Pacific Ocean sediments. Nature 371, 410.

Parkes, R.J., Cragg, B.A., Getliff, J.M., Harvey, S.M., Fry, J.C., Lewis, C.A., Rowland, S.J., 1993. A quantitative study of microbial decomposition of biopolymers in Recent sediments from the Peru Margin. Marine Geology 113, 55-66.

Potter, P.E., Maynard, J.B., Depetris, P.J., 2005. Mud and mudstones: Introduction and overview. Springer Science & Business Media.

Ransom, B., Bennett, R.H., Baerwald, R., Shea, K., 1997. TEM study of in situ organic matter on continental margins: occurrence and the “monolayer” hypothesis. Marine Geology 138, 1-9.

Ray, S.S., 2013. Clay-containing polymer nanocomposites: from fundamentals to real applications. Newnes.

Schultz, L.G., Tourtelot, H., Gill, J.R., Boerngen, J., 1980. Composition and properties of the Pierre Shale and equivalent rocks, northern Great Plains region. US Govt. Print. Off.

Setti, M., Marinoni, L., López-Galindo, A., 2004. Mineralogical and geochemical characteristics (major, minor, trace elements and REE) of detrital and authigenic clay minerals in a Cenozoic sequence from Ross Sea, Antarctica. Clay Minerals 39, 405-421.

Shaldybin, M., Lopushnyak, Y., Goncharov, I., Wilson, M., Wilson, L., Mendis, B., 2017. The mineralogy of the clayey-silty siliceous rocks in the Bazhenov Shale Formation (Upper Jurassic) in the west Siberian Basin, Russia: The role of diagenesis and possible implications for their exploitation as an unconventional hydrocarbon reservoir. Applied Clay Science 136, 75-89.

Shanks, A.L., 2002. The abundance, vertical flux, and still-water and apparent sinking rates of marine snow in a shallow coastal water column. Continental Shelf Research 22, 2045-2064.

Stach, E., 1982. Stach's textbook of coal petrology.

Suárez-Ruiz, I., Al-Juboury, A., 2012. Organic petrology: an overview. Petrology—New Perspectives and Applications.

Suárez-Ruiz, I., Flores, D., Mendonça Filho, J.G., Hackley, P.C., 2012. Review and update of the applications of organic petrology: Part 1, geological applications. International Journal of Coal Geology 99, 54-112.

Taylor, G.H., 1998. Organic petrology: A new handbook incorporating some revised parts of Stach's textbook of coal petrology. Gebruder Borntraeger Verlagsbuchhandlung.

Tiller, K., Smith, L., 1990. Limitations of EGME retention to estimate the surface area of soils. Soil Research 28, 1-26.

Tissot, B.P., Welte, D.H., 1984. Petroleum formation and occurrence. Springer-Verlag.

Wohling, D., Keppel, M., Fulton, S., Costar, A., Sampson, L., Berens, V., 2013. Australian Government initiative on coal seam gas and large coal mining, Arckaringa Basin and Pedirka Basin Groundwater Assessment Projects. Department of Environment, Water and Natural Resources, Adelaide, Australia, p. 10.

Zonneveld, K., Versteegh, G., Kasten, S., Eglinton, T.I., Emeis, K.-C., Huguet, C., Koch, B., de Lange, G.J., De Leeuw, J., Middelburg, J.J., 2010. Selective preservation of organic matter in marine environments; processes and impact on the sedimentary record.

Chapter 3. Clay-organic association as a control on hydrocarbon generation in shale

Habibur M Rahman[a*], Martin Kennedy[a], Stefan Löhr[a], David N Dewhurst[b]

[a] *Department of Earth and Planetary Sciences, Macquarie University, Sydney, New South Wales, Australia*

[b] *CSIRO Energy, Perth, Western Australia, Australia*

* *Corresponding author at: Department of Earth and Planetary Sciences, Macquarie University, Sydney, NSW 2109, Australia. Tel: +61-2-9850-8426.*

E-mail address: mdhabibur.rahman@mq.edu.au, hrahman039@gmail.com

Statement of authors' contribution

This chapter is a published paper in *Organic Geochemistry* (*Rahman et al., 2017*) . This paper has been formatted to conform to the font and referencing style adopted in the thesis. Figures and tables included within the text are prefixed with the chapter number. This chapter compares the hydrocarbon generation potential of two shale fabrics, particulate and nanocomposite, which is the second objective of the thesis. Organic geochemical techniques including RockEval pyrolysis, mineralogy and organic petrology were used to determine the hydrocarbon generation potential of samples with nanocomposite and particulate shale fabric. I am the primary author of this manuscript. I examined data including sample selection, sampling and sample preparation for this study. I performed all the experiments and analyses used in this manuscript except Rock-Eval pyrolysis of some samples. Rock-Eval pyrolysis data of some samples was acquired by Tony Hall

(University of Adelaide). I processed and interpreted all the data derived from the conducted analyses and experiments. I wrote and designed the paper's structure. Martin Kennedy, Stefan Löhr and David Dewhurst carefully reviewed and provided feedbacks and various refinements on the manuscript. Neither this manuscript nor one with similar content under our authorship has been published or is being considered for publication elsewhere, except as described above.

Abstract

Programmed pyrolysis experiments investigating the influence of the mineral matrix on hydrocarbon generation from organic compounds have shown inconclusive results in past studies. This study tests the hypothesis that the inhibitory vs. catalytic influence of clay minerals is dependent on the physical association of the mineral matrix with organic compounds by comparing natural samples from two shale formations with different mineral-organic associations. Samples from the Miocene aged Monterey Formation have a greater area of surface contact between organic matter and mineral surfaces when compared to the more particulate texture and discrete nature of the organic matter in the samples from the Permian aged Stuart Range Formation. Comparison of kerogen extracts to the whole rock (containing mineral and organic matter) samples during programmed pyrolysis shows higher hydrocarbon generation from isolated kerogen compared to the whole rock sample it was extracted from in both Monterey and the Stuart Range Formation samples. The difference between extracted kerogen and whole rock samples is greater and more variable (56 to 210 mgHC/g TOC) in the Stuart

Range than the Monterey Formation (85 to 142 mgHC/gTOC) implying greater hydrocarbon retention by the free mineral surfaces. Temperature of maximum hydrocarbon generation (T_{max}) is greater in whole rock than kerogen isolates (20°C mean) in the Monterey Formation samples, but shows negligible difference (2°C mean) in the samples from the Stuart Range Formation. Standard kerogen typing using Rock-Eval pyrolysis data places the same kerogen as type II to type III on a modified Van Krevelen diagram depending whether it is isolated or pyrolysed with its mineral host. This study identifies that not only the bulk mineralogy and kerogen type but also the degree of surface contact of the phases influence hydrocarbon generation.

Keywords: Hydrocarbon generation, clay catalysis, shale fabric, organoclay nanocomposite, Monterey Formation, Stuart Range Formation.

3.1. Introduction

Fine-grained sedimentary rocks are the most abundant lithology at the earth's surface (Boggs, 2009). Shales host the bulk of organic carbon in the sedimentary record and are the main source of commercially exploitable hydrocarbons in both conventional and unconventional plays (Potter et al., 2005). Their major distinguishing feature is an abundance of clay minerals, commonly comprising > 60 wt.% of the rock (Shaw and Weaver, 1965). Amongst these, illite (I), smectite (S), and their mixed-layer illite-smectite (I-S) intermediates are most abundant, comprising up to 30 % of all sedimentary rocks (Garrels and Mackenzie, 1971). Smectite clays in particular are reactive, high surface area minerals that have long been utilized to catalyze

organic reactions and to provide thermal stability to organic polymers in industrial applications (Varma, 2002; Clark et al., 2013; McCabe and Adams, 2013). The catalytic properties and abundance of clays led to early suggestions that clay minerals may influence hydrocarbon generation in mudstones (Shimoyama and Johns, 1971; Johns, 1979). This view was strengthened by subsequent observations that the diagenetic transformation of smectite to illite occurs over the temperature-depth interval associated with peak oil generation (Hower et al., 1976; Pevear, 1999; Abid and Hesse, 2007; Li et al., 2015).

A large number of experimental studies have investigated the impact of smectite clays on hydrocarbon generation since the idea was first proposed (Shimoyama and Johns, 1971; Galwey, 1972; Johns and Shimoyama, 1972; Johns, 1979; Heller-Kallai et al., 1984; Pan et al., 2010; Yuan et al., 2013). Two distinct experimental approaches can be distinguished, both involving pyrolysis of organic materials in the presence of clays in experiments designed to mimic natural hydrocarbon generation but conducted on laboratory time-scales. One group of experiments compared the hydrocarbon generation potential of kerogen isolates with the same kerogen mixed with standard clay minerals (e.g. Tannenbaum and Kaplan, 1985; Tannenbaum et al., 1986). Other studies compared the hydrocarbon generation potential of synthetic organic compounds such as aminolauric acid by themselves and mixed with standard clay minerals (Yuan et al., 2013). The results of these experimental studies are equivocal. Some identified decreased hydrocarbon yields for kerogen-clay mixtures relative to kerogen isolates (Espitalie et al.,

1980), which was attributed to the retention of heavier hydrocarbon by the clay mineral surfaces. Other studies showed significantly increased hydrocarbon generation where organic materials (either kerogen isolates or synthetic organic compounds) were pyrolysed in the presence of smectite (Tannenbaum and Kaplan, 1985; Pan et al., 2010; Yuan et al., 2013). There is, therefore, no consensus regarding the magnitude or even the direction of clay mineral influence on hydrocarbon generation. More fundamentally, the degree to which the experimental approaches utilised to date are representative of natural hydrocarbon generation in shale is debatable. Shale contains complex mineral assemblages that have little in common with the synthetic mineral mixtures employed by most studies to date. In addition, experimental design has seen little consideration of the morphology of organic matter (i.e. size, shape and distribution relative to the mineral matrix) most specially the degree to which the organic matter is associated with clay mineral surfaces, although this varies widely in shale (Löhr et al., 2015). The fabric of organic matter is potentially an important control on the nature of organo-mineral interactions leading to inhibited or increased hydrocarbon generation.

Organic matter in sedimentary rocks is commonly preserved as discrete, primary particles that have escaped mineralization (Tyson, 1994). However, a growing body of literature documents a class of mineral-bound organic matter that is frequently dominant both in modern organic-rich sediments (Bishop et al., 1992; Keil et al., 1994; Mayer, 1994; Blair and Aller, 2012) and in ancient mudstones (Salmon et al., 2000; Kennedy et al., 2014; Löhr and Kennedy,

2014). The organic matter bound in organoclay aggregates and nanocomposites (Keil et al., 1994; Kennedy et al., 2014) is preferentially preserved during early diagenesis facilitating its sequestration into the sedimentary rock record. In this study, particulate organic matter is considered to be comprised of discrete organic particles that contain no siliciclastic material and are > 5 μm in size. They may have recognizable structure visible under petrographic microscopes. Organic matter domains that are intimately associated or interleaved with clay minerals at < μm scale to form a nanocomposite structure are called organoclay aggregates in this study (Fig. 3.1). This type of organic matter is classically termed amorphous and lacks visible structure using standard organic petrographic techniques. While it is reasonable to expect some mixture of these two classes of organic matter in a typical organic carbon rich shale, the different depositional and diagenetic conditions controlling their occurrence commonly results in the dominance of one type over the other. It is reasonable to predict that the effect of mineral matrices on hydrocarbon generation will differ greatly between these two end members because of the greater area of mineral surface to organic matter contact and potential for mineral catalyzed reactions. This implies that differences in shale texture can result in differences in hydrocarbon generation, even where bulk rock analysis might indicate similar organic matter and clay composition. Varying organic matter-mineral association may therefore provide an explanation for the inconsistent experimental results published to date.

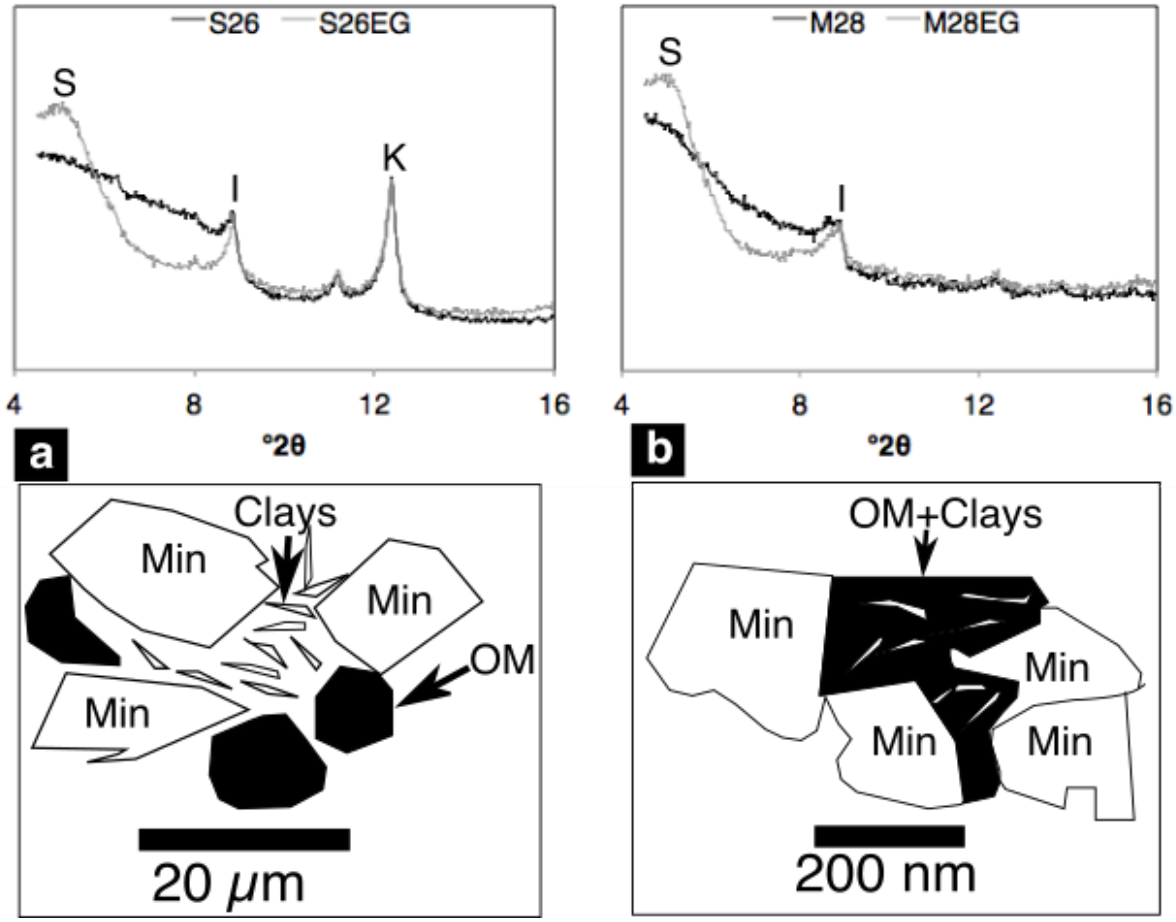

Fig. 3.1. X-ray diffractograms of the < 2μm fraction of air-dried (black) and ethylene glycol-treated (grey) samples of (a) Stuart Range and (b) Monterey Formation. Both smectite (S) and illite (I) are common in these two formations; kaolinite (K) is also present in Stuart Range Formation. The Stuart Range Formation shows discrete, particulate organic matter in mineral matrices and the Monterey Formation is comprised of organic matter intimately associated with clay minerals.

The impact of the mineral matrices on hydrocarbon generation in natural samples considering different degrees of organic matter-mineral association has not been studied to date. It requires integration of bulk geochemical and mineralogical analyses with detailed optical and electron microscopic characterization of organic matter morphology and distribution in shale fabric. In this study, we determine the potential influence of the mineral matrix on hydrocarbon yield and generation temperature for two texturally

different organic rich shales during experimental anhydrous pyrolysis. We explicitly consider the nature of the organic matter-mineral associations by contrasting a suite of samples containing mainly discrete organic matter particles with a suite of samples containing intimately associated (nanometre scale) organic matter with mineral surfaces.

3.2. Materials and Methods

Shale samples were collected from the middle member of the Miocene Monterey Formation of California, USA and the early Permian Stuart Range Formation from the Arckaringa basin of South Australia. The Monterey Formation has been widely studied to understand mechanisms of organic carbon enrichment as well as diagenetic processes including transformation of silica and carbonates (Compton, 1991; Isaacs, 2001; Föllmi et al., 2005; Berndmeyer et al., 2012; Laurent et al., 2015). Due to the high percentage of organic carbon (TOC > 10 %), the Monterey Formation is the most significant source rock in the western USA (Graham and Williams, 1985; Tennyson and Isaacs, 2001). The Stuart Range Formation has recently become topical as one of Australia's most promising potential source rocks (Linc Energy, 2012). Both the Monterey and Stuart Range Formations are organic carbon rich (TOC 1 - 22 %), immature to marginally mature (Ro = 0.30 – 0.60) shales deposited in an intermittently anoxic marine environment (Orr, 1986; Gilby and Foster, 1988; Teln et al., 2001; Tennyson and Isaacs, 2001; Debenham, 2015). Both shales contain sulphur-rich kerogen, Monterey kerogen is characterized as the classical type II-S, with organic sulphur content of 8 to 14 %, while the Stuart Range represents a mixture of type II and type III

kerogen (Tannenbaum and Kaplan, 1985; Orr, 1986; Belin and Huc, 2001; Föllmi et al., 2005; Debenham, 2015).

The middle member of the Monterey Formation is dominated by clay minerals with some detrital quartz and feldspar, diagenetic dolomite and siderite and conspicuous horizons of phosphatic nodules. Biogenic silica and their diagenetic derivatives such as chert and porcelanite are less common in the middle member of the Monterey Formation than in the upper portion in the section studied at Naples Beach, California (Barron, 1986; Garrison et al., 1994; Isaacs, 2001; Föllmi et al., 2005; Berndmeyer et al., 2012; Laurent et al., 2015). Clay mineralogy is dominated by smectite and mixed-layer illite-smectite. Organic matter is dominantly amorphous and intimately associated with clay minerals at the nanometer scale forming organoclay aggregates. The Stuart Range Formation, by contrast, is arkosic silt but also contains a significant fraction of clay minerals that are pore filling (authigenic) and framboidal pyrite (< 14 %) indicating high sulphur abundance during deposition or early diagenesis (Debenham, 2015). Unlike the Monterey Formation, organic matter occurs as discrete particles > 5 μm in size and not directly associated with the authigenic clay mineral fraction.

The broad similarities between kerogen maturity, deposition in a restricted marine environment, presence of similar clay minerals (illite, smectite) and comparable pelagic dominated lithofacies provide an opportunity to contrast the influence of shale texture on hydrocarbon generation in two examples dominated by different organic carbon-mineral associations. Hydrocarbon yields and generation temperature of these two formations were estimated

through anhydrous pyrolysis experiments designed to mimic natural hydrocarbon generation. Pyrolysis experiments were set up to analyse the shale samples and their kerogen isolates in pairs to identify the mineral matrix influence while keeping some major geological variables (e.g. organic content, thermal maturity etc.) broadly constant.

3.2.1. Samples

A total of 17 sub-samples (Table 3.1) were selected for kerogen isolation, bulk mineralogy, optical petrography, electron imaging and subsequent geochemical analyses. The samples were selected based on criteria including, a) high organic content as appropriate for kerogen isolation, b) low thermal maturity and c) characteristic end-member texture (particulate versus amorphous organoclay). Samples from the middle member of the Miocene Monterey Formation were collected from outcrops at the Naples Beach section located west of Santa Barbara, California, USA. The Naples Beach section provides complete exposure in wave-cut coastal cliff outcrops and serves as an informal type locality for studies of the middle member of the Monterey Formation (Hornafius, 1994; Föllmi et al., 2005). Samples were collected from the carbonaceous marl member deposited as a pelagic to hemipelagic sequence described in stratigraphic succession by Isaacs (2001). Samples used for this study include phosphatic mudstone, black shale, calcareous black mudstone, phosphatic shale and calcareous phosphatic shale.

Table 3.1. Lithofacies and TOC (wt.%) of samples studied from Monterey and Stuart Range formations.

Formation	Sample no.	Lithofacies	Depth (m)	TOC (wt.%)
Monterey	M59	Phosphatic mudstone	Outcrop	11.8
	M62	Black shale	Outcrop	21.4
	M22	Calcareous black mudstone	Outcrop	13.0
	M28	Phosphatic shale	Outcrop	16.9
	M33	Black shale	Outcrop	22.7
	M29	Phosphatic shale	Outcrop	5.4
	M21	Calcareous phosphatic shale	Outcrop	9.8
Stuart Range	S43	Fissile black shale	918.06	6.2
	S81	Silty mudstone	897.26	5.9
	S08	Silty Mudstone	951.3	4.7
	S77	Black shale	900.73	7.3
	S99	Argillaceous siltstone	888.5	1.3
	S51	Silty mudstone	990.17	0.06
	S64	Black shale	907.53	6.8
	S12	Silty mudstone	949.65	1.7
	S26	Fissile black shale	934.76	3.2
	S72	Siliceous mudstone	974.64	0.6

Samples of the early Permian Stuart Range Formation were collected from the Arck-1 core stored in the South Australian State core repository. The Arck-1 well was drilled in the Permo-Carboniferous intracratonic Arckaringa basin, located in the central northern part of South Australia (Wohling et al., 2013). The Stuart Range Formation was deposited in quiet, restricted (intermittently anoxic) marine conditions as indicated by intervals of fine-grained laminated silt and mudstone interspersed with decimetre-scale

deposits from density flows and arenaceous foraminifera (Townsend, 1976; Hibburt, 1984; Gilby and Foster, 1988; Alexander et al., 2006; Debenham, 2015). Samples were taken from the laminated, darkest coloured, and finest grained intervals with TOC ranging from 0.6 to 7 wt.%. The samples used for this study include black shale, silty mudstone, argillaceous mudstone and siliceous mudstone (Table 3.1).

3.3. Methods

3.3.1. Whole rock and clay mineralogy

Rock samples were cleaned using compressed air, milled and passed through a 200 μm sieve for bulk geochemical analyses. Mineralogy of the samples was determined by X-ray Diffraction (XRD) (Bruker D8 Advance with a Cu-radiation source) of powdered samples using Bruker Diffrac.Eva software and Crystallography Open Database reference patterns. The clay mineralogy of the samples was determined on Ca-saturated oriented preparations of the < 2 μm fraction (air dried and after treatment with ethylene glycol). The < 2 μm fraction was obtained by centrifugation after carbonate removal with 1 M sodium acetate buffer at pH 5 and 90°C, organic matter removal with NaOCl at pH 9.5 and 90°C, and ultrasonic dispersal following the method described by Löhr and Kennedy (2014).

3.3.2. Organic petrography

Epoxy-mounted sections were prepared by embedding rock samples in a proportional araldite and a hardener mixture. The mounted samples were flattened with different grade sand papers and finally polished with 3 μm and

1 μm diamond paste. Organic petrography was performed in reflected white light mode and fluorescence (ultra-violet) mode using a Nikon Eclipse CiPOL polarising microscope. Macerals were classified in accordance with the procedures of Standards Association of Australia, AS 2856.2 (Australian Standards, 1998) based on the ICCP (International Committee for Coal Petrology) nomenclatures. At least one polished section was studied for each sample. Vitrinite reflectance (Ro) was measured on a subset of samples including three Monterey and four Stuart Range samples, using incident white light under oil immersion using a Zeiss microscope attached with a CRAIC microspectrometer. The Ro value of each sample reported here is a mean of 25-35 measured points.

3.3.3. Scanning electron microscopy (SEM)

Samples were polished using a Hitachi IM4000 Argon Ion Mill system and carbon-coated before SEM analysis. They were imaged using a JEOL Neoscope JCM 6000 SEM, Zeiss EVO MA15 SEM and JEOL JSM 7100F field emission SEM. All SEMs were equipped with energy dispersive x-ray spectroscopy (EDS) systems for elemental analysis. SEM analyses were performed at 12 mm working distance and 15 kV accelerating voltage. Elements with high atomic number backscatter electrons more strongly than the elements with low atomic numbers and thus appear brighter in the BSE photomicrographs (Goldstein et al., 1981). Organic matter appears dark relative to mineral phases in SEM BSE photomicrographs, so that they provide direct visual evidence for the association of minerals and organics in the rock.

3.3.4. Total organic carbon

Total carbon content (TC) for each sample was measured in a Perkin Elmer 2400 Series II CHNS analyzer. Inorganic carbon content (IC) was determined using the pressure-calcimeter method of Sherrod et al. (2002). Total organic carbon (TOC) content was calculated by the differences i.e. TOC = TC – IC.

3.3.5. Mineral surface area

The mineral surface areas (MSA) of the samples was determined using the ethylene glycol monoethyl ether (EGME) method of Tiller and Smith (1990). A factor of 3.2 was used to convert the mass of sorbed EGME (in mg) to mineral surface area (in m^2), based on an assumption of monolayer coverage (Kennedy and Wagner, 2011). Six replicates of a suite of clay mineral standards obtained from the Clay Mineral Society were analysed in the same batch as the samples. MSA was corrected for $CaCO_3$ and organic carbon content, and is reported here as 'silicate MSA'. MSA measured on the clay mineral standards showed good reproducibility (SWy-2: 741 m^2/g ±1.93 %; STx-1b: 771 m^2/g ±1.33 %; IScZ-1: 296 m^2/g ±2.57 %; IMt-2: 141 m^2/g ±1.04 %; n = 6).

3.3.6. Kerogen isolation

Kerogen isolates of each sample were obtained using the method of Durand (1980). Carbonate fractions of the milled samples were dissolved using 4 M hydrochloric acid (HCl). 30 ml of 4 M HCl was added to sample beakers each containing 10 g of sample. The samples were washed several times with deionized water after the removal of carbonate fractions as indicated by the disappearance of the effervescence. The silicate mineral phases were dissolved using hydrofluoric acid (HF). 40 ml of 20 wt.% HF was added to

each sample tube, they were then heated to 60°C and left to react for 24 hours. The treatment was repeated until dissolution of silicate minerals was completed as confirmed by subsequent XRD analysis. The isolated organic matter samples were washed several times with deionized water and oven dried at 40°C. TC of the organic matter isolates was measured to confirm organic matter purity. In total four samples from both Monterey and Stuart Range formations were excluded from further analyses where organic matter isolates have TC < 30 %. It should be noted that pyrite could not be dissolved by the technique used in this study. Some studies have suggested a pyrite removal method using chromous chloride (e.g. Acholla and Orr, 1993), however the method was not implemented here as the presence of pyrite in organic matter isolates was not considered detrimental to the aims of the study.

Organic matter isolates and whole rock samples were solvent extracted to remove the bitumen fraction. Samples were treated ultrasonically in a 9:1 mixture of dichloromethane (DCM) and methanol for 10 minutes followed by 10 minutes settling time. The samples were then stirred and underwent a second stage of ultrasonic treatment for 10 minutes. Solvents were discarded between repeats. This cycle was repeated until all bitumen was removed (4 cycles on average) as indicated by the clear appearance of solvent after the final treatment. The bulk rock samples (10 g of each) were also solvent extracted using the same ultrasonic treatments, ensuring that pyrolysis data of the bulk rock and the kerogen isolates are comparable.

3.3.7. Rock-Eval pyrolysis

The hydrocarbon generation potential (S2) and the temperature of maximum hydrocarbon generation (T_{max}) of both rock samples and their kerogen isolates were determined by Rock-Eval pyrolysis, using a Weatherford Laboratories source rock analyser (SRA). Each sample was measured in triplicate. Thermal maturity of the samples was estimated using the method of Jarvie et al. (2001), which relates measured T_{max} to calculated Ro using the equation: calculated %Ro = 0.0180 × T_{max} - 7.16. The Ro of the samples were calculated from the T_{max} values to compare with the measured Ro values.

3.4. Results

Monterey and Stuart Range formations are both comprised of organic-carbon rich, sulphur-rich shale (Monterey 5 to 23 and Stuart Range 1 to 7 wt.% TOC, Table 3.1) of roughly comparable maturities (Monterey 0.41 to 0.43 %Ro and Stuart Range 0.49 to 0.59 %Ro). However, differences in their depositional environments and diagenetic histories resulted in significantly different mineralogy, grain size, composition of organic matter and distinct textural relationships between organic matter and mineral phases potentially influencing hydrocarbon generation.

The early Permian Stuart Range Formation was deposited in a paraglacial environment during the waning stages of Gondwana glaciation in south Australia. Granular texture and feldspathic (immature) mineralogy of the Formation reflect a dominance of physical weathering processes in a cold climate environment. Silt grains ranging from 5 to 50 μm are dominant and

are comprised of quartz, feldspar and mica (Table 3.2). The grains are angular to subangular and poorly sorted. A significant clay sized fraction evident in Fig. 3.1a and identified by the high MSA that ranges between 179 to 273 m^2/g is composed of smectite and kaolinite (Table 3.2). The majority of clay minerals occur as euhedral phases filling pores (Fig. 3.2c) showing a random orientation indicating a diagenetic rather than a detrital origin. As a result of this diagenetic pore filling distribution, clay minerals were not mixed with organic matter during deposition and are thus not directly physically associated (Fig. 3.2a and 3.2b). There is no correlation between MSA and TOC in bulk sediment analysis (discussed below) indicating no direct relationship.

Table 3.2. Mineral surface area (MSA) and bulk mineralogy of Monterey and Stuart Range formations. Qz = Quartz, Ab = Albite/Plagioclase feldspars, Mc = Microcline, Ca = Calcite, Py = Pyrite, Ch = Chlorite, S = Smectite, I = Illite, Mu = Muscovite, Bt = Biotite, K = Kaolinite, Gp = Gypsum, Fp = Fluorapatite.

Sample No.	Silicate MSA (m2g-1)	Qz	Ab	Mc	Ca	Py	Ch	S	I	Mu	Bt	K	Gp	Fp
M59	318	*	*	*	*	*		*	*		*		*	
M62	676	*	*			*		*	*					
M22	459	*	*	*	*	*		*	*	*	*			
M28	477	*	*	*	*	*		*	*		*			
M33	635	*	*	*	*	*		*	*	*	*			
M29	-	*	*	*		*		*		*	*			*
M21	215	*	*	*	*	*		*	*		*			*
S43	273	*	*			*		*	*	*		*		
S81	222	*	*			*			*	*		*		
S08	259	*	*			*	*	*	*	*		*	*	
S77	264	*	*			*		*	*			*		
S99	-	*	*	*			*		*	*		*		
S51	-	*	*	*		*	*	*	*	*		*		
S64	269	*	*			*		*	*			*	*	
S12	179	*	*	*		*		*	*	*		*		
S26	251	*	*			*		*	*			*	*	
S72	-	*	*	*		*	*		*	*		*		

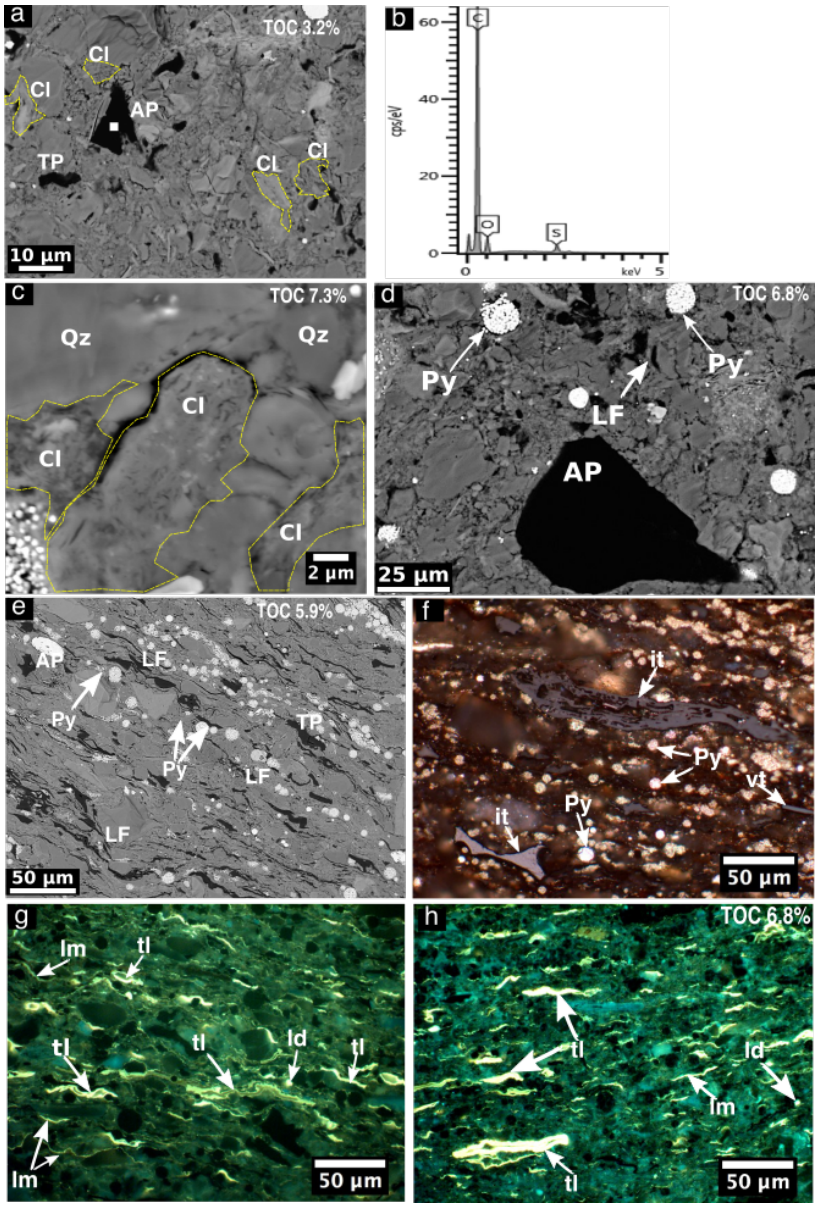

Fig. 3.2. Stuart Range Formation samples. Organic matter (black patches) is visible as discrete particles in photomicrographs at different resolutions (a, d, e). Energy dispersive X-ray analysis showing no aluminium or silicon peak (b, collected from the area marked with a white square in Fig. a reveals that the particulate organic matter is free from clay mineral (Cl) association within them. Fig. c; pore filling smectite clays within dashed outlines. Fig. e; distribution of the three major organic matter morphologies, AP=angular to sub-rounded organic particles, LF=Lamellar organic flakes and TP=Tabular organic particles. Fig. e-g; the same sample under backscatter SEM (e), reflected white (f) and fluorescent (ultra-violet) (g) light microscopy. Fig. h; distribution of liptinite macerals in a section observed under fluorescent light. Liptinite macerals are predominant in the Stuart Range Formation. Abbreviations: vt = vitrinite, it = inertinite, tl = telalginite, lm = lamalginite, ld = liptodetrinite, Py = pyrite, Qz= Quartz.

Organic matter within the Stuart Range Formation is dominated by discrete organic particles ranging in size between 5 and 50 μm. These particles occur in three morphological classes, a) angular to sub-rounded organic particles (AP) b) lamellar organic flakes (LF) and c) tabular organic particles (TP) (Fig. 3.2c and 3.2e). Angular to sub-rounded organic particles of the Stuart Range Shale vary in size from 50 μm to < 5 μm. These appear structure less in SEM BSE micrographs but their shape and sizes suggest that these are the vitrinite and inertinite grains identified by optical microscopy. They are, therefore, derived from the higher plants. Lamellar organic flakes occur parallel to the lamination of the host rock. With a thickness of < 5 μm, they are thinnest compared to the other two particulate organic matter classes (Fig. 3.2e). The lamellar organic flakes correspond to the lamalginite and telalginite grains identified by organic petrography. The third morphology is tabular organic particles with thickness varying from 5 to 10μm (Fig. 3.2e). These correspond to the bituminite including some telalginites and minor amount of sporinites as identified by organic petrography. Telalginite and lamalginite are the most abundant macerals in the Stuart Range Formation with minor sporinite and vitrinite also being common (Fig. 3.2f-h). The liptinite maceral group (e.g. telalginite, lamalginite and sporinite) has high hydrogen content and contains mostly aliphatic compounds, pointing to high potential for hydrocarbon generation compared to the other maceral groups (e.g. vitrinite, inertinite). The presence of vitrinite and inertinite indicates a terrestrial origin for some fraction of the organic matter (Fig. 3.2f). However, the dominantly marine origin of the organic matter is apparent in the predominance of liptinite macerals, high S content and the HI of > 300

mgHC/gTOC in kerogen extracts of some samples (Table 3.3). The Stuart Range Formation comprises a mixture of terrestrial and marine organic matter deposited in an intermittently reducing environment.

The middle member of Monterey Formation is comprised of laminated, intermittently burrowed mudstone recording pelagic to hemipelagic sedimentation. The petrographic images indicate the sediment is dominated by detrital clay minerals that define depositional laminae. This contrasts with the pore filling distribution of clay minerals in the Stuart Range Formation samples. The high MSA values that range from 215 to 676 m^2 /g, (Table 3.2) provide an indication of the high percentage of smectitic layers. Smectite has the highest surface area among common detrital clay minerals in which 100% smectite would equate to ~ 750 m2 /g, it is thus the only clay mineral that can account for these values. Smectite forms in soils influenced by strong seasonality or a primary volcanic source (Chamley, 1989) before being eroded, transported and deposited in marine environments. The 5 to 20 μm quartz grains isolated within the clay matrix likely record re-precipitation of silica-rich pore waters by carbonate replacement or cementation during diagenesis, a process previously described in Monterey Formation by Reimers (2001)

Table 3.3: Rock-Eval pyrolysis data of shale samples from Monterey and Stuart Range formations. Here Cal. Ro is the calculated thermal maturity from T_{max} using (Jarvie et al., 2001) equation and the measured Ro is the thermal maturity of the samples from the vitrinite reflectance measurement.

Sample ID	HI (Rock) (mgHC/g TOC)	Mean HI (Rock) (mgHC/gTOC)	HI (Kero) (mgHC/g TOC)	Mean HI (Kero) (mgHC/gTOC)	Kero HI-Rock HI (ΔHI_{K-R})	Rock Tmax (°C)	Mean Rock Tmax	Kerogen Tmax (°C)	Meaan Kero Tmax (°C)	Rock-Kero Tmax ($\Delta Tmax_{R-K}$)(°C)	Cal. Ro (%)	Measured Ro (%)
M59	346	354	420	440	86	422	422	392	392	30	0.43	0.43
	347		463			422		392				
	369		436			421		391				
M33	400	391	502	512	121	396	397	384	386	11		0.43
	385		486			398		385				
	389		547			396		388				
M28	374	363	470	448	85	408	408	391	389	19	0.19	
	352		441			408		389				
	362		433			409		388				
M21	418	425	543	567	142	422	422	394	393	29	0.44	0.41
	437		569			422		394				
	421		589			422		392				
M62	298	295	455	431	136	396	397	386	385	12		
	303		413			397		384				
	285		425			397		386				
M22	445	445	536	547	102	399	410	390	392	18	0.22	
	454		547			416		393				
	435		559			415		394				
S26	90	89	304	294	205	432	433	431	430	3	0.63	0.55
	89		249			433		430				
	89		330			433		430				
S12	72	74	110	130	56	434	435	428	428	7	0.66	0.59
	77		142			435		428				
	73		139			435		429				
S08	113	109	444	319	210	435	435	432	432	3	0.68	
	106		171			435		432				

	107		341			436		431				
S43	306	238	468	373	135	425	423	422	422	1	0.45	
	206		303			422		422				
	201		347			422		423				
S64	189	179	395	336	157	421	421	421	421	0	0.41	0.49
	172		313			421		421				
	175		300			420		422				
S81	105	100	225	197	97	417	418	418	418	0	0.36	0.51
	98		154			418		418				
	97		212			418		418				
S77	215	211	393	359	148	424	424	424	425	1	0.48	
	206		327			425		426				
	212		356			424		425				

Organic matter of the Monterey Formation is dominated by the liptinite maceral group that include bituminites and minor telalginites (Fig. 3.3g-i). These macerals are typical of a marine environment, and consistent with the HI range of 295 to 445 mgHC/gTOC (Table 3.3). The majority of the organic matter is present as bituminite that is interleaved with clay mineral matrices. This clay-bituminite mixture is similar to the 'mineral bituminous groundmass' defined by the ICCP (International Committee for Coal and Organic Petrology). The organic matter is mostly amorphous with minor telalginites and lamalginite present that is broadly disseminated throughout the sediment. Discrete organic particles are rare and comprise only a small fraction of the total organic matter. This amorphous organic matter is intimately associated with the clay mineral fraction at the nanometer scale (Fig. 3.3a and 3.3b) implying a depositional association with clay minerals similar to the organo-mineral nanocomposites described in other black shales (Kennedy et al., 2002; Kennedy et al., 2014; Löhr and Kennedy, 2014). This petrographic association is consistent with the strong correlation between MSA of the silicate fraction (dominated by smectite minerals) and TOC (R^2 = 0.91) (Fig. 3.4). The EGME surface area provides an approximation of a single monolayer coating of ethylene glycol on mineral surfaces when in equilibrium with an EGME vapour (Cihacek and Bremner, 1979). The monolayer equivalent line is drawn in Fig. 3.4 from the mass addition of ethylene glycol on a series of standard clays exposed to EGME. This reference line demonstrates that the TOC and silicate MSA relationship of Monterey samples are at a ratio similar to the molecular monolayer coating of mineral surfaces by organic compounds. Clay minerals and organic carbon forming

nanocomposites are typically "assembled" in the depositional or early diagenetic setting resulting in a physico-chemical association of organic carbon and mineral surfaces leading to enhanced preservation (Mayer, 1994; Kennedy et al., 2002). This contrasts with the much more limited surface contact between mineral surfaces and organic particles evident in the Stuart Range Formation in which the MSA and TOC do not scale because they are largely unrelated ($R^2 = 0.54$). The TOC is controlled by depositional conditions influencing sedimentation of organic particles while the MSA is dominated by later diagenetic clay minerals filling pores.

The most common organic matter morphology in the Monterey samples is an organoclay laminae (OL). Both discrete and diffusive laminae (i.e. sharp vs. diffusive boundaries) can vary widely in thickness from < 5 μm to > 50 μm. In many cases, the discrete organoclay laminae enclose larger mineral grains (Fig. 3.3a, d, f). The other common morphology observed in the Monterey Formation is sub-rounded grains of organoclay aggregates (OA) that range from 5 to 20μm in size (Fig. 3.3d). While they may look similar to the primary discrete organic particles, their EDX spectra indicate high Al content (Fig. 3.3b) and micron size clay crystals evident in high resolution images (Fig. 3.3e). This indicates that they are not solely organic in nature, rather they are an intimate mixture of clay and organic matter associated at nanometre scales. The third type of morphology is infilling organoclay matrix (OX) (Fig. 3.3f) that has the least organic carbon content. These are dispersed organoclay aggregates occurring as matrix around large mineral grains.

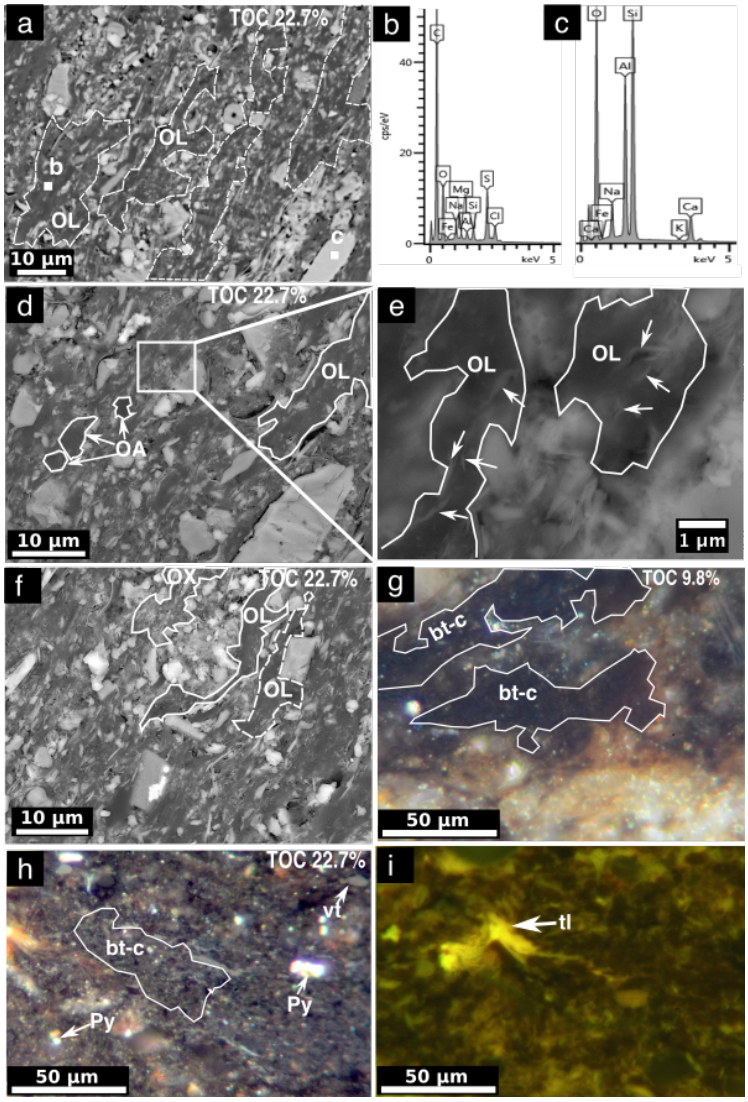

Fig. 3.3. Monterey Formation samples. Organic matter shows a complex association with clay minerals in backscattered SEM photomicrographs (a-f) and optical petrography (g-i). EDS analysis (b) of the area marked by a white square in Fig. (a) confirms the intimate association of clay minerals and organics. Fig. (c): EDS analysis of a feldspar grain marked in Fig. (a) with no carbon peak confirming that the carbon peak observed from the sample are not from the carbon coating done during SEM sample preparation. Fig. (d-f): Three types of organic matter are classified based on their morphology, OL= organoclay laminae, OA= organoclay aggregates and OX= infilling organoclay matrix. The broken outlines indicate diffusive boundaries of OL. The arrows indicate the clay mineral flakes imbedded in organic matter (e). Fig. (g, h); images under reflected white light. Fig. (i); the same section as Fig. h under fluorescent (ultra-violet) light. Here Fig. f, h and i are the same sample. Majority of the organic matter in Monterey samples are bituminite mixed with clay minerals (bt-c); vt= vitrinite, tl = telalginite, Py = pyrite.

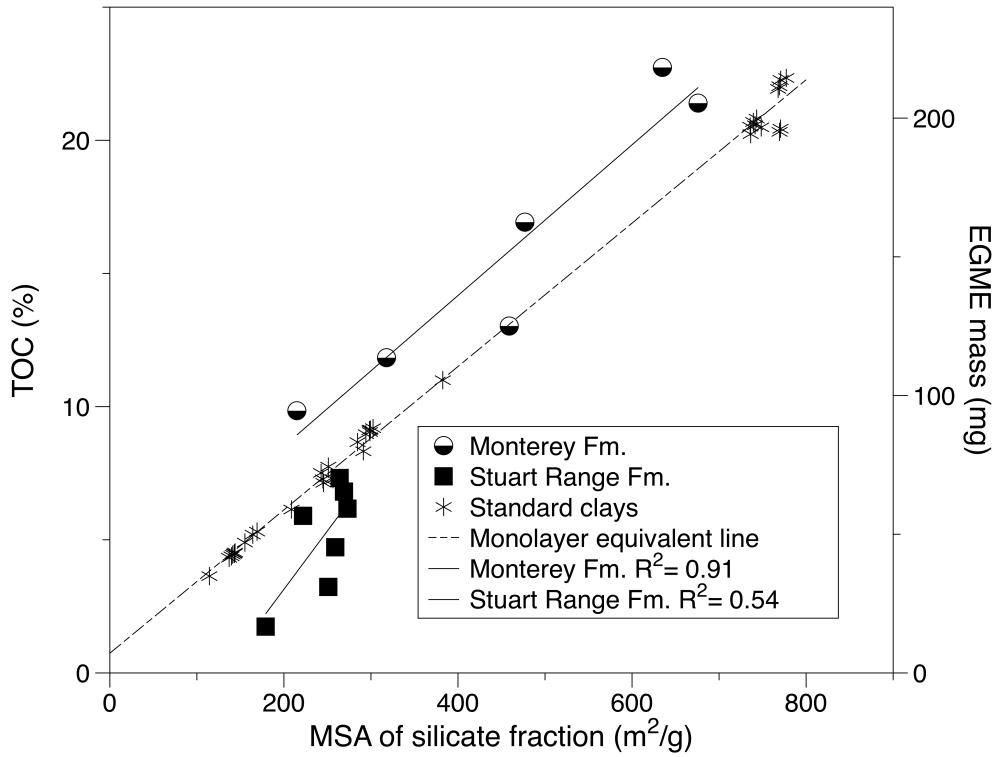

Fig. 3.4. TOC and silicate MSA cross-plots of Monterey and Stuart Range Formations. The Monterey Formation samples show a positive relationship between silicate MSA and TOC over a broad range of values, whereas Stuart Range Formation samples show no apparent relationship between silicate MSA and TOC. The monolayer equivalent line is drawn by measuring mass addition of ethylene glycol to a series of standard clays exposed to EGME. This line is included as a reference only to show how TOC and silicate MSA of the Monterey Formation samples compare to the ratio of a molecular monolayer coating of mineral surfaces by ethylene glycol.

Laboratory pyrolysis experiments provide important information on hydrocarbon generation potential of organic rich, immature samples that attempt to simulate natural hydrocarbon generation in source rocks. The hydrogen index (HI) derived from pyrolysis is a widely accepted proxy of the hydrocarbon generation potential of organic rich sedimentary rocks. Whole rock samples from the Monterey and the Stuart Range formations both show a consistently lower hydrocarbon generation potential for per gram organic carbon than their corresponding kerogen isolates (Fig. 3.5). The difference in HI between the kerogen isolate and the whole rock ($\Delta HI_{K\text{-}R}$) is much greater

in Stuart Range samples relative to Monterey Formation samples. ΔHI_{K-R} in the Monterey ranges from 85 to 142 mgHC/gTOC compared to the Stuart Range at 56 to 210 mgHC/gTOC (Table 3.3). The reduction in HI of the bulk rock relative to the kerogen HI is markedly different for Stuart Range and Monterey samples. Some Stuart Range samples have > 50% reduction in HI, whereas with similar hydrocarbon generation potential (as indicated by the kerogen HI), majority of Monterey samples show a HI reduction of < 20% (Fig. 3.6). ΔHI_{K-R} does not show a relationship with MSA (Table 3.2, and 3.3) suggesting it is not a simple function of the abundance of clay minerals.

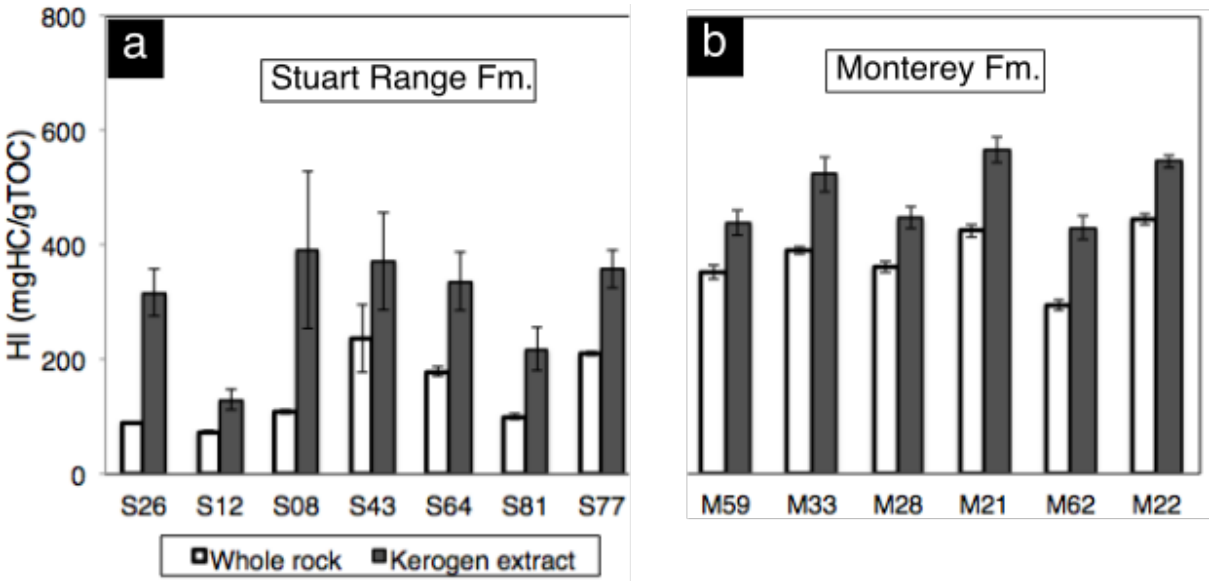

Fig. 3.5. Rock-Eval pyrolysis data of the bulk rock samples and their kerogen isolates shows lower hydrocarbon generation for whole rock samples in the Stuart Range Formation (a) and the Monterey Formation (b). This effect is significantly greater in the Stuart Range Formation. Each sample was run three times to check the reproducibility of data and to recheck the trend of whole rock hydrocarbon generation potential over that of their kerogen isolates and used to calculate standard deviation illustrated with error bars

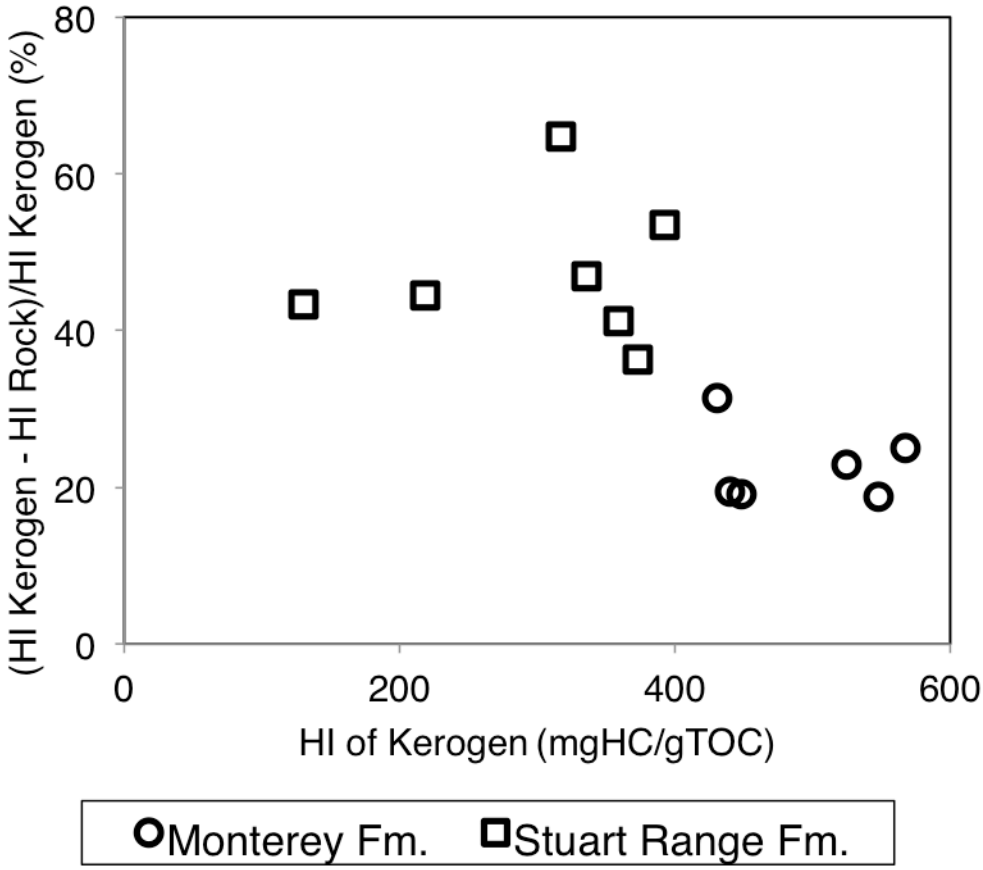

Fig. 3.6. The percentage of the hydrogen index (HI) value in bulk rock samples over the HI value for kerogen extracted from the same samples is greater in the Stuart Range Formation samples compared to Monterey Formation samples. Stuart Range samples show over 50% reduction in HI compared to Monterey samples with a HI reduction of < 20%.

T_{max} is a measure of the temperature at which maximum hydrocarbon generation occurs during pyrolysis of a sample. In general, higher temperature is required for hydrocarbon generation from samples with higher maturity and greater terrestrial organic matter abundance. Kerogen and bulk rock pairs of any given sample contain the same type of organic matter with same thermal maturity; therefore, they should show similar T_{max} during pyrolysis experiments unless the hydrocarbon generation is affected by another parameter. The difference in T_{max} of bulk rock samples to kerogen isolates (ΔT_{max}R-K) of the Monterey Formation ranges from 11 to 30°C,

whereas for the Stuart Range Formation it ranges from -1 to 6°C (Fig. 3.7). The greater ΔT_{max}R-K indicates that higher temperature is required to generate hydrocarbon from the mineral associated organic matter versus the kerogen isolate of the Monterey Formation samples. A similar relationship in Stuart Range Formation is much more subdued. The ΔT_{max}R-K shows an inversely proportional relationship with TOC in both Monterey (R^2 = 0.84) and Stuart Range samples (R^2 = 0.80, Fig. 3.8a). Similarly, in samples of Monterey Formation where organic matter is intimately associated with the clay matrices, ΔT_{max}R-K has a strong inversely proportional relationship with the MSA (R^2 = 0.93, Fig. 3.8b). This relationship does not occur between ΔT_{max}R-K and silicate MSA of the Stuart Range samples (R^2 = 0.42).

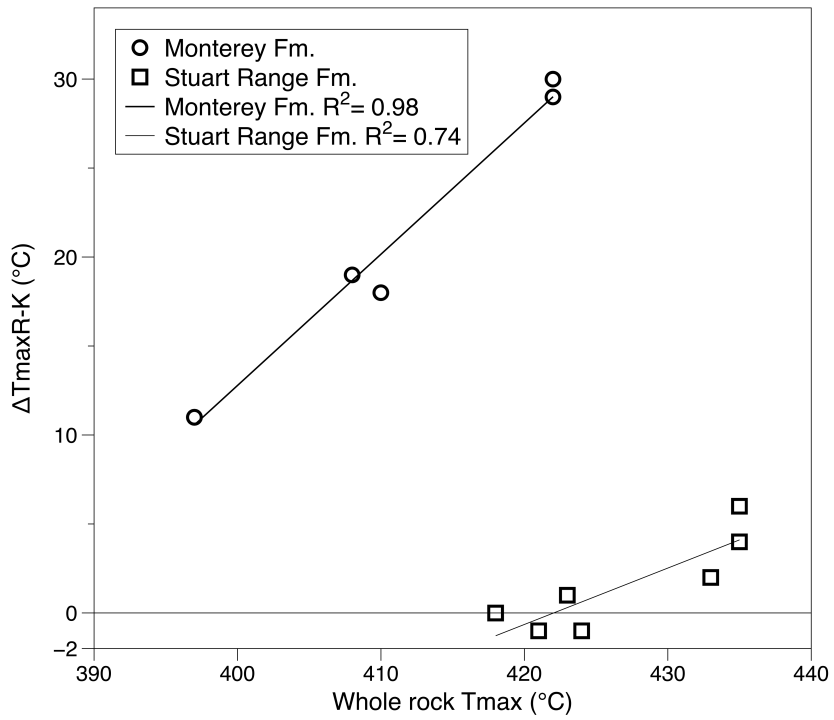

Fig. 3.7. The differences in T_{max} of whole rock compared to the kerogen extracted from the same samples (ΔT_{max}R-K) reaches 30°C depending on the nature of association of organic matter to mineral matrices as observed in Monterey and Stuart Range Formation.

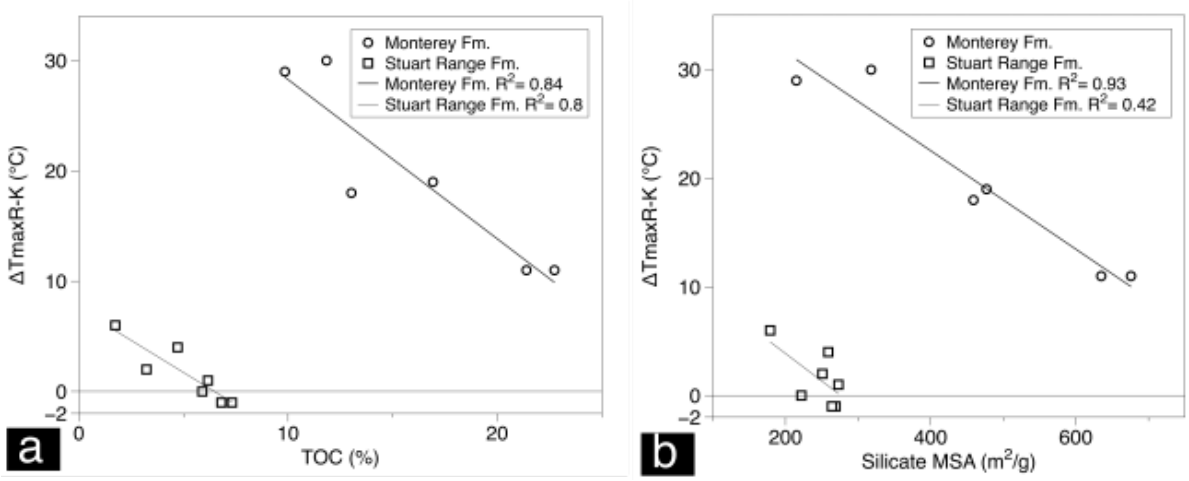

Fig. 3.8. a) An inversely proportional relationship between TOC and ΔT_{max}R-K in both Monterey and Stuart Range formations; b) ΔT_{max}R-K is inversely proportional to the surface area of silicate fraction in the Monterey Formation with no relationship in the Stuart Range Formation.

3.5. Discussion

Previous studies designed to determine the effects of mineral matrix on hydrocarbon generation compared pyrolysis results from isolated organic compounds to those of mineral-organic mixtures (Espitalie et al., 1980; Tannenbaum and Kaplan, 1985). These earlier studies used mixtures of bulk powders and did not explicitly consider the physical relationship between minerals and the organic fraction during analyses of organic-rich rock samples. However, Yuan et al. (2013) showed that the amounts of C_{1-5} hydrocarbon generated during the pyrolysis of a synthetic organic compound (12-aminolauric acid) interlayered with montmorillonite was more than 8 times greater than a simple physical mixture of the same compound with montmorillonite. This result, indicated an important role for spatial association of the organic and inorganic phases, is significant given the very different relationships minerals and organic matter can have in natural shale

that range from interlaminated nanocomposites to discrete micron scale particles. These physical associations may explain some of the variation in hydrocarbon generation during pyrolysis of experimental and natural samples. The sample sets in this study (Monterey and Stuart Range formations) were selected to investigate this potential effect because they provide examples approximating hypothetical end members of the range in physical contact between organic matter and mineral surface area. We hypothesize that depositional environment and diagenetic conditions lead to different physical associations between minerals and organic phases, which, in turn, influence hydrocarbon generation temperature and the yield.

We measured the hydrocarbon yield in bulk rock relative to their kerogen isolates for the Monterey and Stuart Range formations anticipating an increase in yield resulting from clay mineral catalysis, as found in some previous studies (e.g. Johns, 1979; Tannenbaum and Kaplan, 1985; Pan et al., 2010; Yuan et al., 2013; Hu et al., 2014). Further, we anticipated that the intimate mineral-organic carbon associations in the Monterey Formation would exaggerate this effect relative to more discrete particulate carbon that dominates the Stuart Range Formation in keeping with the results of Yuan et al. (2013). However, both Monterey and Stuart Range bulk rocks generated less hydrocarbon compared to their kerogen isolates (Fig. 3.5) in keeping with the result of Espitalie et al. (1980). While Espitalie et al. (1980) were unable to directly determine the mechanism responsible for the difference, they recognised the potential that mineral retention of generated hydrocarbons

could increase with the clay content (and thus reactive surface area) of the sediment.

Our results, however, do not support a simple mineral retention effect on hydrocarbon generation. $\Delta HI_{K\text{-}R}$ does not scale with MSA during pyrolysis in either the Monterey or Stuart Range Formation as would be anticipated if reactive surface area was the sole influence. MSA is dominated by high surface area minerals, particularly smectite minerals which have an order of magnitude greater abundance of mineral surface area relative to other clay minerals such as kaolinite or chlorite and three orders of magnitude greater than quartz or feldspar silt. Smectite also has a surface layer charge capable of coordinating polarized organic molecules and sorbing organic matter within interlayer sites (Lagaly, 1981; Aringhieri, 2004). Among the common and abundant sedimentary clay minerals that are stable on geologic time scales, smectite is considered the most effective mineral catalyst for hydrocarbon generation (Huizinga et al., 1987). While smectite is abundant in both the Stuart Range and the Monterey formations, the measurement of MSA in bulk rock does not directly identify the physical relationship of the organic matter to the mineral surfaces; it indicates only the presence of smectite. Our petrographic studies, however, reveal a very different relationship between the clay mineral and organic matter in the Monterey and Stuart Range formations. In the former, there is an intimate association between organic matter and clay minerals resulting from initial depositional and early diagenetic sedimentary processes (Fig. 3.3). In the latter, there is very limited physical contact between organic matter and clay surfaces because the clays

were formed in pores during late diagenesis (Fig. 3.2).

Both the Monterey and the Stuart Range samples show reduced hydrocarbon yield relative to their kerogen isolates (Fig. 3.5). ΔHI_{K-R}, when expressed as a percentage of kerogen HI, is both more variable and greater in the Stuart Range (up to 3.65%) compared to Monterey Formation (up to 31%) (Fig. 3.6). Though there are subtle differences in thermal maturity and the type of organic matter in the two formations, this cannot explain the significant difference in yield between kerogen isolates and whole rock samples. We argue that it is the difference in fabric, i.e. the nature of organic-mineral association that accounts for the observed differences in ΔHI_{K-R} between the two sample suites. This is consistent with the scaling of TOC with silicate MSA of Monterey samples (Fig. 3.4) at a ratio of molecular monolayer coating of mineral surfaces by organic compounds. By contrast, due to their granular texture, discrete organic particles of the Stuart Range Formation share comparatively little common surfaces with the mineral phases (Fig. 3.2). While the Stuart Range Formation has a significant fraction of clay minerals (including smectite), they are either isolated in pore spaces or only tangentially associated with organic matter (Fig. 3.2). As a consequence, the clay minerals within the Stuart Range Formation are largely free from organic coatings emplaced during deposition or early diagenesis and are therefore able to potentially sorb and retain early-generated hydrocarbons during pyrolysis which may account for the greater ΔHI_{K-R} observed in these samples.

These results imply that any influence of hydrocarbon generation resulting

from mineral association with organic matter begins with initial depositional conditions controlling shale fabric and mineralogy. A first order association between TOC and MSA occurs in many modern and ancient continental margin sediments (Keil et al., 1994; Mayer, 1994; Ransom et al., 1997; Kennedy et al., 2002; Kennedy et al., 2014; Löhr and Kennedy, 2014). MSA is dominated by the presence of clay minerals, particularly the expandable smectite group of clays. In a depositional setting where a significant fraction of the sediment is comprised of detrital clay minerals, complex interactions between organic matter and clay mineral surfaces are likely to occur at nanometre scales leading to significant physical contact between organic carbon and mineral surfaces. In sedimentary environments where detrital clays comprise a limited fraction of sediments such as the paraglacial environment in which the Stuart Range Formation was deposited, organic matter will be accumulated independently of the mineral phase. Clay minerals present will commonly represent late stage authigenic phases not related to the organic matter.

The association of organic matter with mineral surfaces thermally stabilizes organic matter as evident in the ΔT_{max}R-K. This implies an increase in temperature required to crack clay associated organic matter relative to that required for discrete organic particles. This is significant because the exploitation of commercial hydrocarbon depends to some extent on the timing of hydrocarbon generation in source rocks controlled by temperature, which in turn is influenced by the depth of the source rock interval and spatial association with temperature anomalies in the basin. Our results show that

at a given thermal maturity, the ΔT_{max}R-K increases up to 30°C in the Monterey Formation. However, when organic matter is present as discrete particles, in most cases the T_{max} does not differ much between the kerogen isolates and bulk rock samples (Fig. 3.7). In the Monterey Formation samples, a very strong correlation is observed between the bulk rock T_{max} and ΔT_{max}R-K (R^2 = 0.98) indicating an increasing influence of clay minerals with increasing temperature. For any temperature increase in bulk rock T_{max} after 390^0C, there is an almost 80% increase in ΔT_{max}R-K in these samples. By considering only the presence of clay minerals, a 5 to 12°C increase of T_{max} was previously reported for type II and type III kerogen rich shale (Espitalié, 1986). Our results show that T_{max} can be 30°C higher for whole rock samples when compared to the isolated kerogen depending on the nature of the organic matter-mineral association (Fig. 3.7).

In addition to thermal stabilisation of the organic matter by clay minerals, measured ΔT_{max}R-K may also be impacted by the sorption of early-generated hydrocarbons on free clay mineral surfaces. Once sorbed, higher temperatures are required to desorb hydrocarbons as well as for their secondary cracking (Espitalié, 1986), increasing T_{max} of bulk rock samples relative to kerogen. The maximum value of ΔT_{max}R-K occurs within the samples with lowest TOC and there is a reduction in ΔT_{max}R-K with increasing TOC in both sample sets from the Monterey and Stuart Range formations (Fig. 3.8a). ΔT_{max}R-K shows a similar inversely proportional relationship with the silicate MSA in the Monterey shale (R^2 = 0.93) that is not apparent in the Stuart Range shale (R^2 = 0.42, Fig. 3.8b). Given that silicate MSA is almost entirely a function of clay

content (and dominated by smectite clays where present) in our samples, this observation supports the influence of clay minerals on ΔT_{max}R-K in the Monterey Formation but not in the Stuart Range Formation. The observation is consistent with their fabrics, in that the Monterey shale has clay minerals that are intimately associated with organic matter while the Stuart Range shale has a particulate, discrete organic matter fabric. The diagenetic clay minerals in the Stuart Range Formation samples provide mineral surfaces that initially formed free from organic matter; therefore the ΔT_{max}R-K shows less sensitivity to the MSA. However, these mineral surfaces can potentially adsorb hydrocarbons during generation because the surfaces are not occupied by organic compounds as they might be in the case of the Monterey Formation samples. Thus the Stuart Range Formation has a greater potential for retention during hydrocarbon generation. This suggestion is consistent with the relationship observed between the ΔTmaxR-K (i.e. higher mineral retention), TOC and MSA that indicates TOC and surface area are unrelated (Fig. 3.9). That is when higher ΔTmaxR-K is observed in samples with organic carbon free authigenic clay mineral surfaces determined by lower TOC/MSA values (R^2 = 0.78). This relationship is not apparent in the Monterey Formation (R^2 = 0.40) where presumably detrital clay mineral surfaces are coated with organic matter during or shortly after deposition.

To better understand hydrocarbon generation temperature and timing, the physical association of kerogen with mineral surfaces needs to be accounted for in addition to the kerogen type. Kerogen in shale is commonly classified using its hydrogen and oxygen content determined from pyrolysis as type I to

type IV. The samples from the Monterey and Stuart Range Formations show a significant shift in the modified Van Krevelen diagram (van Krevelen, 1961) when whole rock versus kerogen isolates are plotted (Fig. 10) providing a different kerogen type. This diagram is frequently used to predict the origin (marine, terrestrial or lacustrine), potential, maturity and generation products of shale. The evident shift towards lower HI and higher T_{max} from kerogen isolates to whole rock samples in Fig. 3.10 results from the mineral matrix effect resulting in a reclassification of some samples from type II to type III. Kerogen typing may thus be a function of more than the organic matter composition.

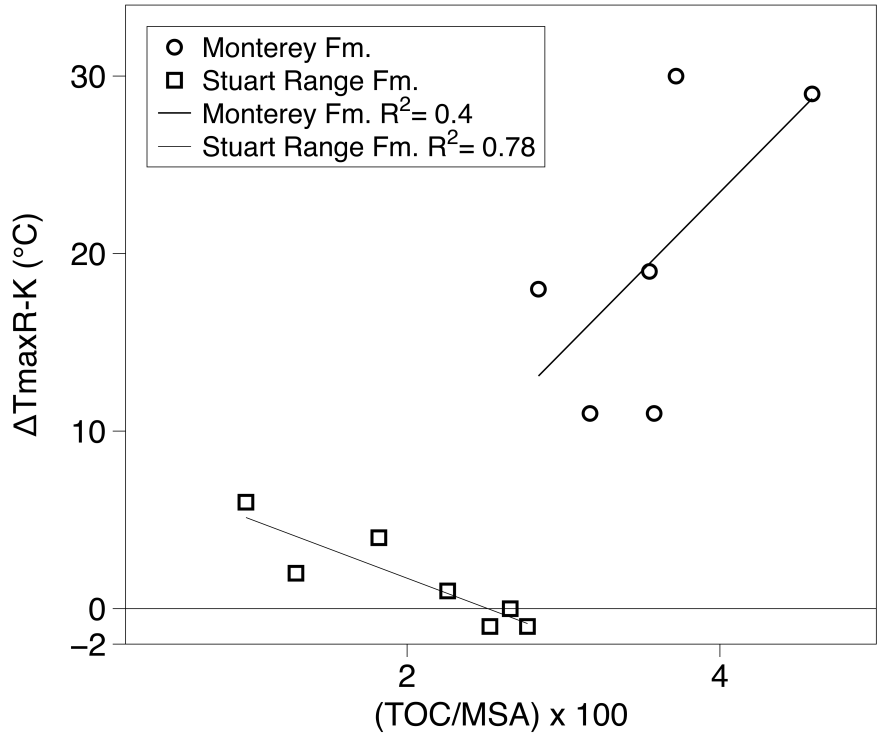

Fig. 3.9. The difference in T_{max} of kerogen isolates and their whole rock (ΔT_{max}R-K) shows an inverse relation with the TOC/MSA in Stuart Range Formation samples. No relationship in Monterey Formation samples is evident. The TOC/MSA is interpreted to represent a general association between mineral surfaces and organic carbon that might have coated the surfaces.

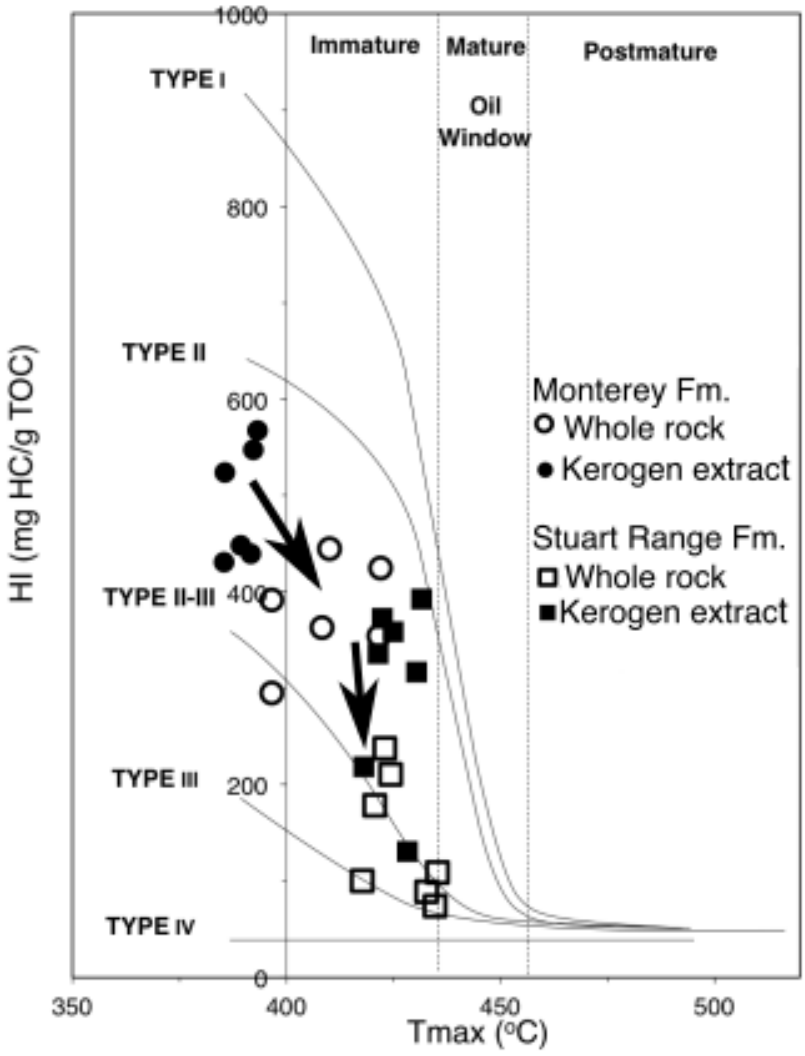

Fig. 3.10: Whole rock compared to kerogen extracted from the same samples plotted on a modified Van Krevelen diagram illustrating the effect minerals have on kerogen typing during pyrolysis. The arrows indicate shifts of kerogen on the crossplot due to their associations with mineral matrices.

Clay minerals have a general retention effect during hydrocarbon generation in organic rich shale. Among the common and geologically stable clay mineral families, smectites have the greatest surface area and potential to adsorb organic matter in depositional or early diagenetic environments to form organoclay aggregates. However, the hydrocarbon retention effects are not entirely controlled by the presence of clay minerals, as some clays may precipitate in pore spaces away from organic carbon. The depositional

environment and type and quantity of detrital versus authigenic clays influence the association between organic matter and mineral surfaces. In the two cases studied here, these associations influence hydrocarbon yield as well as the generation temperature.

3.6. Conclusions

SEM and organic petrography analyses of two organic rich shale formations from South Australia and California, USA, revealed two major types of shale fabric: organoclay aggregates and particulate. In the Monterey Formation, organic matter occurs in a close association with clay minerals at nanometre scale as organoclay aggregates. Organic matter in the Stuart Range Formation, by contrast, occurs as discrete organic particles at μm scale and clay minerals are present as authigenic phases in pores. In the Monterey Formation, detrital clays likely formed clay-organic associations during or soon after deposition of sediments at nanometre scales. In the Stuart Range Formation, pore filling clay minerals formed during diagenesis are spatially unrelated to organic matter. This observation is consistent with the positive relationship between TOC and MSA in Monterey Formation ($R^2 = 0.91$) and the contrasting lack of relationship between TOC and MSA in Stuart Range Formation ($R^2 = 0.54$).

Both the Monterey and Stuart Range formations show retention in hydrocarbon yield due to mineral matrix effects in bulk rock as compared to their kerogen isolates. The magnitude of this retention effect varies with the detrital versus authigenic clay components. Clay mineral surfaces associated

with organic matter during deposition result in less retention during hydrocarbon generation compared to authigenic clay minerals that have organic carbon-free surfaces.

During pyrolysis, shale samples with nanocomposites generate maximum hydrocarbon at higher temperatures compared to shale samples dominated by particulate organic matter. A higher T_{max} difference (between bulk rock and kerogen isolate pairs) is observed in the Monterey Formation samples compared to Stuart Range Formation samples with former varying as much as 30°C between the kerogen isolates and their bulk rock.

A significant shift in kerogen typing between the bulk rock and the extracted kerogen is evident in the modified Van Krevelen diagram. This implies that the shale texture as well as the actual kerogen composition influences this common classification scheme. While limited to two examples of shale fabric, this study suggests that the physical association of organic matter with clay minerals rather than just the presence or absence of particular types of clay minerals may play an important role in determining the temperature and quantity of hydrocarbon generation in shale.

Acknowledgements

The Australian Research Council (ARC) is acknowledged for providing financial support (ARC Linkage Project LP120200086 to M. J. Kennedy) to conduct the research project. We thank Tony Hall from the University of Adelaide for helping with the pyrolysis experiments and XRD analyses. We

are thankful to Simon George from Macquarie University for his assistance on solvent extractions. We acknowledge Neil Sherwood from CSIRO for helping with organic petrography. SEM analyses were conducted using microscope facilities at the Department of Earth and Planetary Sciences and the Biology Microscopy Unit at Macquarie University.

References

Abid, I., Hesse, R., 2007. Illitizing fluids as precursors of hydrocarbon migration along transfer and boundary faults of the Jeanne d'Arc Basin offshore Newfoundland, Canada. Marine and Petroleum Geology 24, 237-245.

Acholla, F.V., Orr, W.L., 1993. Pyrite removal from kerogen without altering organic matter: the chromous chloride method. Energy & fuels 7, 406-410.

Alexander, E.M., Sansome, A., Cotton, T.B., 2006. Lithostratigraphy and environments of deposition, in: Cotton, T.B., Scardigno, M.F., Hibburt, J.E. (Eds.), The Petroleum Geology of South Australia Vol.2: Eromanga Basin. Department of Primary Industry and Resources, Adelaide.

Aringhieri, R., 2004. Nanoporosity Characteristics of Some Natural Clay Minerals and Soils. Clays and Clay Minerals 52, 700-704.

Australian Standards, 1998. AS 2856.2: Coal Petrography. Part 2: Maceral Analysis.

Barron, J.A., 1986. Paleoceanographic and tectonic controls on deposition of the Monterey formation and related siliceous rocks in California. Palaeogeography, Palaeoclimatology, Palaeoecology 53, 27-45.

Belin, S., Huc, A.Y., 2001. Organic Matter Microhabit Within the Monterey Formation (Miocene of California). The Monterey Formation: From Rocks to Molecules, 77.

Berndmeyer, C., Birgel, D., Brunner, B., Wehrmann, L.M., Jöns, N., Bach, W., Arning, E.T., Föllmi, K.B., Peckmann, J., 2012. The influence of bacterial activity on phosphorite formation in the Miocene Monterey Formation, California. Palaeogeography, Palaeoclimatology, Palaeoecology 317–318, 171-181.

Bishop, A., Kearsley, A., Patience, R., 1992. Analysis of sedimentary organic materials by scanning electron microscopy: the application of backscattered electron imagery and light element X-ray microanalysis. Organic Geochemistry 18, 431-446.

Blair, N.E., Aller, R.C., 2012. The fate of terrestrial organic carbon in the marine environment. Annual Review of Marine Science 4, 401-423.

Boggs, S., 2009. Petrology of sedimentary rocks. Cambridge University Press.

Chamley, H., 1989. Clay sedimentology / Hervé Chamley. Springer-Verlag, London New York.

Cihacek, L., Bremner, J., 1979. A simplified ethylene glycol monoethyl ether procedure for assessment of soil surface area. Soil Science Society of America Journal 43, 821-822.

Clark, J., Comerford, J., Macquarrie, D.J., 2013. Green Catalytic Transformations, in: Anastas, P.T., Zimmerman, J.B. (Eds.), Innovations in Green Chemistry and Green Engineering. Springer New York, pp. 37-80.

Compton, J.S., 1991. Porosity reduction and burial history of siliceous rocks from the Monterey and Sisquoc Formations, Point Pedernales area, California. Geological Society of America Bulletin 103, 625-636.

Debenham, N., 2015. Controls on organic carbon enrichment in a Permian Periglacial setting (Arckaringa Basin), MSc Thesis, Earth and Planetary Sciences. Macquarie University, Sydney, pp. 15 - 39.

Durand, B., 1980. Kerogen: Insoluble organic matter from sedimentary rocks. Editions technip.

Espitalié, J., 1986. Use of Tmax as a maturation index for different types of organic matter. Comparison with vitrinite reflectance, Thermal modelling in sedimentary basins. Editions Technip Paris, pp. 475-496.

Espitalie, J., Madec, M., Tissot, B., 1980. Role of mineral matrix in kerogen pyrolysis: influence on petroleum generation and migration. AAPG Bulletin 64, 59-66.

Föllmi, K.B., Badertscher, C., de Kaenel, E., Stille, P., John, C.M., Adatte, T., Steinmann, P., 2005. Phosphogenesis and organic-carbon preservation in the Miocene Monterey Formation at Naples Beach, California—The Monterey hypothesis revisited. Geological Society of America Bulletin 117, 589-619.

Galwey, A.K., 1972. The rate of hydrocarbon desorption from mineral surfaces and the contribution of heterogeneous catalytic-type processes to petroleum genesis. Geochimica et Cosmochimica Acta 36, 1115-1130.

Garrels, R.M., Mackenzie, F.T., 1971. Evolution of sedimentary rocks.

Garrison, R.E., Hoppie, B.W., Grimm, K.A., 1994. Phosphates and dolomites in coastal upwelling sediments of the Peru margin and the Monterey Formation (Naples Beach section), California.

Gilby, A.R., Foster, C.B., 1988. Early Permian palynology of the Arckaringa Basin, South Australia. Palaeontographica Abteilung B, 167-191.

Goldstein, J.I., Newbury, D.E., Echlin, P., Joy, D.C., Fiori, C., Lifshin, E., 1981. Scanning electron microscopy and X-ray microanalysis. A text for biologists, materials scientists, and geologists. Plenum Publishing Corporation.

Graham, S., Williams, L., 1985. Tectonic, depositional, and diagenetic history of Monterey Formation (Miocene), central San Joaquin basin, California. AAPG Bulletin 69, 385-411.

Heller-Kallai, L., Aizenshtat, Z., Miloslavski, I., 1984. The effect of various clay minerals on the thermal decomposition of stearic acid under 'bulk flow'conditions. Clay Miner 19, 779-788.

Hibburt, J.E., 1984. A Review of exploration in the Arckaringa Basin, Report Book 84/1, South Australia, pp. 1887-1983.

Hornafius, J.S., 1994. Field Guide to the Monterey Formation between Santa Barbara and Gaviota, California.

Hower, J., Eslinger, E.V., Hower, M.E., Perry, E.A., 1976. Mechanism of burial metamorphism of argillaceous sediment: 1. Mineralogical and chemical evidence. Geological Society of America Bulletin 87, 725-737.

Hu, M., Cheng, Z., Zhang, M., Liu, M., Song, L., Zhang, Y., Li, J., 2014. Effect of Calcite, Kaolinite, Gypsum, and Montmorillonite on Huadian Oil Shale Kerogen Pyrolysis. Energy & fuels 28, 1860-1867.

Huizinga, B.J., Tannenbaum, E., Kaplan, I.R., 1987. The role of minerals in the thermal alteration of organic matter—III. Generation of bitumen in laboratory experiments. Organic Geochemistry 11, 591-604.

Isaacs, C.M., 2001. Depositional framework of the Monterey formation, California. The Monterey Formation: From Rocks to Molecules, 1-30.

Jarvie, D.M., Claxton, B.L., Henk, F., Breyer, J., 2001. Oil and shale gas from the Barnett Shale, Ft, Worth Basin, Texas (abs.): AAPG Annual Meeting Program, p. A100.

Johns, W.D., 1979. Clay mineral catalysis and petroleum generation. Annual review of Earth and planetary sciences 7, 183.

Johns, W.D., Shimoyama, A., 1972. Clay minerals and petroleum-forming reactions during burial and diagenesis. AAPG Bulletin 56, 2160-2167.

Keil, R.G., Montlucon, D.B., Prahl, F.G., Hedges, J.I., 1994. Sorptive preservation of labile organic matter in marine sediments. Nature 370, 549-552.

Kennedy, M.J., Löhr, S.C., Fraser, S.A., Baruch, E.T., 2014. Direct evidence for organic carbon preservation as clay-organic nanocomposites in a Devonian black shale; from deposition to diagenesis. Earth and Planetary Science Letters 388, 59-70.

Kennedy, M.J., Pevear, D.R., Hill, R.J., 2002. Mineral surface control of organic carbon in black shale. Science 295, 657-660.

Kennedy, M.J., Wagner, T., 2011. Clay mineral continental amplifier for marine carbon sequestration in a greenhouse ocean. Proceedings of the National Academy of Sciences 108, 9776-9781.

Lagaly, G., 1981. Characterization of clays by organic compounds. CLAY MINER. Clay Miner. 16, 1.

Laurent, D., de Kaenel, E., Spangenberg, J.E., Föllmi, K.B., 2015. A sedimentological model of organic-matter preservation and phosphogenesis in the Miocene Monterey Formation at Haskells Beach, Goleta (central California). Sedimentary Geology 326, 16-32.

Li, Y., Cai, J., Song, G., Ji, J., 2015. DRIFT spectroscopic study of diagenetic organic–clay interactions in argillaceous source rocks. Spectrochimica Acta Part A: Molecular and Biomolecular Spectroscopy 148, 138-145.

Linc Energy, 2012. ARCK-1 well completion report, PEL 122, Arckaringa basin, South Australia. Department of State Development, Adelaide.

Löhr, S.C., Baruch, E.T., Hall, P.A., Kennedy, M.J., 2015. Is organic pore development in gas shales influenced by the primary porosity and structure of thermally immature organic matter? Organic Geochemistry 87, 119-132.

Löhr, S.C., Kennedy, M.J., 2014. Organomineral nanocomposite carbon burial during Oceanic Anoxic Event 2. Biogeosciences 11, 4971-4983.

Mayer, L.M., 1994. Surface area control of organic carbon accumulation in continental shelf sediments. Geochimica et Cosmochimica Acta 58, 1271-1284.

McCabe, R.W., Adams, J.M., 2013. Clay Minerals as Catalysts, in: Bergaya, F., Gerhard, L. (Eds.), Developments in Clay Science. Elsevier, UK, pp. 491-538.

Orr, W.L., 1986. Kerogen/asphaltene/sulfur relationships in sulfur-rich Monterey oils. Organic Geochemistry 10, 499-516.

Pan, C., Jiang, L., Liu, J., Zhang, S., Zhu, G., 2010. The effects of calcite and montmorillonite on oil cracking in confined pyrolysis experiments. Organic Geochemistry 41, 611-626.

Pevear, D.R., 1999. Illite and hydrocarbon exploration. Proceedings of the National Academy of Sciences 96, 3440-3446.

Potter, P.E., Maynard, J.B., Depetris, P.J., 2005. Mud and mudstones: Introduction and overview. Springer Science & Business Media.

Rahman, H.M., Kennedy, M., Löhr, S., Dewhurst, D.N., 2017. Clay-organic association as a control on hydrocarbon generation in shale. Organic Geochemistry 105, 42-55.

Ransom, B., Bennett, R.H., Baerwald, R., Shea, K., 1997. TEM study of in situ organic matter on continental margins: occurrence and the "monolayer" hypothesis. Marine Geology 138, 1-9.

Reimers, C.E., 2001. Petrographic clues to processes leading to high organic carbon concentrations in the Naples Beach section of the Monterey Formation. The Monterey Formation, 59-76.

Salmon, V., Derenne, S., Lallier-Vergès, E., Largeau, C., Beaudoin, B., 2000. Protection of organic matter by mineral matrix in a Cenomanian black shale. Organic Geochemistry 31, 463-474.

Shaw, D.B., Weaver, C.E., 1965. The mineralogical composition of shales. Journal of Sedimentary Research 35.

Sherrod, L.A., Dunn, G., Peterson, G.A., Kolberg, R.L., 2002. Inorganic Carbon Analysis by Modified Pressure-Calcimeter Method. Soil Science Society of America Journal 66, 299-305.

Shimoyama, A., Johns, W.D., 1971. Catalytic conversion of fatty acids to petroleum-like paraffins and their maturation. Nature 232, 140-144.

Tannenbaum, E., Huizinga, B.J., Kaplan, I.R., 1986. Role of minerals in thermal alteration of organic matter--II: a material balance. AAPG Bulletin 70, 1156-1165.

Tannenbaum, E., Kaplan, I.R., 1985. Role of minerals in the thermal alteration of organic matter—I: Generation of gases and condensates under dry condition. Geochimica et Cosmochimica Acta 49, 2589-2604.

Teln, N., Hanesand, T., Hermansen, D., Jarvie, D.M., 2001. Characterization of Source Rock Potential, Hydrocarbon Generation, and Maturity in Well OCS-315-1, Offshore Santa Maria Basin, California. The Monterey Formation: From Rocks to Molecules, 310.

Tennyson, M.E., Isaacs, C.M., 2001. Geologic setting and petroleum geology of Santa Maria and Santa Barbara basins, coastal California. The Monterey Formation From Rocks to Molecules, 206-229.

Tiller, K., Smith, L., 1990. Limitations of EGME retention to estimate the surface area of soils. Soil Research 28, 1-26.

Townsend, I.J., 1976. A synthesis of stratigraphic drilling in the Arckaringa Basin, Report of Investigations. South Australia geological Survey, South Australia, pp. 1969 - 1971.

Tyson, R.V., 1994. Sedimentary organic matter : organic facies and palynofacies / R. V. Tyson. London : Chapman & Hall, London.

van Krevelen, D.W., 1961. Coal. Elsevier.

Varma, R.S., 2002. Clay and clay-supported reagents in organic synthesis. Tetrahedron 58, 1235-1255.

Wohling, D., Keppel, M., Fulton, S., Costar, A., Sampson, L., Berens, V., 2013. Australian Government initiative on coal seam gas and large coal mining, Arckaringa Basin and Pedirka Basin Groundwater Assessment Projects. Department of Environment, Water and Natural Resources, Adelaide, Australia, p. 10.

Yuan, P., Liu, H., Liu, D., Tan, D., Yan, W., He, H., 2013. Role of the interlayer space of montmorillonite in hydrocarbon generation: An experimental study based on high temperature-pressure pyrolysis. Applied Clay Science 75-76, 82-91.

Chapter 4. The influence of shale depositional fabric on the kinetics of hydrocarbon generation through control of mineral surface contact area on clay catalysis

Habibur M Rahman[a*], Martin Kennedy[a], Stefan Löhr[a], David N Dewhurst[b], Neil Sherwood[c], Shengyu Yang[d], Brian Horsfield[d]

[a] *Department of Earth and Planetary Sciences, Macquarie University, Sydney, New South Wales 2109, Australia*

[b] *CSIRO Energy, Perth, Western Australia, Australia*

[c] *CSIRO Energy, Sydney, New South Wales 2113, Australia*

[d] *GFZ German Research Centre for Geosciences, Telegrafenberg, 14473 Potsdam, Germany*

* *Corresponding author at: Department of Earth and Planetary Sciences, Macquarie University, Sydney, NSW 2109, Australia. Tel: +61-2-9850-8426.*

E-mail address: mdhabibur.rahman@mq.edu.au, hrahman039@gmail.com

Statement of authors' contribution

This chapter is a published paper in *Geochimica et Cosmochimica Acta* (Rahman et al., 2018). This paper has been formatted to conform to the font and referencing style adopted in the thesis. Figures and tables included within the text are prefixed with the chapter number. This chapter documents the effects of particulate and nanocomposite shale fabrics on hydrocarbon generation kinetics, which is the third objective of the thesis. In this chapter, including high-resolution petrography, bulk kinetic experiments

are performed on particulate and nanocomposite shale samples. I am the primary author of this manuscript. I examined data including sample selection, sampling and sample preparation for this study. I performed all the experiments and analyses used in this manuscript except the kinetic experiment. Kinetic experiment is run by Brian Horsfield at the GFZ German Research Centre for Geosciences, Potsdam, Germany. I processed and interpreted all the data derived from the conducted analyses and experiments. I wrote and designed the paper's structure. Martin Kennedy, Stefan Löhr, David Dewhurst, Neil Sherwood and Brian Hosfield carefully reviewed and provided feedbacks and various refinements on the manuscript. Neither this manuscript nor one with similar content under our authorship has been published or is being considered for publication elsewhere, except as described above.

Abstract

Accurately assessing the temperature and hence the depth and timing of hydrocarbon generation is a critical step in the characterization of a petroleum system. Clay catalysis is a potentially significant modifier of hydrocarbon generation temperature, but experimental studies of clay catalysis show inconsistent or contradictory results. This study tests the hypothesis that source rock fabric itself is an influence on clay mineral catalysis as it controls the extent to which organic matter and clay minerals are physically associated. Two endmember clay-organic fabrics distinguish the source rocks studied: 1) a particulate fabric where organic matter is present as discrete, >5 μm particles and 2) a nanocomposite fabric in which

amorphous organic matter is associated with clay mineral surfaces at sub-micron scale. High-resolution electron imaging and bulk geochemical characterisation confirm that samples of the Miocene Monterey Formation (California) are representative of the nanocomposite source rock endmember, whereas samples from the Permian Stuart Range Formation (South Australia) represent the particulate source rock endmember. Kinetic experiments are performed on paired whole rock and kerogen isolate samples from these two formations using open system, non-isothermal pyrolysis at three different heating rates (0.7, 2 and 5 K/min) to determine the effects of the different shale fabrics on hydrocarbon generation kinetics. Extrapolation to a modelled geological heating rate shows a 20°C reduction in the onset temperature of hydrocarbon generation in Monterey Formation whole rock samples relative to paired kerogen isolates. This result is consistent with the Monterey Formations's nanocomposite fabric where clay catalysis can proceed because reactive clay minerals are intimately associated with organic matter. By contrast, there is no significant difference in the modelled hydrocarbon generation temperature of paired whole rock and kerogen isolates from the Stuart Range Formation. This is consistent with its particulate fabric, where relatively large, discrete organic particles have limited contact with the mineral matrix and the clay minerals are mainly diagenetic and physically segregated within pores. While heating rate may have a control on mineral matrix effects, this result shows that the extent to which organic matter and clay minerals are physically associated could have a significant effect on the timing of hydrocarbon generation, and is a function of the depositional environment and detrital vs diagenetic origin of clay minerals in source rocks.

Keywords: Hydrocarbon generation kinetics, clay catalysis; shale fabric; organoclay nanocomposite; Monterey Formation; Stuart Range Formation

4.1. Introduction

Burial depth, temperature and residence time are the key factors controlling the major physical and chemical transformations of sedimentary organic matter after deposition (Tissot and Welte, 1984), including the generation of liquid and gaseous hydrocarbons from geopolymers (kerogen). An accurate assessment of generation temperature and hence the depth and timing of hydrocarbon generation is an important component of the characterization of a petroleum system using basin modelling and is critical for the success of petroleum exploration. The impact of organic matter type on hydrocarbon generation temperature is well understood (van Krevelen, 1961). By contrast, the influence of reactive clay mineral surfaces, long considered potential catalysts of hydrocarbon generation (Shaw and Weaver, 1965), is not fully resolved. Their influence on hydrocarbon yield is equivocal, and whether and under what conditions mineral surfaces influence hydrocarbon generation temperatures remains poorly constrained.

A potential regulator of clay-mineral catalysis is the extent to which kerogen and mineral surfaces are in physical contact within source rocks. Organic matter in sedimentary rocks commonly comprises discrete, > 5 μm in diameter, primary particles 'floating' in the mineral matrix (Tyson, 1994). In these cases, the extent of mineral-organic matter contact is limited to the external surface area of a given organic particle (Fig. 4.1a). However, a

second class of mineral-associated organic matter is dominant in many examples of modern sediments (e.g. Keil et al., 1994; Mayer, 1994; Blair and Aller, 2012) and ancient thermally immature, organic-rich rocks (e.g. Salmon et al., 2000; Kennedy et al., 2002; Kennedy et al., 2014; Löhr and Kennedy, 2014). In these cases, organic matter and clay minerals are intimately associated at nanometre scales to form organoclay aggregates and nanocomposites. This 'nanocomposite' fabric provides substantially greater contact area between organic compounds and charged mineral surfaces per unit volume of organic matter (Fig. 4.1b) compared to rocks containing more discrete organic matter and this close physical association likely has higher potential to catalyse hydrocarbon generation.

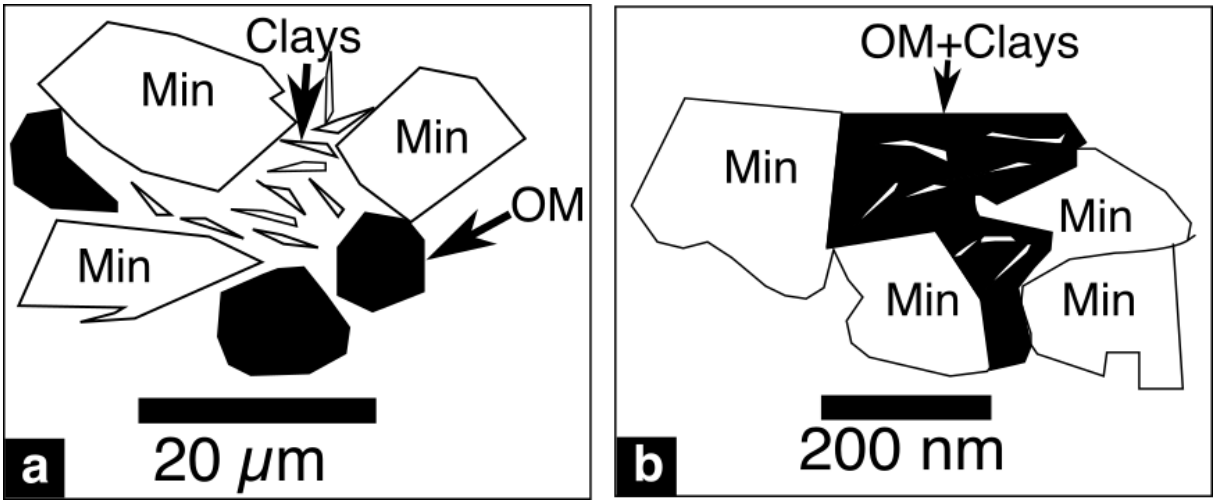

Fig. 4.1: Schematic diagram illustrating the two end member shale fabrics with a) discrete, particulate organic matter, and b) organic matter intimately associated with clay minerals in rock matrices (modified from Rahman et al., 2017).

A number of studies have investigated the potential effects of clay minerals on hydrocarbon generation using laboratory pyrolysis experiments (Shimoyama and Johns, 1971; Galwey, 1972; Johns, 1979; Espitalie et al., 1980; Pan et al., 2010; Yuan et al., 2013). However, Rahman et al. (2017)

were the first to investigate the influence of shale fabric in this context, using Rock-Eval pyrolysis of paired whole rock-kerogen isolate samples corresponding to two endmember fabrics (particulate and nanocomposite) to test mineral matrix effects on hydrocarbon generation. Their results suggest that the varying degree to which organic matter coats and is exposed to reactive clay mineral surfaces influences hydrocarbon yield and temperature of maximum rate of hydrocarbon generation (T_{max}) during experimental pyrolysis. While a reduction in hydrocarbon yield for bulk rock samples relative to their kerogen isolates was observed for both particulate and nanocomposite sample suites, consistent with earlier studies (e.g. Espitalie et al., 1980), the difference in hydrocarbon yield between kerogen isolates and whole rock is generally greater and more variable for the particulate sample suite (56 to 210 mgHC/gTOC for the particulate samples versus 85 to 142 mgHC/gTOC for the nanocomposite samples). The authors attributed this to greater hydrocarbon retention by the free mineral surfaces typical of the diagenetic clay-dominated, particulate organic matter sample suite. Lower retention on the detrital clay mineral surfaces already coated with organic matter was evident for the nanocomposite sample suite. In addition, a greater difference between the whole rock (R) and kerogen (K) isolate T_{max} values was reported for the nanocomposite sample suite (mean $\Delta T_{maxR\text{-}K}$ of 20°C) than for the particulate sample suite (mean $\Delta T_{maxR\text{-}K}$ of 2°C). The question remains if these differences are also evident at lower, geologically relevant temperatures and heating rates that are nine orders of magnitude slower than those employed during laboratory pyrolysis.

Kinetic theory dictates that temperature can be swapped for time as far as organic reactions are concerned, and this is the basis of using first order kinetic models to study the generation of petroleum in time and space (Ungerer and Pelet, 1987; Burnham et al., 1988; Behar et al., 1997; Schenk et al., 1997). This is certainly true for the maturation of aliphatic geopolymers in source rocks for which cracking reactions dominate (Schenk and Horsfield, 1998). Indeed, kinetic models are applied routinely in petroleum system evaluation (Braun and Burnham, 1987; Tissot et al., 1987; Espitalie et al., 1988; Ungerer et al., 1988; Pepper and Corvi, 1995; Peters et al., 2015; Abbassi et al., 2016; Romero-Sarmiento et al., 2016). Dembicki (1992) proposed that the same logic could be applied to organic-inorganic interactions, and suggested that whole rocks be pyrolysed in preference to kerogen concentrates for predicting the extent of petroleum forming reactions in nature. Pelet (1994) and Burnham (1994) argued for clarification of issues related to pyrolysis system design and data processing from that which actually occurs in nature such as the presence or absence of water (Lewan and Roy, 2011). Differences in sample preparation techniques affecting the physical relationship between organic compounds and mineral surfaces also need to be considered. Recently, Yang and Horsfield (2016) related mineral matrix effects on bulk petroleum-forming reactions to heating rate (using MSSV pyrolysis), and demonstrated that the effects are greatly weakened with decreasing heating rate in laboratory experiments implying that the mineral matrix was unlikely to have a significant effect on hydrocarbon generation over geologic time periods in nature.

While an accurate prediction of organic-inorganic reactions in nature is difficult, it is nevertheless instructive to examine the types of reactions occurring under laboratory conditions that are associated with any given lithofacies or organofacies, in other words different genetic combinations of kerogen types and minerals in contrasting rock fabrics. The present study is the first to explore differences in the kinetics of hydrocarbon generation resulting from a contrast in organic-mineral contact area inherent in different shale fabrics with the potential to modify the extent of clay mineral catalysis of hydrocarbon generation. Two shale sample suites with different fabrics were selected based on detailed petrographic analyses: 1) a particulate fabric in which organic matter is present as discrete organic particles >5 μm in diameter and 2) a nanocomposite fabric, in which organic matter and clay mineral surfaces are intimately associated at the nanometer scale to form organoclay aggregates and nanocomposites. Paired whole rock and kerogen isolates from the two sample suites were used in a series of pyrolysis experiments and kinetic modelling to identify any differences in petroleum generation temperature resulting from the physical association between the mineral matrix and organic matter.

4.2. Materials and Methods

4.2.1. Background

Two source rocks with distinct textural relationships between organic matter and minerals were selected as representatives of two shale fabric endmembers: a) the Miocene Monterey Formation of California, USA and b) the early Permian Stuart Range Formation of the Arckaringa Basin, South

Australia. The Monterey Formation is dominated by detrital, high surface area clay minerals and displays a positive relationship between total organic carbon (TOC) content and mineral surface area (MSA) that is proportional to a molecular monolayer coating of organic carbon (Kennedy et al., 2002). Visually, organic matter is intimately dispersed with clay minerals at sub-micron scales. The Stuart Range Formation, by contrast, is dominated by silt-sized detrital grains comprising feldspar and quartz, while clay mineral phases are restricted to diagenetic pore-filling habits. Organic matter is dominated by discrete detrital particles largely unrelated to the clay mineral fraction (Rahman et al., 2017). Both formations were deposited in an intermittently anoxic marine environment (Hibburt, 1984; Orr, 1986; Gilby and Foster, 1988; Tennyson and Isaacs, 2001; Alexander et al., 2006), contain organic matter with varying quantities of sulphur and are of comparable low thermal maturity (see Tannenbaum and Kaplan, 1985; Compton, 1991; Belin and Huc, 2001; Isaacs, 2001; Föllmi et al., 2005; Berndmeyer et al., 2012; Debenham, 2015; Laurent et al., 2015).

4.2.2. Materials

The samples used for this study are a subset of the samples previously characterised by Rahman et al. (2017). Organic rich (TOC: 5 to 21 wt.%) samples (Table 4.1) representing the nanocomposite fabric class were selected from the middle member of the Miocene Monterey Formation at the Naples Beach section located west of Santa Barbara, California, USA. A complete exposure crops out in wave-cut coastal cliffs at the Naples Beach section and is regarded as an informal type locality for the middle member of the

Monterey Formation (Hornafius, 1994; Föllmi et al., 2005). The Monterey Formation as Naples Beach is lithologically variable with phosphatic, carbonate rich, diatomaceous and organic rich laminated intervals.

Table 4.1: Lithofacies and TOC (wt.%) of samples studied from Monterey and Stuart Range formations.

Formation	Sample no.	Lithofacies	Depth (m)	TOC (wt.%)	Bulk kinetics
Monterey	M44	Calcareous black mudstone	Outcrop	16	
	M59	Phosphatic mudstone	Outcrop	11.8	*
	M62	Black shale	Outcrop	21.4	*
	M22	Calcareous black mudstone	Outcrop	13	
	M28	Phosphatic shale	Outcrop	16.9	*
	M33	Black shale	Outcrop	22.7	
	M29	Phosphatic shale	Outcrop	5.4	
	M21	Calcareous phosphatic shale	Outcrop	9.8	*
Stuart Range	S99	Argillaceous siltstone	888.5	1.3	
	S81	Silty mudstone	897.26	5.9	*
	S77	Black shale	900.73	7.3	*
	S64	Black shale	907.53	6.8	*
	S43	Fissile black shale	918.06	6.2	
	S26	Fissile black shale	934.76	3.2	
	S12	Silty mudstone	949.65	1.7	*
	S08	Silty mudstone	951.3	4.7	*
	S72	Siliceous mudstone	974.64	0.6	
	S51	Silty mudstone	990.17	0.06	

Note: * denotes samples selected for bulk kinetic analyses.

We sampled the laminated organic rich intervals from the carbonaceous marl member (Isaacs, 2001) deposited under pelagic to hemipelagic conditions and are mineralogically dominated by clay minerals with minor detrital quartz,

feldspar, diagenetic dolomite and siderite concretions. Horizons containing phosphatic nodules and lithoclasts are indicative of significant reworking of organic matter and condensation, whereas biogenic silica and their diagenetic derivatives such as chert and porcelanite are minor or absent in this interval (Barron, 1986; Garrison et al., 1994; Isaacs, 2001; Föllmi et al., 2005; Berndmeyer et al., 2012; Laurent et al., 2015). Smectite and illite are the most abundant clay minerals present (Fig. 4.2a).

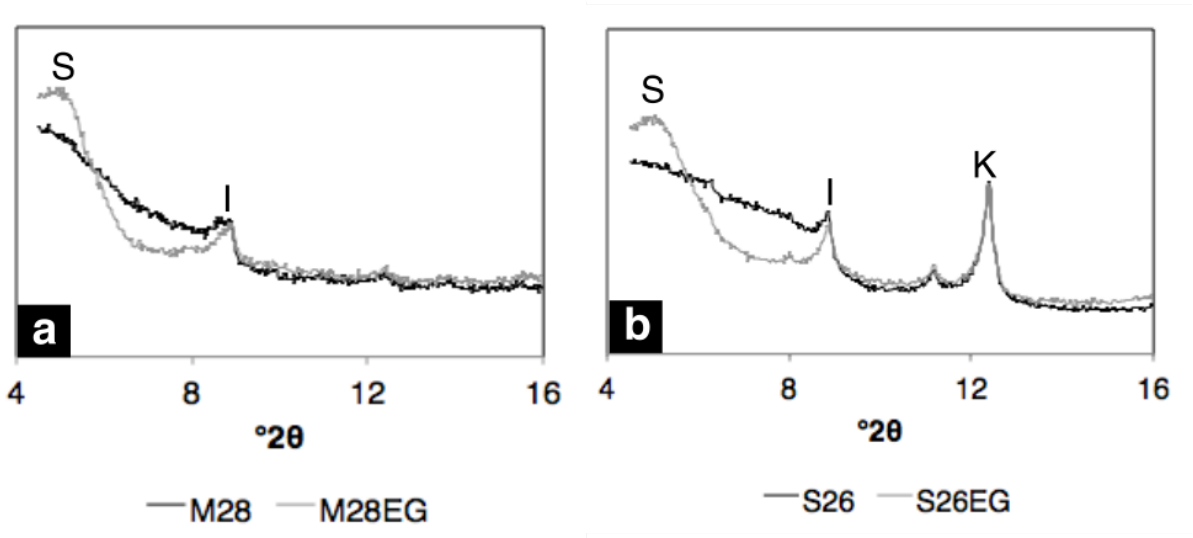

Fig. 4.2. X-ray diffractograms of the < 2 µm fraction of air-dried (black) and ethylene glycol-treated (grey) samples of (a) Monterey (M28 and M28EG respectively) and (b) Stuart Range formations (S26 and S26 EG respectively). Smectite (S) and illite (I) are common in samples of both formations; kaolinite (K) is also present in the Stuart Range samples and is minor in the Monterey samples (modified from Rahman et al., 2017).

A subset of Stuart Range Formation samples (TOC: 2–7 wt.%) was chosen as representatives of the particulate organic matter fabric endmember (Table 1). They were collected from the Arck-1 well core stored at the South Australian

State core repository, and were taken from an interval ranging from 888 to 990 m depth. The samples are typical of the Stuart Range Formation, being feldspar-rich quartz siltstone with authigenic clay minerals including smectite, illite and kaolinite (Fig. 4.2b).

4.2.3. Methods

4.2.3.1. Scanning electron microscopy (SEM) and Nanomin mineral mapping

The samples were polished using a Hitachi IM4000 Argon Ion Mill system and carbon-coated before imaging and mineral mapping on a FEI Teneo field emission SEM equipped with dual EDS (energy dispersive x-ray spectroscopy) detectors (Bruker XFlash Series 6). SEM analyses were performed at 13 mm working distance and 15 kV accelerating voltage. EDS spectra for mineral mapping were collected simultaneously at 200 nm steps and 8 ms acquisition times using the FEI Maps Mineralogy software, followed by classification of the individual EDS spectra using the FEI Nanomin software. Mineral classification is achieved by comparing EDS spectra collected in the mapped area against reference spectra collected on known mineral standards. Unlike earlier SEM-based mineral mapping techniques (e.g. QEMSCAN), the Nanomin mineral classification system can de-convolve mixed X-ray spectra and assign up to three minerals per analysed spot. This is a critical advantage for the correct interpretation of the mixed phase X-ray spectra characteristic of heterogeneous fine-grained sediments, which might otherwise lead to mineral misidentification and erroneous quantitative results. SEM photomicrographs and Nanomin maps provide direct visual

evidence of the range of complex association of minerals and organic matter at the required µm to sub-µm scale.

4.2.3.2. Mineralogy

X-ray Diffraction (XRD) (Bruker D8 Advance with a Cu-radiation source) of micronized powdered samples (including a 10% ZnO internal standard) was used to determine and quantify mineralogy of the samples. Minerals were identified using Bruker Diffrac.Eva software and Crystallography Open Database reference patterns and quantified using RockJock program (Eberl, 2003).

4.2.3.3. Organic petrology

Macerals in the samples were characterized and quantified using point counting in accordance with the procedures of the Australian Standards (1998; AS 2856.2). The delineation of the macerals is based on their morphologies and textures although reflectance is also considered. A minimum of 500 points was counted for each of the white light and fluorescence mode observations on every sample. The maceral analyses are reported as volumetric percentages. Vitrinite reflectance measurements were made using a Zeiss microscope with a 40x oil immersion objective and an interference filter with a pass-band peak of 546 nm in accordance with the AS2456.3 (Australian Standards, 2000). Random reflectances of vitrinite particles were measured using non-polarized light. The average of 30 to 40 measurements (depending on the abundance of vitrinite grains) from each sample is reported as 'mean vitrinite reflectance' of the sample. The vitrinites were identified according to Australian Standards (1998; AS 2856.2). A

transition in reflectance occurs between vitrinite and inertinite because they have the same precursors but differing levels of alteration prior to deposition or during early diagenesis.

4.2.3.4. Kerogen isolation

Kerogen isolates of each whole rock sample were obtained using the method of Durand (1980), as described in detail by Rahman et al. (2017). In brief, powdered aliquots of each sample were treated with hydrochloric acid to remove carbonates, and treated multiple times with 20% hydrofluoric acid (HF) at 60°C until XRD analysis confirmed the complete removal of silicate minerals. The organic matter isolates were ground to similar sizes as the whole rock samples. We assume that there was no or negligible fractionation and alteration of organic matter during demineralization that could affect subsequent comparisons to the whole rock samples. The organic matter concentrates were subsequently extracted to remove the bitumen fraction using a 9:1 mixture of dichloromethane (DCM) and methanol. The bulk rock samples were also solvent extracted to ensure that pyrolysis data of the bulk rock and the kerogen isolates are comparable.

4.2.3.5. Bulk kinetics

Bulk kinetic parameters were assessed by subjecting samples to open-system, non-isothermal pyrolysis at three different linear heating rates (0.7, 2 and 5 K/min) using a Source Rock Analyser (SRA) following standard procedures (Braun and Burnham, 1987). The KINETICS 2000 program was used to optimise the discrete activation-energy (Ea) distribution with a single, variable frequency factor (A). The kinetic experiment results were

extrapolated to a typical geological heating rate (3 K/million year) using the KMOD program.

4.3. Results

4.3.1. Mineral-organic petrography

The sample sets of both Monterey and Stuart Range formations are smectite and illite rich shale (Table 4.2). Different depositional and diagenetic processes have resulted in fundamentally different rock fabrics in these two formations.

The Stuart Range Formation was deposited in a periglacial environment during waning of the Gondwana glaciation in Australia (Menpes et al., 2010). The sediment composition was influenced by a granitic provenance and limited chemical weathering in the cold climate settings and therefore it is compositionally and texturally 'immature'. Backscattered scanning electron (BSE) photomicrographs and Nanomin mineral maps show that silt grains comprising quartz and feldspar are sub-angular to angular, poorly sorted and dominantly 5 to 50 μm in size (Fig. 4.3a, b). The significant clay-sized fraction identified by the high MSA of the sediments (179 to 269 m^2/g; Table 4.2) comprises smectite, illite and kaolinite (Fig. 4.2). BSE photomicrographs and Nanomin mineral maps show that the majority of these clay minerals are pore filling (Fig. 4.3a, c), forming discrete domains of randomly oriented clay minerals with distinct boundaries separating them from the surrounding matrix (Fig. 4.3d). These observations indicate that the majority of clay minerals in the Stuart Range Formation are authigenic. Quartz cements are

Table 4.2. Mineral surface area (MSA) and quantitative mineralogy of samples from Monterey and Stuart Range formations. MSA is measured using the EGME method of Tiller and Smith (1990). Mineralogy is presented as wt. percent based on XRD, not normalized to 100%.

Sample No.	Silicate MSA (m2g-1)	Quartz	Albite	Microcline	Calcite	Pyrite	Chlorite	Smectite + Illite	Muscovite	Biotite	Kaolinite	Gypsum	Fluorapatite
M59	318	8	14	8	12	1		46		5		5	
M62	676	8	14					78					
M28	477	9	15	7	1			63		5			
M33	635	7	14	9	2	1		60	3	3			
M21	215	3	5	6	52	1		27		2			3
S81	222	41	4			16		23	9		7		
S08	259	33	8			11	7	16	12		7	5	
S77	264	28	6			9		45			11		
S64	269	34	5			6		44			9	2	
S12	179	30	7	13		3		29	9		8		
S26	251	35	4			2		48			9	1	

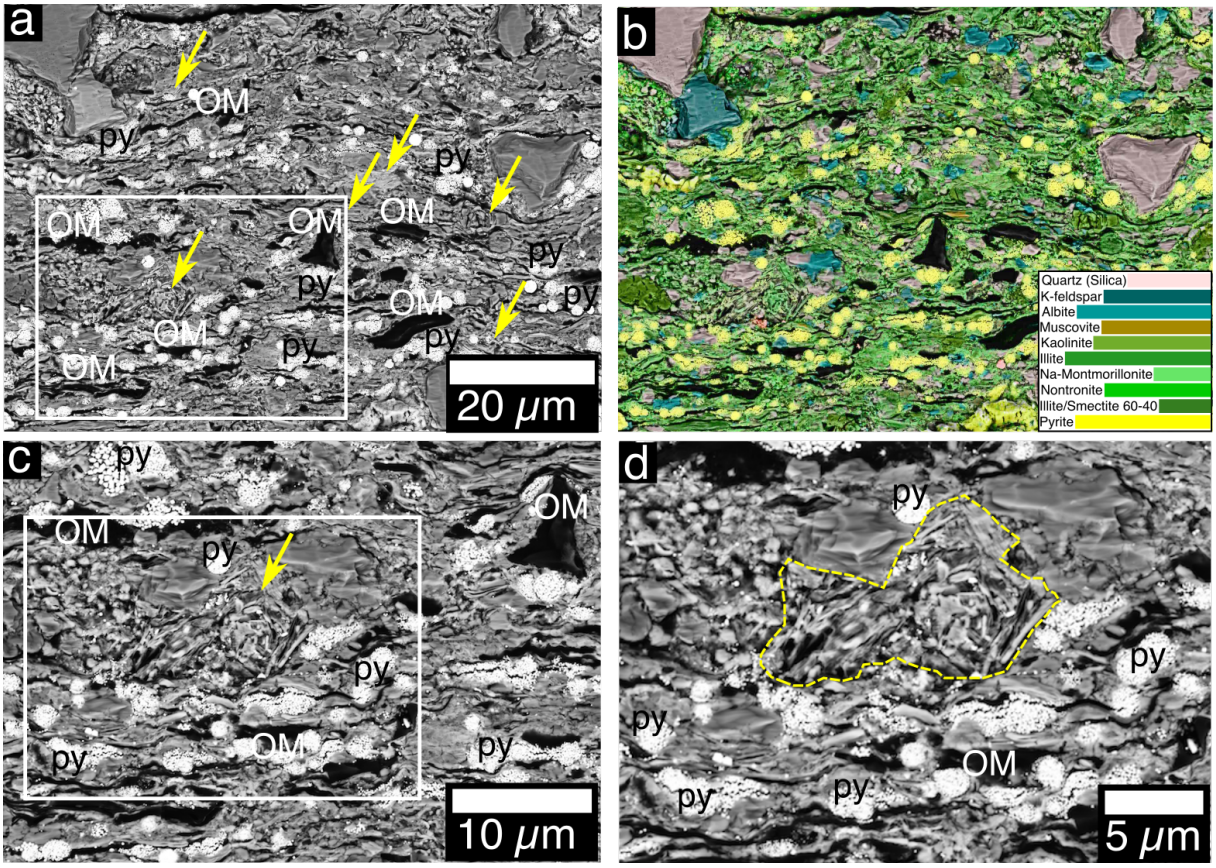

Fig. 4.3. SEM photomicrographs and Nanomin mineral map of a Stuart Range Formation sample (S81). a, c, d: Backscattered SEM photomicrographs at sequentially higher resolutions showing discrete organic matter (OM) and abundant pyrite framboids (py). Pore-filling clay minerals are indicated by arrows on Fig. a, c and dashed outline on Fig. d. b: Nanomin mineral map of the same view as Fig. a shows the abundance of smectite clays (green), pyrite framboids (yellow), quartz (grey) and feldspars (blues).

present both as fine-grained authigenic crystals and as overgrowths of detrital quartz. Pyrite framboids consisting of densely packed submicron-size pyrite crystals are abundant in the Stuart Range samples. The size of the framboids varies from 2 to 20 μm in diameter. In some sections, polyframboid aggregates containing multiple single framboids of different sizes are also present (Fig. 4.3d).

BSE imaging shows organic matter in the Stuart Range samples to be present as sub-angular to angular particles as well as elongated organic stringers

(Fig. 4.3c). Organic petrological analyses show that telalginite and lamalginite are the most abundant macerals present (51 to 83% on a mineral-free basis); vitrinite and reworked vitrinite/inertinite are common but less abundant (10 to 29%; Table 4.3; Fig. 4.4a, b). The presence of vitrinite and inertinite indicates a terrestrial contribution, although the predominance of alginite, including prasinophyte cysts is consistent with a marine depositional environment. Oxidation rims on vitrinite and inertinite grains are common in sample S08 and less common in sample S77. These rims indicate a possible oxidation effect on the terrestrial organic matter prior to, or during deposition, but they were not observed in other samples.

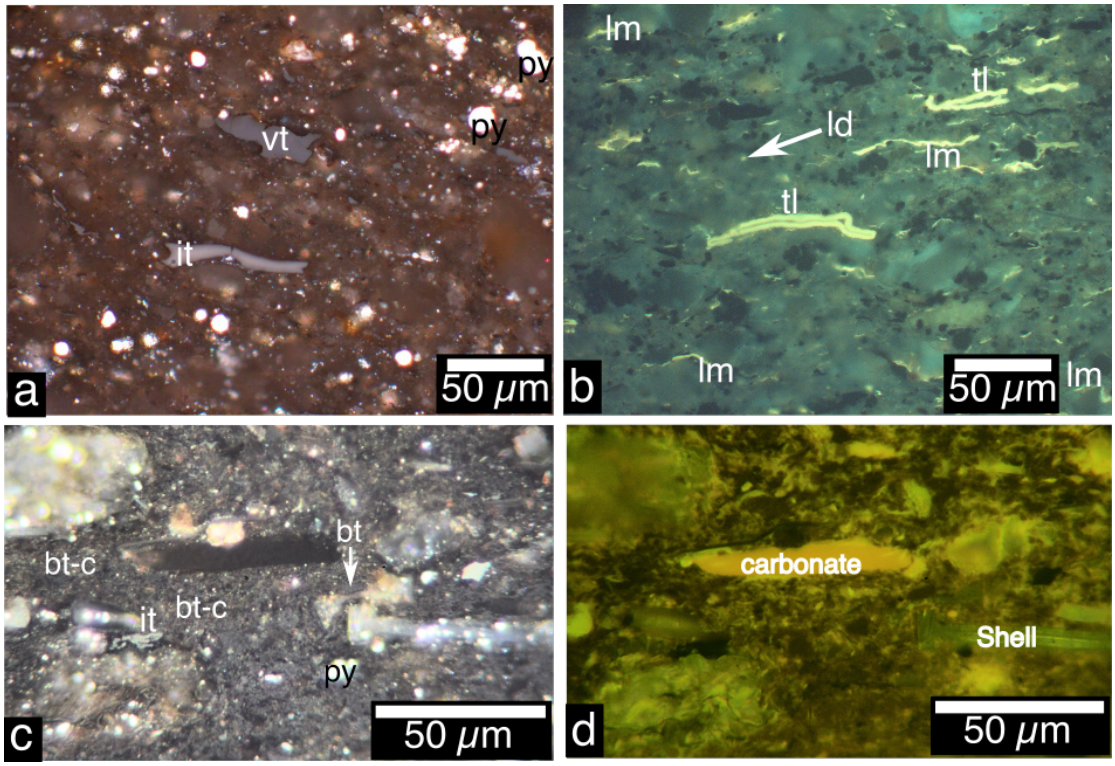

Fig. 4.4: Photomicrographs of samples of Stuart Range (S12; a, b) and Monterey formations (M21; c, d). a: Vitrinite (vt) and inertinite (it) represent the terrestrial fraction of organic matter in Stuart Range Formation samples. Pyrite framboids (py) are abundant. b: Telalginite (tl) and lamalginite (lm) are the dominant

liptinite macerals in Stuart Range samples and liptodetrinite (ld) is also common. c: Bituminite-clay mixtures (bt-c) are the major form of organic matter in the Monterey Formation samples. Pyrite framboids are abundant. d. Same field of view as for c, showing dull fluorescing bituminite (bt). Here, a and c are observations under reflected white light and b and d under UV/blue light; all observations on samples under oil immersion.

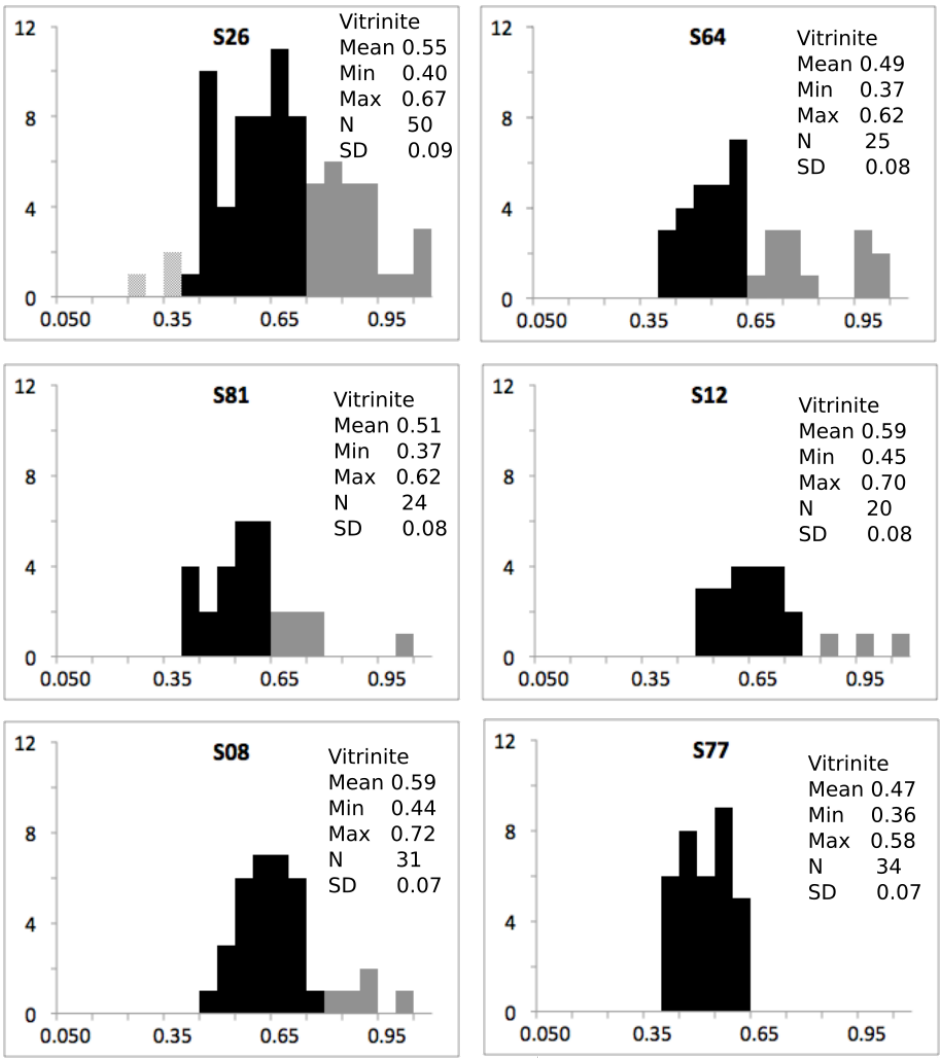

Fig. 4.5: Random vitrinite reflectance (VR) measurements of Stuart Range Formation samples. Mean VR values ranging from 0.47 to 0.59 %R_o indicates the samples are thermally immature to marginally mature for hydrocarbon generation. N = number of measurements per sample, SD = standard deviation.

Table 4.3: Maceral analyses illustrate that telalginite and lamalginite are the dominant macerals in the Stuart Range Formation samples. Data are reported here as volume percent on a mineral-free basis.

Sample No.	TOC wt.(%)	Telalginite (%)	Lamalginite (%)	Sporinite (%)	Liptodetrinite (%)	Micrinite (%)	Bituminite (%)	Vitrinite (%)	Inertinite/reworked vitrinite (%)
S81	5.9	24	27	8	9	1	1	15	14
S12	1.7	21	40	4	6	< 1	5	11	12
S26	3.2	27	31	4	6	1	8	9	13
S64	6.8	30	24	6	6	< 1	11	11	12
S77	7.3	25	37	3	4	2	3	6	20
S08	4.7	63	20	1	5	< 1	< 1	2	8

The vitrinite reflectance (VR) analyses show that organic matter in the Stuart Range samples are thermally immature to marginally mature for oil generation (0.47 to 0.59 % Ro; Fig. 4.5), although the VR values may underestimate the thermal maturity due to the effects of VR suppression, which is common in marine rocks (e.g. Wilkins et al., 1992). The samples from the Monterey Formation comprise laminated, intermittently burrowed mudstone recording pelagic to hemipelagic sedimentation in a periodically restricted marine shelf to offshore setting. Alkali feldspar, quartz, smectite and illite are the major minerals present (Table 4.2). Quartz grains 5 to 20 μm diameter (Fig. 4.6a, b) have an aeolian source or have formed as diagenetic precipitates from silica-rich pore waters, as carbonate replacement or cements, a process reported for the Monterey Formation by Reimers (2001). The majority of the clay minerals comprise flaky crystals of smectite and mixed layer illite-smectite oriented along laminations and in some cases are deformed around rigid grains (Fig. 4.6c, d), indicative of differential compaction during initial sediment burial. These observations suggest that the majority of the smectitic clays in the Monterey Formation samples are detrital. The mineralogy also indicates a dominance of chemical over physical weathering in the provenance area with either a strong seasonality or a primary volcanic source (Chamley, 1989). Pores/voids are separated from organic matter based on their darker isotopic black color appearance compared to the lighter grey appearance and apparent relief within organic matter evident in BSE observations. The organic matter is mostly amorphous (occurring as bituminite) and is widely disseminated throughout the rocks; discrete macerals are rare. Where present, these discrete organic particles

have a distinct contact with the rock matrix (Fig. 4.6b), but the bituminite is intimately associated with clay minerals. Sub-micron size clay flakes embedded within the bituminite are identified with the aid of high-resolution BSE photomicrographs and Nanomin mineral maps. The organoclay aggregate domains vary from sub-angular to angular shapes and mostly have diffuse boundaries with the mineral matrices, although some have sharp contacts (Fig. 6c, d).

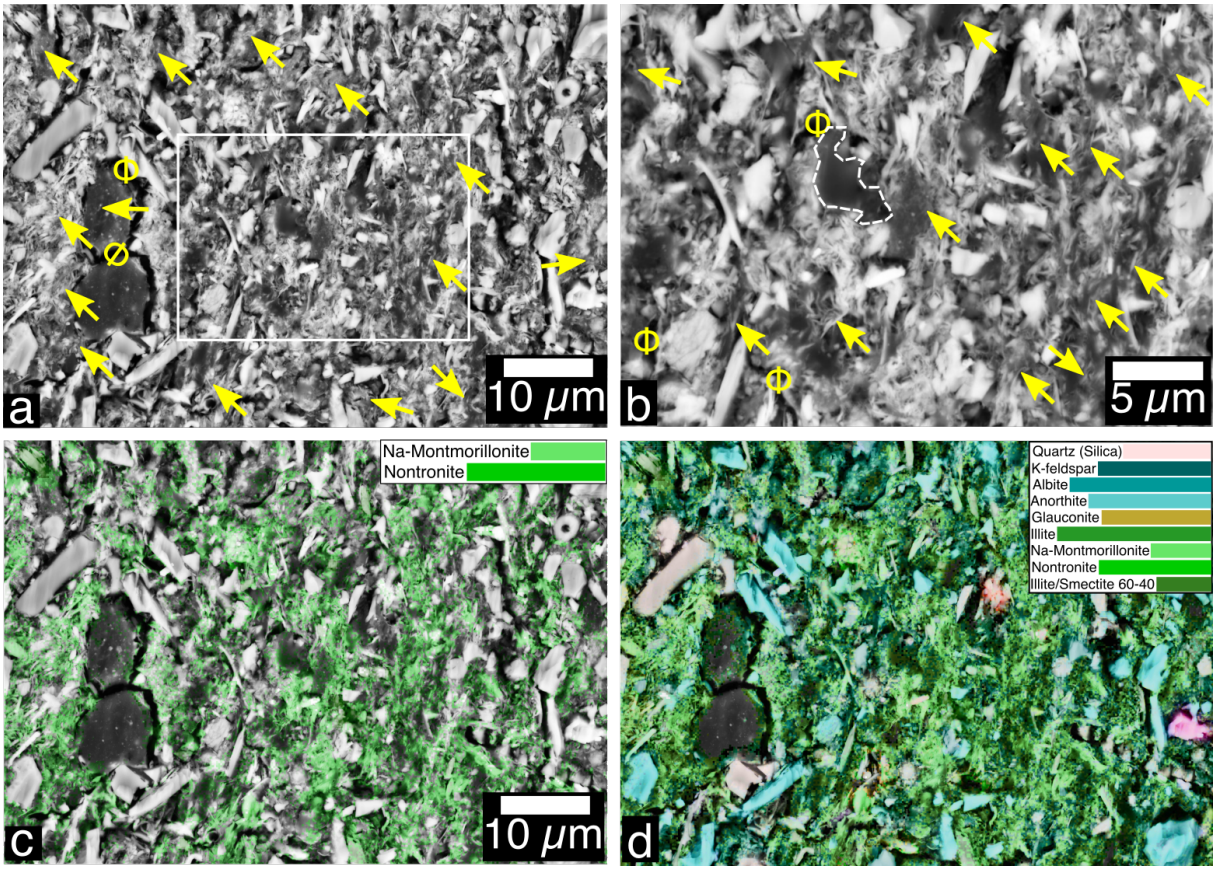

Fig. 4.6: a, b: Backscattered SEM photomicrographs of a Monterey sample (M28). Arrows indicate clay mineral flakes closely associated with organic matter at sub-micron scales. Some of the visible fracture porosity (Φ) in the sample could be formed during the sample preparation for SEM. Dashed outline (b) indicates rare occurrence of discrete organic particle in Monterey samples. c, d: Nanomin mineral maps for smectites (c) and all minerals (d). Discrete quartz (grey) and feldspar grains (blue) are present in the fine clay-organic matrix. Submicron size smectite-illite flakes (green) occur within organic matter.

Consistent with the BSE-SEM and Nanomin results, organic petrographic analyses show >70% of the organic matter in the Monterey Formation samples comprises bituminite mixed with clay minerals (Fig. 4.4c, d; Table 4.4). Telalginite (4 - 9% on a mineral free basis), liptodetrinite (2 - 4%) and vitrinite (< 1 - 2 %) are the other macerals present in these samples (Table 4.4). The VR analyses indicate that the Monterey Formation samples are thermally immature for oil generation (0.36 to 0.43 %Ro) (Fig. 4.7), although similar to the VR for the Stuart Range Formation samples, they may underestimate thermal maturity due to suppression (e.g. Wilkins et al., 1992).

Organic and inorganic petrography of the Monterey and Stuart Range formation sample sets confirm that they are representative of two endmember shale fabric classes (nanocomposite and particulate respectively) and therefore are suitable for comparing the effects of shale fabric on hydrocarbon generation kinetics.

4.3.2. Hydrocarbon generation kinetics

Hydrocarbon generation kinetic data differ between the Monterey and Stuart Range formation samples. Consistent with the similar maceral proportions for the suite of Stuart Range Formation samples, all of the kerogen isolates have similar activation energy distributions and frequency factors (Fig. 4.8, Table 4.3). The paired whole rock and kerogen isolates for S77, S81, S64 have similar, narrow activation energy distributions (mostly from 51 to 55 kcal/mol) and similar frequency factors (3.21E+13 to 1.64E+14 /sec) (Fig. 4.8). This observation is consistent with the negligible T_{max} shift between whole-rock and kerogen isolate pairs (2°C mean difference; Table 4.5). Both whole

rock and kerogen isolates of S08 and to a lesser extent S12 have narrower activation energy distributions (52 to 56 kcal/mol for kerogen and bulk rock of S08 and 51 to 56 kcal/mol for kerogen and bulk rock of S12) than for the other samples.

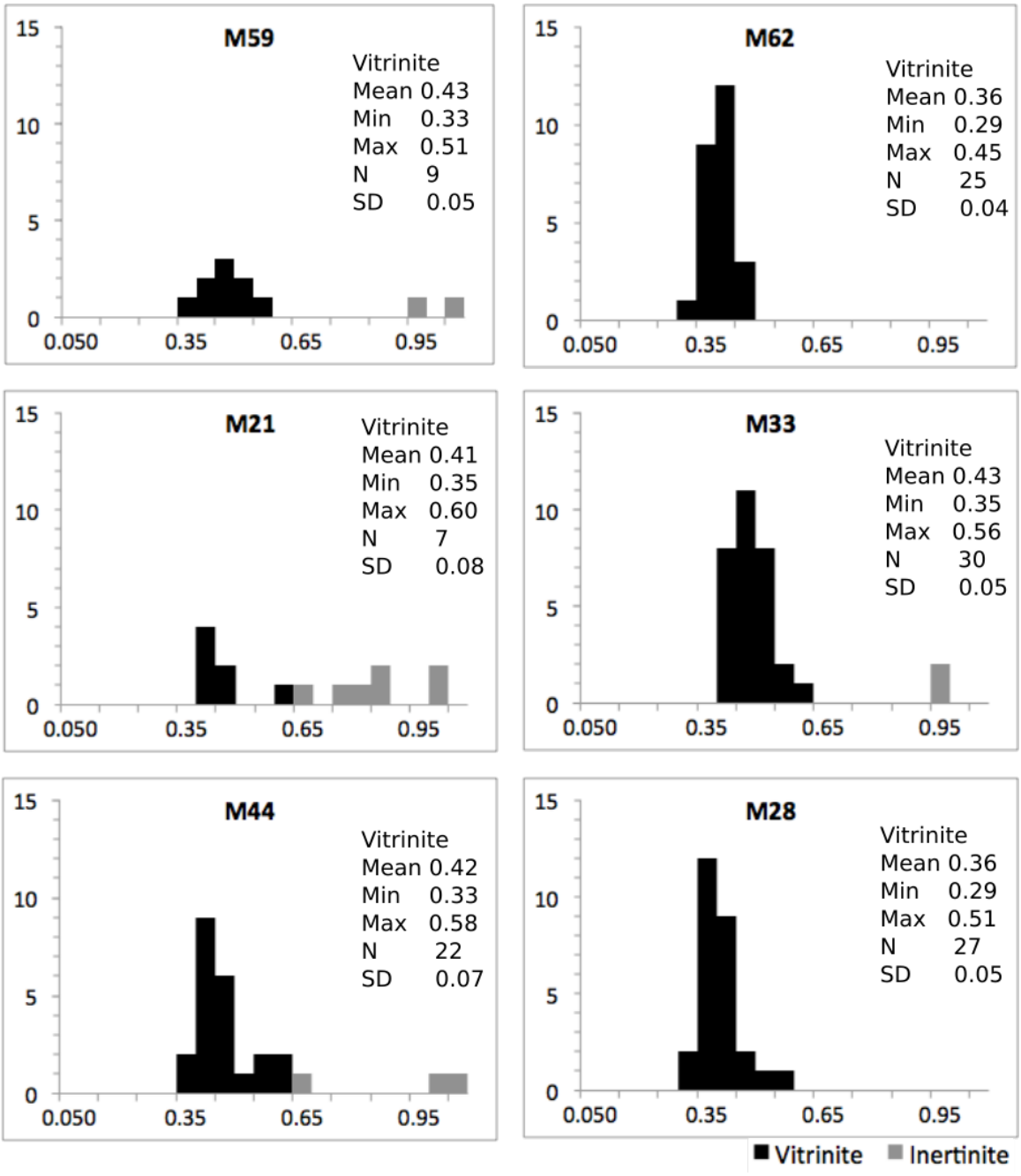

Fig. 4.7: Random vitrinite reflectance (VR) measurements of Monterey Formation samples. Mean VR values ranging from 0.36 to 0.43 $\%R_o$ indicates the samples are thermally immature for hydrocarbon generation. N = number of measurements, SD = standard deviation.

Table 4.4: Quantitative maceral analyses demonstrate the dominance of bituminite-clay mixtures over the other forms of organic matter in samples of Monterey Formation. Data are reported here as volume percent on a mineral-free basis.

Sample No.	TOC wt.(%)	Sporinite (%)	Telalginite (%)	Lamalginite (%)	Liptodetrinite (%)	Micrinite (%)	Bituminite (%)	Vitrinite (%)	Inertinite/reworked vitrinite (%)	Bituminite-clay mixture (%)
M33	22.7	<1	4	<1	2	<1	18	<1	<1	74
M59	11.8	<1	4	<1	2	2	11	<1	<1	79
M21	9.8	<1	4	<1	2	<1	16	<1	<1	77
M44	16	<1	4	<1	2	<1	21	2	<1	70
M28	16.9	<1	9	1	4	<1	2	<1	2	80
M62	21.4	<1	5	<1	3	<1	5	1	<1	83

Table 4.5: Rock-Eval pyrolysis results of the samples of Monterey and Stuart Range formations. Here, Cal. %Ro is the calculated thermal maturity from T_{max} using Jarvie et al. (2001) equation (from Rahman et al., 2017)).

Sample No.	HI (Rock) (mgHC/gTOC)	Mean HI (Rock) (mgHC/gTOC)	HI (Kero) (mgHC/gTOC)	Mean HI (Kero) (mgHC/gTOC)	Kero HI-Rock HI (ΔHI_{K-R})	Rock Tmax (°C)	Mean Rock Tmax	Kerogen Tmax (°C)	Mean Kero Tmax (°C)	Rock-Kero Tmax ($\Delta Tmax_{R-K}$) (°C)	Cal. Ro (%)
M59	346	354	420	440	86	422	422	392	392	30	0.43
	347		463			422		392			
	369		436			421		391			
M33	400	391	502	512	121	396	397	384	386	11	
	385		486			398		385			
	389		547			396		388			
M28	374	363	470	448	85	408	408	391	389	19	0.19
	352		441			408		389			
	362		433			409		388			
M21	418	425	543	567	142	422	422	394	393	29	0.44
	437		569			422		394			
	421		589			422		392			
M62	298	295	455	431	136	396	397	386	385	12	
	303		413			397		384			
	285		425			397		386			
S26	90	89	304	294	205	432	433	431	430	3	0.63
	89		249			433		430			
	89		330			433		430			
S12	72	74	110	130	56	434	435	428	428	7	0.66
	77		142			435		428			
	73		139			435		429			
S08	113	109	444	319	210	435	435	432	432	3	0.68
	106		171			435		432			
	107		341			436		431			

S64	189	179	395	336	157	421	421	421	421	0	0.41
	172		313			421		421			
	175		300			420		422			
S81	105	100	225	197	97	417	418	418	418	0	0.36
	98		154			418		418			
	97		212			418		418			
S77	215	211	393	359	148	424	424	424	425	1	0.48
	206		327			425		426			
	212		356			424		425			

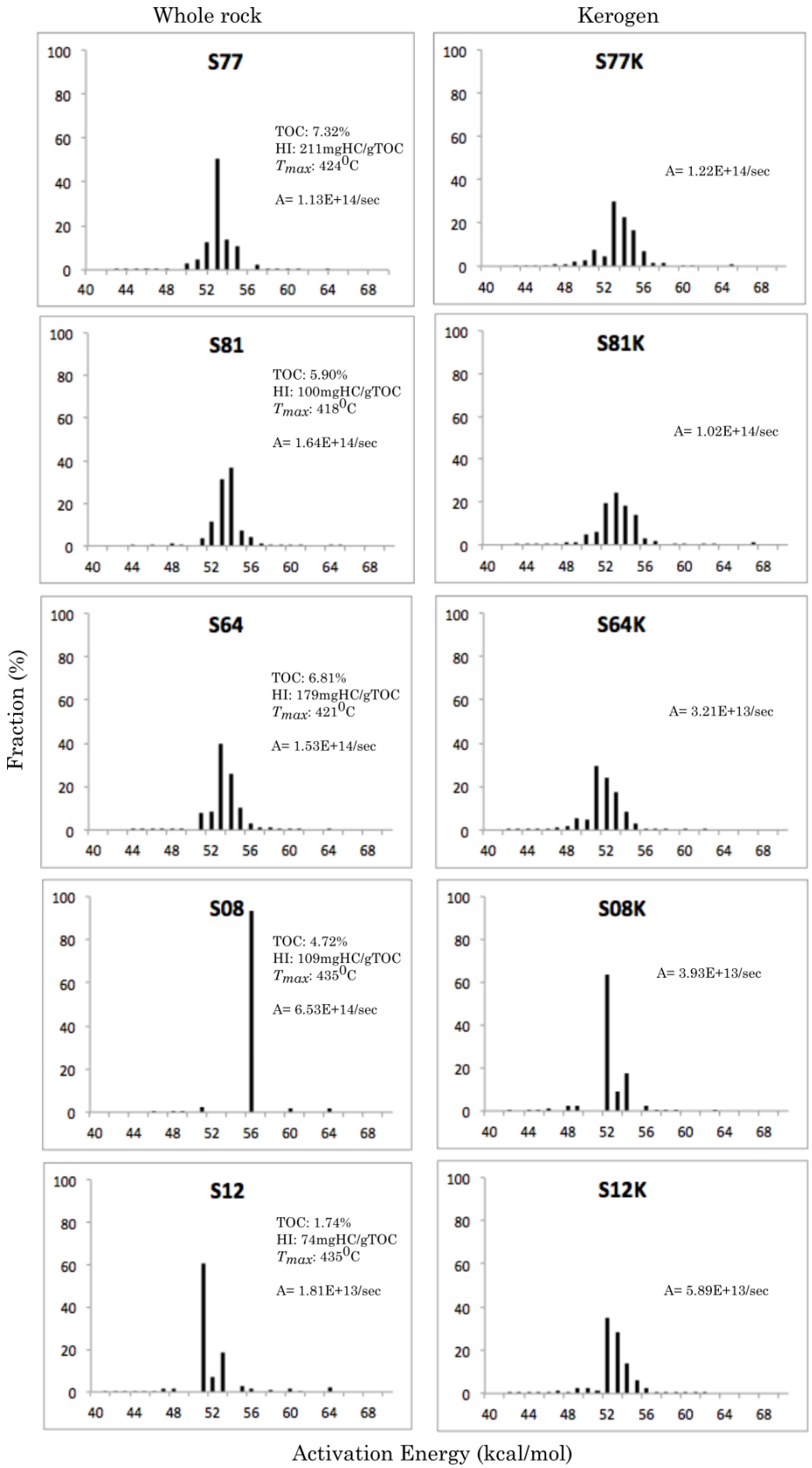

Fig 4.8: Activation energy (E_a) distribution and frequency factor (A) of samples from the Stuart Range Formation. The narrow distribution of activation energy indicates homogenous kerogen structure. Kerogen isolate sample numbers end with K.

With the exception of S08, all Stuart Range Formation kerogen and bulk rock samples show similar modelled generation curves, reaching a transformation ratio of 80% at about 150°C (Fig. 4.9). Overall, the Stuart Range samples demonstrate generation kinetics similar to those for marine shales in general (Behar et al., 1997) and indicate negligible mineral matrix effects on hydrocarbon generation.

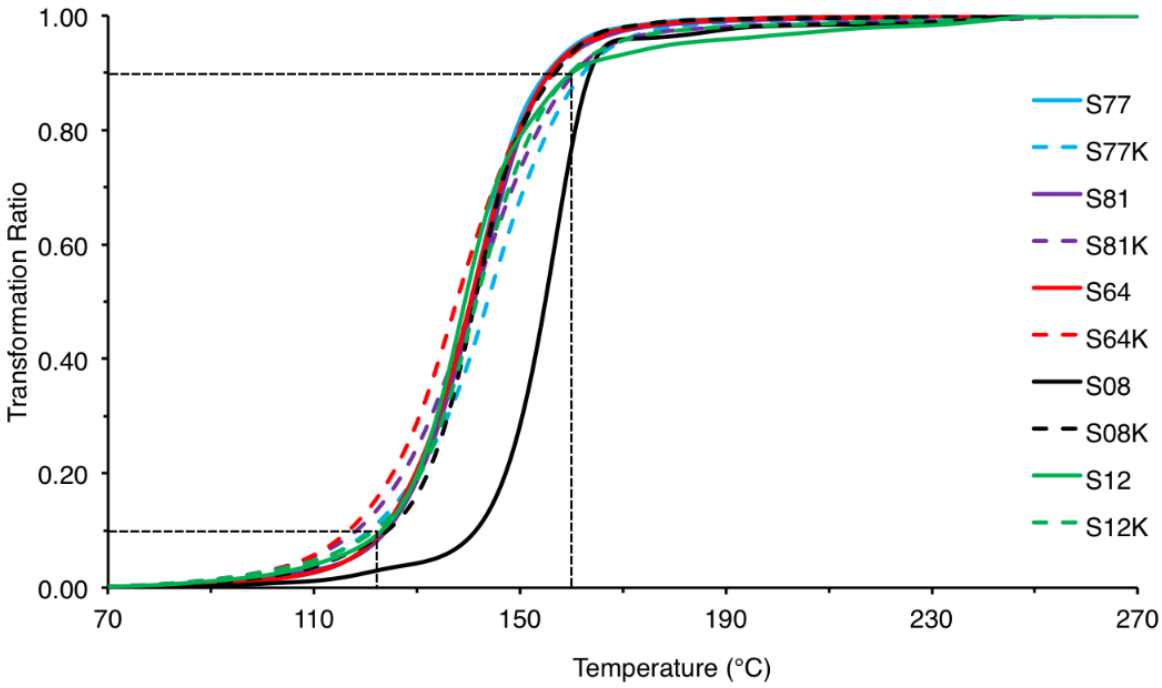

Fig 4.9: Geological extrapolation of hydrocarbon generation from the Stuart Range Formation samples assuming a typical geological heating rate of 3K/million year. Except sample S08, all samples show similar hydrocarbon generation patterns for the kerogen isolates (sample numbers ending with K) and whole rock samples.

Consistent with the similar maceral proportions for the Monterey Formation samples (Table 4.4), the kerogen isolates have similar, low, peak activation energies (below 20% for all samples) coupled with wide activation energy distributions (51 to 70 kcal/mol) (Fig. 4.10). The broad activation energy distribution implies that the Monterey Formation kerogens have a variety of

bond strengths. Whole-rock samples M59, M28 and M21 show coherent bulk kinetic results having lower activation energies than for their corresponding

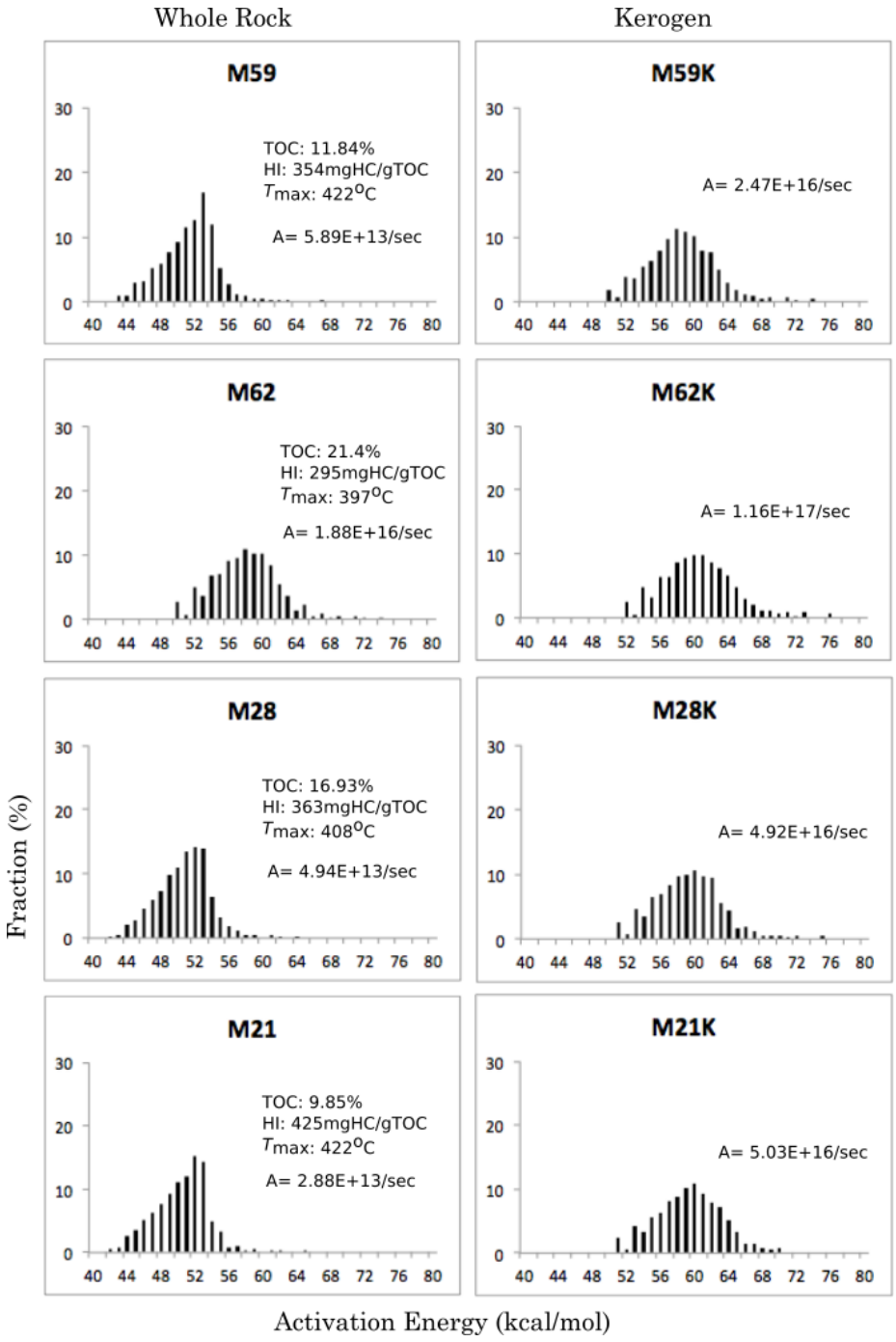

Fig 4.10: Activation energy (E_a) distribution and frequency factor (A) of samples from the Monterey Formation. The wide distribution and low peaks of activation energy indicates heterogeneous kerogen structure. Kerogen isolate sample numbers end with K.

kerogen isolates (peak 53 to 54 kcal/mol for whole rock and 58 to 61 kcal/mol for kerogen). Geological extrapolation further highlights the differences between the kinetic parameters for whole-rock and kerogen samples. All of the kerogens give similar generation curves, reaching transformation ratios of 80% at about 173°C. With the exception of M62, organic matter in the whole rock samples is generally more labile than the kerogen isolates, reaching a transformation ratio of 80% at 150°C (Fig. 4.11). Organic matter in the M62 kerogen and whole rock samples has a higher thermal stability than for the other samples.

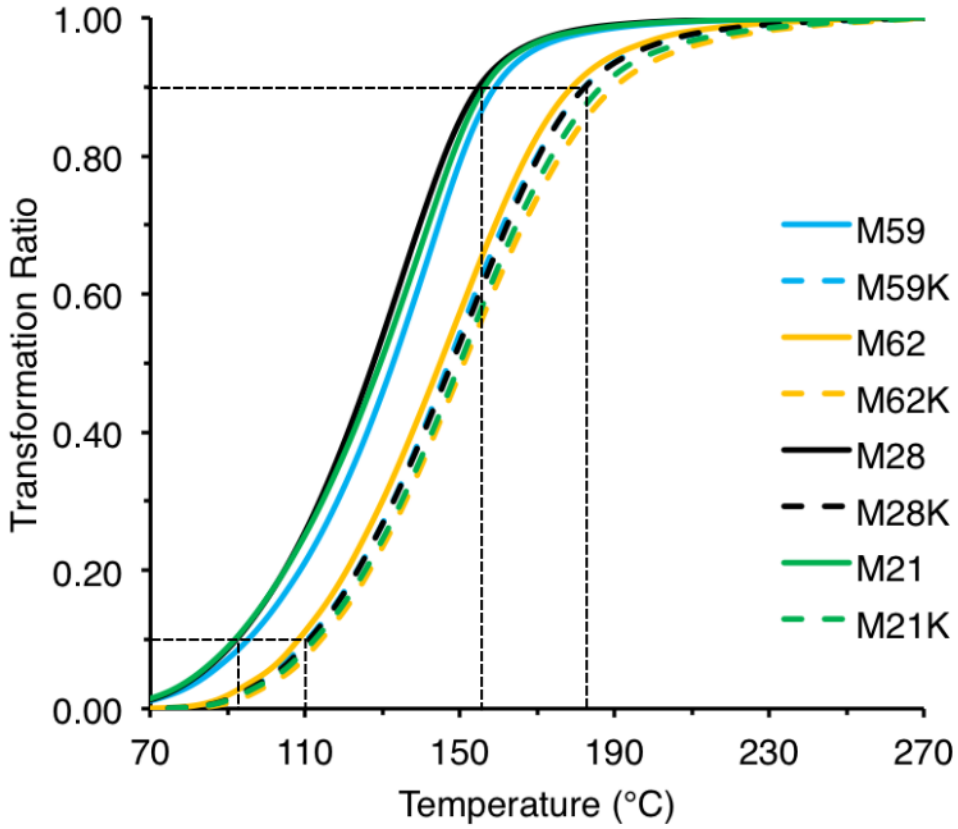

Fig 4.11: Geological extrapolation of hydrocarbon generation from the Monterey Formation samples assuming a typical geological heating rate of 3 K/million year. Except for one sample (M62), the whole rock samples generate hydrocarbons at substantially lower temperatures than for the isolated kerogens. Kerogen sample numbers end with K.

4.4. Discussion

Major differences in fabric, and the degree of organo-mineral association in particular exist in organic-rich shales. Samples from the Monterey and Stuart Range formations exhibit two significantly different fabrics, with fundamentally distinct degrees of mineral surface contact per unit volume of organic matter. The pyrolysis results are consistent with our hypothesis that shale fabric influences clay mineral catalysis of hydrocarbon generation at laboratory heating rates, i.e. they show a reduced hydrocarbon generation temperature in whole-rock vs. kerogen isolates only in nanocomposite source rock samples and not in particulate source rock samples resulting from a catalytic effect.

Table 4.6 presents a synopsis of some kinetic experiments performed on shales from different depositional environments and having different kerogen types. The activation energy peaks and distribution patterns for both the Monterey and Stuart Range formation samples studied are broadly comparable to those for other marine source rocks (e.g. Schaefer et al., 1990; Dieckmann et al., 2000; Schenk and Dieckmann, 2004; Dieckmann, 2005; Romero-Sarmiento et al., 2016). It should be noted that some of the variation in activation energy and frequency factors presented in Table 6 could be due to different experimental conditions applied in the different laboratories, such as heating rates and pyrolysis method (open vs. closed).

Table 4.6: A synopsis of some published bulk kinetic experiments on shale.

Source Rock	Depositional Env.	Sample type	Kerogen type	Heating rates (K/min)	Activation energy (Ea) (KCal/mol)	Frequency factor (A) (/S)	Pyrolysis method	Reference
Green River	Lacustrine	Rock	I	0.1, 0.7, 5	Narrow (51-58) peak 56	1.1071E+15	Open system	Dieckmann (2005)
Toarcian shale	Marine	Rock	II	0.1, 0.7, 5	Wide (46 to 62) peak 56	9.6372E+14	Open system	
Sulfur rich shale (Southern Europe)	Not listed	Rock	II-S	0.1, 0.7, 5	Wide (41 to 56) peak 51	2.6187E+13	Open system	
Green River	Lacustrine	Rock	I	0.1, 0.7, 5	53	2.79E+15	Open systen	Schenk and Dieckmann (2004)
Toarcian Shale	Marine	Rock	II	0.1, 0.7, 5	55	2.17E+16	Open system	
Westphalian coals	Terrestrial	Rock	III	0.1, 0.7, 5	65	6.37E+15	Open system	
Green River	Lacustrine	Kerogen	I	2, 5, 10, 15	Very narrow (52 to 54) peak 54	7.4E+13	Open system	Behar et al. (1997)
Toarcian Shale	Marine	Kerogen	II	2, 5, 10, 15	Wide (46 to 64) peak 54	1.6E+14	Open system	
Monterey	Marine	Kerogen	II-S	2, 5, 10, 15	Wide (44 to 60) peak 48, 50	2.5E+13	Open system	
Mahakam Delta Coals	Terrestrial	Kerogen	III	2, 5, 10, 15	Wide (50 to 70) peak 58	3E+15	Open system	
Yanchang Formation	Lacustrine	Rock	II	0.7, 2, 5, 15	Wide (48 to 70) peak 58, 52, 50, 54	2.2E+12 to 4.57E+14	Open system	Han et al. (2014)
Toolebuc Shale	Marine	Rock+kerogen	II	0.7, 2, 5	R:Wide (48 to 61) peak 54 K: (48 to 63)peak 56	R: 2.27E+14 K: 7.74E+14	Open system	Yang and Horsfield (2016)
Bowland Shale	Marine	Rock+kerogen	II	0.7, 2, 5	R: Wide (48 to 61) peak 54 K: wide (46 to 54) peak 50	R: 2.34E+14 K: 1.22E+13	Open system	
Alum Shale	Marine	Rock+keroge	II	0.7, 2, 5	R: Wide (51 to 61) peak 56	R: 9.43E+14	Open system	

		n			K: wide (51 to 61) peak 56	K: 8.98E+14		
Lucaogou Formation	Lacustrine	Rock	I	0.03, 0.3	Wide (42 to 62	1.98E+13 to 5.27E+13	Close system	Xiang et al. (2016)
Duvernay Formation	Marine	Rock	II	0.1, 0.7, 5	Wide and narrow (different samples) (52 to 69) peak 54, 61, 55, 61, 56, 63	2.29E+16 /min to 1.29E+18 /min	Open system	Dieckmann et al. (2000)
Toarcian Shale	Marine	Rock	II	0.1, 0.7, 5	Wide (50 to 59) peak 54, 59, 60	1.1E+16 to 1.3E+17 /min	Open system	Schaefer et al. (1990)
Kimmeridge Mudstone	Marine	Rock	II	0.1, 0.7, 5	Wide (54 to 70) peak 57	1.2E+17 /min	Open system	
Montney Formation	Marine	Kerogen	II	5, 10, 15, 25	Wide (46 to 60) peak 54	1.9E+14	Open system	Romero-Sarmiento et al. (2016)
Doig Formation	Marine	Kerogen	II	5, 10, 15, 25	Wide (44 to 62) peak 54	1.2E+14	Open system	

With the exception of S08, all Stuart Range samples have similar narrow activation energy distributions, typical of many marine source rocks (Schaefer et al., 1990), and have similar hydrocarbon generation patterns in geological extrapolation for kerogen and whole rock (Fig. 4.9). The S08 sample also shows a very restricted, high activation energy distribution (57 kcal/mol, Fig. 4.8). Similar properties have been described before for homogenous kerogen in lacustrine shale with very high HI (504 mgHC/gTOC) where kerogen cracks relatively slowly in a high, narrow temperature range during bulk kinetic experiments (Pepper and Dodd, 1995). The HI of sample S08 is however much lower (109 mgHC/gTOC). The single, high activation energy of S08 could be the result of the structure of kerogen comprising alicyclic and oxygen containing moieties that crack at a similar thermal stress (see Horsfield et al., 1994). Comparison of the raw experimental kinetics data of S08 with those of another low HI sample (S12, HI = 74 mgHC/gTOC) demonstrates that hydrocarbon is generated from S08 in a narrower temperature range responsible for the single high activation energy (Fig. 4.12). This observation is consistent with the high proportion of alginite, in particular telalginite (63%), relative to other macerals such as vitrinite and inertinite for sample S08 (Table 4.3).

The Monterey Formation samples show consistently low peaks and wide activation energy distributions (Fig. 4.10) indicating heterogeneous kerogen structure. Some of the range in activation energies is likely due to the presence of alginite as well as the dominant bituminite. Monterey Formation kerogen is classified as type II-S due to the presence of high amounts (8 to 14

%) of organically bound sulphur in the kerogen (Orr, 1986). Reynolds et al. (1995) studied the bulk generation kinetics of a sample set from the Monterey Formation from the Naples Beach section and reported a wide distribution of activation energies (46 to 71 kcal/mol), consistent with the findings of the present study. A similar low peak (below 21 %) and wide activation energy distribution (41 to 59 kcal/mol) is also reported for a sulphur-rich shale from southern Europe (Dieckmann, 2005). The presence of strong carbon-carbon bonds in addition to the weaker carbon-sulphur bonds in the bituminite is responsible for the low peaks and wide distributions of activation energies. Geological extrapolation of the generation kinetics of the whole rock and kerogen isolate samples (Fig. 4.11) show that the whole rock samples are significantly less stable (except M62, discussed below) than their kerogen isolate counterparts. We attribute these differences to clay mineral catalysis.

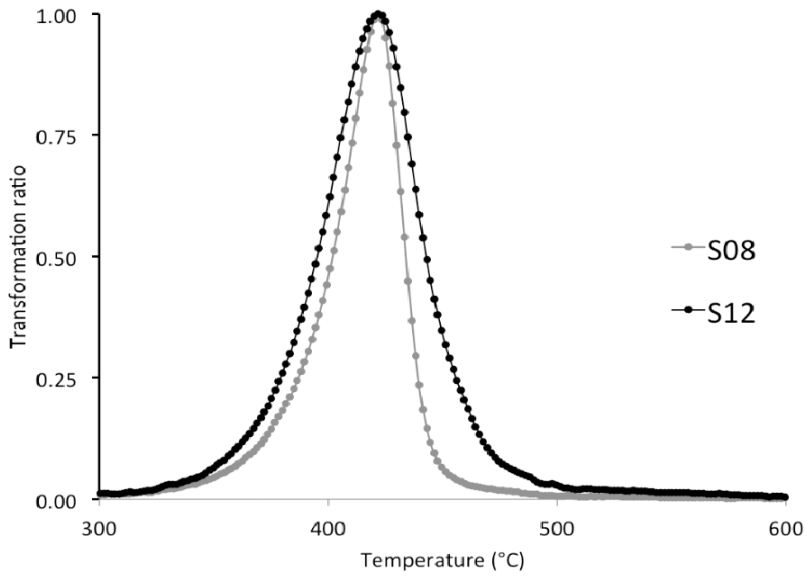

Fig. 4.12: Experimental raw data of whole rock sample S08 (grey) and sample S12 (black) at a heating rate of 0.7 K/min after normalization. The hydrocarbon generation from S08 occurred over a shorter temperature range, which is responsible for the single high activation energy distribution.

The existence of both Brønsted (ability to donate a proton, H^+) and Lewis acid sites (ability to act as an electron-pair acceptor) in clay minerals (Varma, 2002) make them potential natural catalysts for organic matter cracking during hydrocarbon generation (Johns, 1979; Wu et al., 2012). In the case of layered clay minerals (e.g. smectites), the hydrated and dehydrated cations in the interlayer space are the sources of Brønsted and Lewis acidity respectively (Wu et al., 2012). The expanded interlayer space allows clay minerals such as smectite to intercalate organic matter with the consequent formation of clay-organic nanocomposites. The interlayer occurrence of organic matter in smectite clays is supported by several lines of evidence: 1) the observation that linear MSA to TOC correlations in organic-rich shales commonly extend to high surface areas including the smectite interlayer surfaces (e.g. Kennedy et al., 2002), 2) the fact that smectite interlayer spaces of organic-rich clay fractions remain propped open at temperatures greatly exceeding the smectite interlayer dehydration temperature (Löhr and Kennedy, 2014), as well as 3) bulk compositional and direct imaging evidence for the release of formerly interlayered organic matter following smectite illitization with increasing thermal maturity (Kennedy et al., 2014; Berthonneau et al., 2016). This provides a potential explanation for the clay mineral catalysis in Monterey Formation samples where layered smectite clays are intimately associated with organic matter at the nanometre scale. Demineralization to extract the kerogen removes the reactive smectite surfaces and thus removes the clay catalytic effects.

Horsfield and Douglas (1980) reported similar mineral matrix effects as observed in this study, where they produced higher yields of low molecular weight pyrolysis products for isolated kerogen mixed with bentonite as compared to isolated kerogen alone. Dembicki (1992) studied the mineral matrix effects for Kimmeridge shale samples and their results show that smectite clays (e.g. montmorillonite) shift the activation energies to lower values for samples with lower organic matter contents (1-2 wt.% TOC); with increments in organic matter content, the catalytic effects are less and the activation energy becomes more similar to that for the isolated kerogens. As mentioned above, our results show similar mineral matrix effects of shifting activation energy towards lower values for Monterey samples which have nanocomposite fabrics and no apparent mineral matrix effects for Stuart Range samples which have a particulate fabric (Fig. 4.9, 11). A study by Yang and Horsfield (2016) indicates that a component of clay mineral catalysis reported in pyrolysis experiments may be artifacts of the high temperatures and fast-heating rates associated with laboratory pyrolysis, and that catalysis is therefore likely to be less important in natural geological settings than seen experimentally. This is consistent with earlier work by Dieckmann et al. (2000). The Yang and Horsfield (2016) study does not, however, completely preclude the possibility that catalytic activity takes place in natural settings. Furthermore, there was no consideration given to shale fabrics and the influence of varying amounts of contact area shared between mineral surfaces and organic compounds.

The effect of clay catalysis at laboratory heating rates is significant in rocks with nanocomposite fabric, where clay minerals are intimately associated with organic matter. With the exception of one sample (M62), geological extrapolation of the Monterey samples which have nanocomposite fabric shows that at the onset of modelled hydrocarbon generation (10% transformation ratio), whole rock samples generate hydrocarbons at an average 20°C lower than that for their kerogen isolates (Fig. 4.11). At 90% transformation ratio, the difference is 30°C. This indicates that clay mineral catalysis affects modelled hydrocarbon generation from its onset throughout its progression to the hydrocarbon kitchen (the temperature-depth zone where the majority of the hydrocarbon generation occurs) in laboratory conditions. If this were to occur in nature, this would represent a critical influence on the timing and yield of hydrocarbon generation for a wide variety of clay-rich sedimentary rocks under geological conditions where geothermal gradients are typically in the range of 2 to 5°C /100m in sedimentary basins (Pan et al., 2016). This could lead to a difference in the predicted onset of generation of up to 1.5 km in burial depth.

Environmental control on clay mineral catalysis

The close association of organic matter and detrital minerals in the Monterey Formation has been previously reported, with early studies suggesting this is the product of adsorption of organic matter on clay minerals in the water column (e.g. Isaacs, 1983) and subsequent co-transport of organic matter and detrital minerals as fecal pellets (e.g. Dunbar and Berger, 1981). While we cannot rule out water column adsorption of organic matter to clay surfaces,

fecal pellets do not appear to be a major component of the Monterey samples studied here. Furthermore, nanocomposites are clearly not restricted to fecal pellets, rather they appear as a distinct rock fabric comprising specific maceral content (Fig. 4.4c, 4.4d, 4.6). Depositional environment controls the composition of detrital clay minerals and discrete organic particles while diagenetic processes determine the intercalation and formation of nanocomposites in sediments. The fabric of shale depends on the amount of detrital clay and type of organic matter introduced during deposition and subsequent modification by diagenesis. In the Naples Beach section, the Monterey Formation was deposited in a slope setting dominated by hemipelagic contributions, limited dilution of organic carbon, and slow sediment accumulation rates (0.5 to 9 mg/cm2/yr) (Isaacs, 2001). The TOC content of the Monterey Formation samples is inversely proportional to sediment accumulation rate (Isaacs, 2001) and directly proportional to MSA and hence smectite abundance. A slow accumulation rate provides an increased residence time in the most microbially active, early diagenetic zone close to the sediment-water interface (Parkes et al., 1993a). This is likely to facilitate diagenetic and microbial modification of primary organic matter such that it interacts and becomes associated with reactive detrital clay surfaces (e.g. Bennett et al., 1999; Ransom et al., 1999) to form organoclay aggregates and nanocomposites (Fig. 4.6) within the Monterey Formation.

Limited chemical weathering associated with cold climate conditions of the early Permian in South Australia restricted the abundance of detrital clay minerals in the Stuart Range Formation. Since the majority of the smectite

clays in the Stuart Range samples are restricted to a pore filling habit, and thus authigenic, a limited relationship exists between TOC and MSA. During deposition and early diagenesis of the Stuart Range sediments, few detrital, reactive clay minerals were present (as compared to the Monterey Formation) to associate with organic compounds dissolved in seawater or pore waters. Moreover, compared to the Monterey Formation samples, the amounts of terrestrial organic matter and discrete alginite is greater in the Stuart Range samples. These fractions are less likely to become intimately associated with clays such that the primary organic matter fraction is preserved as distinct particles in the rock matrix (Fig. 4.3). This observation is consistent with the bulk kinetics results of Stuart Range samples showing negligible or no clay catalytic effects on hydrocarbon generation.

One Monterey sample (M62) demonstrates no clay catalytic effect during geological extrapolation of hydrocarbon generation, unlike the other Monterey samples where significant clay catalysis is observed (Fig. 4.11). The quantity of authigenic smectites in M62 is greater than for other Monterey samples and textures of the smectite grains suggest that these are formed later with diagenetic alteration of volcanic glass. Unlike other Monterey samples, where detrital smectites predominate, the smectites in M62 have minimal contact area with the organic matter (Fig. 4.13), leading to negligible catalytic effects.

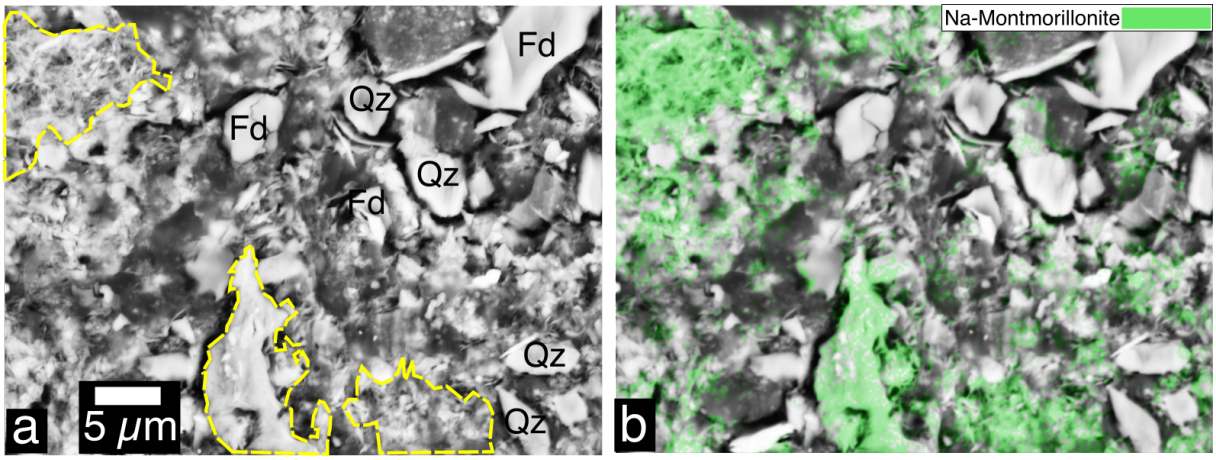

Fig 4.13: a: BSE photomicrographs of a Monterey sample (M62). The dashed outlines indicate randomly oriented clay crystals forming discrete grains; these are interpreted as altered volcanic glass particles. b: Nanomin mineral mapping of the same view shows that the diagenetic clays are smectites. Fd = Feldspar, Qz = Quartz.

4.5. Conclusions

A low supply of terrigenous sediments, high primary organic productivity and slow sediment accumulation rate for the Monterey Formation resulted in an organic rich shale with an intimate association of organic matter and clay minerals as organoclay aggregates and nanocomposites. In the Stuart Range Formation, limited chemical weathering of precursor periglacial sediments restricted the presence of detrital clay minerals and the organic matter is preserved as discrete particles that are mainly >5 μm in size.

Organic matter in the Stuart Range samples comprises mainly telalginite and lamalginite along with sporinite, liptodetrinite, bituminite, micrinite, vitrinite and inertinite. By contrast, most of the organic matter in the Monterey Formation samples comprises bituminite, in large part intimately associated with smectite. The Monterey samples have nanocomposite fabrics

and have organic carbon contents and hydrogen indices that exceed those of the Stuart Range samples. These two endmember shale fabrics, particulate and nanocomposite, control the physical contact of reactive clay surfaces to labile organic matter in the rocks.

Bulk kinetic experiments suggest that the Monterey sample kerogens are structurally heterogeneous, potentially due to the presence of alginite as well as the dominant bituminite and the abundance of both strong C-C and weaker C-S bonds. As indicated by the narrow range in distribution of activation energies, the Stuart Range sample kerogens appear to be comparatively homogenous, even though vitrinite and inertinite are present as well as the dominant alginite. Since the higher plant-derived organic matter has lower hydrogen content, however, they would contribute less oil generation, than for the alginites. Comparison of the hydrocarbon generation kinetics of paired kerogen isolates versus whole rock samples demonstrates that the onset temperature of hydrocarbon generation is reduced by 20°C for samples having nanocomposite fabric. This is attributed to clay catalysis. No clay mineral catalytic effect was observed in shale samples with particulate fabric.

The intimate contacts of smectite surfaces with organic matter induce maximum catalytic effects for hydrocarbon generation in the Monterey Formation samples. The results of this study suggest that the processes leading to particulate or nanocomposite fabrics in shale, controlled by the depositional setting and diagenesis of sediments, influences the clay catalytic effects on hydrocarbon generation temperature and thus burial depth of generation. Hydrocarbon source rocks with nanocomposite fabric are likely to

start generation at significantly shallower depths, up to 1500m shallower, than for a source rock with particulate fabric, provided the mineralogy and organic matter of the two rocks are comparable.

Acknowledgements

The Australian Research Council (ARC) is acknowledged for providing financial support (ARC Linkage Project LP120200086 to M. J. Kennedy) to conduct the research project. We thank Simon George, Macquarie University for assistance with solvent extractions. SEM analyses were conducted using microscope facilities at the Department of Earth and Planetary Sciences and the Biology Microscopy Unit at Macquarie University. We thank three anonymous reviewers and the editor for their insightful and constructive comments.

References

Abbassi, S., Edwards, D.S., George, S.C., Volk, H., Mahlstedt, N., di Primio, R., Horsfield, B., 2016. Petroleum potential and kinetic models for hydrocarbon generation from the Upper Cretaceous to Paleogene Latrobe Group coals and shales in the Gippsland Basin, Australia. Organic Geochemistry 91, 54-67.

Abid, I., Hesse, R., 2007. Illitizing fluids as precursors of hydrocarbon migration along transfer and boundary faults of the Jeanne d'Arc Basin offshore Newfoundland, Canada. Marine and Petroleum Geology 24, 237-245.

Acholla, F.V., Orr, W.L., 1993. Pyrite removal from kerogen without altering organic matter: the chromous chloride method. Energy & fuels 7, 406-410.

Ahn, J., Peacor, D., 1986. Transmission and analytical electron microscopy of the smectite-to-illite transition. Clays and Clay Minerals 34, 165-179.

Alexander, E.M., Sansome, A., Cotton, T.B., 2006. Lithostratigraphy and environments of deposition, in: Cotton, T.B., Scardigno, M.F., Hibburt, J.E. (Eds.), The Petroleum Geology of South Australia Vol.2: Eromanga Basin. Department of Primary Industry and Resources, Adelaide.

Alldredge, A.L., Silver, M.W., 1988. Characteristics, dynamics and significance of marine snow. Progress in oceanography 20, 41-82.

Aplin, A.C., Macquaker, J.H., 2011. Mudstone diversity: Origin and implications for source, seal, and reservoir properties in petroleum systems. AAPG Bulletin 95, 2031-2059.

Aringhieri, R., 2004. Nanoporosity Characteristics of Some Natural Clay Minerals and Soils. Clays and Clay Minerals 52, 700-704.

Arthur, M.A., Sageman, B.B., 1994. Marine shales: depositional mechanisms and environments of ancient deposits. Annual review of Earth and planetary sciences 22, 499-551.

Australian Standards, 1998. AS 2856.2: Coal Petrography. Part 2: Maceral Analysis.

Australian Standards, 2000. AS2456.3: Microscopical determination of the reflectance of coal macerals. Standards Association of Australia.

Barron, J.A., 1986. Paleoceanographic and tectonic controls on deposition of the Monterey formation and related siliceous rocks in California. Palaeogeography, Palaeoclimatology, Palaeoecology 53, 27-45.

Barron, J.A., Isaacs, C.M., 2001. Updated chronostratigraphic framework for the California Miocene. The Monterey Formation: From Rocks to Molecules. Columbia University Press, New York, 393-395.

Behar, F., Vandenbroucke, M., Tang, Y., Marquis, F., Espitalie, J., 1997. Thermal cracking of kerogen in open and closed systems: determination of kinetic parameters and stoichiometric coefficients for oil and gas generation. Organic Geochemistry 26, 321-339.

Belin, S., 1992. Application of backscattered electron imaging to the study of source rocks microtextures. Organic Geochemistry 18, 333-346.

Belin, S., Huc, A.Y., 2001. Organic Matter Microhabit Within the Monterey Formation (Miocene of California). The Monterey Formation: From Rocks to Molecules, 77.

Bennett, R.H., Ransom, B., Kastner, M., Baerwald, R.J., Hulbert, M.H., Sawyer, W.B., Olsen, H., Lambert, M.W., 1999. Early diagenesis: impact of organic matter on mass physical properties and processes, California continental margin. Marine Geology 159, 7-34.

Berndmeyer, C., Birgel, D., Brunner, B., Wehrmann, L.M., Jöns, N., Bach, W., Arning, E.T., Föllmi, K.B., Peckmann, J., 2012. The influence of bacterial activity on phosphorite formation in the Miocene Monterey Formation, California. Palaeogeography, Palaeoclimatology, Palaeoecology 317–318, 171-181.

Berthonneau, J., Grauby, O., Abuhaikal, M., Pellenq, R.J.-M., Ulm, F.J., Van Damme, H., 2016. Evolution of organo-clay composites with respect to thermal maturity in type II organic-rich source rocks. Geochimica et Cosmochimica Acta 195, 68-83.

Bishop, A., Kearsley, A., Patience, R., 1992. Analysis of sedimentary organic materials by scanning electron microscopy: the application of backscattered electron imagery and light element X-ray microanalysis. Organic Geochemistry 18, 431-446.

Blair, N.E., Aller, R.C., 2012. The fate of terrestrial organic carbon in the marine environment. Annual Review of Marine Science 4, 401-423.

Boggs, S., 2009. Petrology of sedimentary rocks. Cambridge University Press.

Braun, R.L., Burnham, A.K., 1987. Analysis of chemical reaction kinetics using a distribution of activation energies and simpler models. Energy & fuels 1, 153-161.

Brincat, D., Abbott, G.D., 2001. Some aspects of the molecular biogeochemistry of laminated and massive rocks from the Naples Beach Section (Santa Barbara-Ventura Basin). The Monterey Formation: From Rocks to Molecules. Columbia University Press, New York, 140-149.

Brown, D., Rhodes, C., 1997. Brønsted and Lewis acid catalysis with ion-exchanged clays. Catalysis Letters 45, 35-40.

Burnham, A.K., 1994. Comments on "The effects of the mineral matrix on the determination of kinetic parameters using modified Rock-Eval pyrolysis" by H. Dembicki Jr, and the resulting comment by R. Pelet. Organic Geochemistry 21, 985-986.

Burnham, A.K., Braun, R.L., Samoun, A.M., 1988. Further comparison of methods for measuring kerogen pyrolysis rates and fitting kinetic parameters. Organic Geochemistry 13, 839-845.

Calvert, S., Nielsen, B., Fontugne, M., 1992. Evidence from nitrogen isotope ratios for enhanced productivity during formation of eastern Mediterranean sapropels.

Carr, L., Korsch, R., Preiss, W., Menpes, S., Holzschuh, J., 2012. Key features of new deep seismic reflection lines across frontier sedimentary basins in central Australia: the Arckaringa, Officer, Amadeus and Georgina Basins. ASEG Extended Abstracts 2012, 1-4.

Chamley, H., 1989. Clay sedimentology / Hervé Chamley. Springer-Verlag, London New York.

Cihacek, L., Bremner, J., 1979. A simplified ethylene glycol monoethyl ether procedure for assessment of soil surface area. Soil Science Society of America Journal 43, 821-822.

Clark, J., Comerford, J., Macquarrie, D.J., 2013. Green Catalytic Transformations, in: Anastas, P.T., Zimmerman, J.B. (Eds.), Innovations in Green Chemistry and Green Engineering. Springer New York, pp. 37-80.

Compton, J.S., 1991. Porosity reduction and burial history of siliceous rocks from the Monterey and Sisquoc Formations, Point Pedernales area, California. Geological Society of America Bulletin 103, 625-636.

Debenham, N., 2015. Controls on organic carbon enrichment in a Permian Periglacial setting (Arckaringa Basin), MSc Thesis, Earth and Planetary Sciences. Macquarie University, Sydney, pp. 15 - 39.

Dembicki, H., 1992. The effects of the mineral matrix on the determination of kinetic parameters using modified Rock Eval pyrolysis. Organic Geochemistry 18, 531-539.

Dieckmann, V., 2005. Modelling petroleum formation from heterogeneous source rocks: the influence of frequency factors on activation energy distribution and geological prediction. Marine and Petroleum Geology 22, 375-390.

Dieckmann, V., Horsfield, B., Schenk, H.J., 2000. Heating rate dependency of petroleum-forming reactions: implications for compositional kinetic predictions. Organic Geochemistry 31, 1333-1348.

Drits, V., Sakharov, B., Lindgreen, H., Salyn, A., 1997. Sequential structure transformation of illite-smectite-vermiculite during diagenesis of Upper Jurassic shales from the North Sea and Denmark. Clay Minerals 32, 351-371.

Dunbar, R.B., Berger, W.H., 1981. Fecal pellet flux to modern bottom sediment of Santa Barbara Basin (California) based on sediment trapping. Geological Society of America Bulletin 92, 212-218.

Durand, B., 1980. Kerogen: Insoluble organic matter from sedimentary rocks. Editions technip.

Eberl, D.D., 2003. User Guide to RockJock - A Program for Determining Quantitative Mineralogy from X-Ray Diffraction Data, Open-File Report, - ed.

Ehrlich, H.L., 1996. How microbes influence mineral growth and dissolution. Chemical Geology 132, 5-9.

Eslinger, E., Highsmith, P., Albers, D., DeMayo, B., 1979. Role of iron reduction in the conversion of smectite to illite in bentonites in the Disturbed Belt, Montana. Clays and Clay Minerals 27, 327-338.

Espitalié, J., 1986. Use of Tmax as a maturation index for different types of organic matter. Comparison with vitrinite reflectance, Thermal modelling in sedimentary basins. Editions Technip Paris, pp. 475-496.

Espitalie, J., Madec, M., Tissot, B., 1980. Role of mineral matrix in kerogen pyrolysis: influence on petroleum generation and migration. AAPG Bulletin 64, 59-66.

Espitalie, J., Ungerer, P., Irwin, I., Marquis, F., 1988. Primary cracking of kerogens. Experimenting and modelling C 1, C 2–C 5, C 6–C 15 and C 15+ classes of hydrocarbons formed. Organic Geochemistry 13, 893-899.

Föllmi, K.B., Badertscher, C., de Kaenel, E., Stille, P., John, C.M., Adatte, T., Steinmann, P., 2005. Phosphogenesis and organic-carbon preservation in the Miocene Monterey Formation at Naples Beach, California—The Monterey hypothesis revisited. Geological Society of America Bulletin 117, 589-619.

Galwey, A.K., 1972. The rate of hydrocarbon desorption from mineral surfaces and the contribution of heterogeneous catalytic-type processes to petroleum genesis. Geochimica et Cosmochimica Acta 36, 1115-1130.

Garrels, R.M., Mackenzie, F.T., 1971. Evolution of sedimentary rocks.

Garrison, R.E., Hoppie, B.W., Grimm, K.A., 1994. Phosphates and dolomites in coastal upwelling sediments of the Peru margin and the Monterey Formation (Naples Beach section), California.

Gilby, A.R., Foster, C.B., 1988. Early Permian palynology of the Arckaringa Basin, South Australia. Palaeontographica Abteilung B, 167-191.

Goldstein, J.I., Newbury, D.E., Echlin, P., Joy, D.C., Fiori, C., Lifshin, E., 1981. Scanning electron microscopy and X-ray microanalysis. A text for biologists, materials scientists, and geologists. Plenum Publishing Corporation.

Graham, S., Williams, L., 1985. Tectonic, depositional, and diagenetic history of Monterey Formation (Miocene), central San Joaquin basin, California. AAPG Bulletin 69, 385-411.

Han, S., Horsfield, B., Zhang, J., Chen, Q., Mahlstedt, N., di Primio, R., Xiao, G., 2014. Hydrocarbon Generation Kinetics of Lacustrine Yanchang Shale in Southeast Ordos Basin, North China. Energy & fuels 28, 5632-5639.

Hartnett, H.E., Keil, R.G., Hedges, J.I., Devol, A.H., 1998. Influence of oxygen exposure time on organic carbon preservation in continental margin sediments. Nature 391, 572-575.

Hedges, J.I., 1992. Global biogeochemical cycles: progress and problems. Marine chemistry 39, 67-93.

Hedges, J.I., Keil, R.G., 1995. Sedimentary organic matter preservation: an assessment and speculative synthesis. Marine chemistry 49, 81-115.

Heller-Kallai, L., Aizenshtat, Z., Miloslavski, I., 1984. The effect of various clay minerals on the thermal decomposition of stearic acid under 'bulk flow'conditions. Clay Miner 19, 779-788.

Hibburt, J.E., 1984. A Review of exploration in the Arckaringa Basin, Report Book 84/1, South Australia, pp. 1887-1983.

Hornafius, J.S., 1994. Field Guide to the Monterey Formation between Santa Barbara and Gaviota, California.

Horsfield, B., Curry, D., Bohacs, K., Littke, R., Rullkötter, J., Schenk, H., Radke, M., Schaefer, R., Carroll, A., Isaksen, G., 1994. Organic geochemistry of freshwater and alkaline lacustrine sediments in the Green River Formation of the Washakie Basin, Wyoming, USA. Organic Geochemistry 22, 415-440.

Horsfield, B., Douglas, A., 1980. The influence of minerals on the pyrolysis of kerogens. Geochimica et Cosmochimica Acta 44, 1119-1131.

Hower, J., Eslinger, E.V., Hower, M.E., Perry, E.A., 1976. Mechanism of burial metamorphism of argillaceous sediment: 1. Mineralogical and chemical evidence. Geological Society of America Bulletin 87, 725-737.

Hu, M., Cheng, Z., Zhang, M., Liu, M., Song, L., Zhang, Y., Li, J., 2014. Effect of Calcite, Kaolinite, Gypsum, and Montmorillonite on Huadian Oil Shale Kerogen Pyrolysis. Energy & fuels 28, 1860-1867.

Huizinga, B.J., Tannenbaum, E., Kaplan, I.R., 1987. The role of minerals in the thermal alteration of organic matter—III. Generation of bitumen in laboratory experiments. Organic Geochemistry 11, 591-604.

Isaacs, C.M., 1983. Compositional variation and sequence in the Miocene Monterey Formation, Santa Barbara coastal area, California. SEPM, 117-132.

Isaacs, C.M., 2001. Depositional framework of the Monterey formation, California. The Monterey Formation: From Rocks to Molecules, 1-30.

Isaacs, C.M., Pollastro, R.M., Barron, J.A., Ingle Jr, J.C., Bukry, D., Dunbar, R.B., Keller, M.A., Tomson, J.H., Lewan, M.D., 2001. Geologic and

Paleontologic Features of Rock Samples in the Cooperative Monterey Organic Geochemistry Study, Naples Beach and Lions Head Sections, California. The Monterey Formation: From Rocks to Molecules, 373.

Jahnke, R.A., 1990. Early diagenesis and recycling of biogenic debris at the seafloor, Santa Monica Basin, California. Journal of marine research 48, 413-436.

Jarvie, D.M., Claxton, B.L., Henk, F., Breyer, J., 2001. Oil and shale gas from the Barnett Shale, Ft, Worth Basin, Texas (abs.): AAPG Annual Meeting Program, p. A100.

Jinsheng, G., 2009. Coal, Oil Shale, Natural Bitumen, Heavy Oil and Peat - Volume II.

Johns, W.D., 1979. Clay mineral catalysis and petroleum generation. Annual review of Earth and planetary sciences 7, 183.

Johns, W.D., Shimoyama, A., 1972. Clay minerals and petroleum-forming reactions during burial and diagenesis. AAPG Bulletin 56, 2160-2167.

Keil, R., Mayer, L., 2014. Mineral matrices and organic matter. Treatise on geochemistry 12, 337-359.

Keil, R.G., Montlucon, D.B., Prahl, F.G., Hedges, J.I., 1994. Sorptive preservation of labile organic matter in marine sediments. Nature 370, 549-552.

Kellendonk, F., Heinerman, J., van Santen, R., 1987. Clay-activated isomerization reactions. Preparative Chemistry using supported reagents, 455.

Kennedy, M.J., Löhr, S.C., Fraser, S.A., Baruch, E.T., 2014. Direct evidence for organic carbon preservation as clay-organic nanocomposites in a

Devonian black shale; from deposition to diagenesis. Earth and Planetary Science Letters 388, 59-70.

Kennedy, M.J., Pevear, D.R., Hill, R.J., 2002. Mineral surface control of organic carbon in black shale. Science 295, 657-660.

Kennedy, M.J., Wagner, T., 2011. Clay mineral continental amplifier for marine carbon sequestration in a greenhouse ocean. Proceedings of the National Academy of Sciences 108, 9776-9781.

Kim, J., Dong, H., Seabaugh, J., Newell, S.W., Eberl, D.D., 2004. Role of Microbes in the Smectite-to-Illite Reaction. Science 303, 830-832.

Klemme, H., Ulmishek, G.F., 1991. Effective petroleum source rocks of the world: stratigraphic distribution and controlling depositional factors (1). AAPG Bulletin 75, 1809-1851.

Kuila, U., McCarty, D.K., Derkowski, A., Fischer, T.B., Topór, T., Prasad, M., 2014. Nano-scale texture and porosity of organic matter and clay minerals in organic-rich mudrocks. Fuel 135, 359-373.

Lagaly, G., 1981. Characterization of clays by organic compounds. CLAY MINER. Clay Miner. 16, 1.

Lagaly, G., Ogawa, M., Dékány, I., 2013. Clay mineral organic interactions. Handbook of clay science.

Laurent, D., de Kaenel, E., Spangenberg, J.E., Föllmi, K.B., 2015. A sedimentological model of organic-matter preservation and phosphogenesis in the Miocene Monterey Formation at Haskells Beach, Goleta (central California). Sedimentary Geology 326, 16-32.

Lazar, O.R., Bohacs, K.M., Macquaker, J.H., Schieber, J., Demko, T.M., 2015. Capturing key attributes of fine-grained sedimentary rocks in outcrops,

cores, and thin sections: nomenclature and description guidelines. Journal of Sedimentary Research 85, 230-246.

Lewan, M.D., Roy, S., 2011. Role of water in hydrocarbon generation from Type-I kerogen in Mahogany oil shale of the Green River Formation. Organic Geochemistry 42, 31-41.

Li, Y., Cai, J., Song, G., Ji, J., 2015. DRIFT spectroscopic study of diagenetic organic–clay interactions in argillaceous source rocks. Spectrochimica Acta Part A: Molecular and Biomolecular Spectroscopy 148, 138-145.

Linc Energy, 2012. ARCK-1 well completion report, PEL 122, Arckaringa basin, South Australia. Department of State Development, Adelaide.

Lochte, K., Turley, C., 1988. Bacteria and cyanobacteria associated with phytodetritus in the deep sea. Nature 333, 67.

Löhr, S.C., Baruch, E.T., Hall, P.A., Kennedy, M.J., 2015. Is organic pore development in gas shales influenced by the primary porosity and structure of thermally immature organic matter? Organic Geochemistry 87, 119-132.

Löhr, S.C., Kennedy, M.J., 2014. Organomineral nanocomposite carbon burial during Oceanic Anoxic Event 2. Biogeosciences 11, 4971-4983.

Lynch, F.L., Mack, L.E., Land, L.S., 1997. Burial diagenesis of illite/smectite in shales and the origins of authigenic quartz and secondary porosity in sandstones. Geochimica et Cosmochimica Acta 61, 1995-2006.

Macquaker, J.H., Adams, A., 2003. Maximizing information from fine-grained sedimentary rocks: An inclusive nomenclature for mudstones. Journal of Sedimentary Research 73, 735-744.

Macquaker, J.H., Keller, M.A., Davies, S.J., 2010. Algal blooms and "marine snow": Mechanisms that enhance preservation of organic carbon in ancient fine-grained sediments. Journal of Sedimentary Research 80, 934-942.

Macquaker, J.H., Taylor, K.G., Keller, M., Polya, D., 2014. Compositional controls on early diagenetic pathways in fine-grained sedimentary rocks: Implications for predicting unconventional reservoir attributes of mudstones. AAPG Bulletin 98, 587-603.

Mayer, L.M., 1994. Surface area control of organic carbon accumulation in continental shelf sediments. Geochimica et Cosmochimica Acta 58, 1271-1284.

McCabe, R.W., Adams, J.M., 2013. Clay Minerals as Catalysts, in: Bergaya, F., Gerhard, L. (Eds.), Developments in Clay Science. Elsevier, UK, pp. 491-538.

Menpes, S., Korsch, R., Carr, L., 2010. 2008 Gawler Craton-Officer Basin-Musgrave Province-Amadeus Basin (GOMA) seismic survey, 08GA-OM1: Geological interpretation of the Arckaringa Basin, GOMA (Gawler Craton–Officer Basin–Musgrave Province–Amadeus Basin) Seismic and MT Workshop 2010, p. 16.

Milliken, K.L., Ko, L.T., Pommer, M., Marsaglia, K.M., 2014. SEM petrography of Eastern Mediterranean sapropels: Analogue data for assessing organic matter in oil and gas shales. Journal of Sedimentary Research 84, 961-974.

Ming, Q., Xilin, R., Dazhong, T., Jian, X., Wolf, M., 1994. Petrographic and geochemical characterization of pale and dark brown coal from Yunnan Province, China. International Journal of Coal Geology 25, 65-92.

Müller, P.J., Suess, E., 1979. Productivity, sedimentation rate, and sedimentary organic matter in the oceans—I. Organic carbon preservation. Deep Sea Research Part A. Oceanographic Research Papers 26, 1347-1362.

Nadeau, P., Wilson, M., McHardy, W., Tait, J., 1985. The conversion of smectite to illite during diagenesis: evidence from some illitic clays from bentonites and sandstones. Mineralogical Magazine 49, 393-400.

Orr, W.L., 1986. Kerogen/asphaltene/sulfur relationships in sulfur-rich Monterey oils. Organic Geochemistry 10, 499-516.

Pakdel, H., Roy, C., Kalkreuth, W., 1999. Oil production by vacuum pyrolysis of Canadian oil shales and fate of the biological markers. Fuel 78, 365-375.

Pan, C., Jiang, L., Liu, J., Zhang, S., Zhu, G., 2010. The effects of calcite and montmorillonite on oil cracking in confined pyrolysis experiments. Organic Geochemistry 41, 611-626.

Pan, L., Xiao, X., Tian, H., Zhou, Q., Cheng, P., 2016. Geological models of gas in place of the Longmaxi shale in Southeast Chongqing, South China. Marine and Petroleum Geology 73, 433-444.

Parkes, R.J., Cragg, B.A., Bale, S., Getlifff, J., Goodman, K., Rochelle, P.A., Fry, J.C., Weightman, A.J., Harvey, S., 1994. Deep bacterial biosphere in Pacific Ocean sediments. Nature 371, 410.

Parkes, R.J., Cragg, B.A., Getliff, J., Harvey, S., Fry, J.C., Lewis, C., Rowland, S., 1993a. A quantitative study of microbial decomposition of biopolymers in Recent sediments from the Peru Margin. Marine Geology 113, 55-66.

Parkes, R.J., Cragg, B.A., Getliff, J.M., Harvey, S.M., Fry, J.C., Lewis, C.A., Rowland, S.J., 1993b. A quantitative study of microbial decomposition of biopolymers in Recent sediments from the Peru Margin. Marine Geology 113, 55-66.

Pelet, R., 1994. Comments on the paper "The effects of the mineral matrix on the determination of kinetic parameters using modified Rock-Eval pyrolysis" by H. Dembicki Jr, Org. Geochem., 18, 531–539 (1992). Organic Geochemistry 21, 979-981.

Pepper, A.S., Corvi, P.J., 1995. Simple kinetic models of petroleum formation. Part I: oil and gas generation from kerogen. Marine and Petroleum Geology 12, 291-319.

Pepper, A.S., Dodd, T.A., 1995. Simple kinetic models of petroleum formation. Part II: oil-gas cracking. Marine and Petroleum Geology 12, 321-340.

Perry, E., Hower, J., 1970. Burial diagenesis in Gulf Coast pelitic sediments. Clays and Clay Minerals 18, 165-177.

Peters, K.E., Burnham, A.K., Walters, C.C., 2015. Petroleum generation kinetics: Single versus multiple heating-ramp open-system pyrolysis. AAPG Bulletin 99, 591-616.

Pevear, D.R., 1999. Illite and hydrocarbon exploration. Proceedings of the National Academy of Sciences 96, 3440-3446.

Pollard, C.O., 1971. Semidisplacive mechanism for diagenetic alteration of montmorillonite layers to illite layers. Geological Society of America Special Papers 134, 79-94.

Potter, P.E., Maynard, J.B., Depetris, P.J., 2005. Mud and mudstones: Introduction and overview. Springer Science & Business Media.

Rahman, H.M., Kennedy, M., Löhr, S., Dewhurst, D.N., 2017. Clay-organic association as a control on hydrocarbon generation in shale. Organic Geochemistry 105, 42-55.

Rahman, H.M., Kennedy, M., Löhr, S., Dewhurst, D.N., Sherwood, N., Yang, S., Horsfield, B., 2018. The influence of shale depositional fabric on the kinetics of hydrocarbon generation through control of mineral surface contact area on clay catalysis. Geochimica et Cosmochimica Acta 220, 429-448.

Ransom, B., Bennett, R.H., Baerwald, R., Hulbert, M.H., Burkett, P.-J., 1999. In situ conditions and interactions between microbes and minerals in fine-grained marine sediments: A TEM microfabric perspective. American Mineralogist 84, 183-192.

Ransom, B., Bennett, R.H., Baerwald, R., Shea, K., 1997. TEM study of in situ organic matter on continental margins: occurrence and the “monolayer” hypothesis. Marine Geology 138, 1-9.

Ray, S.S., 2013. Clay-containing polymer nanocomposites: from fundamentals to real applications. Newnes.

Reimers, C.E., 2001. Petrographic clues to processes leading to high organic carbon concentrations in the Naples Beach section of the Monterey Formation. The Monterey Formation, 59-76.

Reynolds, J.G., Burnham, A.K., Mitchell, T.O., 1995. Kinetic analysis of California petroleum source rocks by programmed temperature micropyrolysis. Organic Geochemistry 23, 109-120.

Romero-Sarmiento, M.-F., Euzen, T., Rohais, S., Jiang, C., Littke, R., 2016. Artificial thermal maturation of source rocks at different thermal maturity levels: Application to the Triassic Montney and Doig formations in the Western Canada Sedimentary Basin. Organic Geochemistry 97, 148-162.

Salmon, V., Derenne, S., Lallier-Vergès, E., Largeau, C., Beaudoin, B., 2000. Protection of organic matter by mineral matrix in a Cenomanian black shale. Organic Geochemistry 31, 463-474.

Schaefer, R., Schenk, H., Hardelauf, H., Harms, R., 1990. Determination of gross kinetic parameters for petroleum formation from Jurassic source rocks of different maturity levels by means of laboratory experiments. Organic Geochemistry 16, 115-120.

Schenk, H., Horsfield, B., 1998. Using natural maturation series to evaluate the utility of parallel reaction kinetics models: an investigation of Toarcian shales and Carboniferous coals, Germany. Organic Geochemistry 29, 137-154.

Schenk, H.J., Di Primio, R., Horsfield, B., 1997. The conversion of oil into gas in petroleum reservoirs. Part 1: Comparative kinetic investigation of gas generation from crude oils of lacustrine, marine and fluviodeltaic origin by programmed-temperature closed-system pyrolysis. Organic Geochemistry 26, 467-481.

Schenk, H.J., Dieckmann, V., 2004. Prediction of petroleum formation: the influence of laboratory heating rates on kinetic parameters and geological extrapolations. Marine and Petroleum Geology 21, 79-95.

Schultz, L.G., Tourtelot, H., Gill, J.R., Boerngen, J., 1980. Composition and properties of the Pierre Shale and equivalent rocks, northern Great Plains region. US Govt. Print. Off.

Setti, M., Marinoni, L., López-Galindo, A., 2004. Mineralogical and geochemical characteristics (major, minor, trace elements and REE) of detrital and authigenic clay minerals in a Cenozoic sequence from Ross Sea, Antarctica. Clay Minerals 39, 405-421.

Shaldybin, M., Lopushnyak, Y., Goncharov, I., Wilson, M., Wilson, L., Mendis, B., 2017. The mineralogy of the clayey-silty siliceous rocks in the Bazhenov Shale Formation (Upper Jurassic) in the west Siberian Basin, Russia: The role of diagenesis and possible implications for their exploitation as an unconventional hydrocarbon reservoir. Applied Clay Science 136, 75-89.

Shanks, A.L., 2002. The abundance, vertical flux, and still-water and apparent sinking rates of marine snow in a shallow coastal water column. Continental Shelf Research 22, 2045-2064.

Shaw, D.B., Weaver, C.E., 1965. The mineralogical composition of shales. Journal of Sedimentary Research 35.

Sherrod, L.A., Dunn, G., Peterson, G.A., Kolberg, R.L., 2002. Inorganic Carbon Analysis by Modified Pressure-Calcimeter Method. Soil Science Society of America Journal 66, 299-305.

Shimoyama, A., Johns, W.D., 1971. Catalytic conversion of fatty acids to petroleum-like paraffins and their maturation. Nature 232, 140-144.

Stach, E., 1982. Stach's textbook of coal petrology.

Suárez-Ruiz, I., Al-Juboury, A., 2012. Organic petrology: an overview. Petrology—New Perspectives and Applications.

Suárez-Ruiz, I., Flores, D., Mendonça Filho, J.G., Hackley, P.C., 2012. Review and update of the applications of organic petrology: Part 1, geological applications. International Journal of Coal Geology 99, 54-112.

Tannenbaum, E., Huizinga, B.J., Kaplan, I.R., 1986. Role of minerals in thermal alteration of organic matter--II: a material balance. AAPG Bulletin 70, 1156-1165.

Tannenbaum, E., Kaplan, I.R., 1985. Role of minerals in the thermal alteration of organic matter—I: Generation of gases and condensates under dry condition. Geochimica et Cosmochimica Acta 49, 2589-2604.

Taylor, G.H., 1998. Organic petrology: A new handbook incorporating some revised parts of Stach's textbook of coal petrology. Gebruder Borntraeger Verlagsbuchhandlung.

Teln, N., Hanesand, T., Hermansen, D., Jarvie, D.M., 2001. Characterization of Source Rock Potential, Hydrocarbon Generation, and Maturity in Well OCS-315-1, Offshore Santa Maria Basin, California. The Monterey Formation: From Rocks to Molecules, 310.

Tennyson, M.E., Isaacs, C.M., 2001. Geologic setting and petroleum geology of Santa Maria and Santa Barbara basins, coastal California. The Monterey Formation From Rocks to Molecules, 206-229.

Tiller, K., Smith, L., 1990. Limitations of EGME retention to estimate the surface area of soils. Soil Research 28, 1-26.

Tissot, B., Pelet, R., Ungerer, P., 1987. Thermal history of sedimentary basins, maturation indices, and kinetics of oil and gas generation. AAPG Bulletin 71, 1445-1466.

Tissot, B.P., Welte, D.H., 1984. Petroleum formation and occurrence. Springer-Verlag.

Townsend, I.J., 1976. A synthesis of stratigraphic drilling in the Arckaringa Basin, Report of Investigations. South Australia geological Survey, South Australia, pp. 1969 - 1971.

Tyson, R., 2001. Sedimentation rate, dilution, preservation and total organic carbon: some results of a modelling study. Organic Geochemistry 32, 333-339.

Tyson, R., 2005. The "productivity versus preservation" controversy: cause, flaws, and resolution. SPECIAL PUBLICATION-SEPM 82, 17.

Tyson, R.V., 1994. Sedimentary organic matter : organic facies and palynofacies / R. V. Tyson. London : Chapman & Hall, London.

Ungerer, P., Behar, F., Villalba, M., Heum, O.R., Audibert, A., 1988. Kinetic modelling of oil cracking. Organic Geochemistry 13, 857-868.

Ungerer, P., Pelet, R., 1987. Extrapolation of the kinetics of oil and gas formation from laboratory experiments to sedimentary basins. Nature 327, 52-54.

van Krevelen, D.W., 1961. Coal. Elsevier.

Vandenbroucke, M., Largeau, C., 2007. Kerogen origin, evolution and structure. Organic Geochemistry 38, 719-833.

Varma, R.S., 2002. Clay and clay-supported reagents in organic synthesis. Tetrahedron 58, 1235-1255.

Wilkins, R.W., Wilmshurst, J.R., Russell, N.J., Hladky, G., Ellacott, M.V., Buckingham, C., 1992. Fluorescence alteration and the suppression of vitrinite reflectance. Organic Geochemistry 18, 629-640.

Wohling, D., Keppel, M., Fulton, S., Costar, A., Sampson, L., Berens, V., 2013. Australian Government initiative on coal seam gas and large coal mining, Arckaringa Basin and Pedirka Basin Groundwater Assessment Projects. Department of Environment, Water and Natural Resources, Adelaide, Australia, p. 10.

Wu, L.M., Zhou, C.H., Keeling, J., Tong, D.S., Yu, W.H., 2012. Towards an understanding of the role of clay minerals in crude oil formation, migration and accumulation. Earth-Science Reviews 115, 373-386.

Xiang, B., Li, E., Gao, X., Wang, M., Wang, Y., Xu, H., Huang, P., Yu, S., Liu, J., Zou, Y., 2016. Petroleum generation kinetics for Permian lacustrine source rocks in the Junggar Basin, NW China. Organic Geochemistry 98, 1-17.

Yang, S., Horsfield, B., 2016. Some Predicted Effects of Minerals on the Generation of Petroleum in Nature. Energy & fuels 30, 6677-6687.

Yuan, P., Liu, H., Liu, D., Tan, D., Yan, W., He, H., 2013. Role of the interlayer space of montmorillonite in hydrocarbon generation: An experimental study based on high temperature-pressure pyrolysis. Applied Clay Science 75-76, 82-91.

Zonneveld, K., Versteegh, G., Kasten, S., Eglinton, T.I., Emeis, K.-C., Huguet, C., Koch, B., de Lange, G.J., De Leeuw, J., Middelburg, J.J., 2010.

Selective preservation of organic matter in marine environments; processes and impact on the sedimentary record.

Chapter 5: Conclusions

This study demonstrates two major fabrics in shale resulting from distinctive depositional settings and diagenesis of detrital minerals. Shale samples from the Monterey Formation of California, USA is compared with samples from Stuart Range Formation of South Australia. Samples of the Monterey Formation contain abundant high surface area detrital clay minerals deposited in a tropical climate, whereas, Stuart Range shale is deposited in a cold climate setting without the influence of detrital clays. Results reveal a strong control of detrital mineralogy and diagenesis on physical association of organic matter and mineral matrices in shale. Samples from both Monterey and Stuart Range formation comprise clay minerals with abundant smectite. However, smectites in the Monterey samples are detrital and have a genetic link with the deposition of organic matter. Subsequently, organic matter in the Monterey samples is preserved in nanocomposite fabric showing an intimate association with clay minerals at sub-micron scales as organoclay aggregates and nanocomposites. This intimate physical association is also consistent with a strong positive relationship between TOC and MSA in the Monterey samples ($R^2 = 0.91$). On the contrary, the smectites in Stuart Range samples are pore-filling and authigenic. They do not have a genetic connection with the organic matter during deposition, since high surface area clays are formed later during diagenesis. As a result, organic matter preserved in the Stuart Range Formation does not show any association with clay minerals and preserved as discrete organic particles. This is consistent

with the apparent absence of a relationship between TOC and MSA of Stuart Range samples ($R^2 = 0.54$).

Distinct differences are observed in organic matter morphology in samples of Monterey and Stuart Range formations having nanocomposites and particulate fabric respectively. The morphology of organic matter in Monterey Formation is classified as a) organoclay laminae b) organoclay aggregates and c) infilling organoclay matrix. Organoclay laminae are the most common organic matter morphology observed in the Monterey samples. The maceral content of the samples from Monterey and Stuart Range formations is consistent with SEM observations. Almost three-quarters of macerals in samples of Monterey Formation (bituminite) are intimately mixed with mostly smectite clay minerals. Organic matter in samples of Stuart Range Formation are mostly present as discrete particles of > 5μm. According to their texture, they can be classified as a) angular to sub-angular organic particles (AP), b) lamellar organic flakes (LF), and c) tabular organic particles (TP). Quantitative maceral analyses identified telalginite, lamalginite, sporinite, bituminite, vitrinite and inertinite in the Stuart Range samples. With some minor expected overlap, the AP, LF and TP mostly represent the vitrinite/inertinite, lamalginite and telalgninite macerals respectively. None of the samples of Stuart Range Formation show an intimate association of mineral matrix with organic matter. These two endmember shale fabrics, particulate and nanocomposite, control the physical contact of reactive clay surfaces to labile organic matter in sediments.

Clay mineral catalytic effects on hydrocarbon generation are tested in

particulate and nanocomposite sample sets comparing keorgen isolate and whole-rock pairs using Rock-Eval pyrolysis technique. The differences in shale fabrics have a significant effect on clay mineral catalysis on hydrocarbon generation by controlling the physical association of the two phases. Both Monterey and the Stuart Range formations show retention in hydrocarbon yield due to mineral matrix effects in bulk rock as compared to their kerogen isolates. Clay mineral surfaces associated with organic matter during deposition result in less retention during hydrocarbon generation compared to authigenic clay minerals that have organic carbon-free surfaces. During Rock-Eval pyrolysis, shale samples with nanocomposites generate maximum hydrocarbon at higher temperatures compared to shale samples dominated by particulate organic matter. A higher T_{max} difference (between bulk rock and kerogen isolate pairs) is observed in the Monterey Formation samples compared to Stuart Range Formation samples with former varying as much as 30°C between the kerogen isolates and their bulk rock.

Bulk kinetic experiments suggest that Monterey sample kerogens are structurally heterogenous, possibly due to the abundance of both strong C-C and weaker C-S bonds. The Stuart Range sample kerogens have relatively homogenous structure. Results of this study are consistent with the hypothesis that the physical association of organic matter and mineral matrices has a significant impact on hydrocarbon generation kinetics. Comparison of the hydrocarbon generation kinetics of paired kerogen isolates versus whole rock samples for both shale demonstrates that the onset temperature of hydrocarbon generation is reduced by 20°C in samples with

nanocomposite fabric. This is attributed to clay catalysis. No clay mineral catalytic effect was observed in shale samples with particulate fabric.

A significant shift in kerogen typing between the bulk rock and the extracted kerogen is evident in the modified van Krevelen diagram. This implies that the shale fabric as well as the actual kerogen composition influences this common classification scheme. The intimate contacts of smectite surfaces with organic matter induce maximum catalytic effects during hydrocarbon generation in the Monterey Formation samples. The results of this study suggest that processes leading to particulate and nanocomposite fabric in shale have strong influences on hydrocarbon generation by regulating clay catalysis as observed through laboratory pyrolysis. Hydrocarbon source rocks with nanocomposite fabric potentially will start generation at lower depth (due to clay catalysis) compared to a source rock with particulate fabric given the mineralogy and organic content of the two rocks is similar. Thus the consideration of organic matter-clay mineral fabrics can have a significant impact on source rock characterization and geological modelling of both conventional and unconventional petroleum systems.

5.1. Recommendations for future work

This thesis presents evidences that organic matter and clay mineral fabrics can function as a natural regulator of clay catalysis during hydrocarbon generation. The physical association of organic matter can alter the yield, temperature of hydrocarbon generation and thus affect the hydrocarbon generation window. The control of these physical associations on composition

of generated hydrocarbon is not known yet. A study on well characterized selective natural shale/mudstone sample sets representing different kerogen types (type I, II, III) and clay mineralogy can provide important information on the control of shale fabric on hydrocarbon composition.

The kinetic experiments performed on nanocomposite and particulate shale samples show significant influence of clay mineral-organic association on kinetic parameters at laboratory pyrolysis. However, a fundamental limitation of any pyrolysis technique is to mimic the natural geological setting in the laboratory mostly because geologically the generation of hydrocarbon occurs in many orders of magnitude slower and at a much lower temperature than those performed in laboratory pyrolysis. A potential study with well-characterized sample sets representing particulate and nanocomposite fabric can be used for comparison of kinetic experiments with multiple different heating rates. This study can provide information on the potential influence of heating rates on the control of shale fabric on hydrocarbon generation kinetics.

Appendices

Appendix 1. Methods

A1.1. Whole rock and clay mineralogy

Rock samples were cleaned using compressed air, milled and passed through a 200 μm sieve for bulk geochemical analyses. Mineralogy of the samples was determined by X-ray Diffraction (XRD) (Bruker D8 Advance with a Cu-radiation source) of powdered samples using Bruker Diffrac.Eva software and Crystallography Open Database reference patterns. The clay mineralogy of the samples was determined on Ca-saturated oriented preparations of the < 2 μm fraction (air dried and after treatment with ethylene glycol). The < 2 μm fraction was obtained by centrifugation after carbonate removal with 1 M sodium acetate buffer at pH 5 and 90°C, organic matter removal with NaOCl at pH 9.5 and 90°C, and ultrasonic dispersal.

A1.2. Scanning Electron Microscopy (SEM)

Samples were polished using a Hitachi IM4000 Argon Ion Mill system and carbon-coated before SEM analysis. They were imaged using a JEOL Neoscope JCM 6000 SEM, Zeiss EVO MA15 SEM and JEOL JSM 7100F field emission SEM. All SEMs were equipped with energy dispersive x-ray spectroscopy (EDS) systems for elemental analysis. SEM analyses were performed at 12 mm working distance and 15 kV accelerating voltage. Elements with high atomic number backscatter electrons more strongly than the elements with low atomic numbers and thus appear brighter in the BSE photomicrographs. Organic matter appears dark relative to mineral phases in

SEM BSE photomicrographs, so that they provide direct visual evidence for the association of minerals and organics in the rock.

A1.3. Nanomin Mineral Mapping

The Nanomin automated mineralogy and petrography technique was used for mineral mapping of the samples on an FEI Taneo field emission SEM equipped with dual Bruker Series 6 EDS detectors. Nanomin is a recently introduced technology to determine and map the mineralogy of fine-grained, heterogenous rock samples such as shale. Nanomin compares EDS spectra collected in the mapped area against reference spectra collected on known mineral standards. An X-ray spacing of 200 nm and 8 ms acquisition time were used for EDS mapping of the samples for Nanomin analyses. The Nanomin mineral classification system can de-convolve mixed X-ray spectra and assign up to three minerals per analysed spot, a significant advancement compared to earlier SEM-based mineral mapping techniques (e.g. QEMSCAN). This allows for improved interpretation of the mixed phase X-ray spectra characteristic of fine-grained sediments. Nanomin mineral maps provide visual information on the distribution of different mineral phases at micron resolution.

A1.4. Mineral Surface Area (MSA)

The mineral surface areas (MSA) of the samples were determined using the 'free surface' procedure of ethylene glycol monoethyl ether (EGME) method (Tiller and Smith, 1990). Calcium chloride (1 M) was added the samples to ensure that the same cation (Ca) is on the exchange sites of all samples. The amount of EGME retained was assumed to represent complete monolayer

coverage on all surfaces. A factor of 3.2 was used to convert the mass of sorbed EGME (in mg) to mineral surface area (in m^2), based on an assumption of monolayer coverage. Six replicates of a suite of clay mineral standards obtained from the Clay Mineral Society were analysed in the same batch as the samples. MSA was corrected for $CaCO_3$ and organic carbon content, and is reported here as 'silicate MSA'. MSA measured on the clay mineral standards showed good reproducibility (SWy-2: 741 m^2/g ±1.93 %; STx-1b: 771 m^2/g ±1.33 %; IScZ-1: 296 m^2/g ±2.57 %; IMt-2: 141 m^2/g ±1.04 %; n = 6).

A1.5. Total Organic Carbon (TOC)

Total carbon content (TC) for each sample was measured in a Perkin Elmer 2400 Series II CHNS analyzer. Inorganic carbon content (IC) was determined using the pressure-calcimeter method (Sherrod et al., 2001). Rock samples were milled and passed through a 200 μm sieve. The samples were weighed to 200 mg and transferred to glass vials and 5 mL of 4 M HCl/3% $FeCl_2$ was added to each vial. Seven $CaCO_3$ standards of 200mg, 150mg, 100mg, 75mg, 50mg, 25mg and 10mg were weighed and placed into vials containing acid. Each standards were run as duplicate. Four vials were also included as blanks containing only the acid and an empty micro-centrifuge tube. The vials were sealed and rigorously shaken to start the reaction. After one hour of contact time (shaking them once more at the 30 minute mark), the maximum pressure from vials was recorded using a manometer. The weight and pressure of the standards and pressure recorded in each sample is then used to calculate the equivalent mass of $CaCO_3$ in each sample. Total organic carbon (TOC) content was calculated by the differences i.e. TOC = TC – IC.

A1.6. Kerogen isolation

Carbonate fractions of the milled samples were dissolved using 4 M hydrochloric acid (HCl). 30 ml of 4 M HCl was added to sample beakers each containing 10 g of sample. The samples were washed several times with deionized water after the removal of carbonate fractions as indicated by the disappearance of the effervescence. The silicate mineral phases were dissolved using hydrofluoric acid (HF). 40 ml of 20 wt.% HF was added to each sample tube, they were then heated to 60°C and left to react for 24 hours. The treatment was repeated until dissolution of silicate minerals was completed as confirmed by subsequent XRD analysis. The isolated organic matter samples were washed several times with deionized water and oven dried at 40°C. TC of the organic matter isolates was measured to confirm organic matter purity. In total four samples from both Monterey and Stuart Range formations were excluded from further analyses where organic matter isolates have TC < 30 %. It should be noted that pyrite could not be dissolved by the technique used in this study. Some studies have suggested a pyrite removal method using chromous chloride, however the method was not implemented here as the presence of pyrite in organic matter isolates was not considered detrimental to the aims of the study.

Organic matter isolates and whole rock samples were solvent extracted to remove the bitumen fraction. Samples were treated ultrasonically in a 9:1 mixture of dichloromethane (DCM) and methanol for 10 minutes followed by 10 minutes settling time. The samples were then stirred and underwent a second stage of ultrasonic treatment for 10 minutes. Solvents were discarded

between repeats. This cycle was repeated until all bitumen was removed (4 cycles on average) as indicated by the clear appearance of solvent after the final treatment. The bulk rock samples (10 g of each) were also solvent extracted using the same ultrasonic treatments, ensuring that pyrolysis data of the bulk rock and the kerogen isolates are comparable.

A1.7. Rock-Eval pyrolysis

The hydrocarbon generation potential (S_2) and the temperature of maximum hydrocarbon generation (T_{max}) of both rock samples and their kerogen isolates were determined by Rock-Eval pyrolysis, using a Weatherford Laboratories source rock analyser (SRA). Each sample was measured in triplicate. Thermal maturity of the samples was estimated using the method of Jarvie et al. (2001), which relates measured T_{max} to calculated Ro using the equation: calculated %Ro = 0.0180 × T_{max} - 7.16. The Ro of the samples were calculated from the T_{max} values to compare with the measured Ro values.

A1.8. Organic Petrology

Macerals in the samples were characterized and quantified using point counting in accordance with the procedures of the Standards Association of Australia (AS2856.2). A minimum of 500 points were counted for each of the white and fluorescent light observations on every sample. The maceral analyses are reported as volume precents. Vitrinite reflectance measurements were made using a Zeiss microscope with a 40x oil immersion objective and an interference filter with a pass-band peak of 546 nm in accordance with the AS2456.3. Random reflectances of vitrinite particles were measured using non-polarized light. The average of 30 to 40 measurements (depending on the

abundance of vitrinite grains) from each sample is reported as 'mean vitrinite reflectance' of the sample.

A1.9. Bulk Kinetics

Bulk kinetic parameters were assessed by subjecting samples to open-system, non-isothermal pyrolysis of 10-20 mg of extracted samples at three different linear heating rates (0.7, 2 and 5 K/min) using a Source Rock Analyser (SRA) following standard procedures (Braun and Burnham, 1987). The KINETICS 2000 program was used for the optimization of the discrete activation-energy (Ea) distribution with a single, variable frequency factor (A). The kinetic experiment results were extrapolated to a typical geological heating rate (3 K/million year) using the KMOD program.

Appendix 2. Rock_Eval FID pyrogram of whole rock samples from the Stuart Range Formation

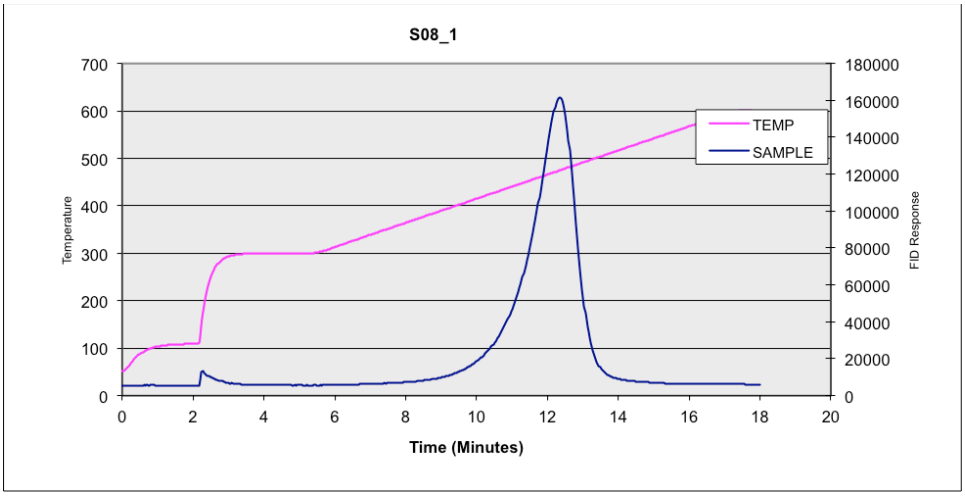

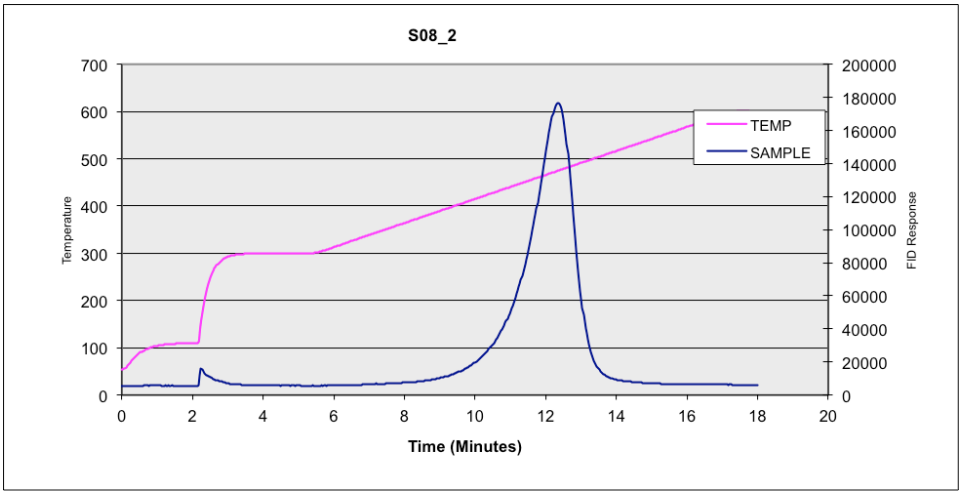

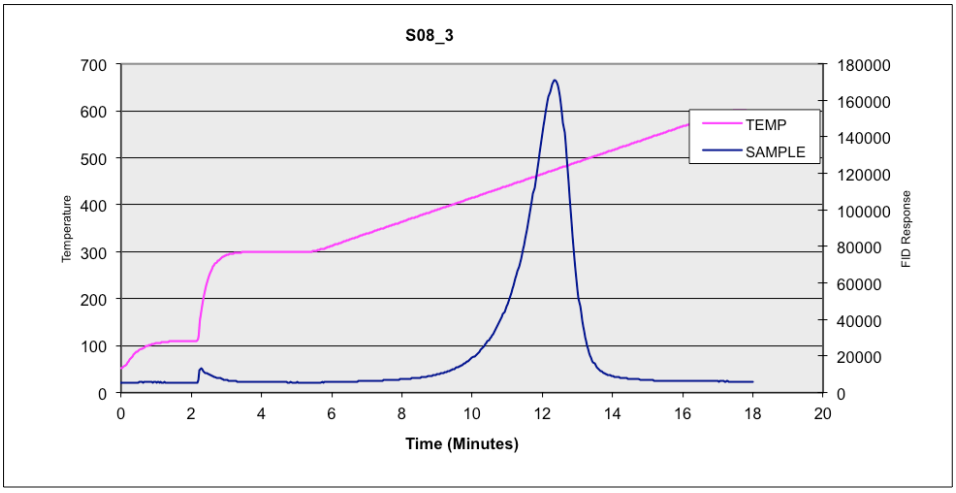

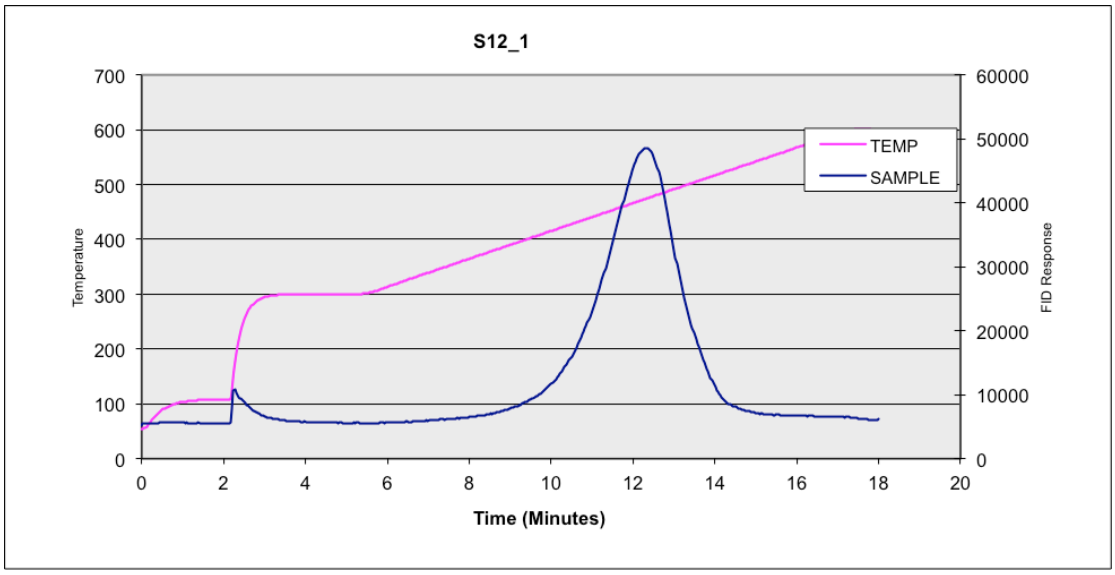
S12_1
Temperature
FID Response
TEMP
SAMPLE
Time (Minutes)
0
100
200
300
400
500
600
700
0
10000
20000
30000
40000
50000
60000
0
2
4
6
8
10
12
14
16
18
20

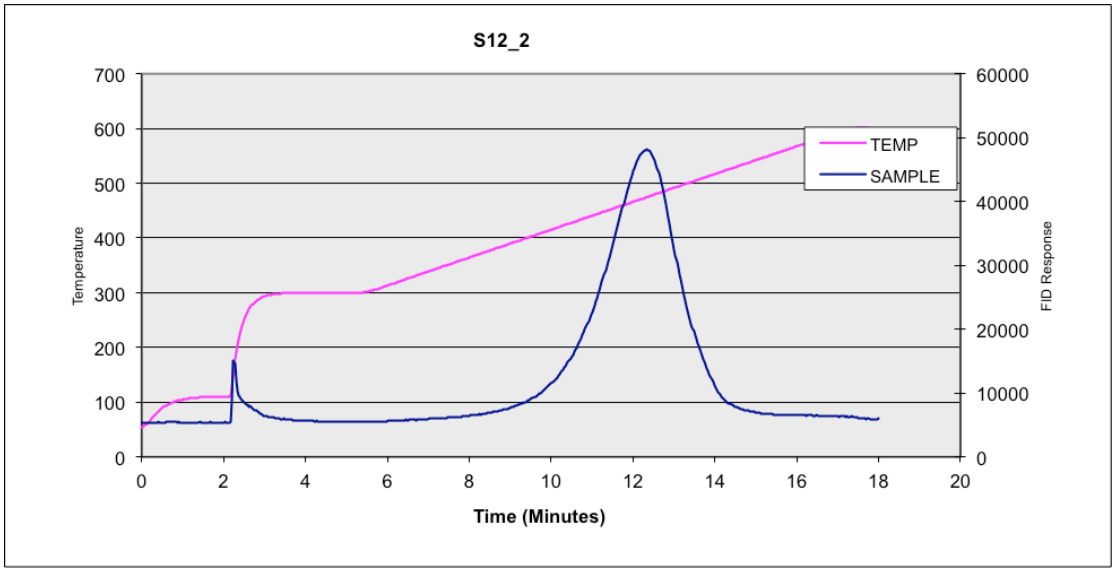
S12_2
Temperature
FID Response
TEMP
SAMPLE
Time (Minutes)
0
100
200
300
400
500
600
700
0
10000
20000
30000
40000
50000
60000
0
2
4
6
8
10
12
14
16
18
20

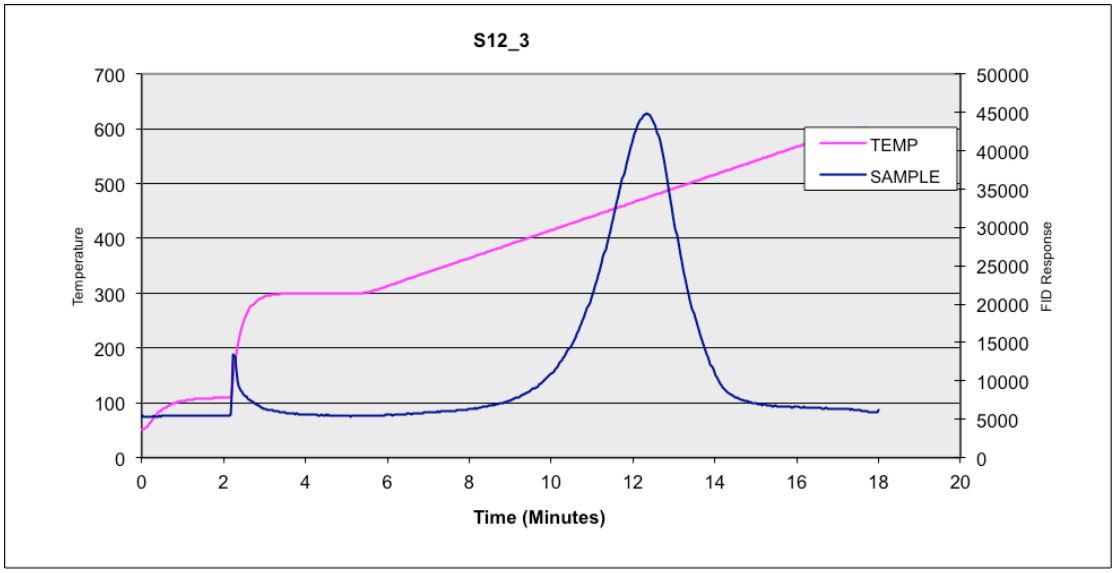
S12_3
Temperature
FID Response
TEMP
SAMPLE
Time (Minutes)
0
100
200
300
400
500
600
700
0
5000
10000
15000
20000
25000
30000
35000
40000
45000
50000
0
2
4
6
8
10
12
14
16
18
20

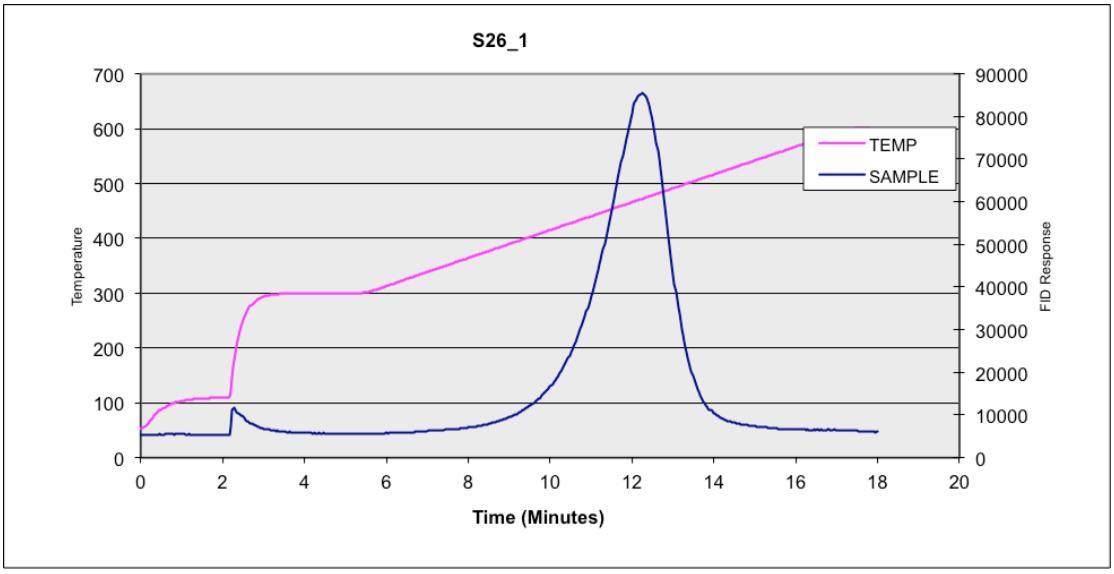
S26_1
Temperature
FID Response
TEMP
SAMPLE
Time (Minutes)

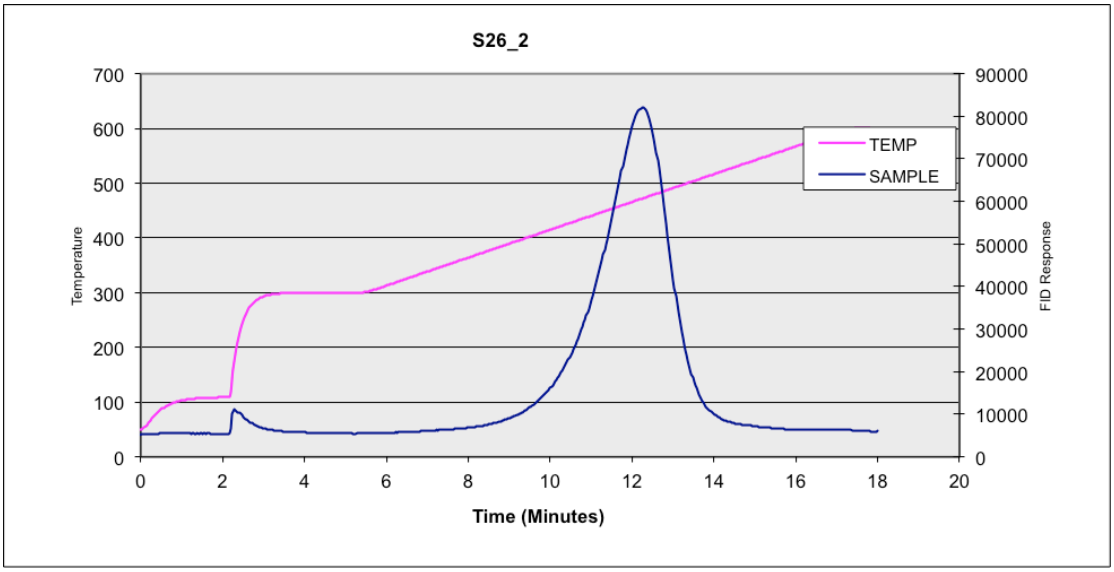
S26_2
Temperature
FID Response
TEMP
SAMPLE
Time (Minutes)

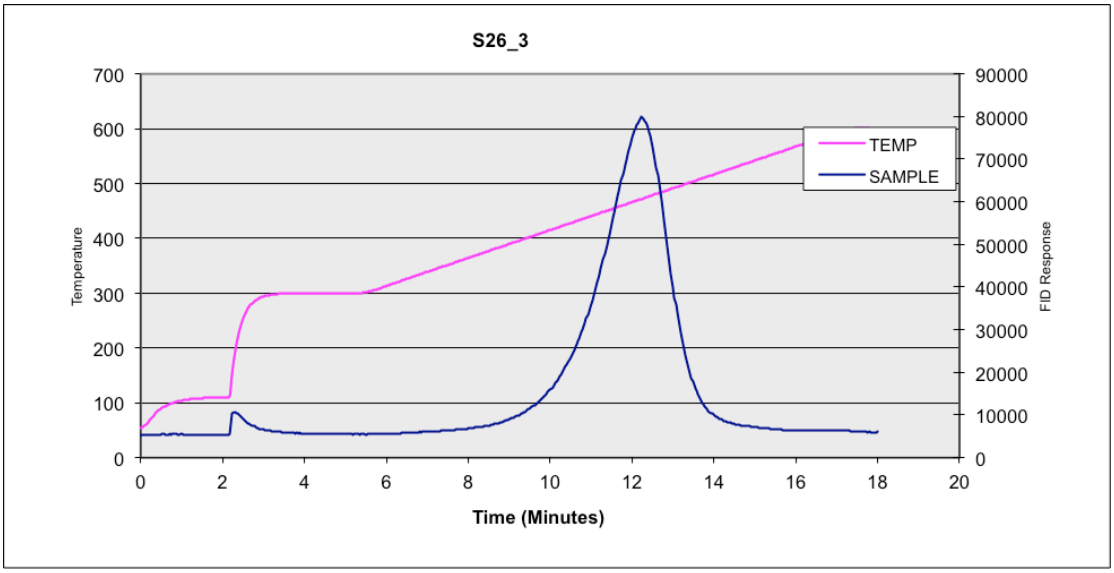
S26_3
Temperature
FID Response
TEMP
SAMPLE
Time (Minutes)

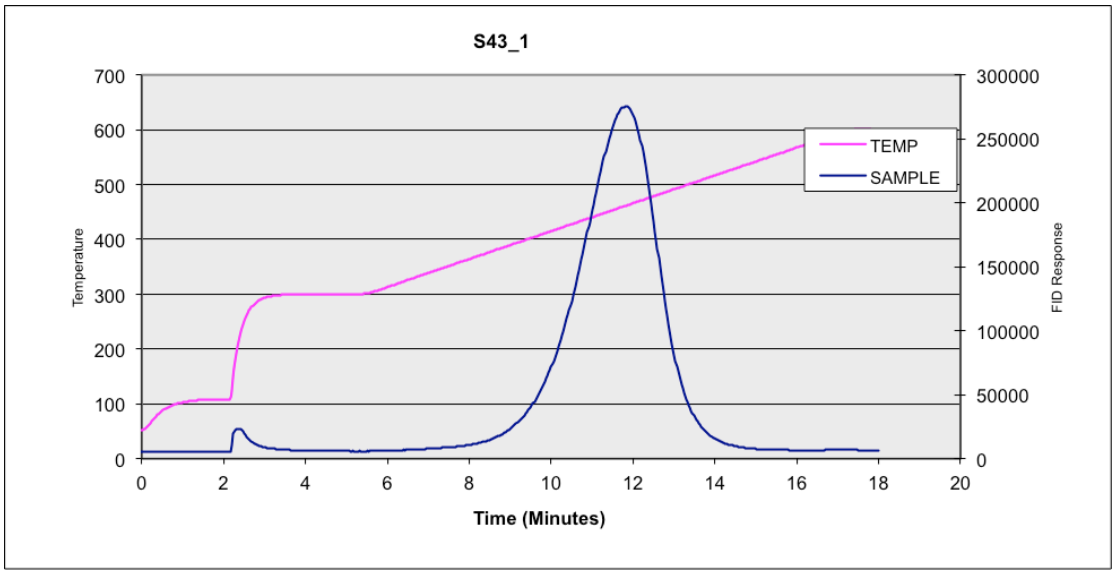
S43_1
Temperature
FID Response
TEMP
SAMPLE
Time (Minutes)

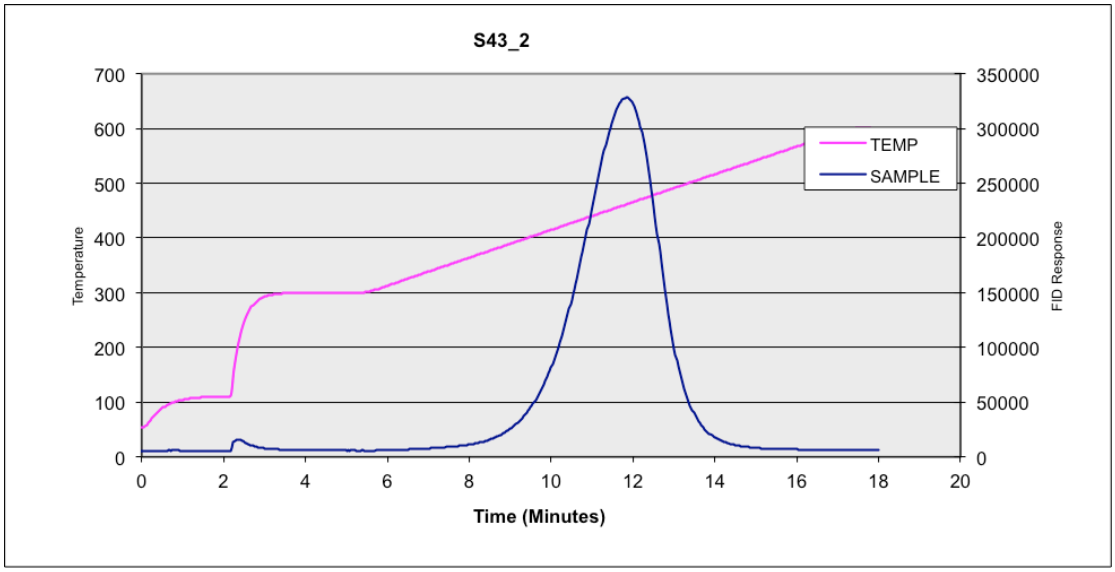
S43_2
Temperature
FID Response
TEMP
SAMPLE
Time (Minutes)

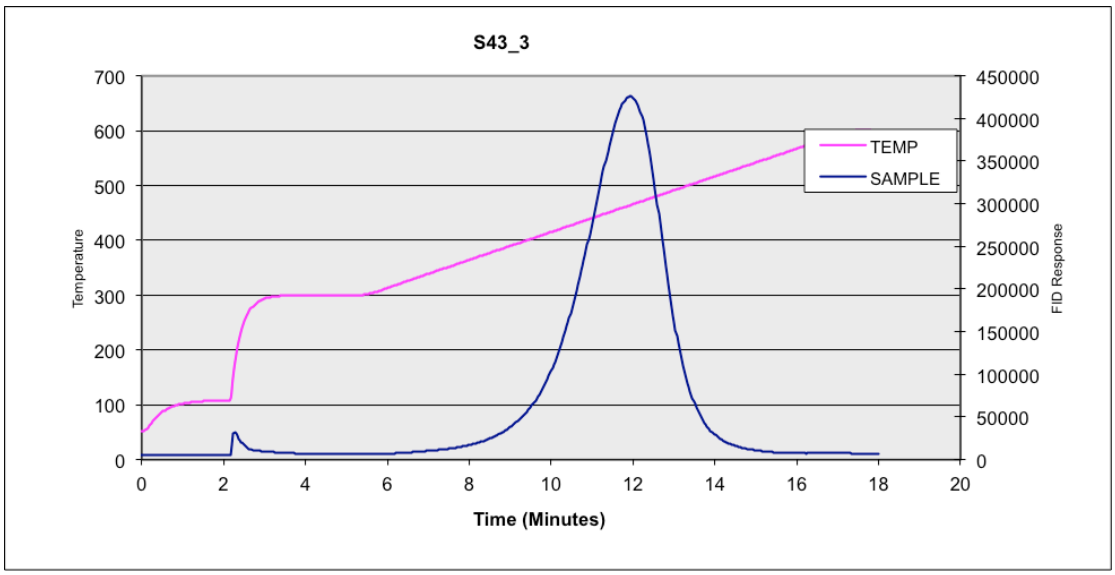
S43_3
Temperature
FID Response
TEMP
SAMPLE
Time (Minutes)

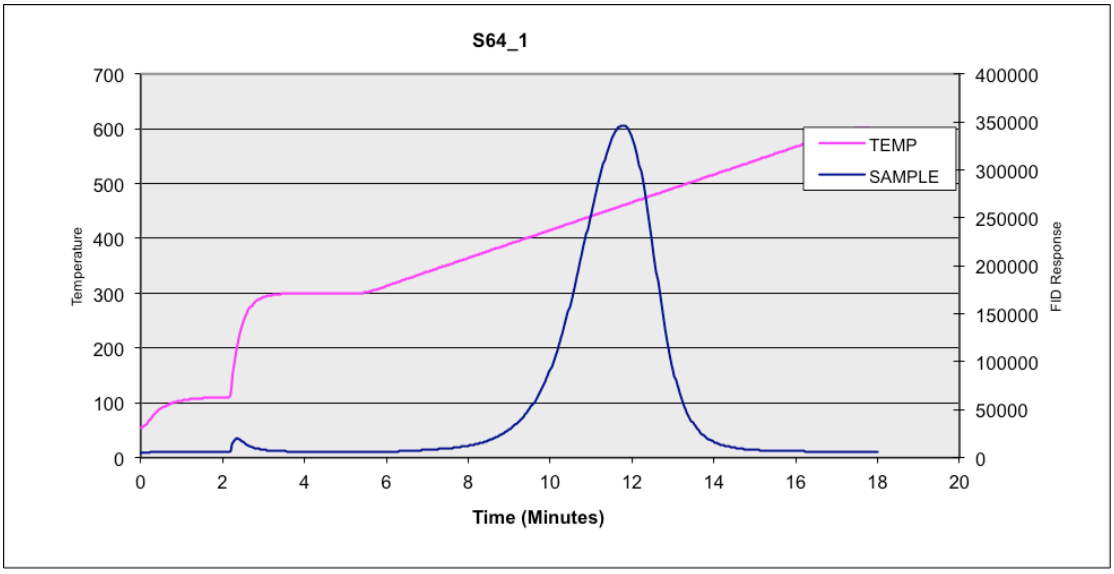
S64_1
Temperature
FID Response
TEMP
SAMPLE
Time (Minutes)

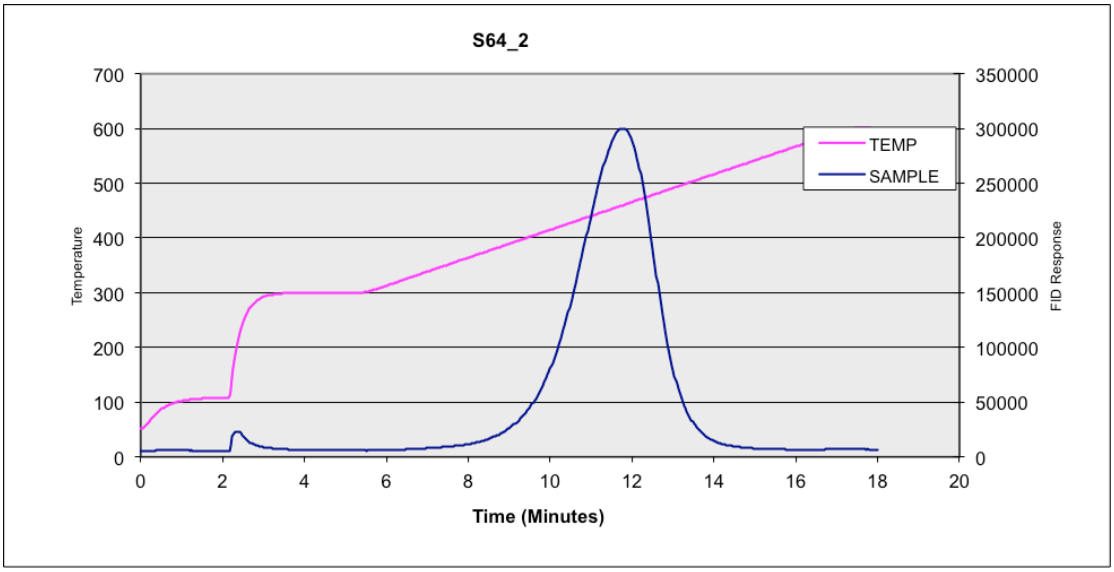
S64_2
Temperature
FID Response
TEMP
SAMPLE
Time (Minutes)

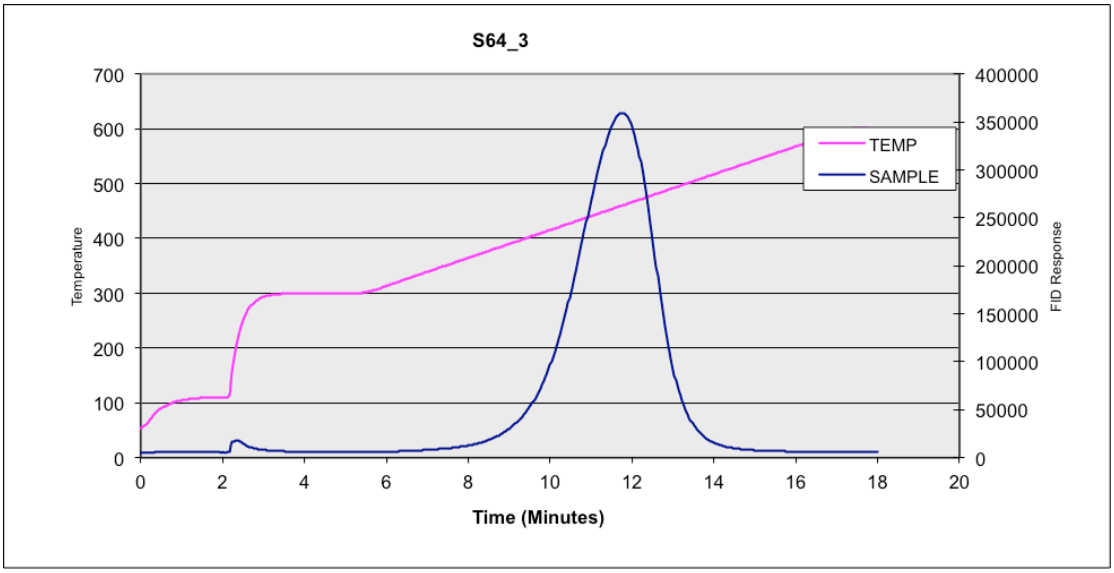
S64_3
Temperature
FID Response
TEMP
SAMPLE
Time (Minutes)

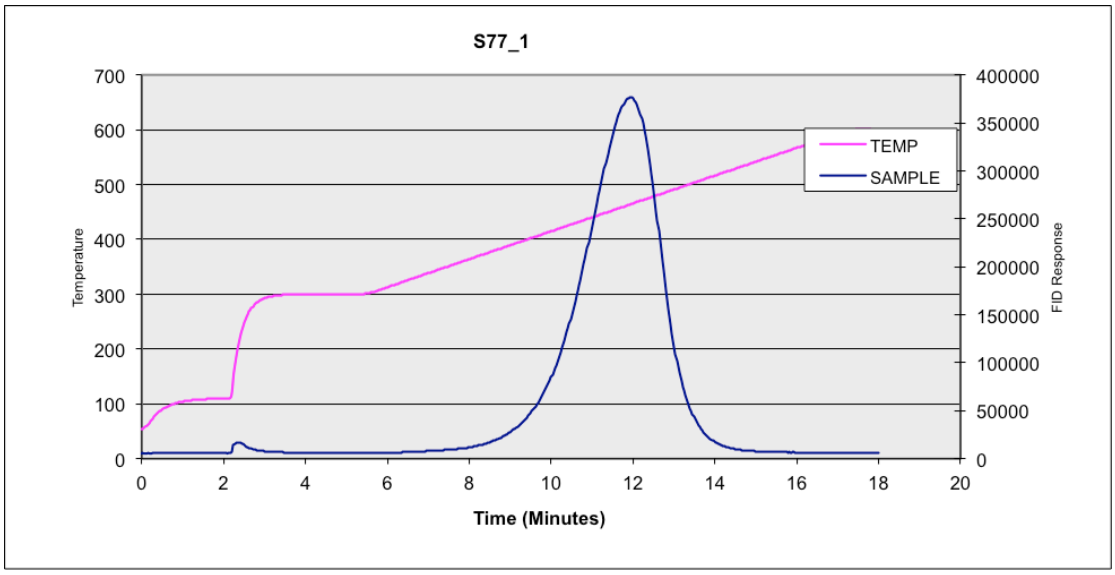
S77_1
Temperature
FID Response
Time (Minutes)
TEMP
SAMPLE
0
100
200
300
400
500
600
700
0
50000
100000
150000
200000
250000
300000
350000
400000
0
2
4
6
8
10
12
14
16
18
20

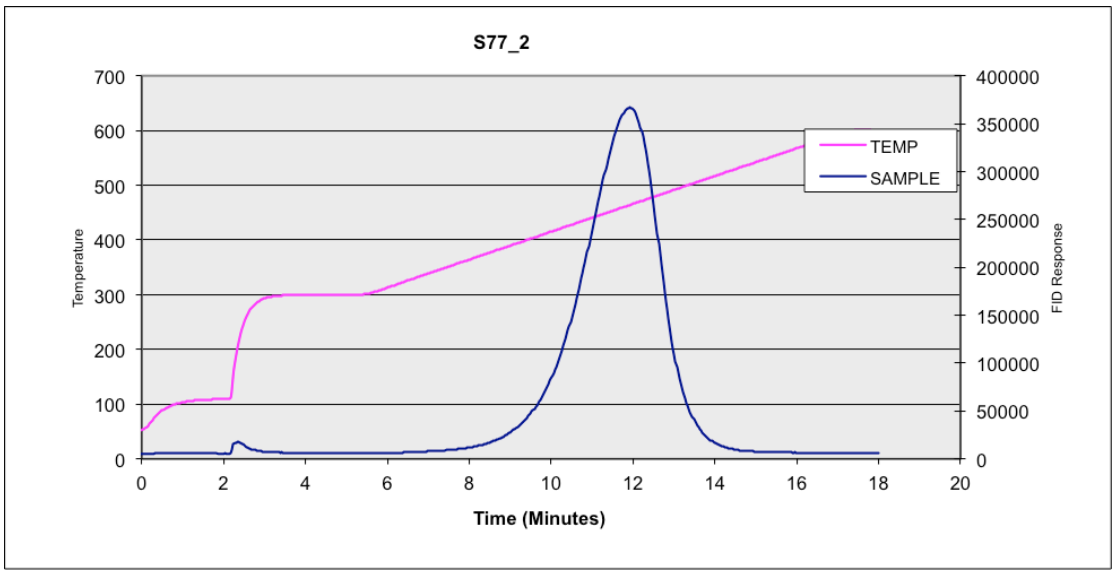
S77_2
Temperature
FID Response
Time (Minutes)
TEMP
SAMPLE
0
100
200
300
400
500
600
700
0
50000
100000
150000
200000
250000
300000
350000
400000
0
2
4
6
8
10
12
14
16
18
20

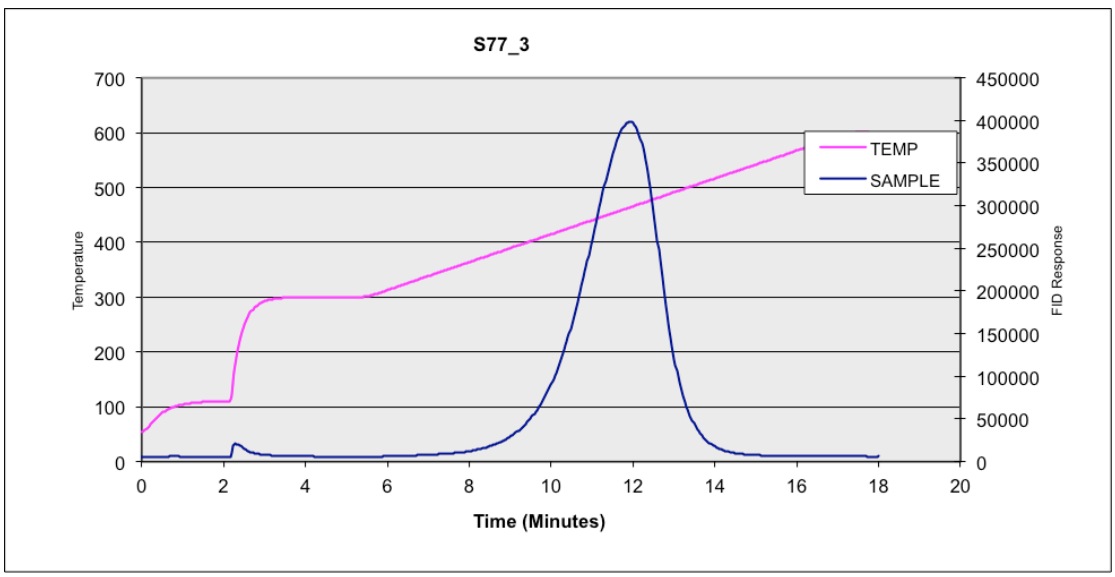
S77_3
Temperature
FID Response
Time (Minutes)
TEMP
SAMPLE
0
100
200
300
400
500
600
700
0
50000
100000
150000
200000
250000
300000
350000
400000
450000
0
2
4
6
8
10
12
14
16
18
20

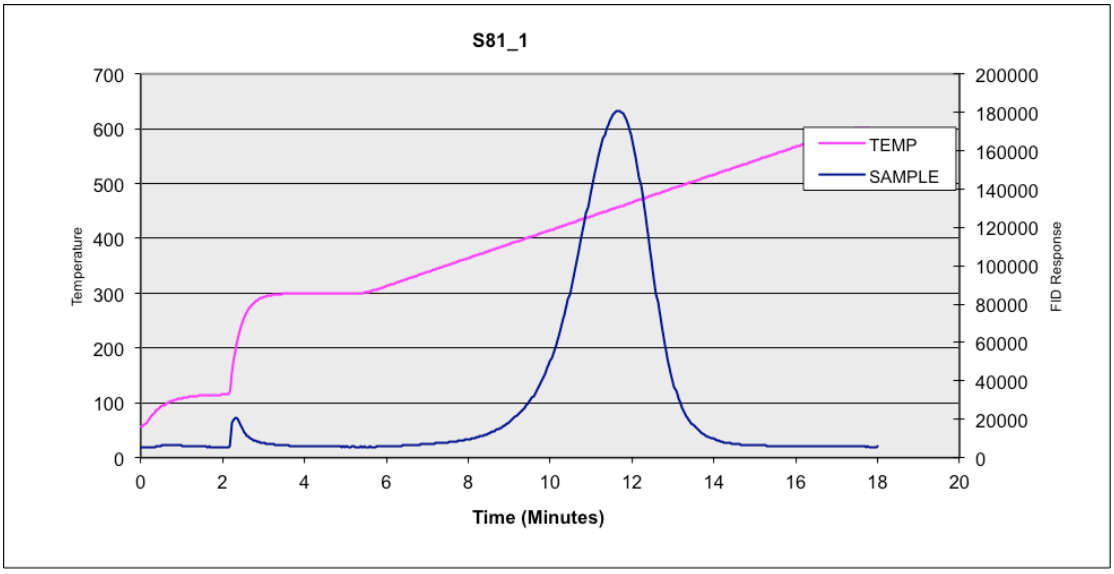
S81_1
Temperature
FID Response
TEMP
SAMPLE
Time (Minutes)

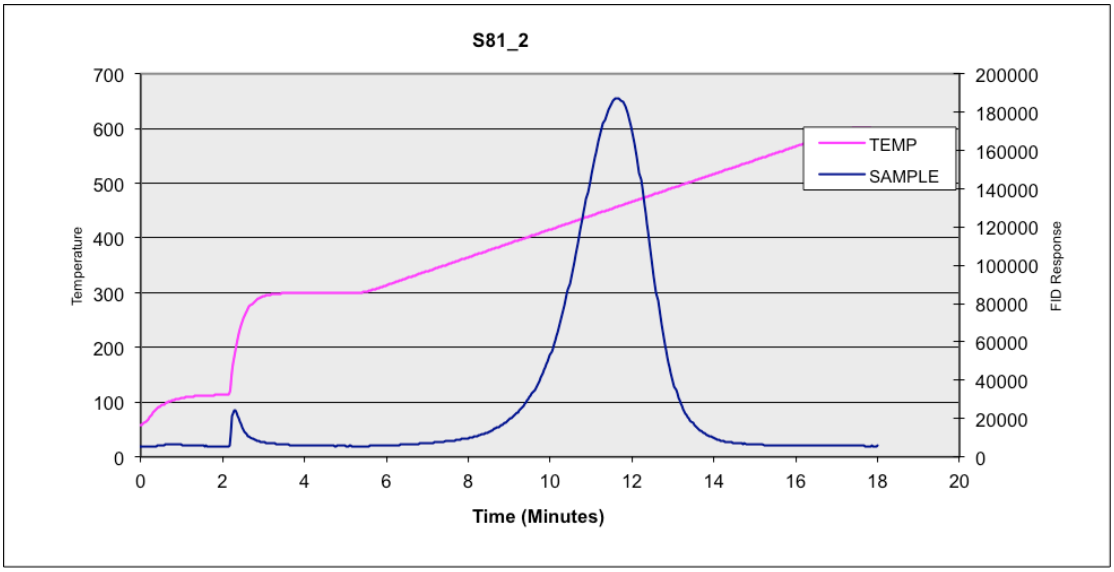
S81_2
Temperature
FID Response
TEMP
SAMPLE
Time (Minutes)

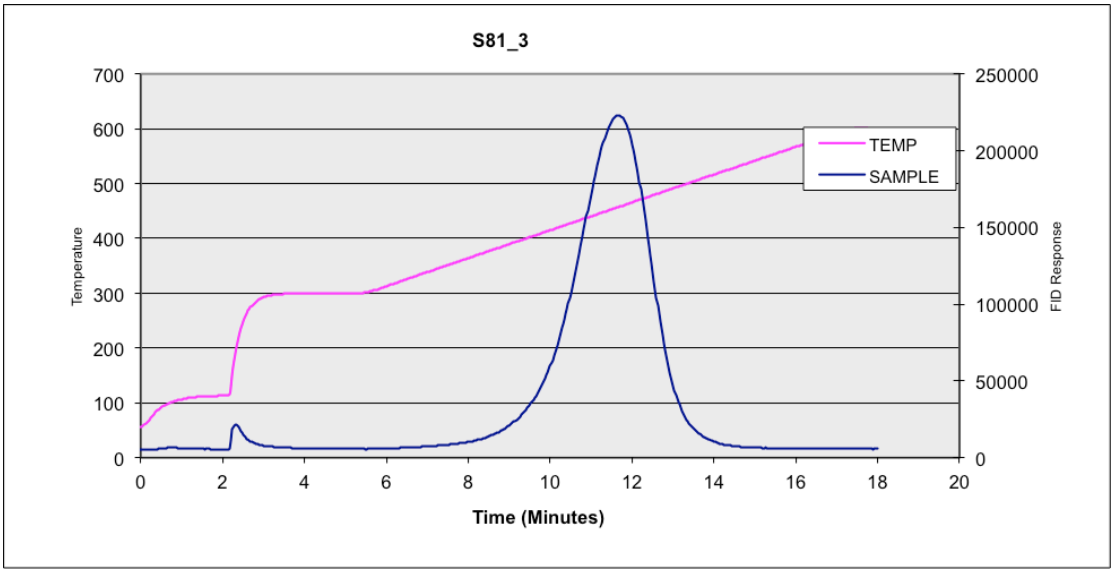
S81_3
Temperature
FID Response
TEMP
SAMPLE
Time (Minutes)

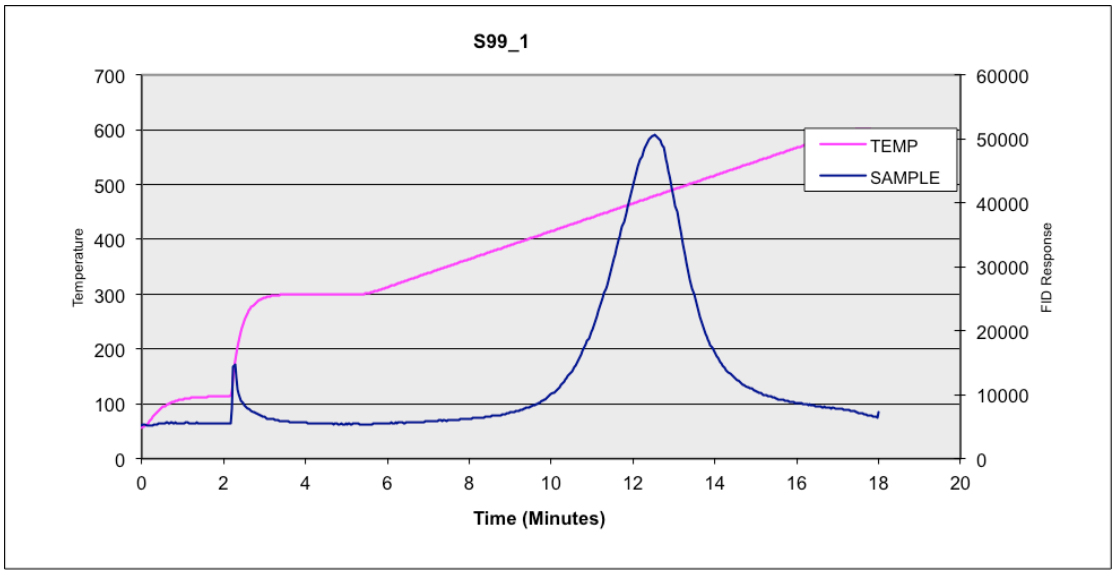
S99_1
Temperature
FID Response
TEMP
SAMPLE
Time (Minutes)
0
100
200
300
400
500
600
700
0
10000
20000
30000
40000
50000
60000
0
2
4
6
8
10
12
14
16
18
20

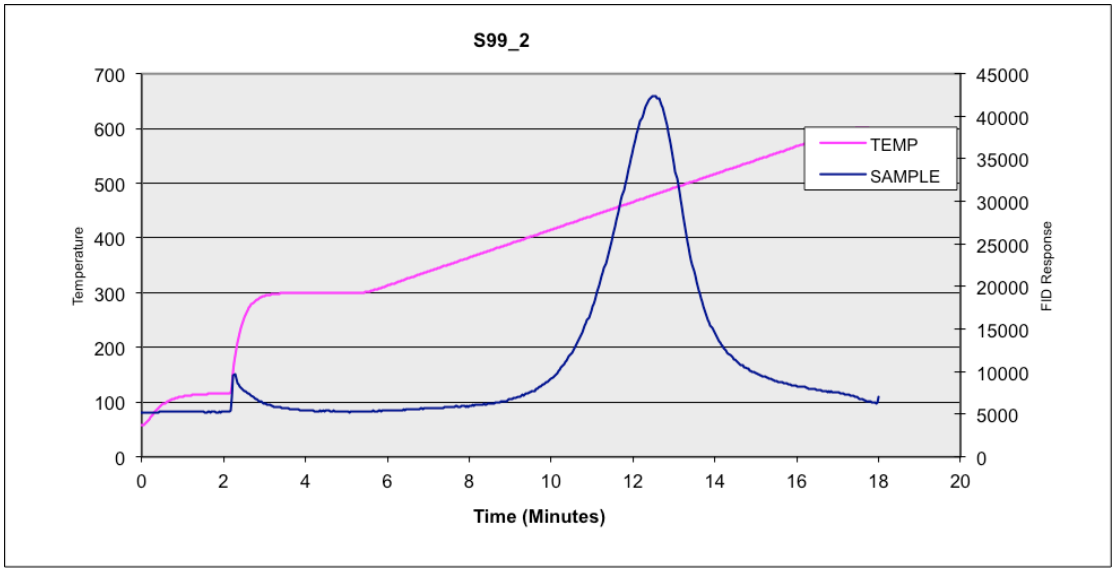
S99_2
Temperature
FID Response
TEMP
SAMPLE
Time (Minutes)
0
100
200
300
400
500
600
700
0
5000
10000
15000
20000
25000
30000
35000
40000
45000
0
2
4
6
8
10
12
14
16
18
20

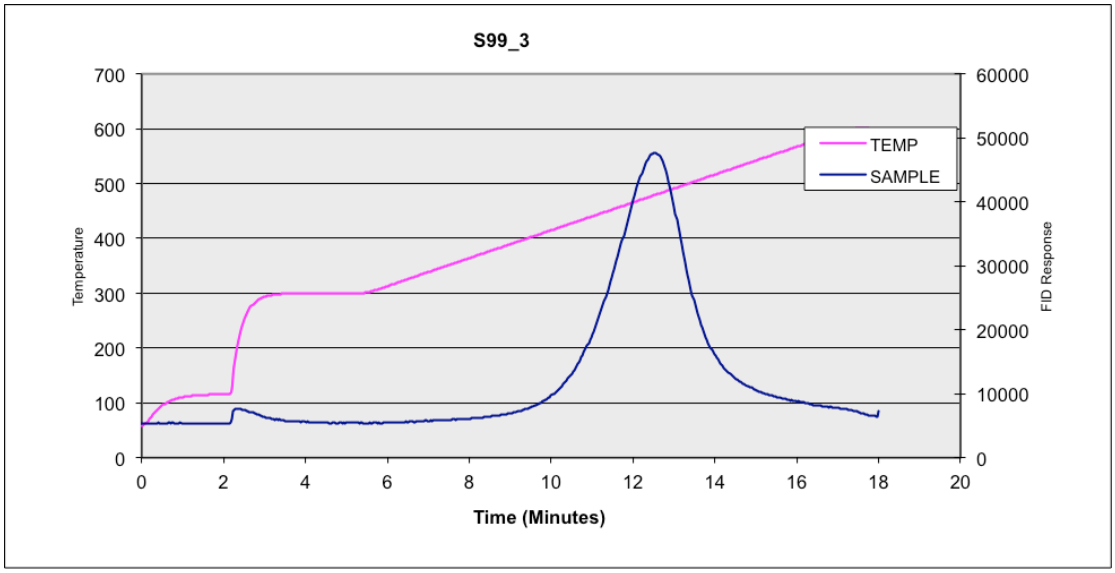
S99_3
Temperature
FID Response
TEMP
SAMPLE
Time (Minutes)
0
100
200
300
400
500
600
700
0
10000
20000
30000
40000
50000
60000
0
2
4
6
8
10
12
14
16
18
20

Appendix 3. Rock-Eval FID pyrogram of kerogen isolate of samples of the Stuart Range Formation.

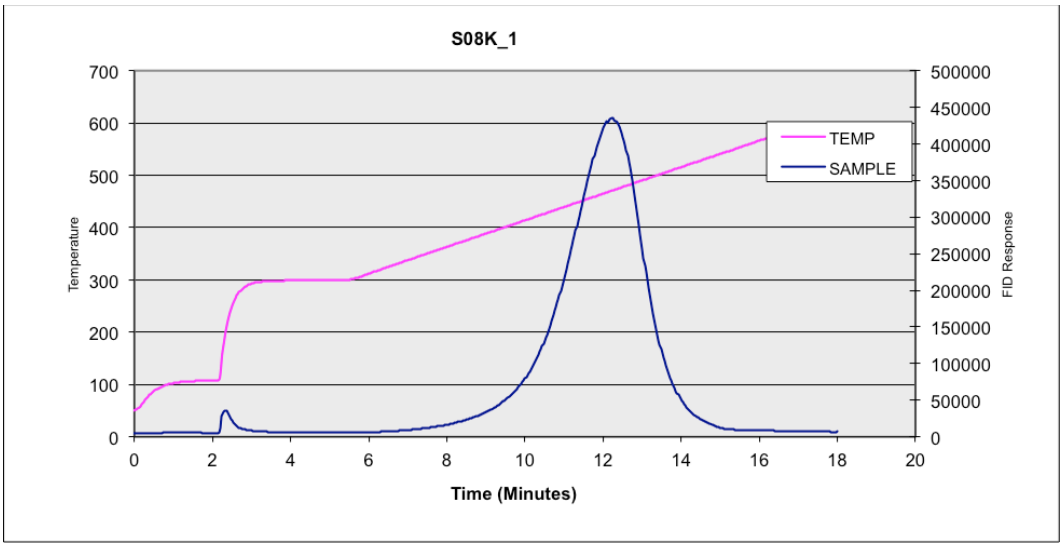

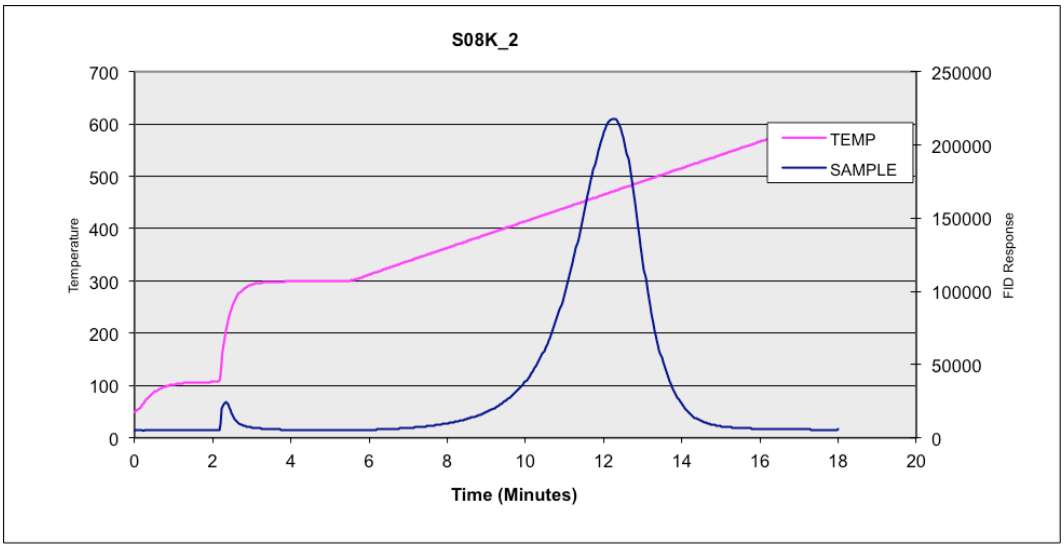

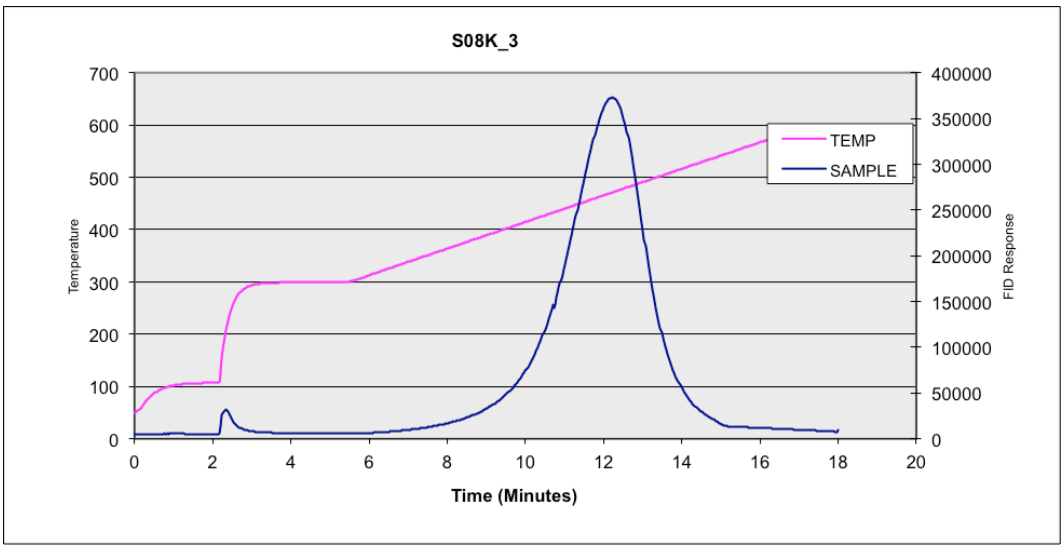

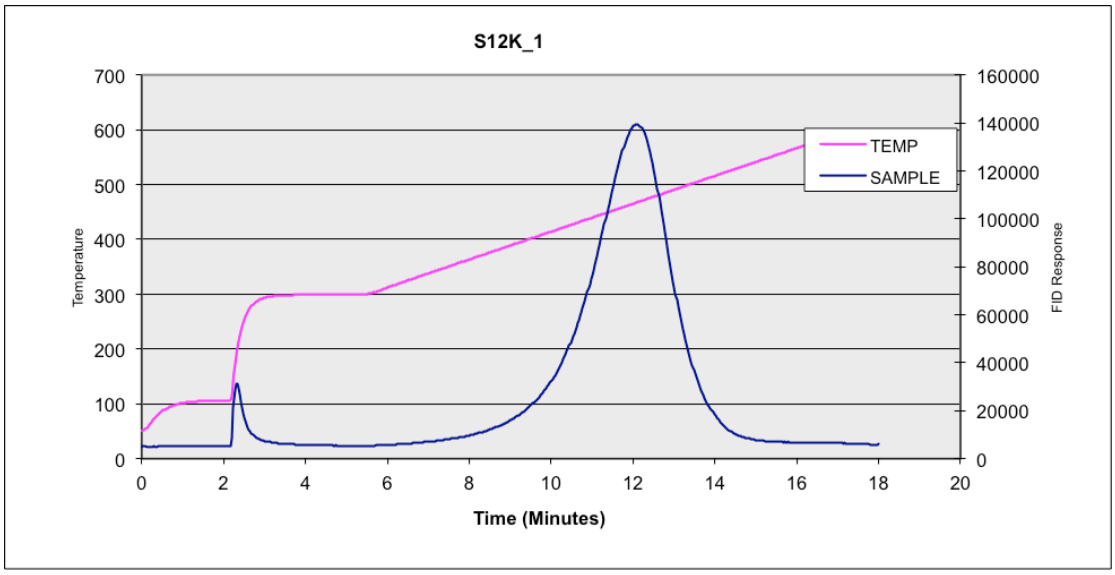
S12K_1
Temperature
FID Response
Time (Minutes)
TEMP
SAMPLE
0
100
200
300
400
500
600
700
0
20000
40000
60000
80000
100000
120000
140000
160000
0
2
4
6
8
10
12
14
16
18
20

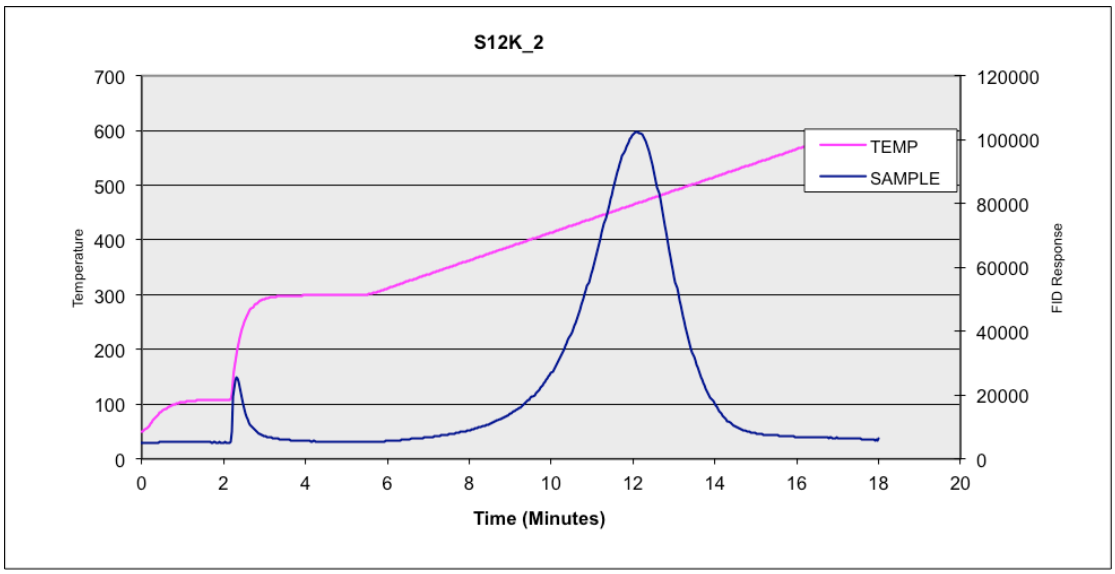
S12K_2
Temperature
FID Response
Time (Minutes)
TEMP
SAMPLE
0
100
200
300
400
500
600
700
0
20000
40000
60000
80000
100000
120000
0
2
4
6
8
10
12
14
16
18
20

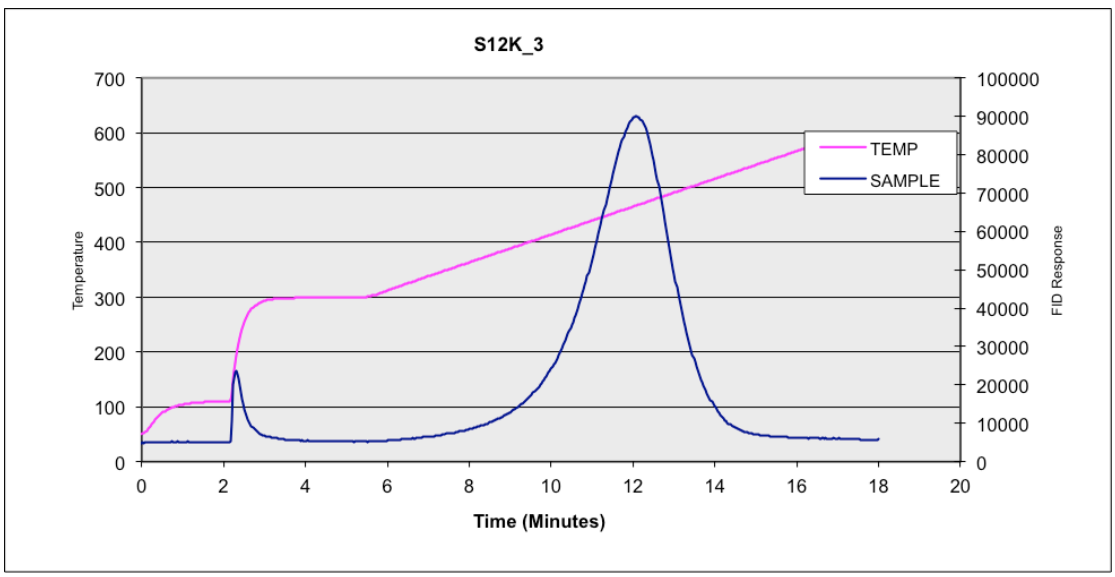
S12K_3
Temperature
FID Response
Time (Minutes)
TEMP
SAMPLE
0
100
200
300
400
500
600
700
0
10000
20000
30000
40000
50000
60000
70000
80000
90000
100000
0
2
4
6
8
10
12
14
16
18
20

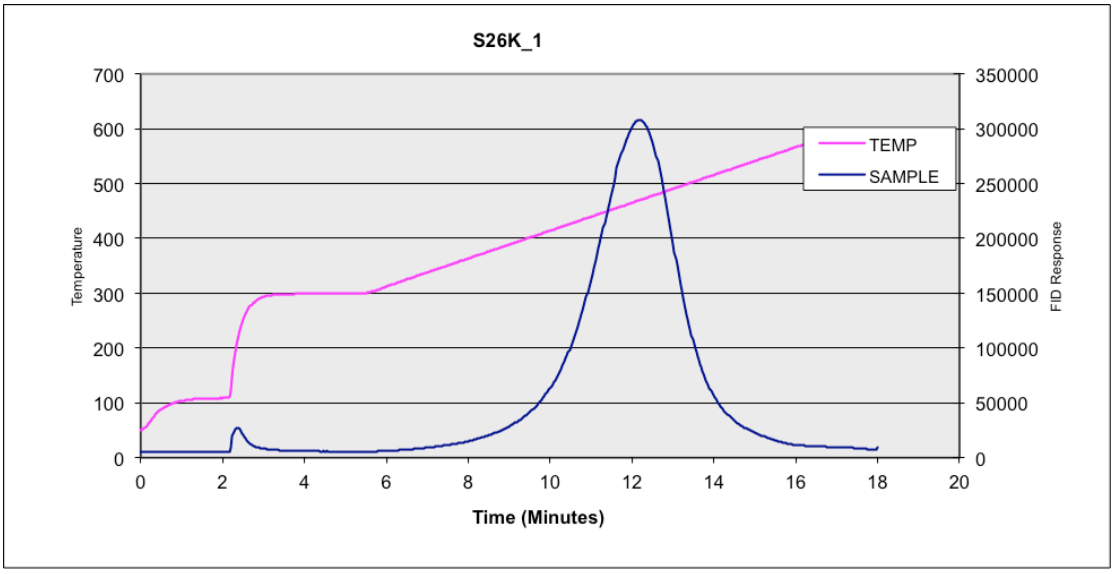
S26K_1
Temperature
FID Response
TEMP
SAMPLE
Time (Minutes)

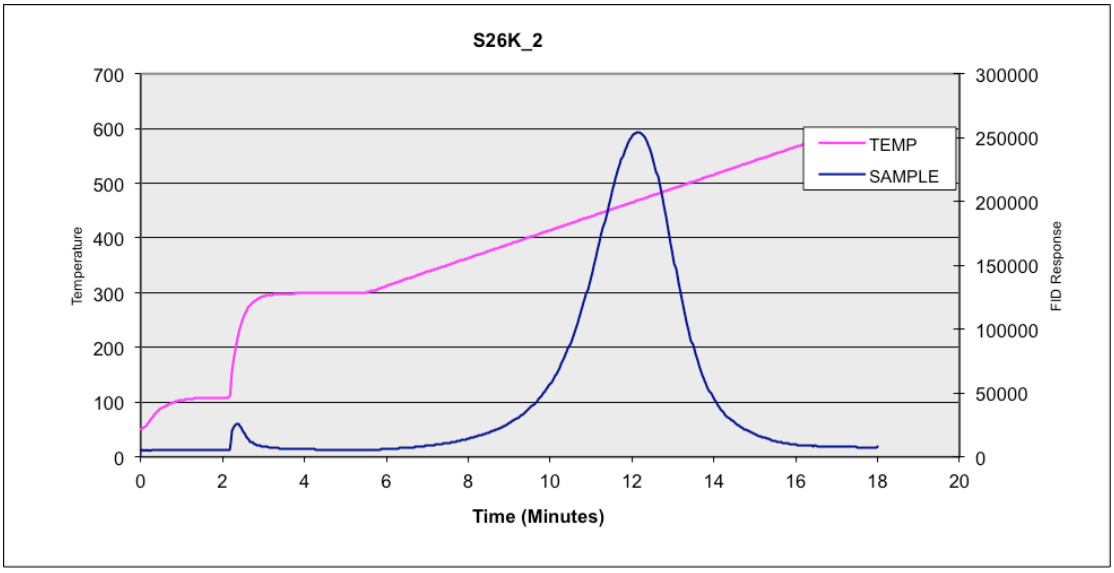
S26K_2
Temperature
FID Response
TEMP
SAMPLE
Time (Minutes)

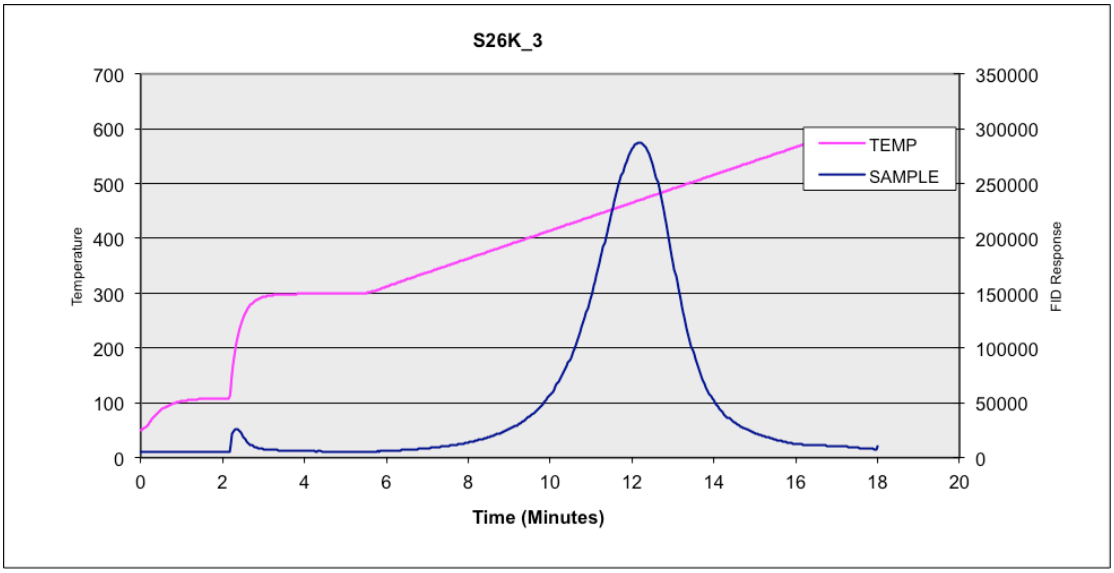
S26K_3
Temperature
FID Response
TEMP
SAMPLE
Time (Minutes)

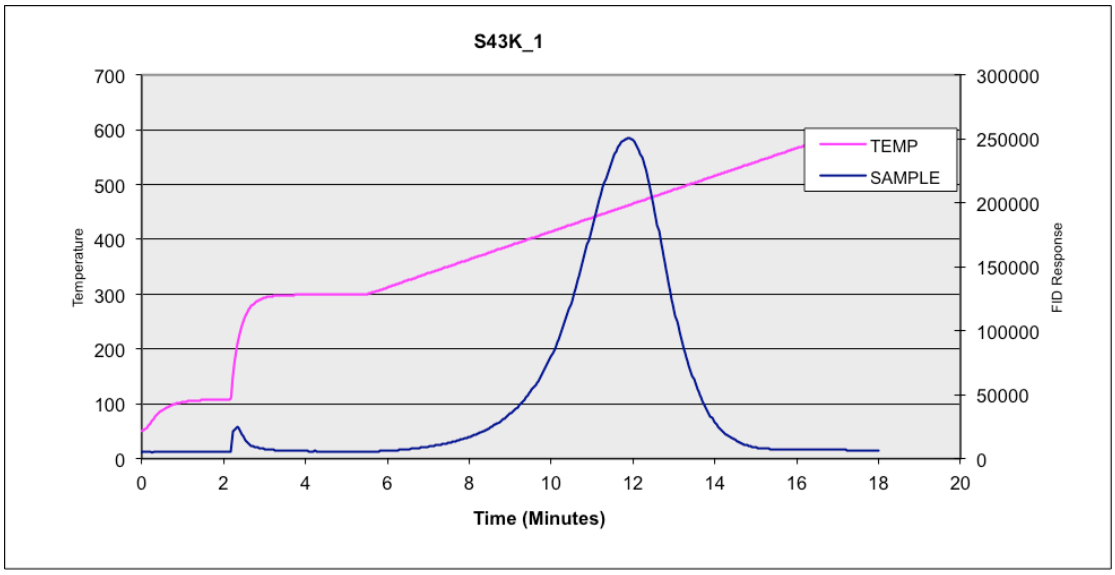
S43K_1
Temperature
FID Response
TEMP
SAMPLE
Time (Minutes)

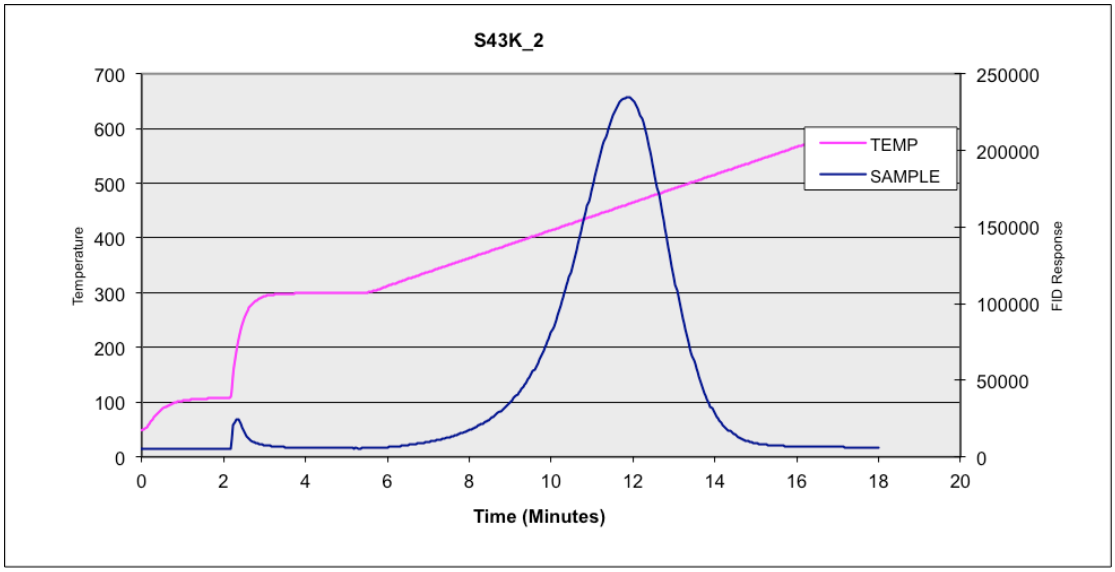
S43K_2
Temperature
FID Response
TEMP
SAMPLE
Time (Minutes)

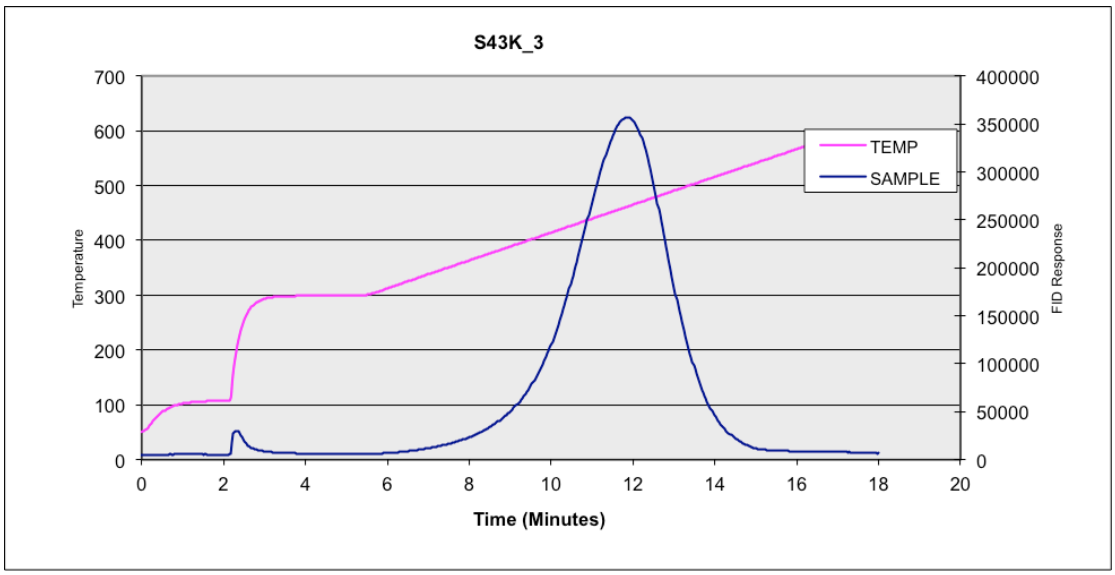
S43K_3
Temperature
FID Response
TEMP
SAMPLE
Time (Minutes)

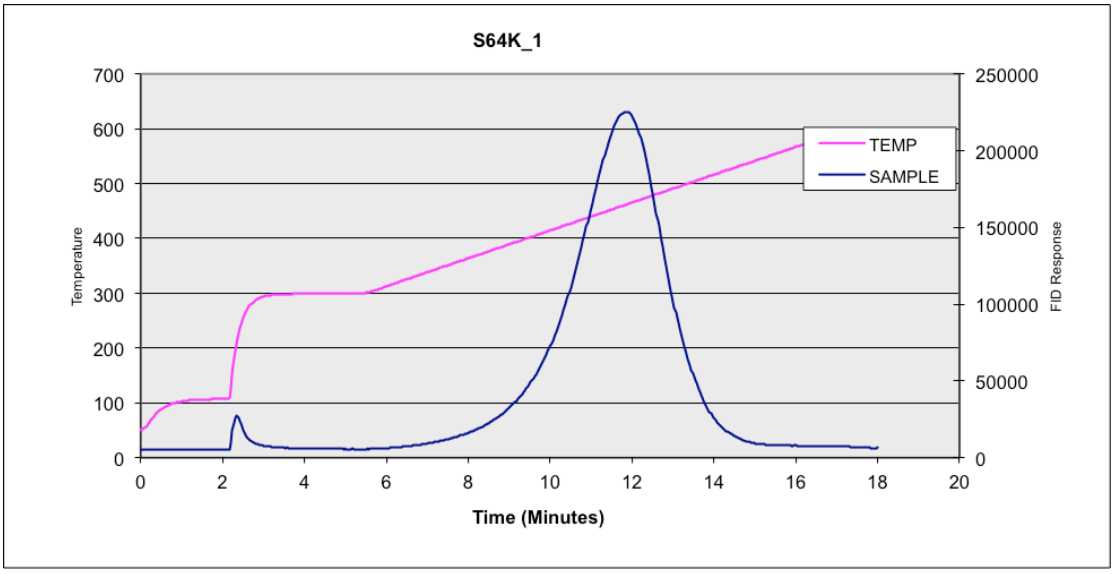
S64K_1
Temperature
FID Response
TEMP
SAMPLE
Time (Minutes)

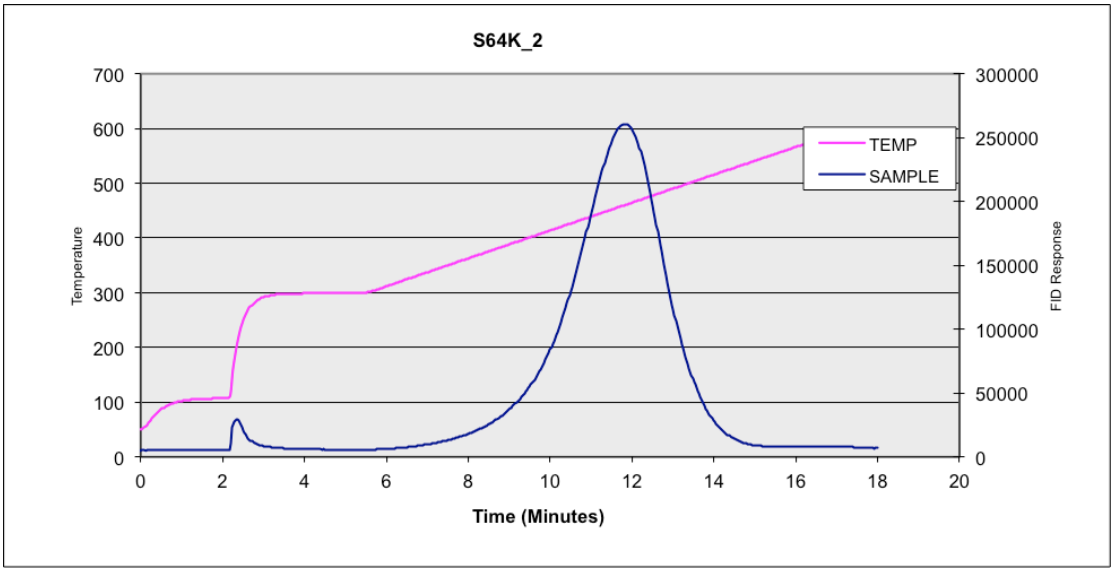
S64K_2
Temperature
FID Response
TEMP
SAMPLE
Time (Minutes)

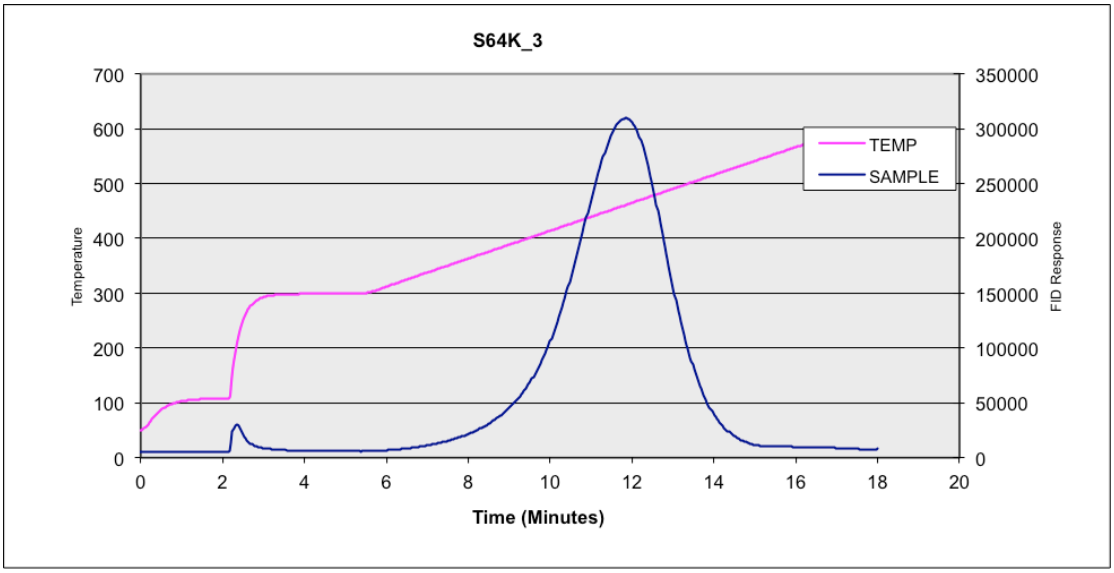
S64K_3
Temperature
FID Response
TEMP
SAMPLE
Time (Minutes)

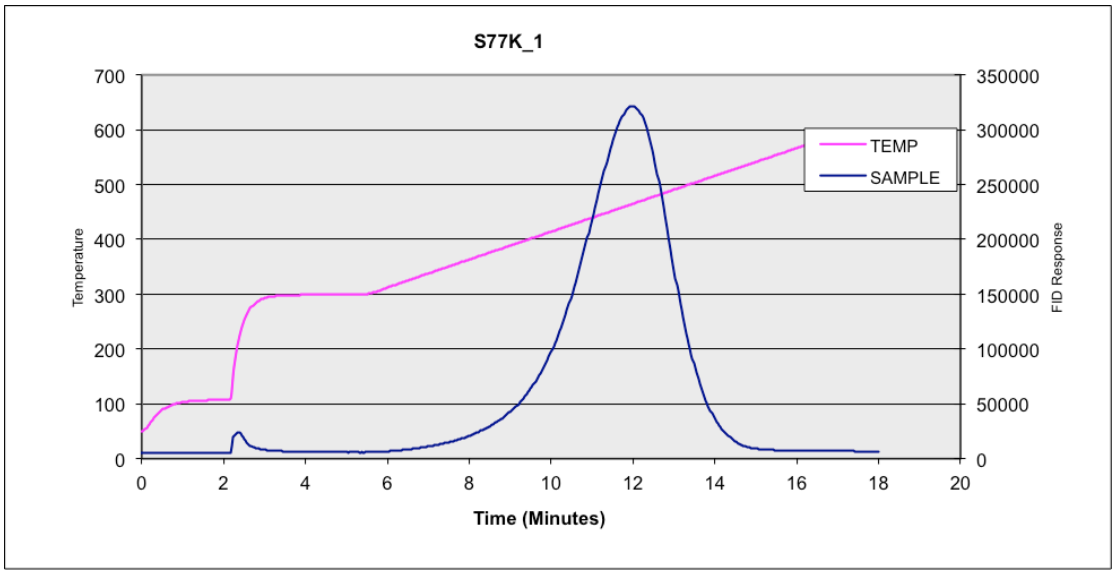
S77K_1
Temperature
FID Response
TEMP
SAMPLE
Time (Minutes)

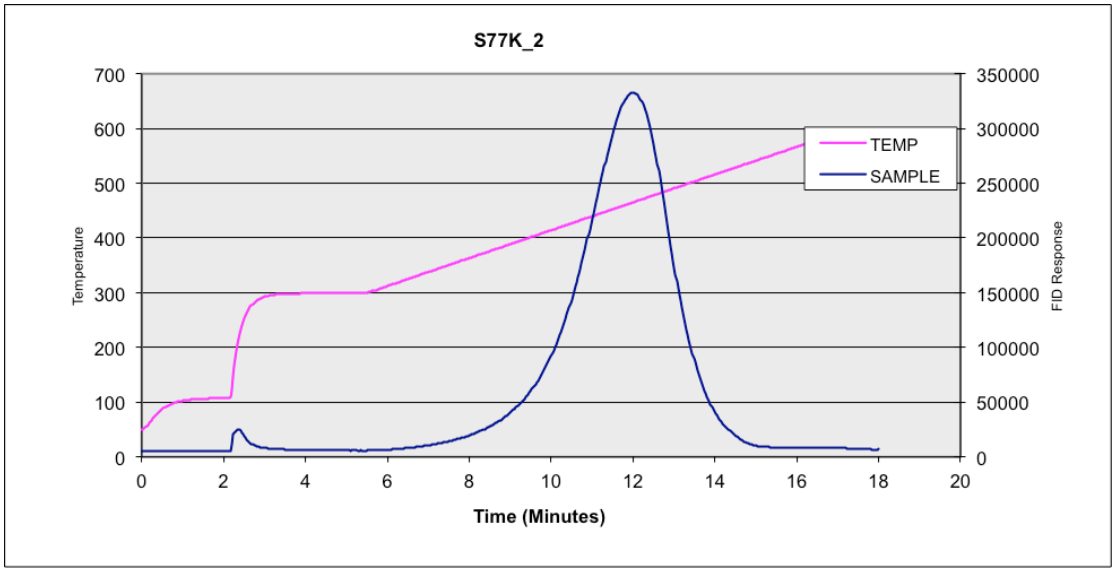
S77K_2
Temperature
FID Response
TEMP
SAMPLE
Time (Minutes)

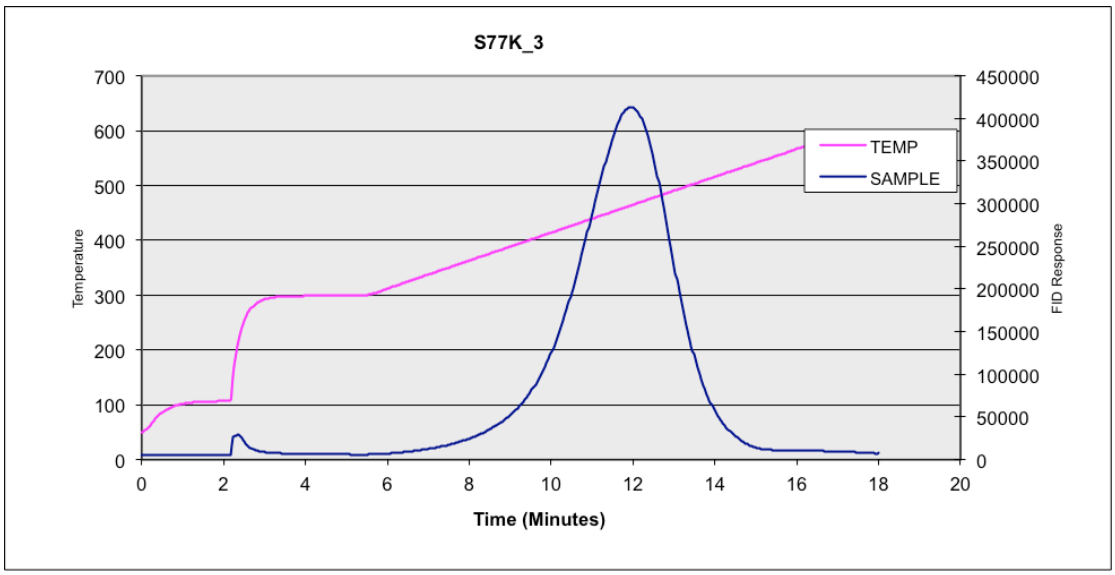
S77K_3
Temperature
FID Response
TEMP
SAMPLE
Time (Minutes)

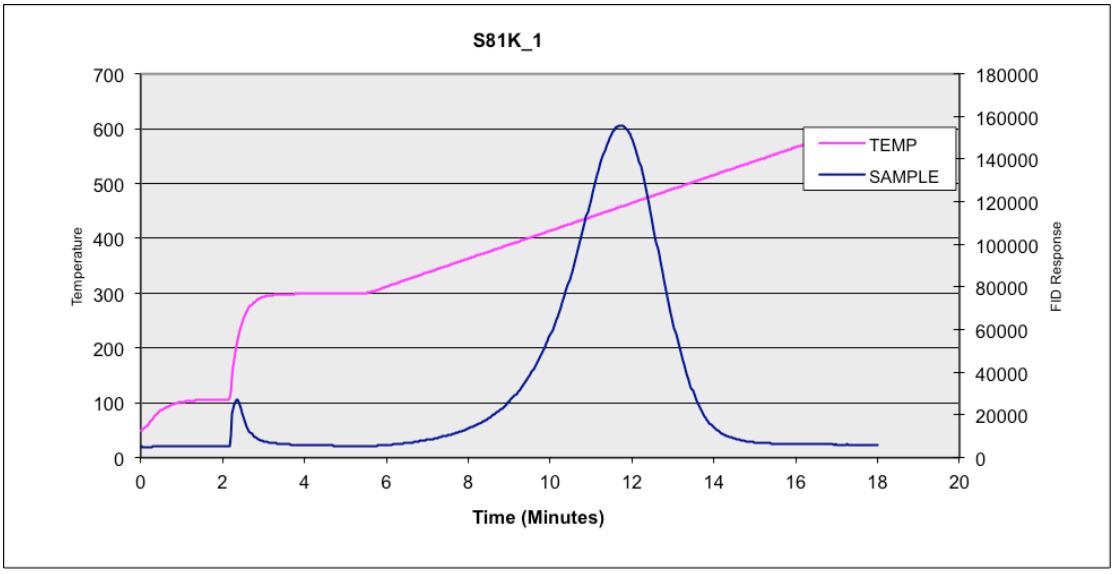
S81K_1
Temperature
FID Response
TEMP
SAMPLE
Time (Minutes)

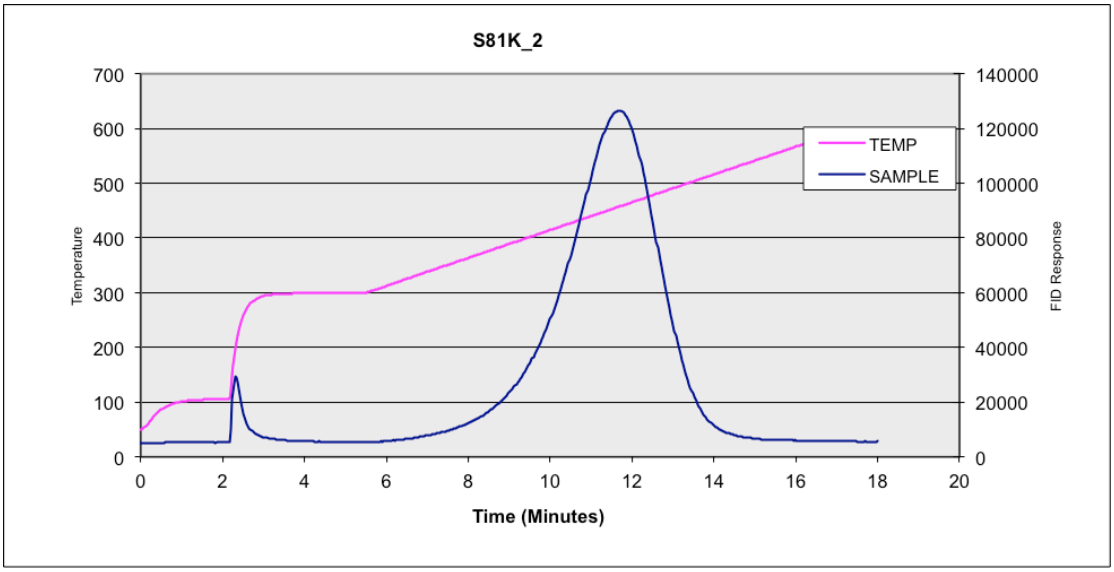
S81K_2
Temperature
FID Response
TEMP
SAMPLE
Time (Minutes)

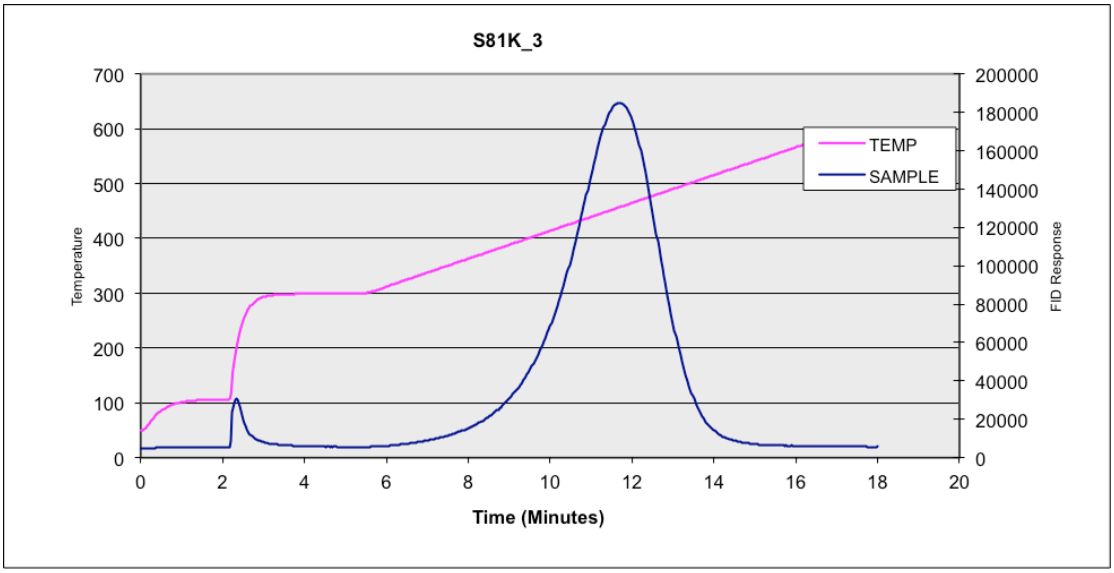
S81K_3
Temperature
FID Response
TEMP
SAMPLE
Time (Minutes)

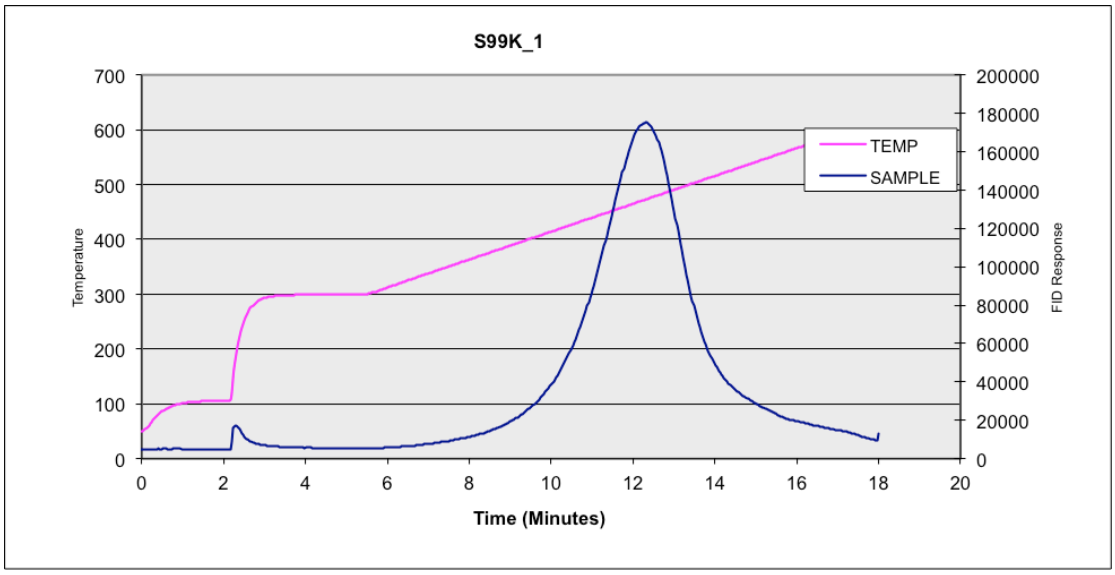
S99K_1
Temperature
FID Response
TEMP
SAMPLE
Time (Minutes)

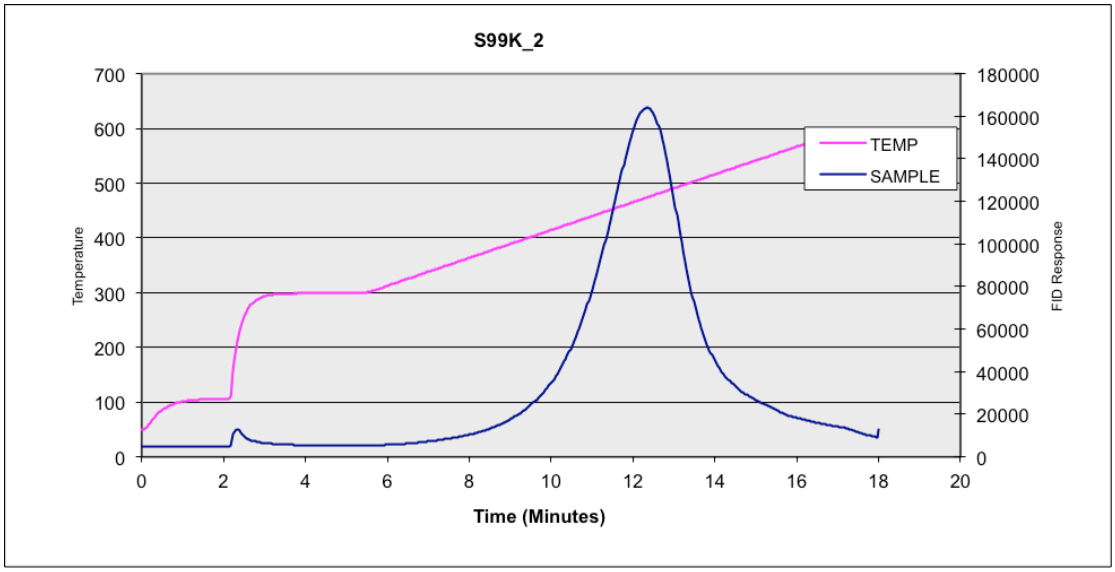
S99K_2
Temperature
FID Response
TEMP
SAMPLE
Time (Minutes)

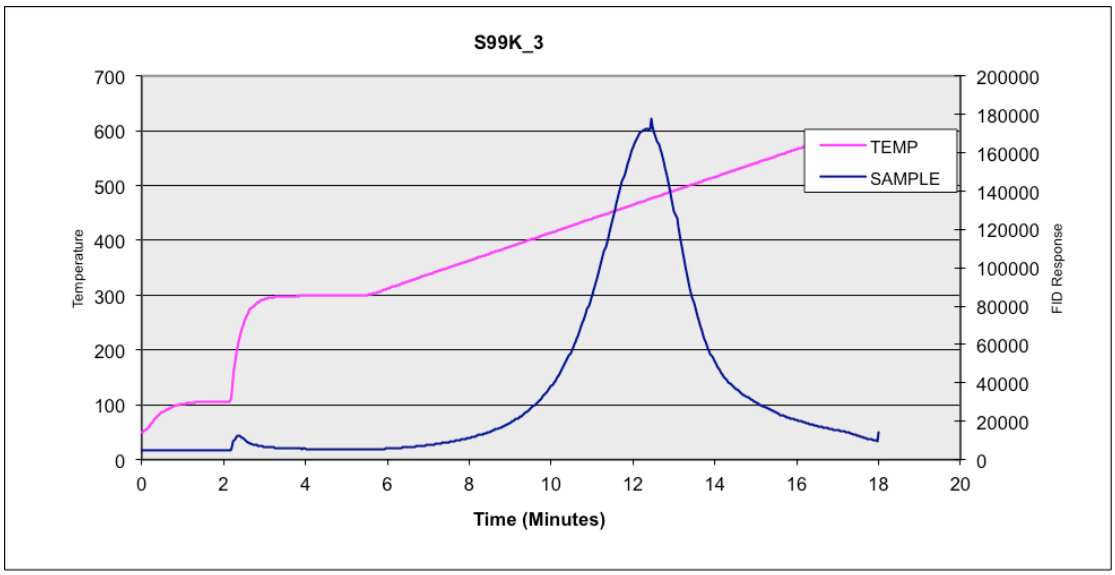
S99K_3
Temperature
FID Response
TEMP
SAMPLE
Time (Minutes)

Appendix 4. Rock-Eval FID pyorgram of whole rock samples of the Monterey Formation.

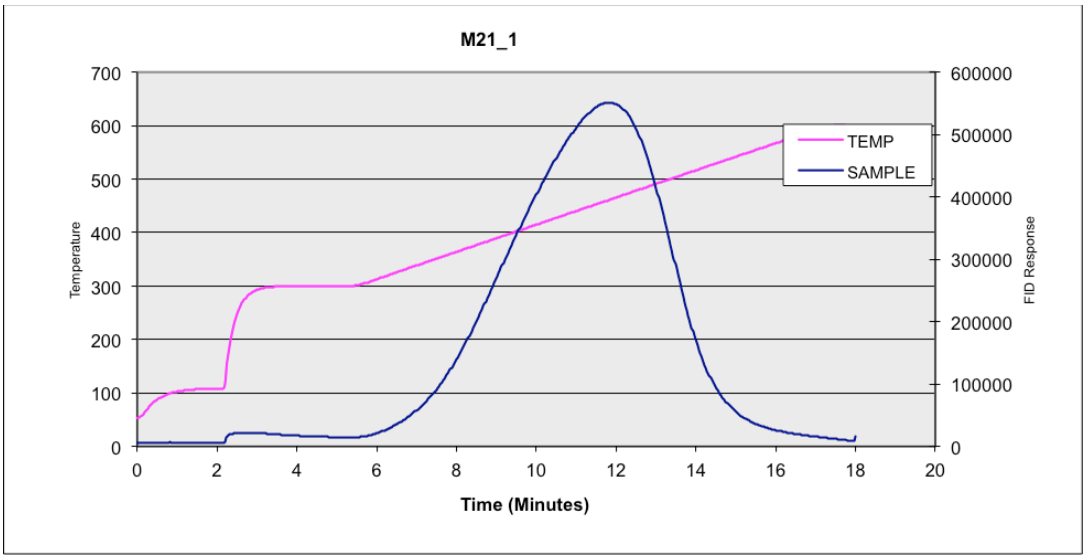

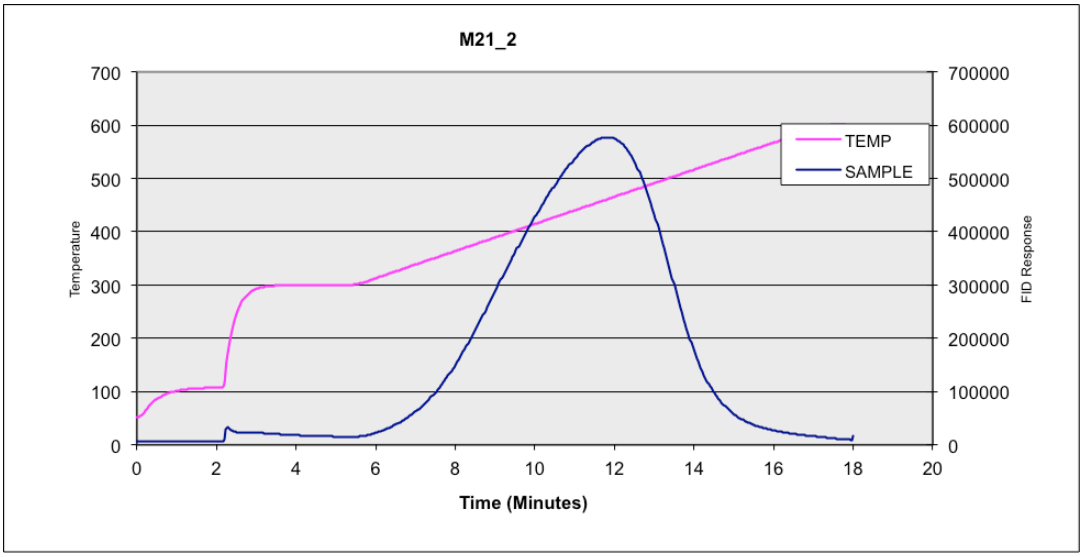

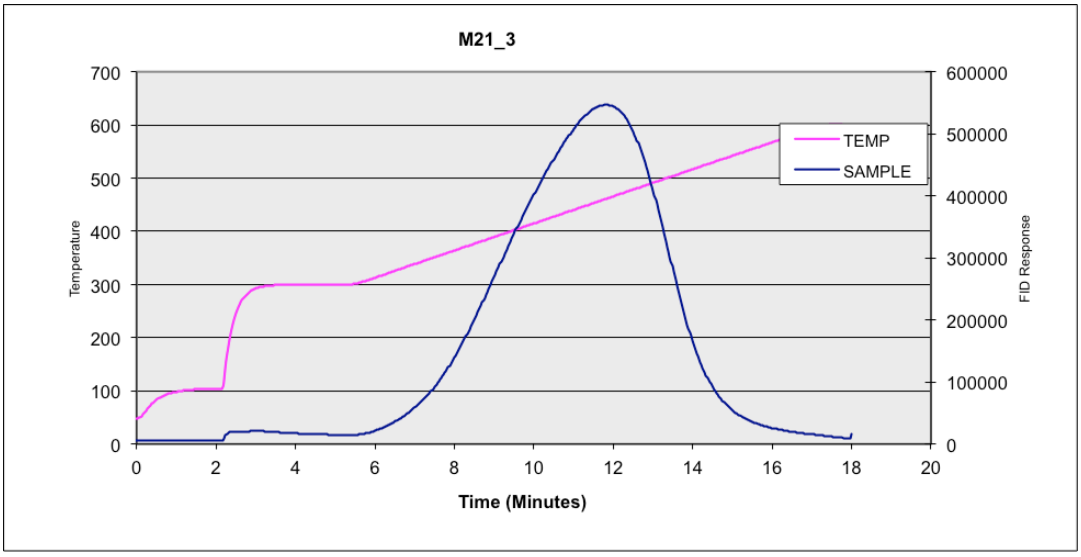

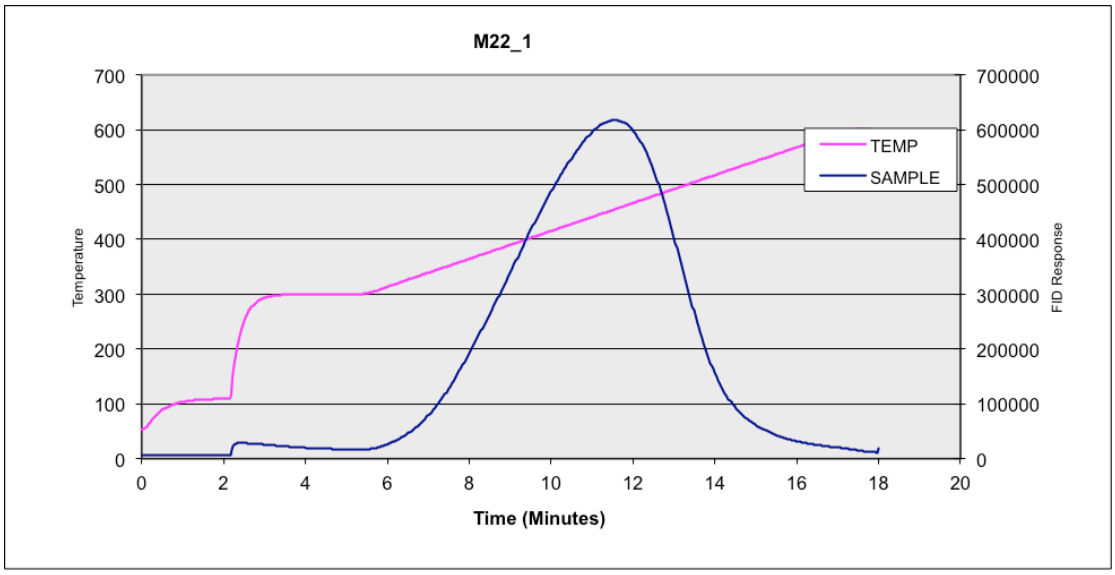
M22_1
Temperature
FID Response
TEMP
SAMPLE
Time (Minutes)
0
100
200
300
400
500
600
700
0
100000
200000
300000
400000
500000
600000
700000
0
2
4
6
8
10
12
14
16
18
20

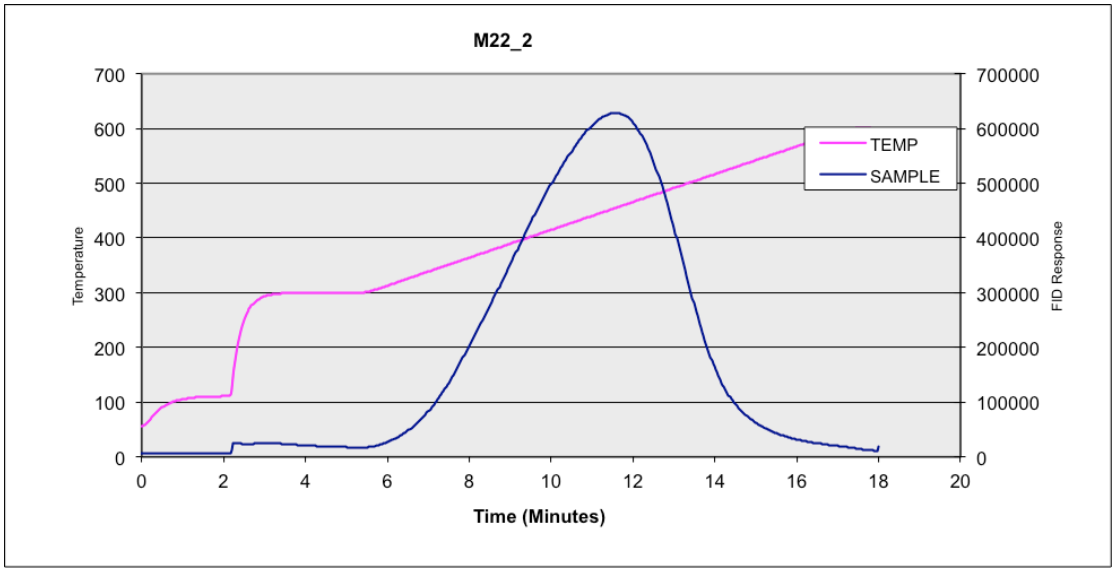
M22_2
Temperature
FID Response
TEMP
SAMPLE
Time (Minutes)
0
100
200
300
400
500
600
700
0
100000
200000
300000
400000
500000
600000
700000
0
2
4
6
8
10
12
14
16
18
20

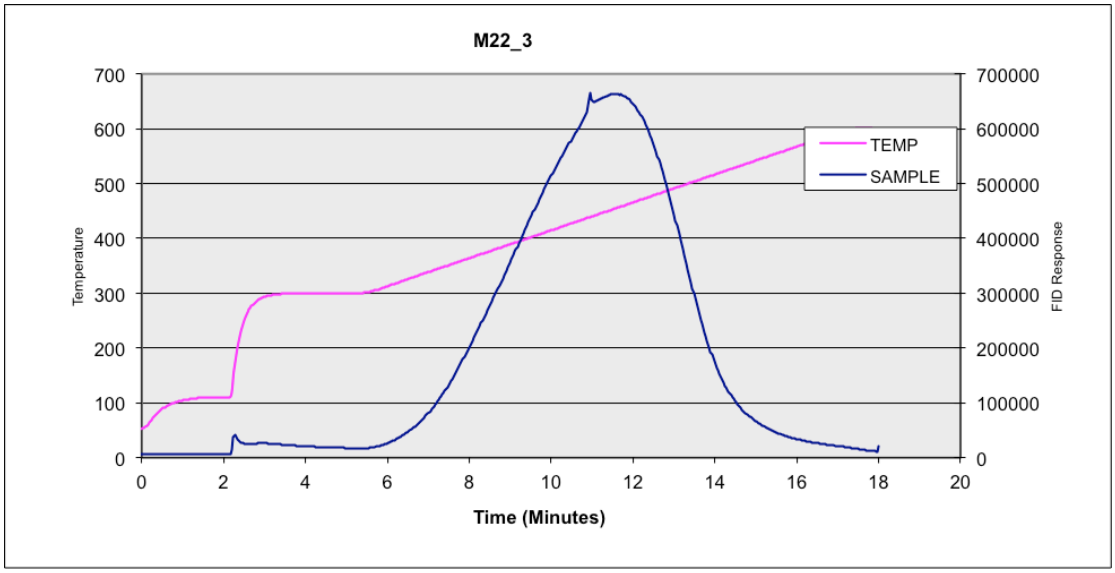
M22_3
Temperature
FID Response
TEMP
SAMPLE
Time (Minutes)
0
100
200
300
400
500
600
700
0
100000
200000
300000
400000
500000
600000
700000
0
2
4
6
8
10
12
14
16
18
20

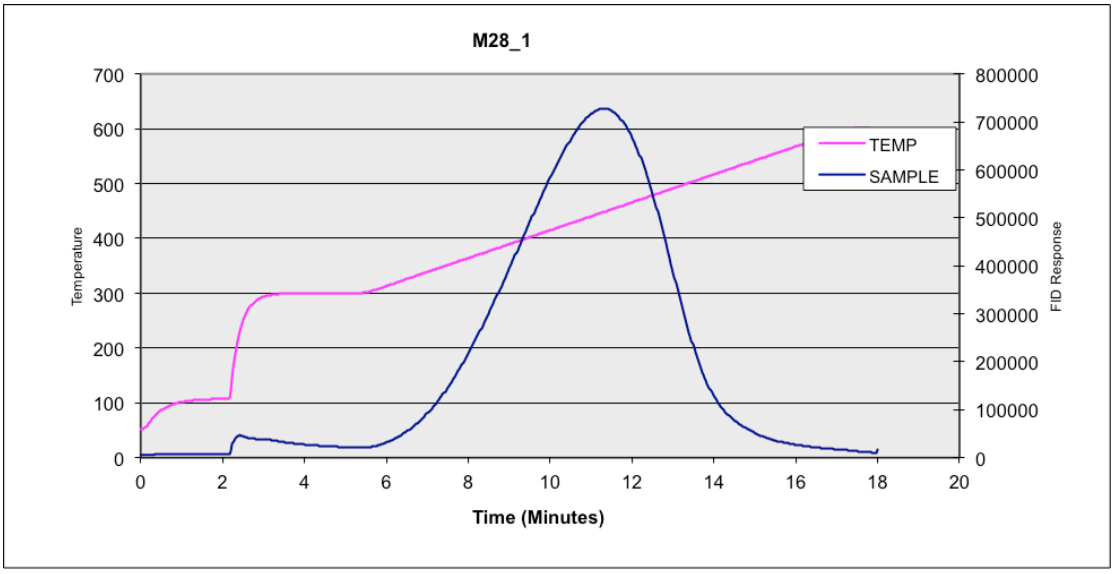
M28_1
Temperature
FID Response
TEMP
SAMPLE
Time (Minutes)
0
100
200
300
400
500
600
700
0
100000
200000
300000
400000
500000
600000
700000
800000
0
2
4
6
8
10
12
14
16
18
20

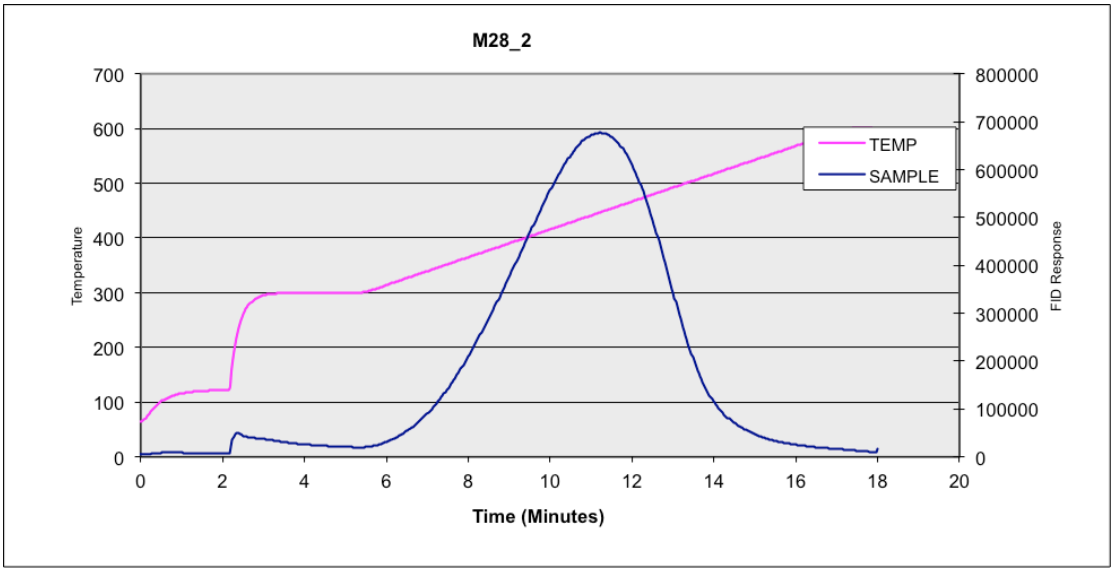
M28_2
Temperature
FID Response
TEMP
SAMPLE
Time (Minutes)
0
100
200
300
400
500
600
700
0
100000
200000
300000
400000
500000
600000
700000
800000
0
2
4
6
8
10
12
14
16
18
20

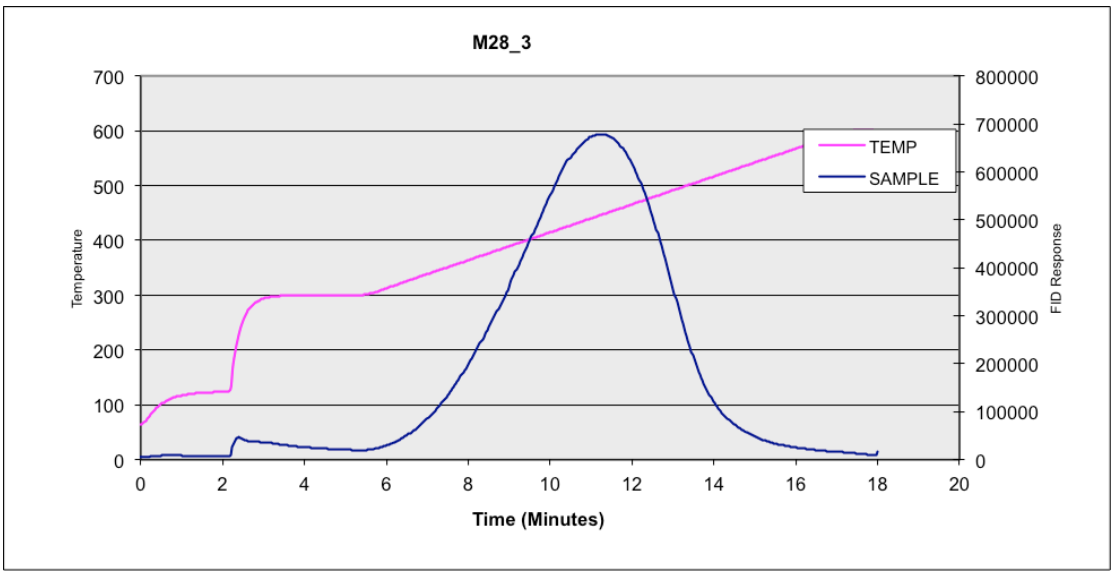
M28_3
Temperature
FID Response
TEMP
SAMPLE
Time (Minutes)
0
100
200
300
400
500
600
700
0
100000
200000
300000
400000
500000
600000
700000
800000
0
2
4
6
8
10
12
14
16
18
20

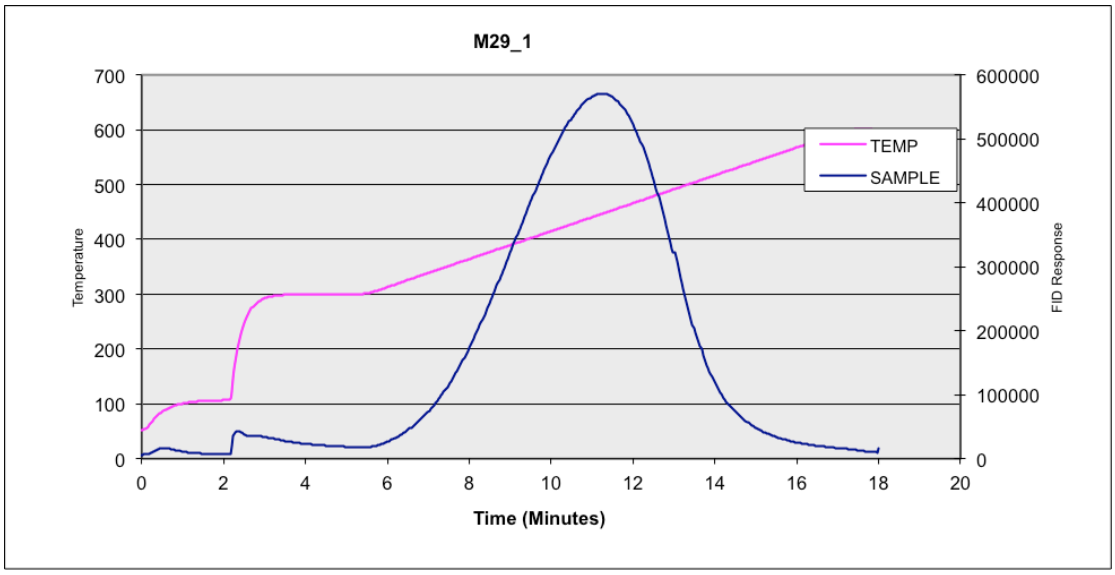
M29_1
Temperature
FID Response
TEMP
SAMPLE
Time (Minutes)
0
100
200
300
400
500
600
700
100000
200000
300000
400000
500000
600000
0
2
4
6
8
10
12
14
16
18
20

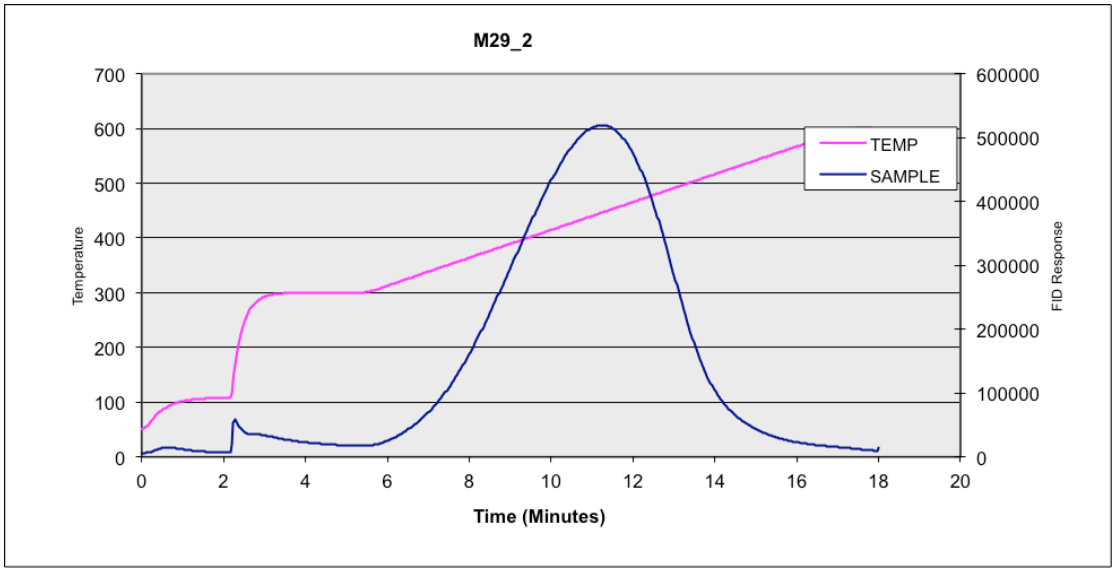
M29_2
Temperature
FID Response
TEMP
SAMPLE
Time (Minutes)
0
100
200
300
400
500
600
700
100000
200000
300000
400000
500000
600000
0
2
4
6
8
10
12
14
16
18
20

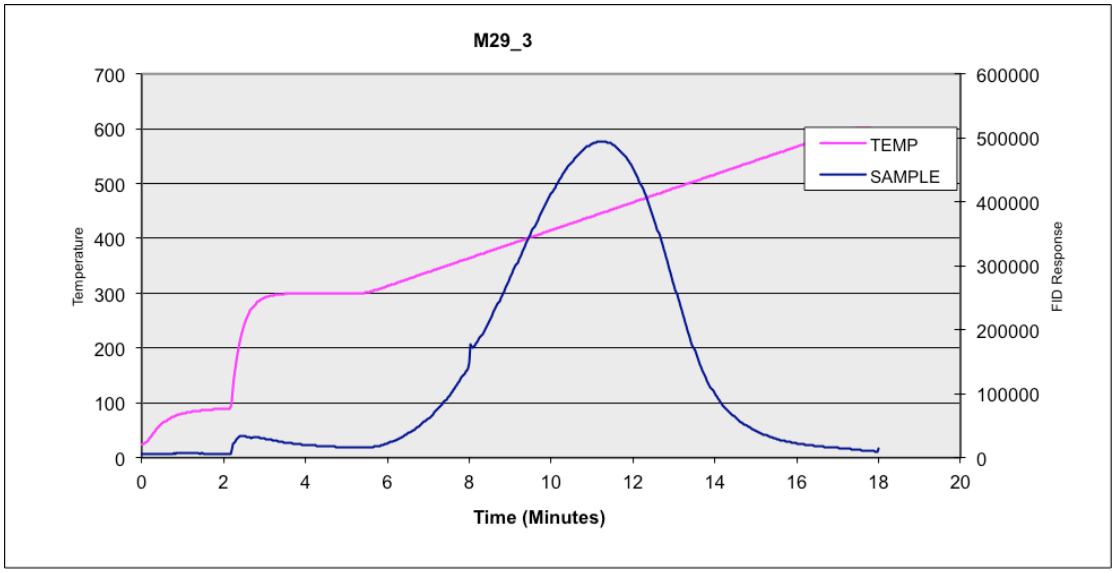
M29_3
Temperature
FID Response
TEMP
SAMPLE
Time (Minutes)
0
100
200
300
400
500
600
700
100000
200000
300000
400000
500000
600000
0
2
4
6
8
10
12
14
16
18
20

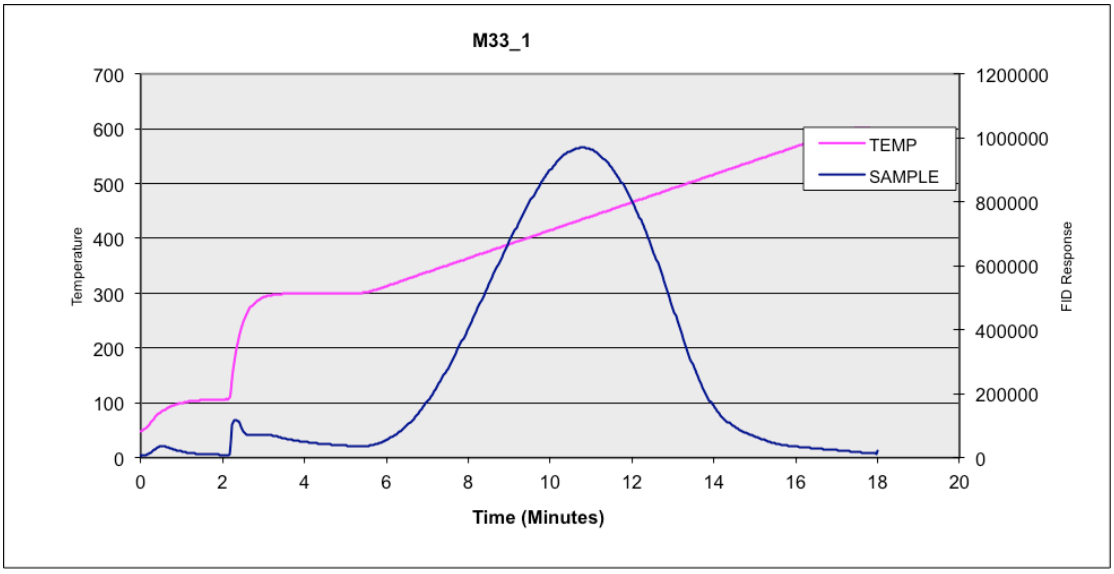
M33_1
Temperature
FID Response
TEMP
SAMPLE
Time (Minutes)
0
100
200
300
400
500
600
700
0
200000
400000
600000
800000
1000000
1200000
0
2
4
6
8
10
12
14
16
18
20

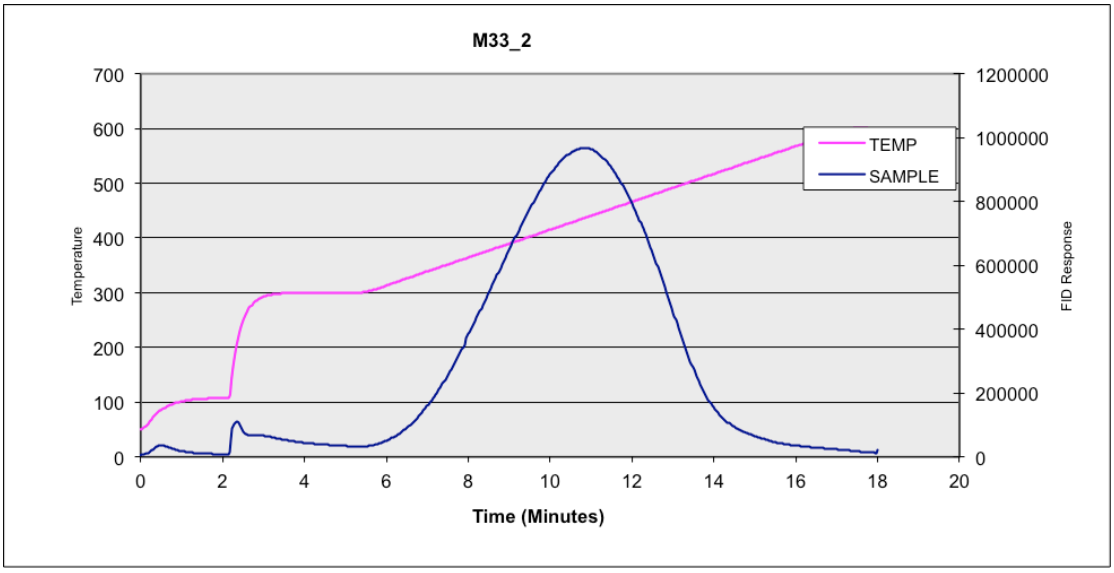
M33_2
Temperature
FID Response
TEMP
SAMPLE
Time (Minutes)
0
100
200
300
400
500
600
700
0
200000
400000
600000
800000
1000000
1200000
0
2
4
6
8
10
12
14
16
18
20

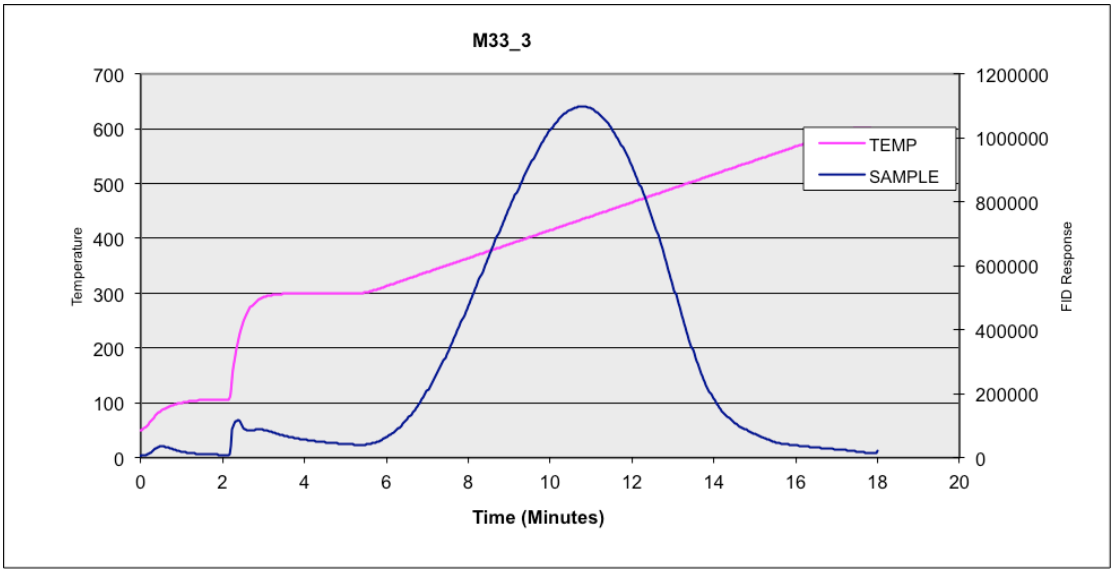
M33_3
Temperature
FID Response
TEMP
SAMPLE
Time (Minutes)
0
100
200
300
400
500
600
700
0
200000
400000
600000
800000
1000000
1200000
0
2
4
6
8
10
12
14
16
18
20

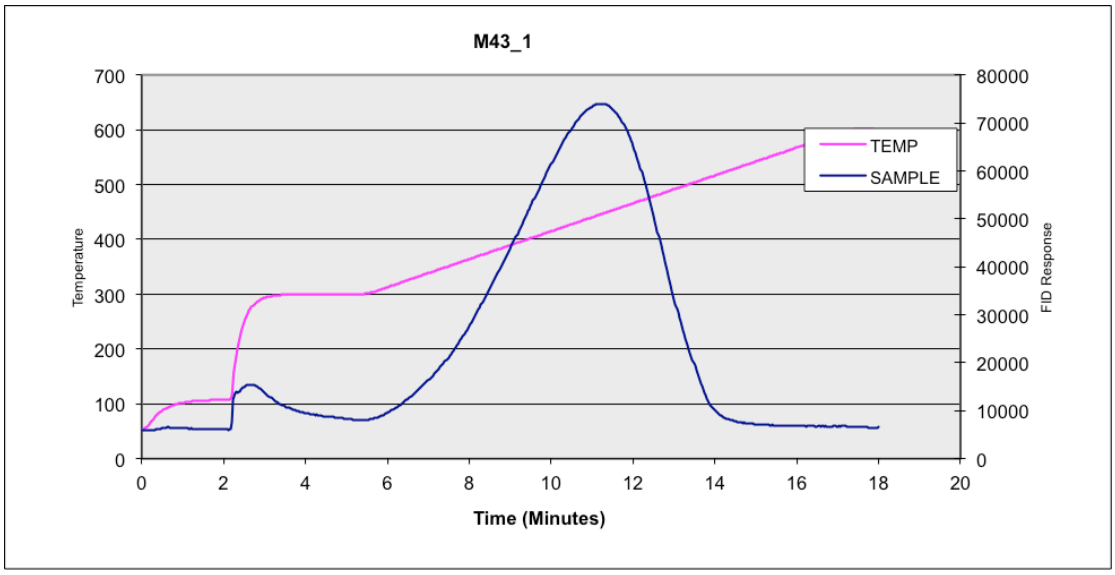
M43_1
Temperature
FID Response
TEMP
SAMPLE
Time (Minutes)
0
100
200
300
400
500
600
700
0
10000
20000
30000
40000
50000
60000
70000
80000
0
2
4
6
8
10
12
14
16
18
20

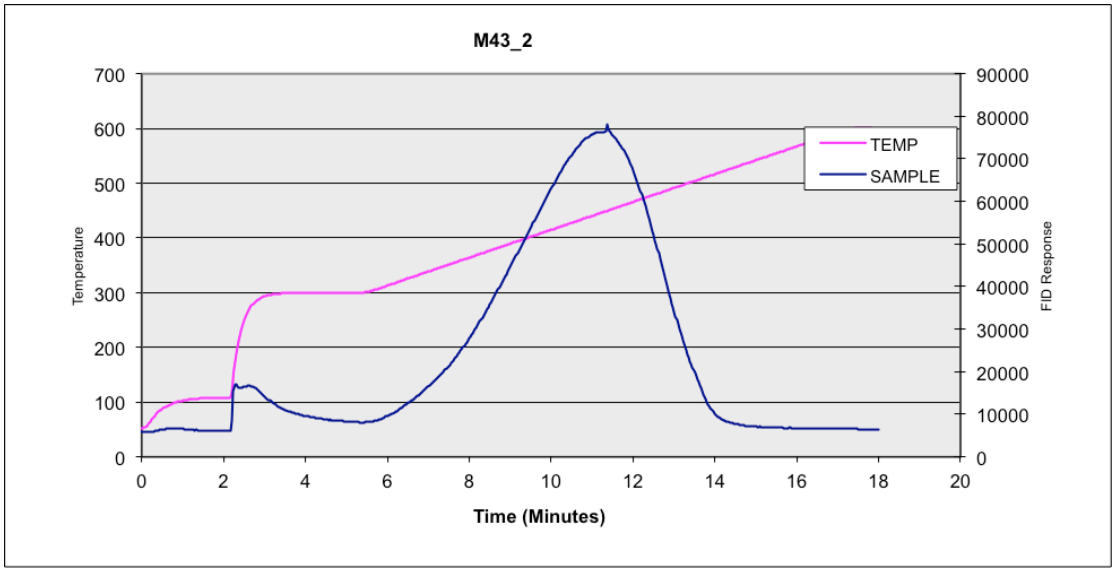
M43_2
Temperature
FID Response
TEMP
SAMPLE
Time (Minutes)
0
100
200
300
400
500
600
700
0
10000
20000
30000
40000
50000
60000
70000
80000
90000
0
2
4
6
8
10
12
14
16
18
20

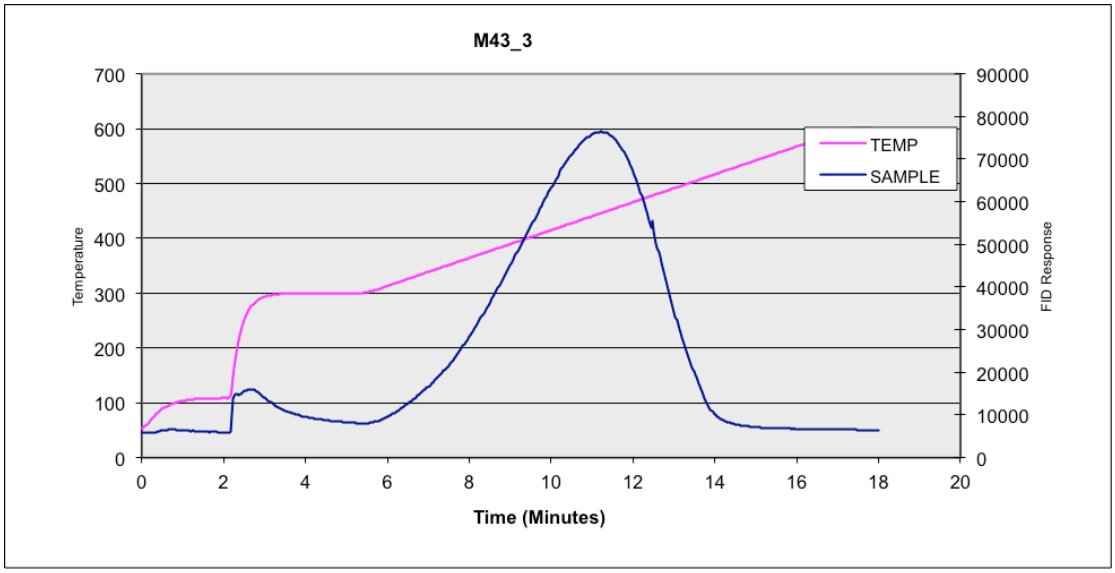
M43_3
Temperature
FID Response
TEMP
SAMPLE
Time (Minutes)
0
100
200
300
400
500
600
700
0
10000
20000
30000
40000
50000
60000
70000
80000
90000
0
2
4
6
8
10
12
14
16
18
20

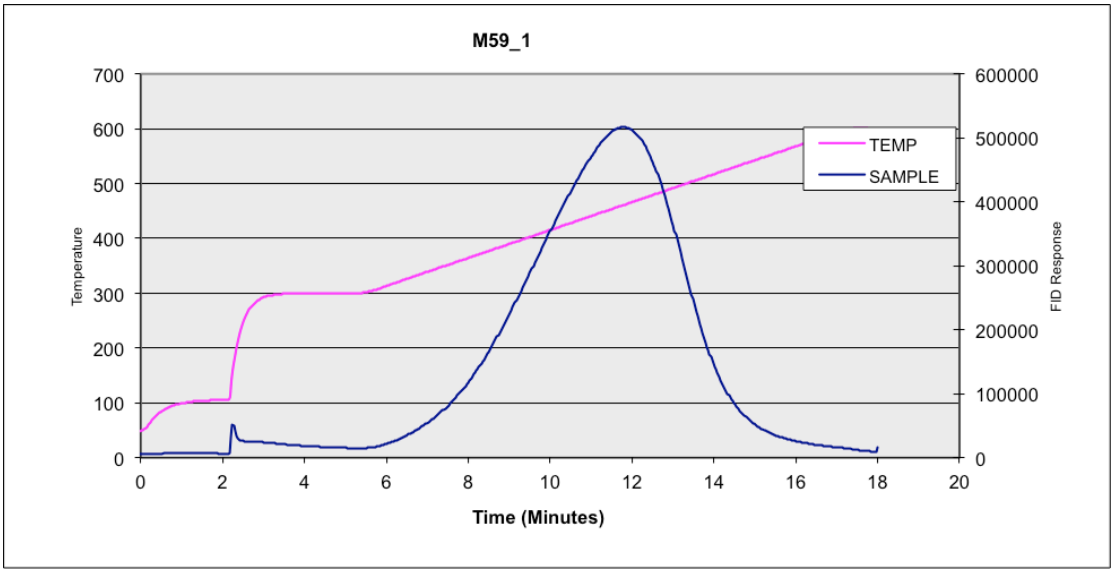
M59_1
Temperature
FID Response
TEMP
SAMPLE
Time (Minutes)
0
100
200
300
400
500
600
700
0
100000
200000
300000
400000
500000
600000
0
2
4
6
8
10
12
14
16
18
20

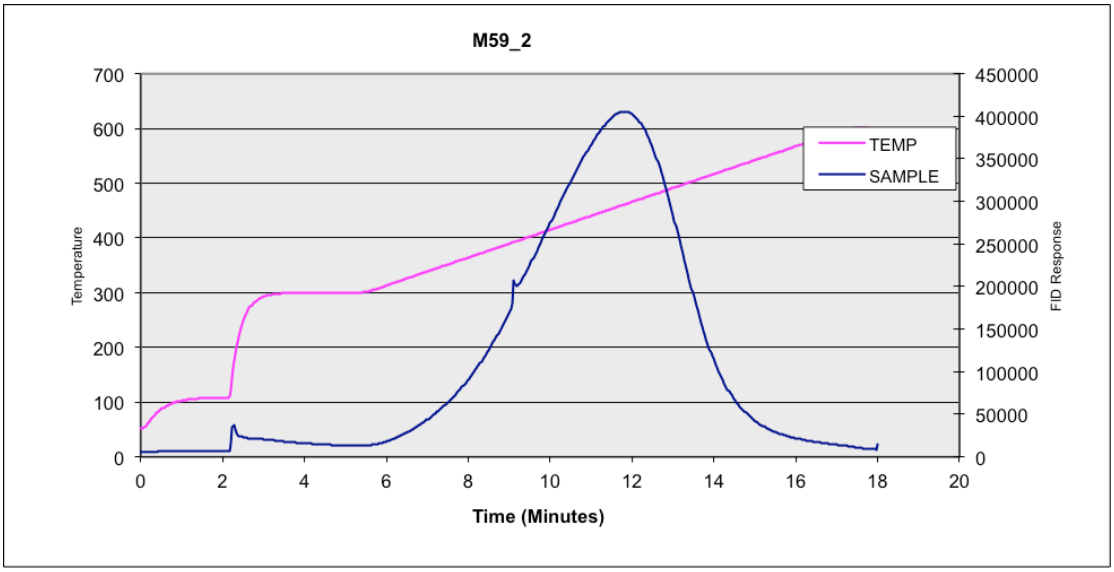
M59_2
Temperature
FID Response
TEMP
SAMPLE
Time (Minutes)
0
100
200
300
400
500
600
700
0
50000
100000
150000
200000
250000
300000
350000
400000
450000
0
2
4
6
8
10
12
14
16
18
20

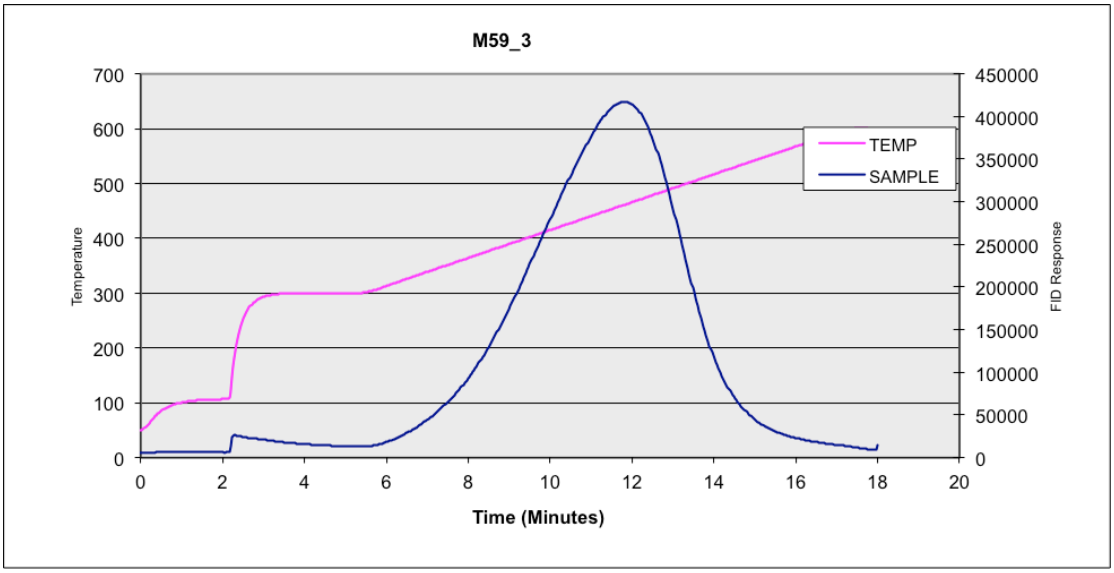
M59_3
Temperature
FID Response
TEMP
SAMPLE
Time (Minutes)
0
100
200
300
400
500
600
700
0
50000
100000
150000
200000
250000
300000
350000
400000
450000
0
2
4
6
8
10
12
14
16
18
20

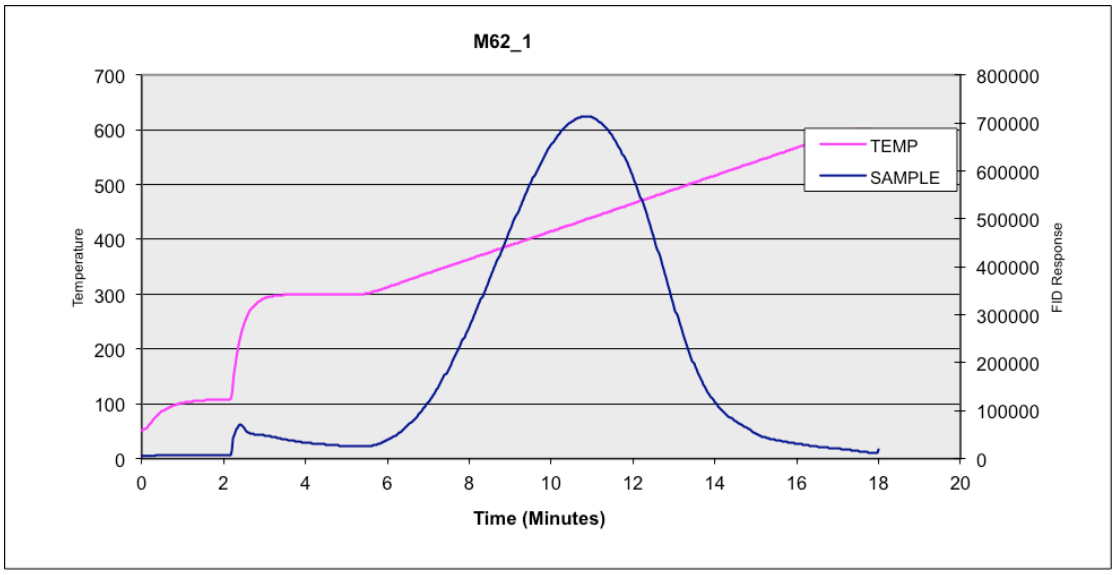
M62_1
Temperature
FID Response
TEMP
SAMPLE
Time (Minutes)

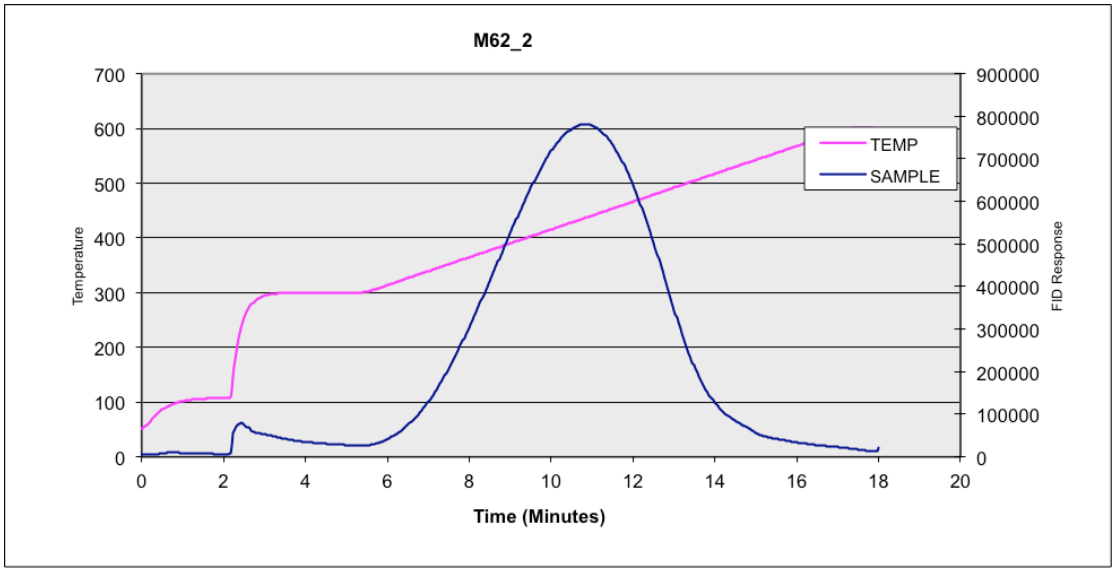
M62_2
Temperature
FID Response
TEMP
SAMPLE
Time (Minutes)

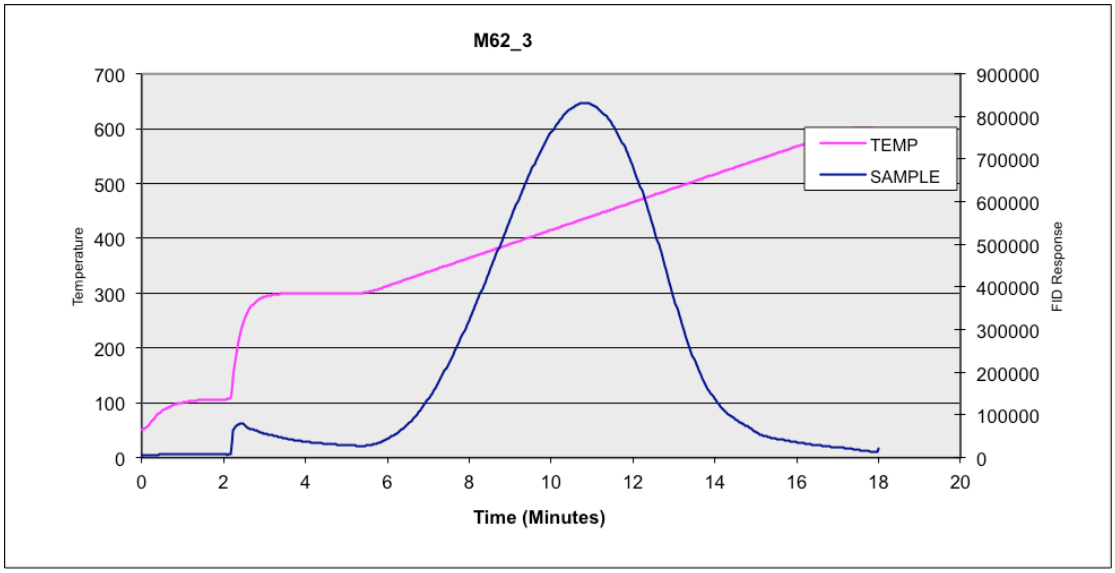
M62_3
Temperature
FID Response
TEMP
SAMPLE
Time (Minutes)

Appendix 5. Rock-Eval FID pyrograms of kerogen isolate of samples of the Monterey Formation

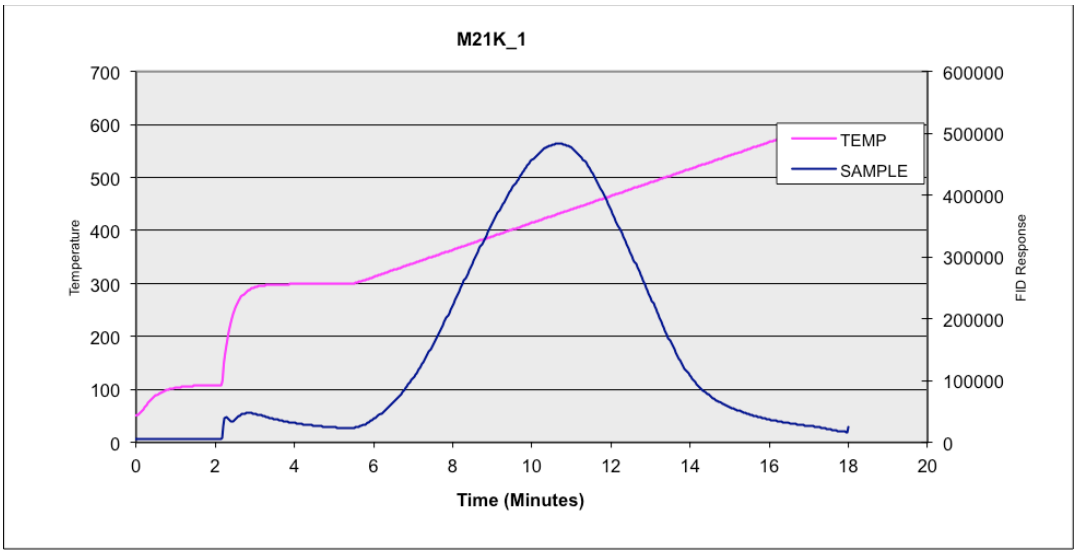

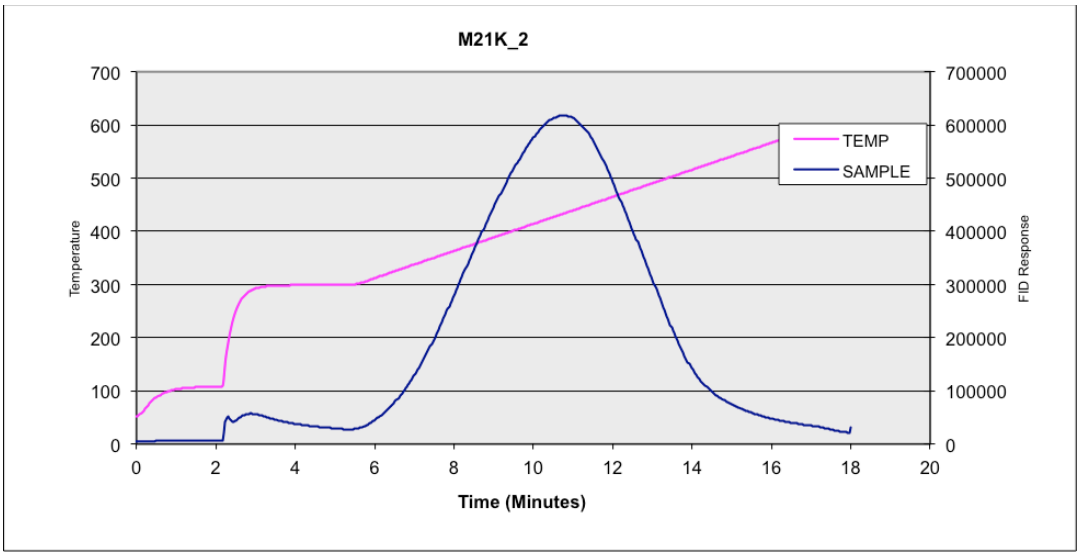

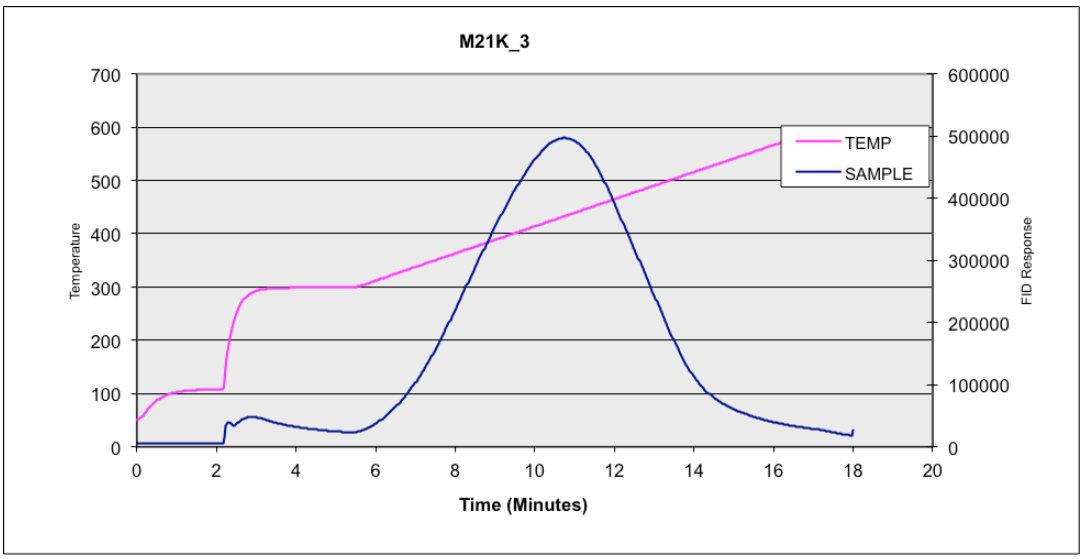

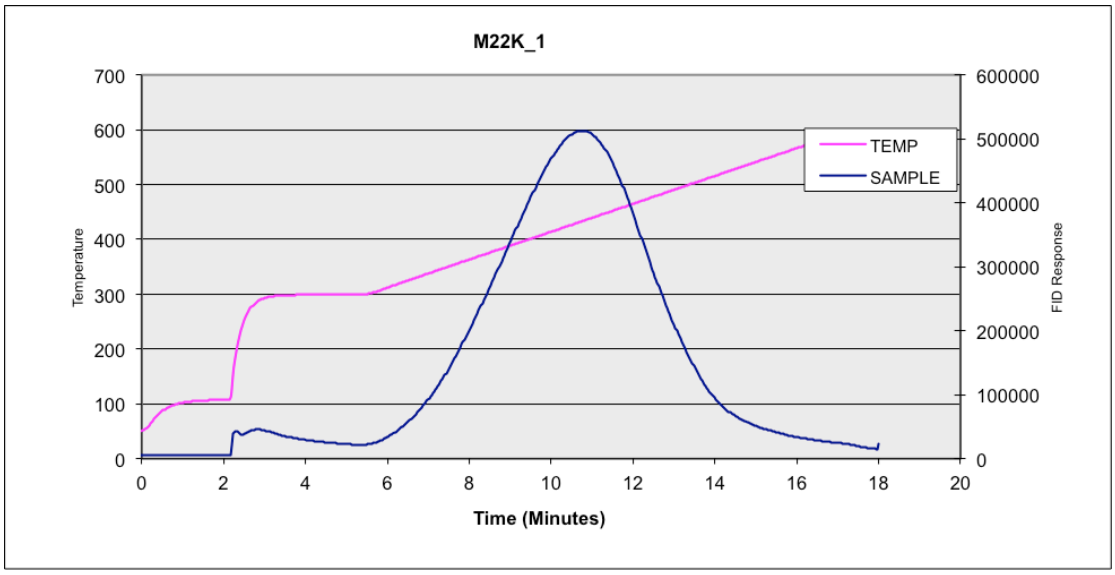
M22K_1
Temperature
FID Response
TEMP
SAMPLE
Time (Minutes)
0
100
200
300
400
500
600
700
100000
200000
300000
400000
500000
600000
0
2
4
6
8
10
12
14
16
18
20

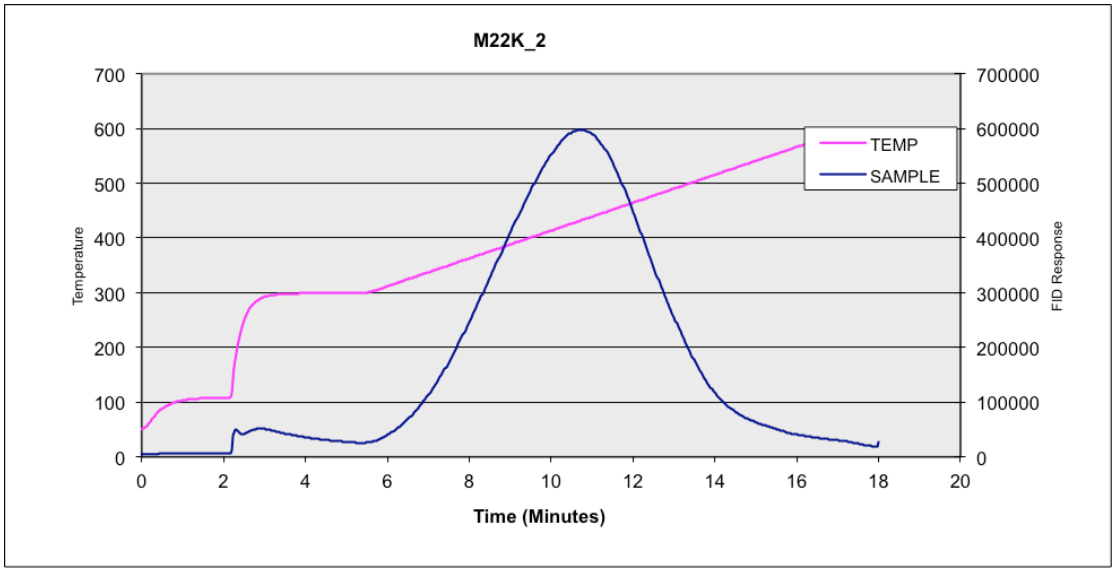
M22K_2
Temperature
FID Response
TEMP
SAMPLE
Time (Minutes)
0
100
200
300
400
500
600
700
100000
200000
300000
400000
500000
600000
700000
0
2
4
6
8
10
12
14
16
18
20

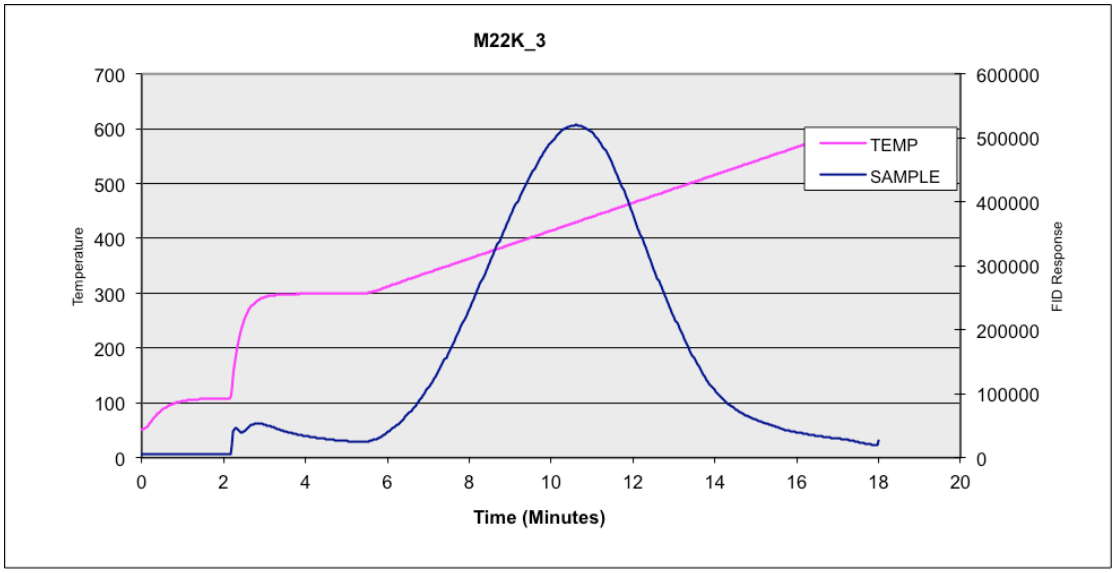
M22K_3
Temperature
FID Response
TEMP
SAMPLE
Time (Minutes)
0
100
200
300
400
500
600
700
100000
200000
300000
400000
500000
600000
0
2
4
6
8
10
12
14
16
18
20

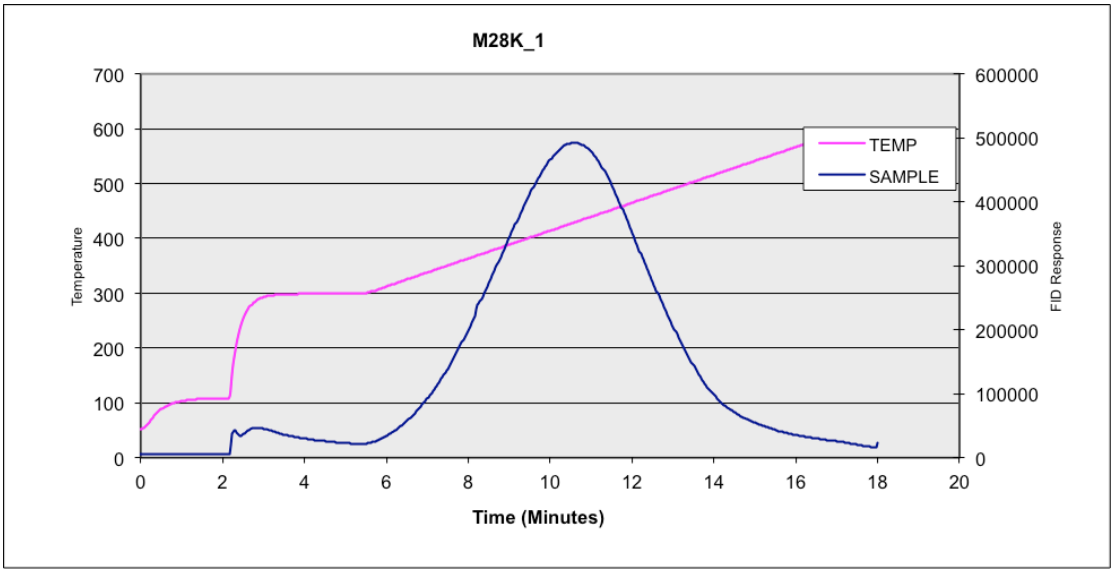
M28K_1
Temperature
FID Response
TEMP
SAMPLE
Time (Minutes)

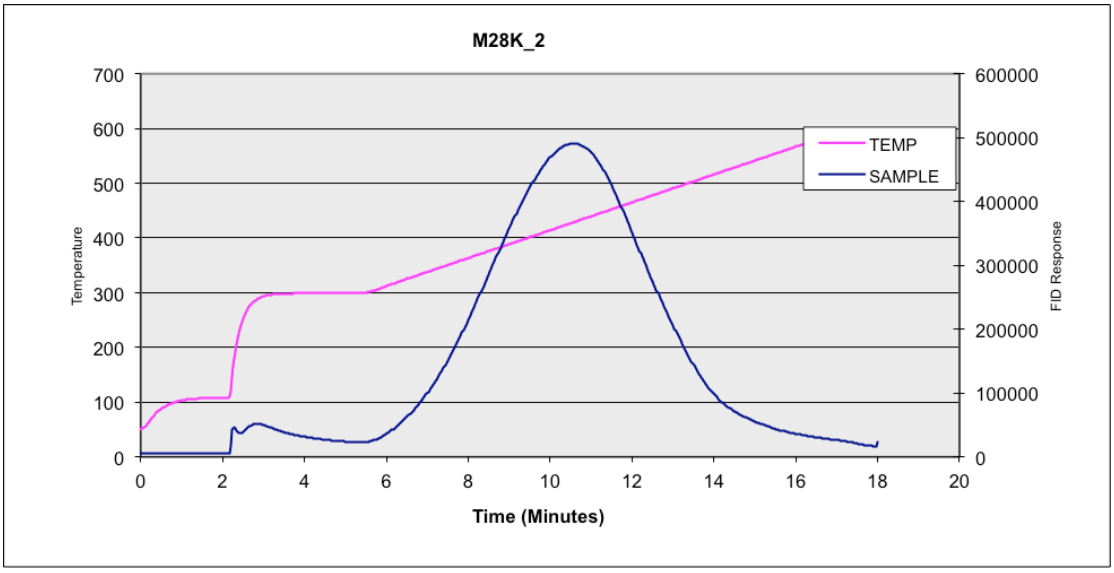
M28K_2
Temperature
FID Response
TEMP
SAMPLE
Time (Minutes)

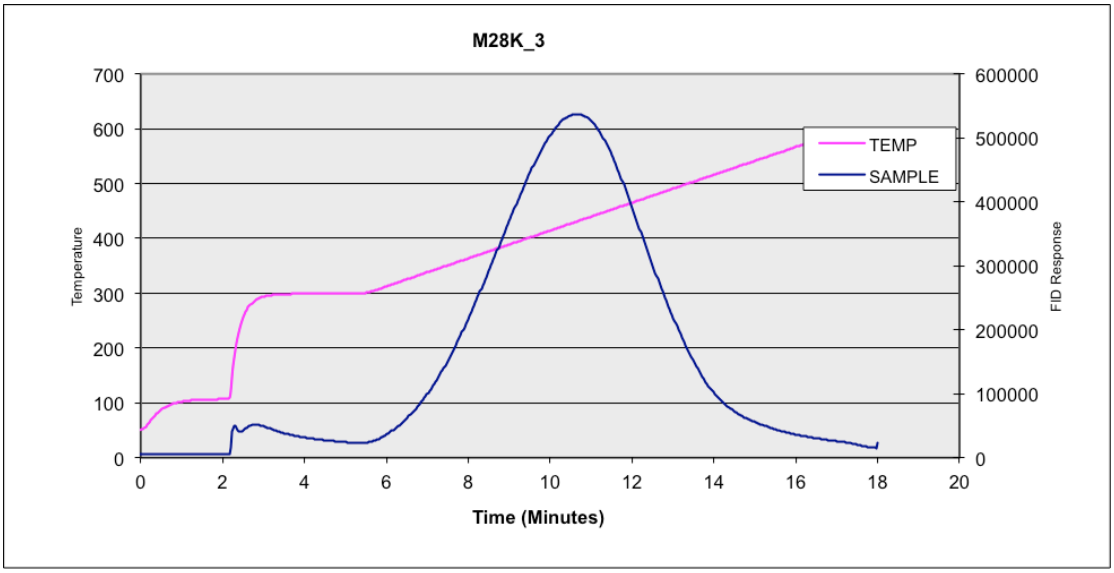
M28K_3
Temperature
FID Response
TEMP
SAMPLE
Time (Minutes)

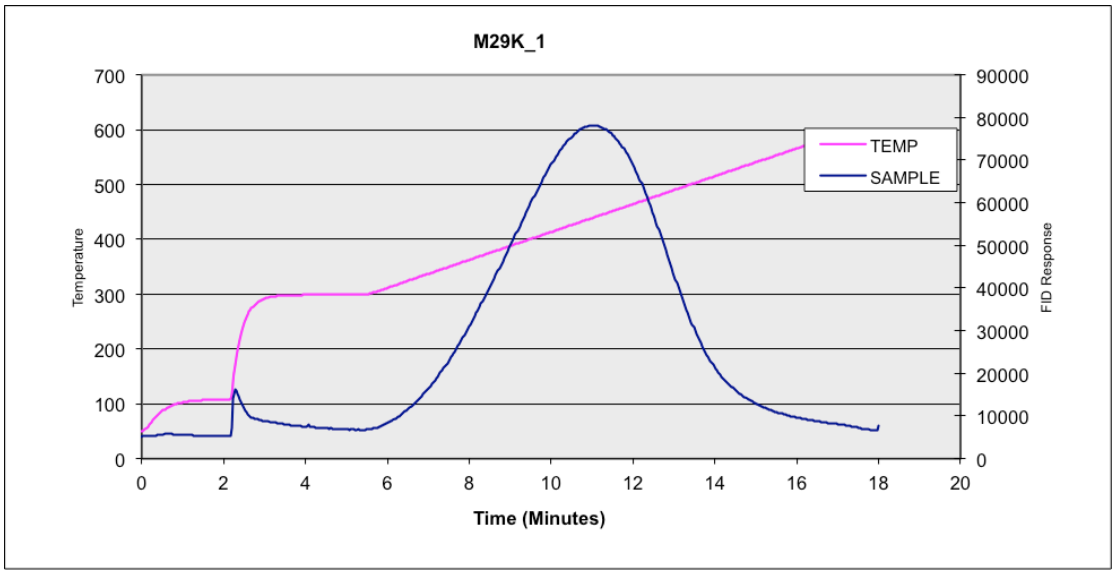
M29K_1
Temperature
FID Response
TEMP
SAMPLE
Time (Minutes)

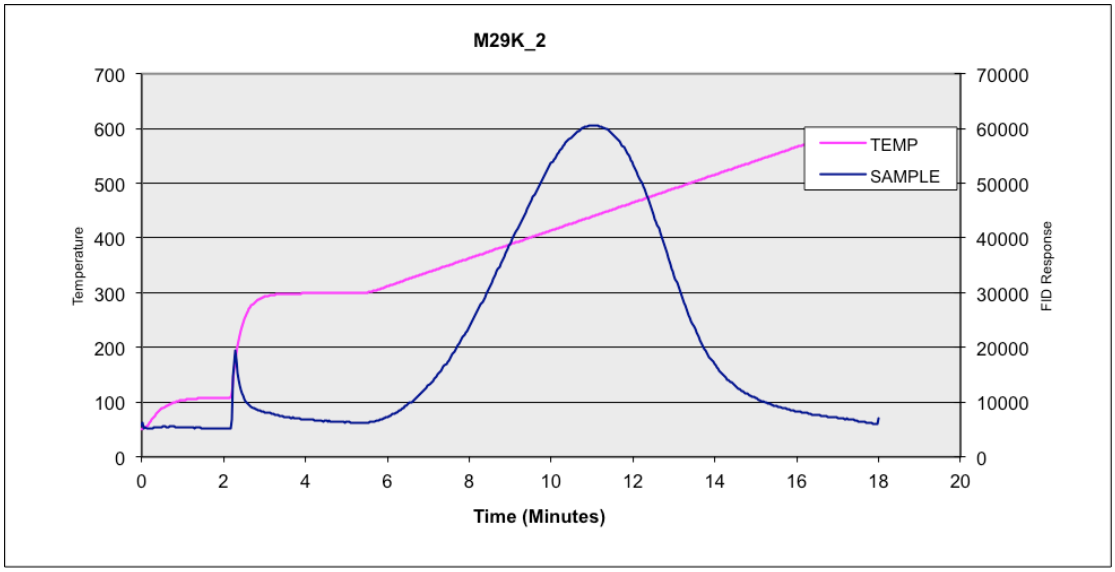
M29K_2
Temperature
FID Response
TEMP
SAMPLE
Time (Minutes)

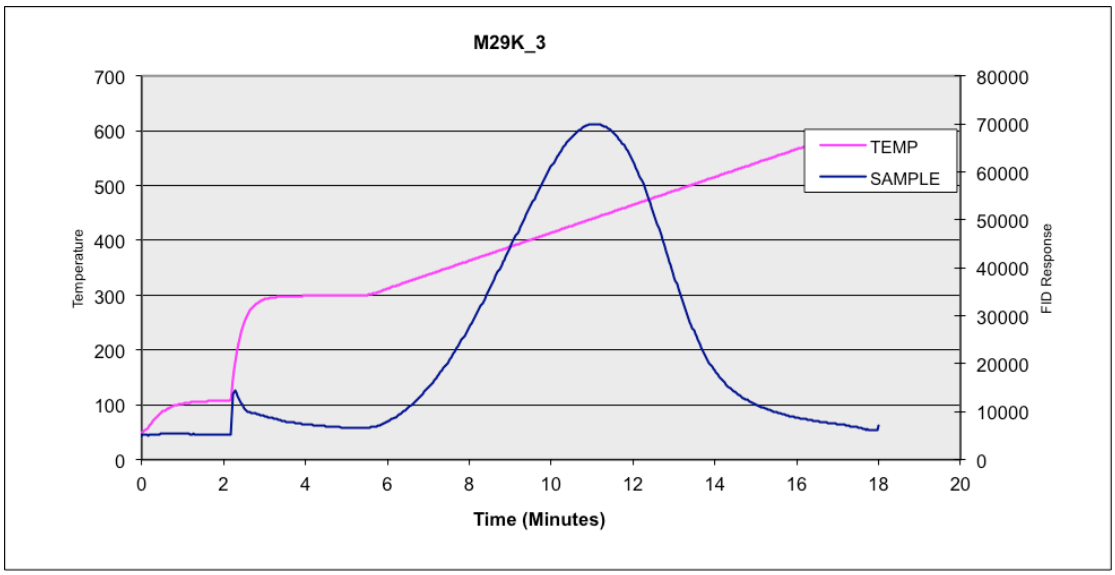
M29K_3
Temperature
FID Response
TEMP
SAMPLE
Time (Minutes)

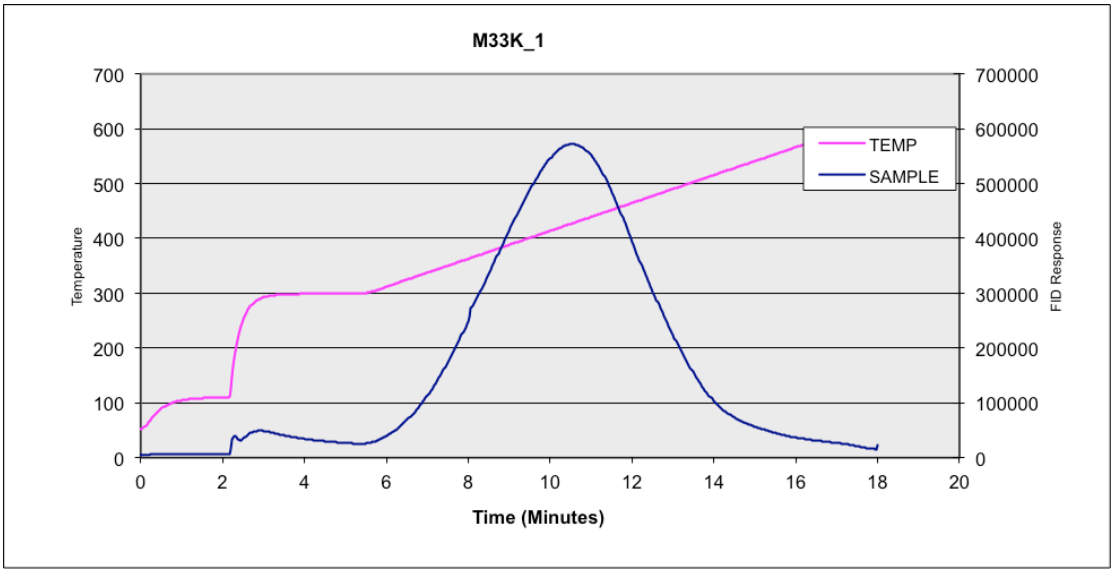
M33K_1
Temperature
FID Response
TEMP
SAMPLE
Time (Minutes)

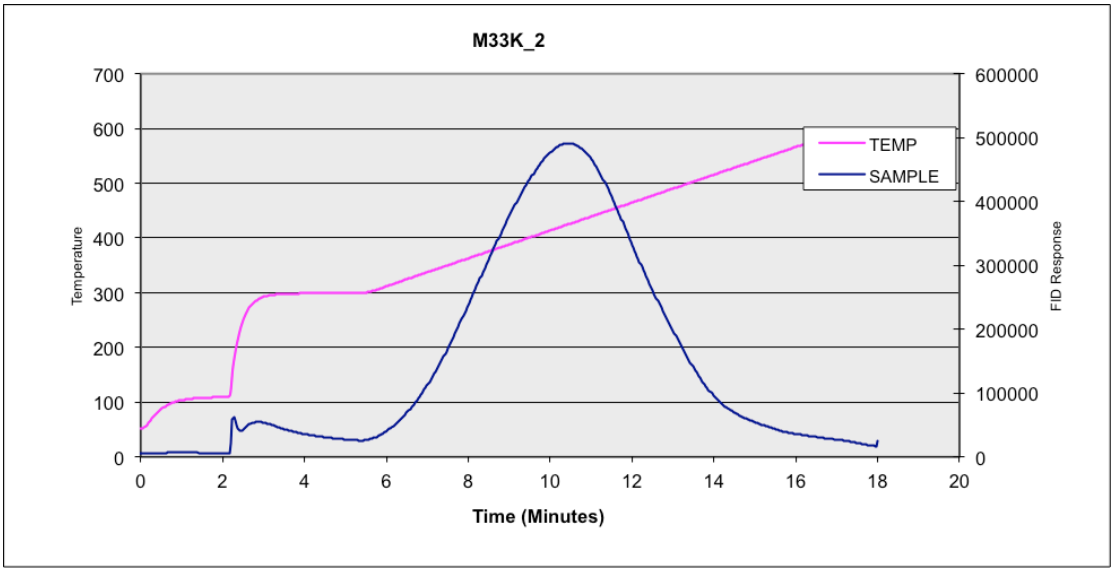
M33K_2
Temperature
FID Response
TEMP
SAMPLE
Time (Minutes)

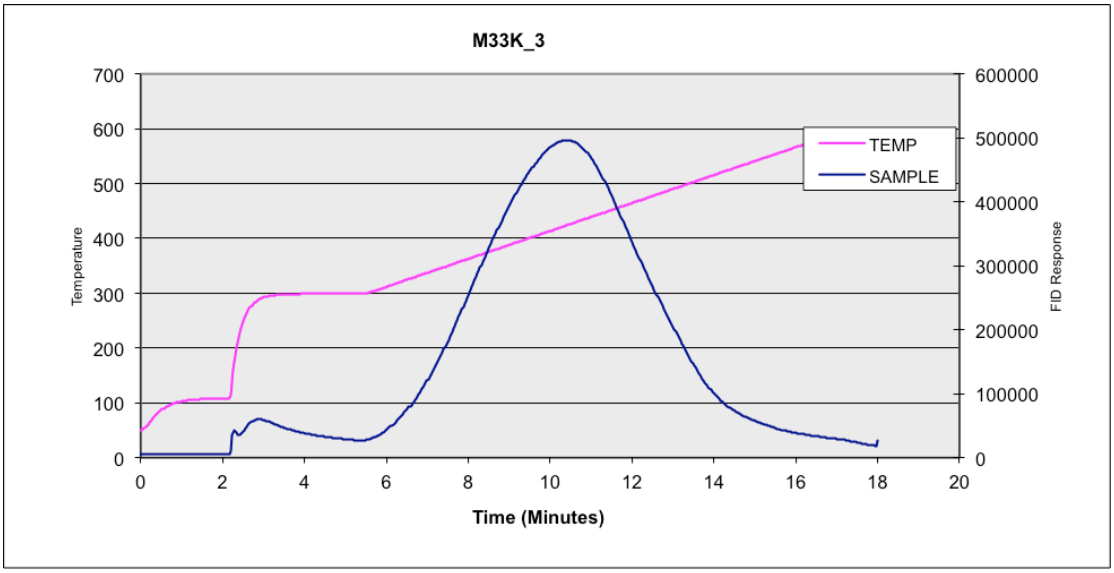
M33K_3
Temperature
FID Response
TEMP
SAMPLE
Time (Minutes)

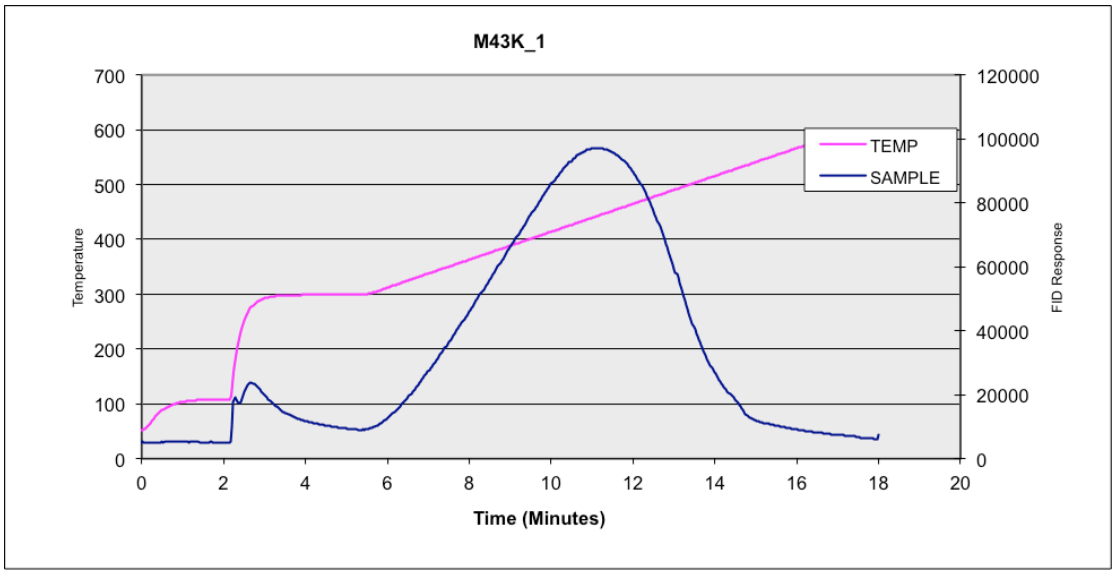
M43K_1
Temperature
FID Response
TEMP
SAMPLE
Time (Minutes)
0
100
200
300
400
500
600
700
0
20000
40000
60000
80000
100000
120000
0
2
4
6
8
10
12
14
16
18
20

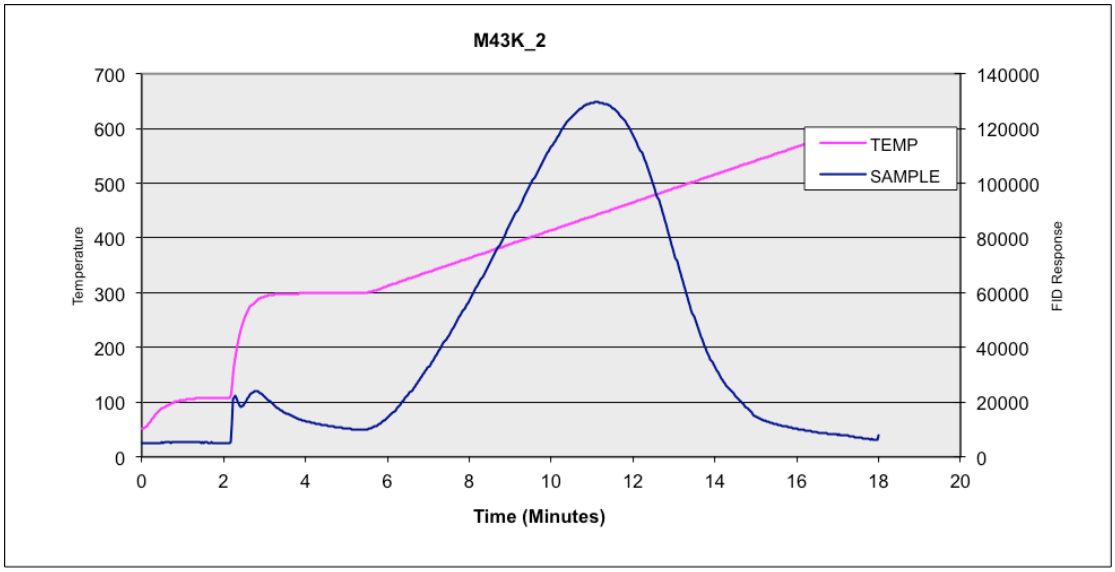
M43K_2
Temperature
FID Response
TEMP
SAMPLE
Time (Minutes)
0
100
200
300
400
500
600
700
0
20000
40000
60000
80000
100000
120000
140000
0
2
4
6
8
10
12
14
16
18
20

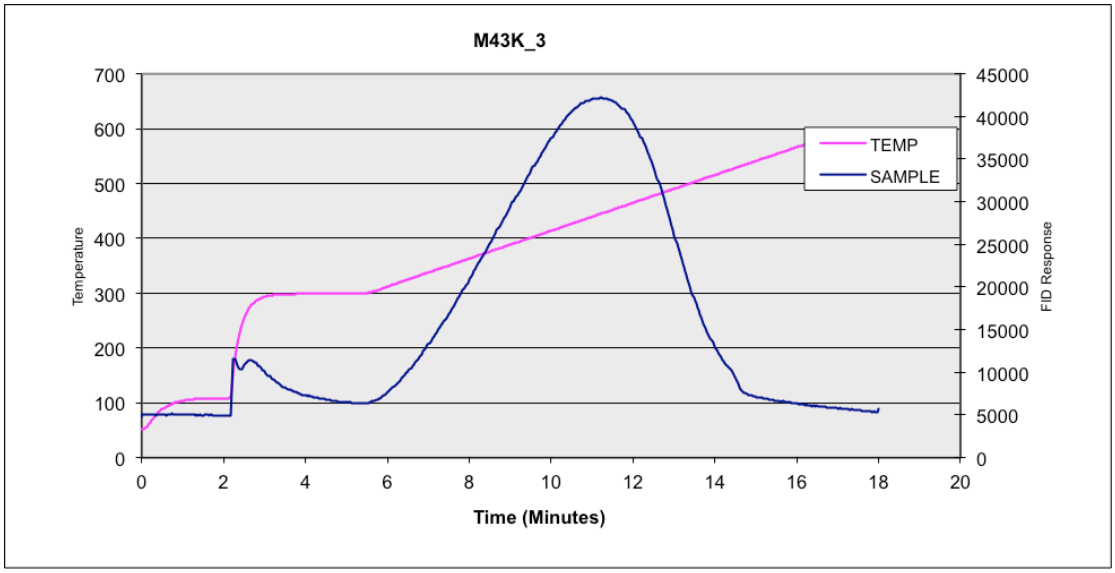
M43K_3
Temperature
FID Response
TEMP
SAMPLE
Time (Minutes)
0
100
200
300
400
500
600
700
0
5000
10000
15000
20000
25000
30000
35000
40000
45000
0
2
4
6
8
10
12
14
16
18
20

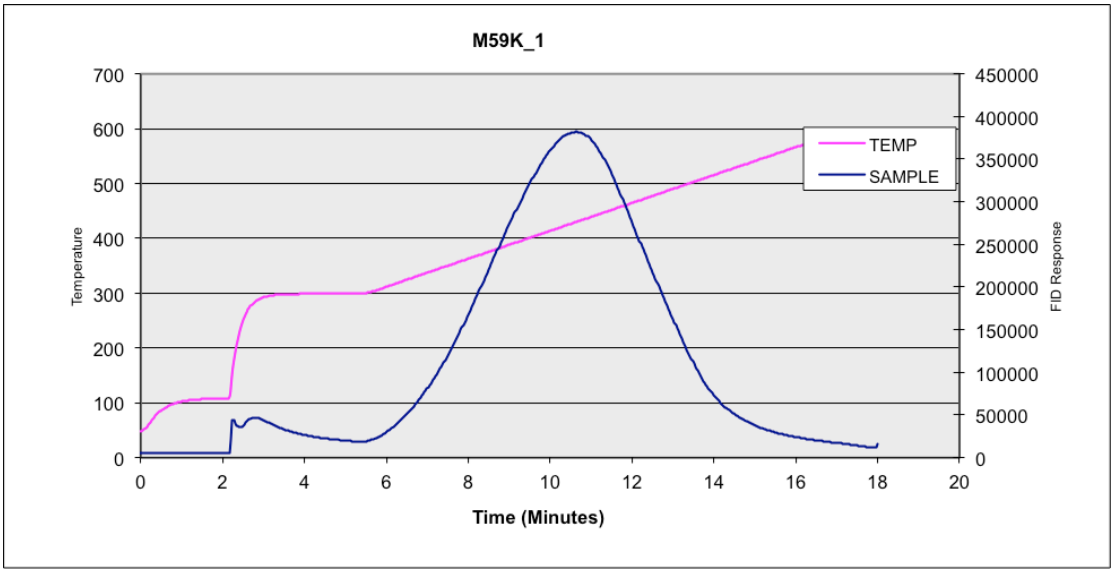
M59K_1
Temperature
FID Response
TEMP
SAMPLE
Time (Minutes)

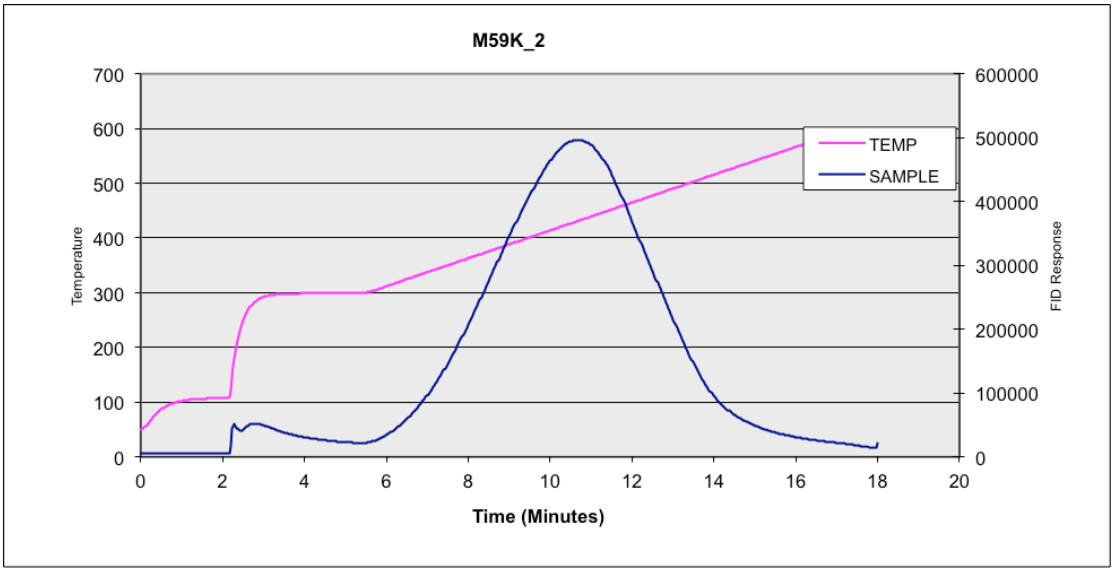
M59K_2
Temperature
FID Response
TEMP
SAMPLE
Time (Minutes)

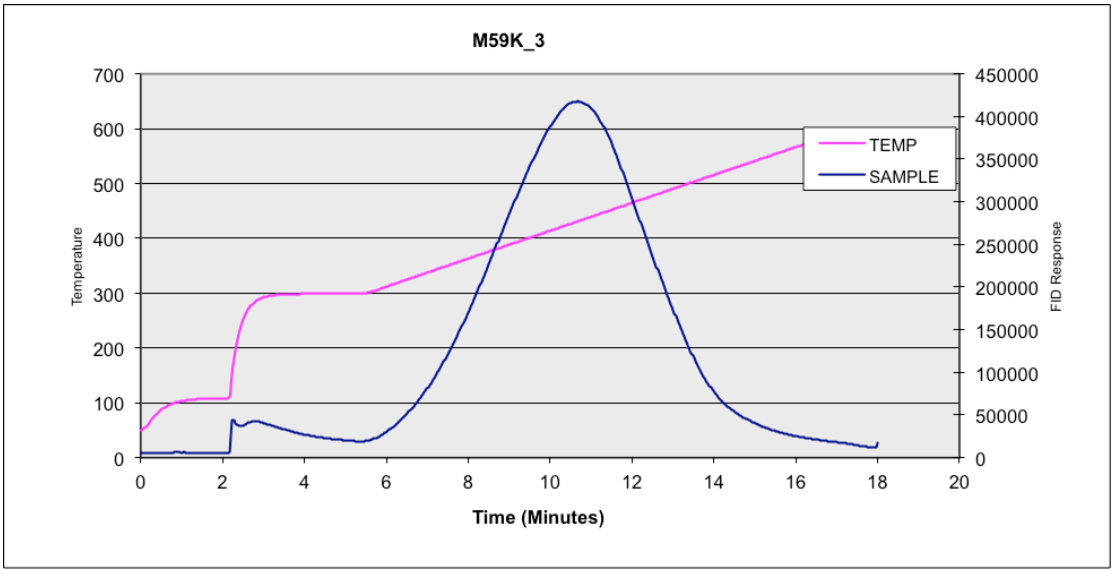
M59K_3
Temperature
FID Response
TEMP
SAMPLE
Time (Minutes)

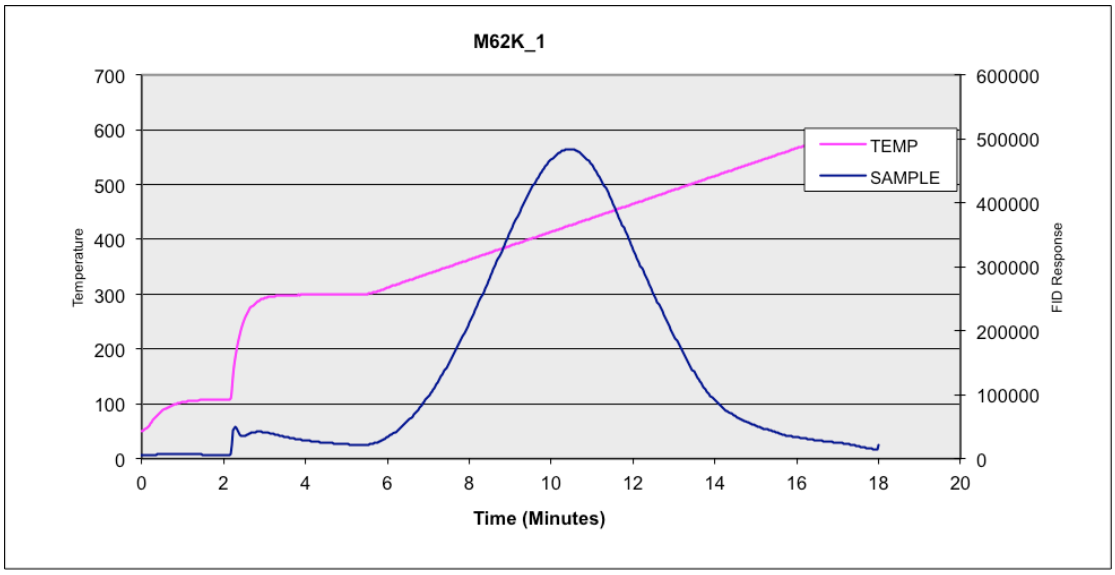
M62K_1
Temperature
FID Response
TEMP
SAMPLE
Time (Minutes)
0
100
200
300
400
500
600
700
0
100000
200000
300000
400000
500000
600000
0
2
4
6
8
10
12
14
16
18
20

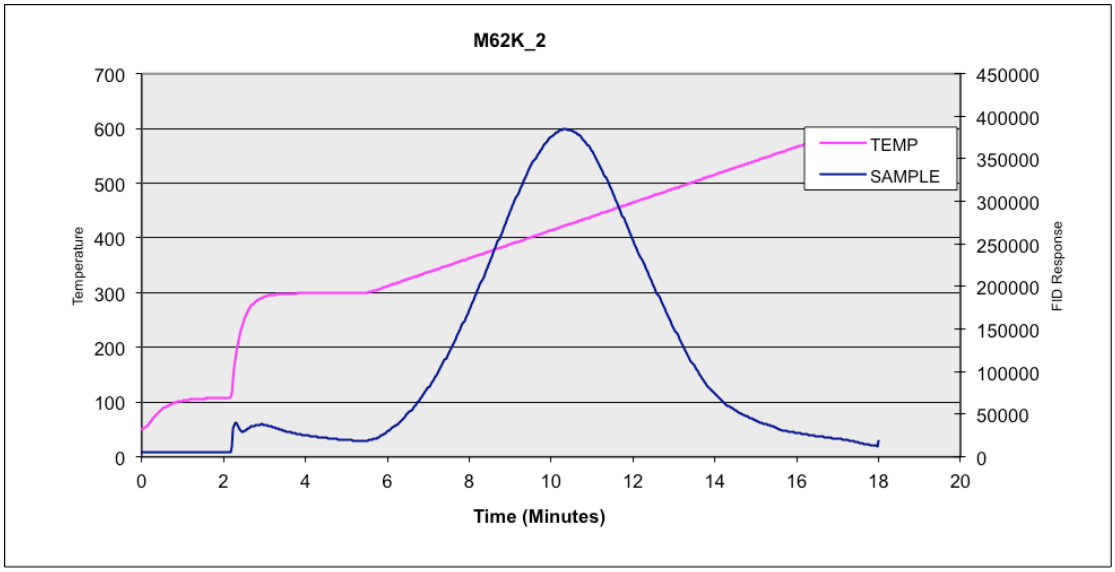
M62K_2
Temperature
FID Response
TEMP
SAMPLE
Time (Minutes)
0
100
200
300
400
500
600
700
0
50000
100000
150000
200000
250000
300000
350000
400000
450000
0
2
4
6
8
10
12
14
16
18
20

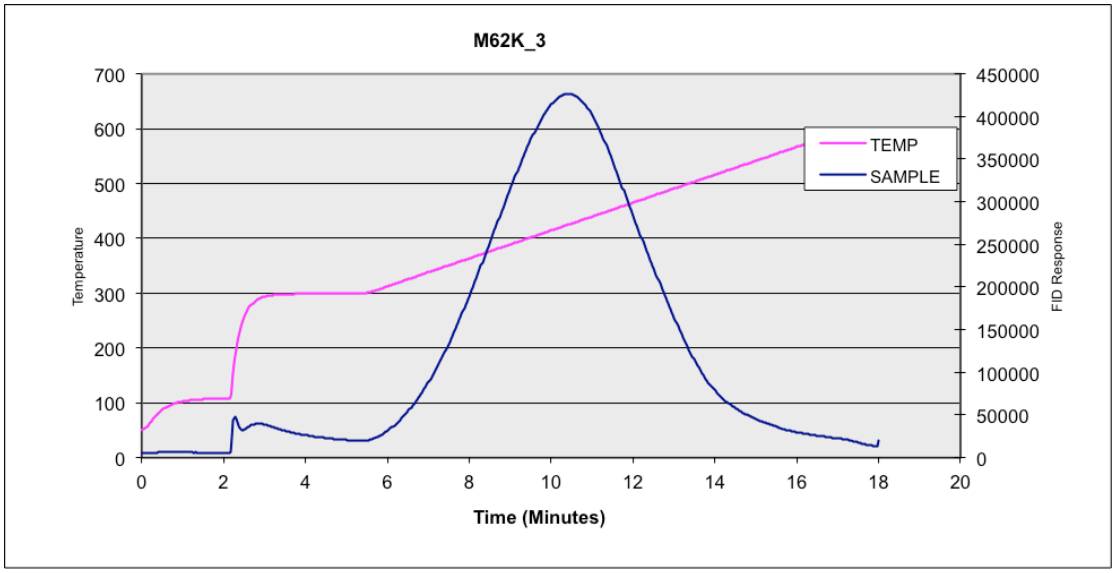
M62K_3
Temperature
FID Response
TEMP
SAMPLE
Time (Minutes)
0
100
200
300
400
500
600
700
0
50000
100000
150000
200000
250000
300000
350000
400000
450000
0
2
4
6
8
10
12
14
16
18
20